To the Graduate Council:

I am submitting herewith a thesis written by Jon William Jessee entitled "The Development Of A Natural Convection Heat Transfer Research Facility." I have examined the final copy of this thesis for form and content and recommend that it be accepted in partial fulfillment of the requirements for the degree of Master of Science, with a major in Mechanical Engineering.

Robert J. Krane, Major Professor

We have read this thesis
and recommend its acceptance:

Accepted for the Council:

Vice Provost
and Dean of the Graduate School

STATEMENT OF PERMISSION TO USE

In presenting this thesis in partial fulfillment of the requirements for a Master's degree at The University of Tennessee, Knoxville, I agree that the Library shall make it available to borrowers under rules of the Library. Brief quotations from this thesis are allowable without special permission, provided that accurate acknowledgment of the source is made.

Permission for extensive quotation from or reproduction of this thesis may be granted by the Head of Interlibrary Services when the proposed use of the material is for scholarly purposes. Any copying or use of the material in this thesis for financial gain shall not be allowed without my written permission.

Signature Robert J. Kane for J. Jessee (deceased)

Date August 19, 1985

THE DEVELOPMENT OF A NATURAL CONVECTION HEAT TRANSFER RESEARCH FACILITY

A Thesis

Presented for the

Master of Science

Degree

The University of Tennessee, Knoxville

Jon William Jessee

August 1985

PREFACE

A number of minor editorial changes were made to this thesis after the untimely death of the author, Jon William Jessee. This work was performed by his friends and colleagues:

Mr. Thomas J. Phillips

Mr. Peter E. Raad

Mr. Abdollah H. Tabrizi

Mr. Seid-Ahmed Mohammed Said.

Their unselfish gift of time enabled the completion of this work.

Robert J. Krane, Professor

ABSTRACT

The Mechanical and Aerospace Engineering Department of the University of Tennessee, Knoxville, has dedicated a laboratory exclusively to the study of natural convection heat transfer. A major decision in the development of the laboratory was to employ optical instrumentation whenever possible. Thus, a Mach-Zehnder interferometer (MZI) is used for measuring fluid temperatures, a laser doppler velocimeter (LDV) for measuring fluid velocities, and a Wollaston prism interferometer for measuring heat fluxes at fluid-solid interfaces.

The basic objectives accomplished in the performance of the thesis project are:

(1) The development and documentation of the detailed experimental procedures required for using the Mach-Zehnder interferometer and laser doppler velocimeter to make measurements in natural convection flows,

(2) The design and construction of the experimental apparatus necessary for an investigation of optimal enclosure shapes for internal natural convetion flows, and

(3) The application of the experimental procedures developed for the Mach-Zehnder interferometer and laser doppler velocimeter to measure the velocity and temperature profiles in the optimal enclosure

shape apparatus when this apparatus was assembled in the form of a two-dimensional square enclosure with isothermal vertical walls and adiabatic horizontal walls.

An additional experiment was performed using the natural convection flow on a vertical, constant-heat-flux plate to check the accuracy of determining wall heat fluxes from temperature profiles measured with the Mach-Zehnder interferometer.

In summary, this thesis:

(1) Describes the operation, in both theory and practice, of the MZI and LDV,

(2) Presents the design and construction details of the two experimental devices,

(3) Lists the detailed procedures for setting-up the experiments and taking the required data,

(4) Explains and illustrates with examples the data reduction procedures, and

(5) Presents the results of the experiments along with an uncertainty analysis.

TABLE OF CONTENTS

CHAPTER		PAGE
INTRODUCTION		1
I.	DESCRIPTION OF INSTRUMENTS	3
	A. Mach-Zehnder Interferometer	3
	1. The Idealized MZI	3
	2. The Real MZI	19
	3. Relationships Between Fringe Shifts and Temperature Changes	34
	4. The End Effect Error	37
	5. The Refraction Error	44
	B. The Mach-Zehnder Interferometer of Aerolab, Inc.	45
	1. General Description	45
	2. The Mercury Arc Light Source	47
	3. The Helium-Neon Laser Light Source	50
	4. Alignment of the Aerolab MZI	54
	5. Viewing and Recording the Output of the Interferometer	65
	6. Establishment and Alignment of the Desired Fringe Pattern	73
	C. The Laser Doppler Velocimeter	81
	1. Principles of Operation	82
	2. A General Description of the Thermo-Systems, Inc. LDV System	92
	3. Alignment and Operation of the TSI LDV System	98
	4. The Model 1090 Tracker	113
II.	DESIGN OF EXPERIMENTS	125
	A. Introductory Remarks	125
	B. The Two-Dimensional Enclosure Experiment	126
	1. Basic Design Features	126
	2. Design of the Vertical Walls	128
	3. The Thermocouple System	131
	4. Design of the Horizontal Walls	133
	5. Design of the Support Structure and End Windows	135
	6. Design of the Positioning System	142
	C. The Vertical Flat Plate Experiment	146
III.	ASSEMBLY AND OPERATION OF EXPERIMENTS	150
	A. Preliminary Remarks	150
	B. The Heated Vertical Plate Experiment	150
	1. Introduction	150
	2. Preparation of the Plate	151
	3. Mounting the Plate	152
	4. Power Supply	154

5. Camera Alignment and Focusing 154
6. Plate Alignment 157
7. Adjustment of the MZI 168
8. Performance of the Experiment 173
C. The Enclosure Experiment 182
1. Thermocouple Calibration 182
2. Preparation of the Vertical Walls 183
3. Assembly of the Enclosure 185
4. Alignment of the Enclosure and its Support and Transport System 187
5. Alignment of the LDV System with respect to the Enclosure 195
6. Enclosure Alignment and Focusing for the MZI 205
7. Final Assembly and Preparation of the Enclosure Including Window Alignment . . 207
8. Performance of the Enclosure Experiment . 214

IV. DATA REDUCTION TECHNIQUES AND RESULTS OF THE EXPERIMENTS 224
A. Introduction 224
B. Techniques for Reducing the Mach-Zehnder Data for the Heated Plate Experiment. 224
C. Physical Interpretation of the Results of the Heated Plate Experiment 251
D. Techniques for Reducing the Mach-Zehnder Data for the Internal Cavity Experiment. . . 253
E. Techniques for Reducing the LDV Data for the Internal Cavity Experiment 264
F. Physical Interpretation of the Results of the Internal Cavity Experiment 270

V. ERROR ANALYSIS 274
A. Introduction 274
B. Uncertainty Analysis of the MZI Data for the Cavity Experiment 274
C. Uncertainty Analysis of the LDV Data for the Cavity Experiment 283

VI. SUMMARY AND RECOMMENDATIONS 289
A. Summary 289
B. Recommendations for Future Research 290

LIST OF REFERENCES 295

APPENDICES 298
APPENDIX A. END-EFFECT CALCULATIONS 299
APPENDIX B. AN ALTERNATIVE COLLIMATION TECHNIQUE FOR THE MACH-ZEHNDER INTERFEROMETER . . 302
APPENDIX C. OPERATION OF CAMERA AND FILM DEVELOPMENT 304
APPENDIX D. WALL ANGULAR ALIGNMENT 306

APPENDIX E. OPERATION OF THE CIRCULATING BATHS . . . 309
APPENDIX F. TEMPERATURE DATA FOR THE HEATED PLATE EXPERIMENT 313
APPENDIX G. TEMPERATURE DATA FOR THE HOT AND COLD WALLS OF THE CAVITY 321
APPENDIX H. PARTICLE GENERATORS FOR SEEDING FLOWS FOR LASER DOPPLER VELOCIMETRY 327
APPENDIX I. CAVITY VELOCITY DATA MEASURED WITH THE LDV 330
APPENDIX J. THE MEASURING MICROSCOPE 334
APPENDIX K. PROPERTY VALUES AND EQUATIONS FOR AIR . 337
APPENDIX L. CAVITY END EFFECT ANALYSIS 339
APPENDIX M. CAVITY TEMPERATURE DATA FROM THE MZI . . 346

VITA. 358

LIST OF FIGURES

FIGURE PAGE

1. Basic optical design of the Mach-Zehnder interferometer 4
2. Optical arrangement for wedge fringe formation . . . 9
3. Enlargement of the beam intersection region of Figure 2 10
4. Fringe formation due to the effects of a heated plate in the test section 14
5. Light source arrangements for the Mach-Zehnder interferometer 21
6. Effect of focusing on image formation 28
7. A possible assumption for the end effect about a plate in free air 39
8. Notation for correction of end effect error 41
9. Layout of Aerolab, Inc. Mach-Zehnder interferometer 46
10. The mercury arc light source mounted on the interferometer 49
11. The laser light source mounted on the interferometer 51
12. Condenser and diaphragm assembly for the laser light source 52
13. The collimation tool used with the interferometer . 59

14. The collimation tool in use suspended inside the interferometer 60
15. The viewing screen and its stand used with the interferometer 66
16. The camera and its focusing track on the stand as used with the interferometer 67
17. The "camera alignment tool" mounted on the apron of the camera 69
18. Schematic of the Laser Doppler Velocimeter in dual beam, forward scatter mode with details illustrating the principle of operation 83
19. The Laser Doppler Velocimeter system in dual beam, backscatter mode with the optional frequency shifter in place 88
20. The view through the magnifier of the Model 10096 aligment tool 109
21. The Thermo-Systems, Inc. Model 1090 Tracker . . . 114
22. Cross sectional view of the test enclosure and the support arrangement 127
23. Thermocouple locations on the hot and cold walls and their identifying numbers 132
24. Cross section of the test enclosure illustrating details of the end windows 136
25. The "linear positioner" or "track" with the "carriage" for supporting and transporting the experimental device 143

26. Cutaway view of the electrically heated vertical plate 148

27. The vertical plate mounted on the enclosure package and within the test beam of the interferometer 153

28. Exposure for scale factor determination and to illustrate focusing 156

29. The viewing screen in place in the interferometer for alignment of the experiment with the test beam 161

30. Schematic of the "reflection-off-the-wall" alignment technique and the alignment tool 162

31. The "alignment tool" in place in the interferometer for alignment of the experiment with the test beam 163

32. The test plate at air temperature showing straight wedge fringes along with the shadows of the wires of the collimation tool 172

33. Exposure of the heated plate with the RHS in "best" alignment (angular adjustment knob at 9) 177

34. Exposure of the heated plate at a wider fringe spacing than the previous figure and adjusted for average alignment of the two sides 179

35. Exposure of the heated plate with the MZI in the infinite fringe setting showing isotherm fringes . 180

36. Schematic of the enclosure and mounting arrangement 188
37. Detail of the support bracket's attachment to the vertical dovetail slider 192
38. Alignment and focusing tool 197
39. Tool for aligning laser beams to a surface 200
40. Exposure of the scale at the L/2 location for scale factor determinaton 208
41. Schematic of the "reflection-off-the-glass" technique for aligning a glass end window to be perpendicular to the optical axis 213
42. Exposure of the cavity at operating temperature showing approximate isotherm fringes 216
43. Exposure of the isothermal cavity with wedge fringes 218
44. Exposure of the cavity at operating temperature with a wedge fringe field 219
45. Reproduction of a form for recording measuring microscope data from interferograms 234
46. Distances x and x may be measured in order to interpolate the fringe number at intermediate locations between fringe intercepts 241
47. Reproduction of a form for recording and reducing interferogram data 245
48. Temperature profiles about the heated plate . . . 252

49. Horizontal temperature distributions within the cavity 265
50. Form for recording LDV data 266
51. Centerline velocity profiles within the cavity . . 269
52. Temperature profile along the vertical centerline within the cavity 272
53. Thermocouple millivolt potential versus temperature data as given in the Omega Engineering Inc, catalog for the 50-60 oC range 316
54. Thermocouple millivolt potential versus temperature for the 20-30 oC range 317
55. Thermocouple millivolt potential versus temperature forthe 30-40 oC range 324
56. Thermocouple millivolt potential versus temperature for the 0-10 oC range 325
57. Photograph of the measuring microscope 335
58. Assumed end effects for a heated plate in free air (A) and for the influence of an end window in an internal cavity (B) 342

LIST OF TABLES

TABLE PAGE

1. Value of x'20 and y'20 readings for several alignment trials of the test cavity to the LDV's laser beams 206
2. Measuring microscope coordinate locations for the centerline fringe in exposure 071580-2 (unheated plate) 228
3. Measuring microscope coordinate locations for the centerline fringe and fringe intercepts in exposure 071580-3 (heated plate, RHS in "best" alignment) 231
4. Measuring microscope coordinate locations for the centerline fringe and fringe intercepts in exposure 071580-5 (heated plate, average alignment) 236
5. Fringe location measurements for interferogram 071580-6 (infinite fringe field) 238
6. Measuring microscope data for interferogram 071580-3 with interpolations between fringe intercepts 243
7. Fringe number and temperature data for interferogram 071580-3 with fringe number interpolations 250

8. Interferogram analysis and temperature data at the y = 0.5H traverse for the internal cavity . . 258

9. Values obtained for repeated measurements at the x = 0.5L location along with the S-value differences, S 280

10. Cold wall temperature, T, obtained by interpolation from second-order fits, and measurement error, T-TC, where TC = 7.24 oC . . . 282

11. Temperature data for the heated plate 314

12. Hot and cold wall temperature data for the calibration and main operating tests 323

13. Thermometer data for the hot and cold wall calibration tests 326

14. Temperature data for: y' = 0.2675 inch; y = 1.53 mm; y/H = 0.038 347

15. Temperature data for: y' = 0.3515 inch; y = 3.86 mm; y/H = 0.097 348

16. Temperature data for: y' = 0.5025 inch; y = 8.05 mm; y/H = 0.202 349

17. Temperature data for: y' = 0.6355 inch; y = 11.74 mm; y/H = 0.295 350

18. Temperature data for: y' = 0.7838 inch; y = 15.85 mm; y/H = 0.399 351

19. Temperature data for: y' = 0.9318 inch; y = 19.96 mm; y/H = 0.502 352

20. Temperature data for: y' = 1.0645 inch;
y = 23.64 mm; y/H = 0.595 353
21. Temperature data for: y' = 1.2130 inch;
y = 27.76 mm; y/H = 0.698 354
22. Temperature data for: y' = 1.3632 inch;
y = 31.93 mm; y/H = 0.803 355
23. Temperature data for: y' = 1.4963 inch;
y = 35.62 mm; y/H = 0.896 356
24. Temperature data for: y' = 1.5965 inch;
y = 38.40 mm; y/H = 0.966 357

INTRODUCTION

The study of natural convection heat transfer is important to provide understanding of heat transfers from structures and equipment. To further heat transfer research, the Mechanical and Aerospace Engineering Department of the University of Tennessee, Knoxville, has dedicated a laboratory exclusively to the study of natural convection. This laboratory features two instruments especially well suited to measurements of natural convection flows: a Mach-Zehnder Interferometer for fluid temperature measurements and a Laser Doppler Velocimeter for fluid velocity measurements. After the research leading to this thesis was started, a third major instrumentation system was acquired: a Wallaston Prism Interferometer for heat flux measurements. These instruments are especially applicable to natural convection studies because they employ only optical probes within the test space; that is, there is no disturbance of the test fluid by physical probes such as hot-wire anemometers or thermocouples--only light beams of low power enter the test space. This is important because typical natural convection flows are relatively weak; hence, a physical probe could introduce significant deviations from an undisturbed form of the flow.

This thesis is intended as a "users manual" for the

Natural Convection Laboratory. The theories of operation and techniques for setup and use of the principle instruments will be explained. The design of two natural convection experiments will be presented along with the application of the instruments to these experiments. Finally, methods of data reduction will be illustrated, and the actual data from the experiments will be shown.

CHAPTER I

DESCRIPTION OF INSTRUMENTS

The theories of operation and techniques of setup and adjustment for both the Mach-Zehnder Interferometer and the Laser Doppler Velocimeter will be described.

A. Mach-Zehnder Interferometer

The Mach-Zehnder Interferometer (abbreviated as MZI) was named after L. Zehnder and L. Mach who each independently described its design in 1891 and 1892, respectively [1], [2]. Though there are numerous interferometer designs, the MZI is especially well suited to heat transfer studies and, thus, seems to be one of the most popular instruments for quantitative studies in this field. The optical layout and principles of operation of the MZI will now be described, beginning with a simplified "ideal" model and later adding the complicating factors.

The Idealized MZI

The basic optical design of the MZI is illustrated in Figure 1. Light rays from a monochromatic point light source are collimated by a lens into a beam of parallel rays. This collimated beam then strikes a beam splitter, BS1, which divides the incident beam into two parts, which are usually of equal intensity. One of the beams is called

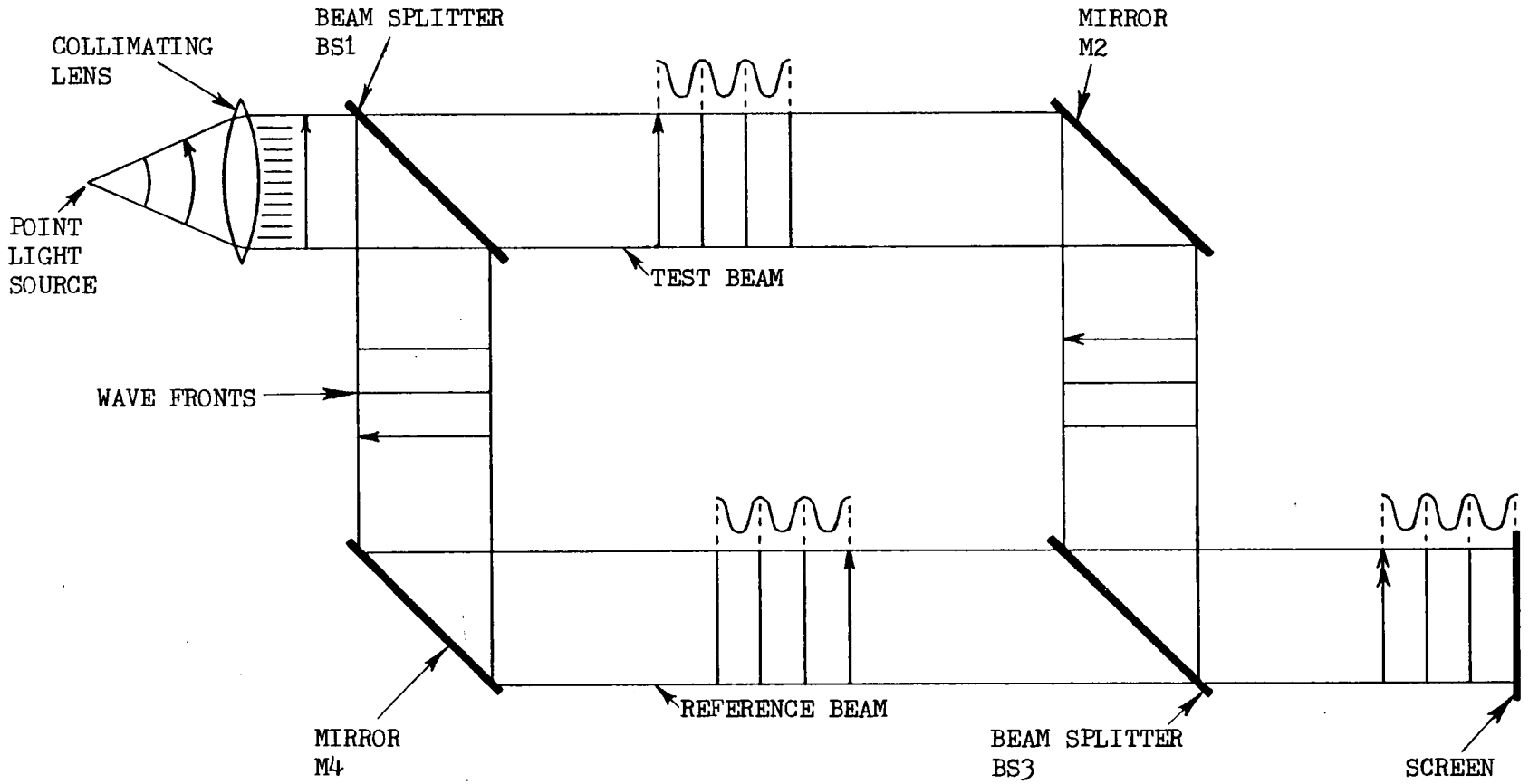


Figure 1. Basic optical design of the Mach-Zehnder interferometer.

the "test beam" or "measuring beam," and the other is called the "reference beam." Beam splitters employed in an MZI usually consist of a dielectric coating on a thick glass carrier; in the diagram, only the coating is shown. The two beams leaving the first beam splitter are deflected by two flat relay mirrors, labeled M2 and M4, which cause the two beams to intersect at the second beam splitter, labeled BS3. Although it is called a beam splitter and is identical to BS1, it combines the two incident beams into a single beam that exits parallel to the collimated beam from the light source.

The functioning of an interferometer may be more throughly understood if light is described in mathematical terms. The following equations and explanations are largely from Wilkie and Fisher [3].

To a first approximation, rays of light may be described by the equation

$$y = a \sin\left(\frac{2\pi}{\lambda}(x - vt)\right)$$

where y is the transverse displacement, a the amplitude, λ the wavelength, and v the phase velocity of a sinusoidal waveform moving in a direction x in a time t.

Rewriting the equation

$$y = a \sin\left(2\pi\frac{x}{\lambda} - \omega t\right)$$

where $2\pi\frac{x}{\lambda}$ is a "phase" associated with the wave train and

ω is the angular velocity.

If two wave trains of the same frequency are superimposed, the resultant wave is given by addition

$$y = y_1 + y_2 = a_1 \sin(2\pi\frac{x_1}{\lambda_1} - \omega t) + a_2 \sin(2\pi\frac{x_2}{\lambda_2} - \omega t)$$

Thus

$$y = A \sin(\theta - \omega t) \qquad [1]$$

where

$$A^2 = a_1^2 + a_2^2 + 2a_1a_2\cos(2\pi(\frac{x_1}{\lambda_1} - \frac{x_2}{\lambda_2})) \qquad [2]$$

and

$$\theta = \tan^{-1}\frac{a_1\sin 2\pi\frac{x_1}{\lambda_1} + a_2\sin 2\pi\frac{x_2}{\lambda_2}}{a_1\cos 2\pi\frac{x_1}{\lambda_1} + a_2\cos 2\pi\frac{x_2}{\lambda_2}} \qquad [3]$$

The resultant wave train is another sine wave but its amplitude depends not only on the amplitudes of the two superimposed waves but also on their phase relationship. If $\cos 2\pi(\frac{x_1}{\lambda_1} - \frac{x_2}{\lambda_2})$ is +1, then $A = a_1 + a_2$ and the wave trains are said to be "in-phase." If $\cos 2\pi(\frac{x_1}{\lambda_1} - \frac{x_2}{\lambda_2})$ is -1, then $A = a_1 - a_2$ and the waves are said to be "out-of-phase."

Applying the above results to the MZI, the two wave trains are the two halves of the split beam after they are superimposed by the second beam splitter, BS3. Assuming that the wave trains are of equal intensity, $a_1 = a_2 = a$

and $\lambda_1 = \lambda_2 = \lambda$. For in-phase wave trains, $\cos 2\pi \left(\frac{x_1 - x_2}{\lambda}\right)$ $= +1$, implying that $|x_1 - x_2| = 0, \lambda, 2\lambda, 3\lambda, \ldots$, or, in other words, the difference between the two trains must be a whole number of wavelengths at locations where the waves are in-phase. This condition is also referred to as "constructive interference." The amplitude A is equal to $\pm(a_1 + a_2) = \pm 2a$ which is its maximum value; hence, a location where wave trains are in-phase is a location of maximum brightness. Considering the out-of-phase condition, $\cos 2\pi \left(\frac{x_1 - x_2}{\lambda}\right) = -1$ when $|x_1 - x_2| = \lambda/2, 3\lambda/2, 5\lambda/2, \ldots$; that is, there must be a half wavelength plus any whole number of wavelengths difference between the two trains at locations where the waves are exactly out-of-phase. This condition is referred to as "destructive interference." The resulting amplitude A is $\pm(a_1 - a_2) = 0$; hence, a location where waves are out-of-phase appears dark. The amplitude varies sinusoidally between being completely in-phase and completely out-of-phase.

The lines drawn across the beams in Figure 1 represent wavefronts. A wavefront is a surface or contour that connects regions of the same phase. In this case, they are chosen to coincide with the crests of the light waves, as is indicated by the sine waves drawn next to the beams. Spherical wave fronts emanate from the point light source; the (ideal) collimating lens refracts the rays to form flat

wave fronts. The two beam splitters and the two mirrors are assumed to be flat, plus the medium traversed by the light is assumed to be optically homogeneous. Thus, the flat wavefronts remain flat throughout the interferometer. Due to the rectangular configuration of the optical path, the test and reference beams are superimposed by BS3 exactly in-phase so that constructive interference occurs in the combined beam. A viewing screen is interposed in this output beam to make it visible. Note that the intensity of the light is uniform over the screen but varies with time as the sinusoidal light waves reach the screen. To the eye, however, the screen appears constantly illuminated since it receives about 10^{16} light pulses per second--a rate far beyond the eye's ability to follow.

In Figure 2, the light path is altered from the configuration in Figure 1. Mirror M2 is rotated counterclockwise from the 45^{o} position and splitter BS3 is translated and rotated such that the central ray of the test beam now forms an angle with the central ray of the reference beam and the point of intersection is in the plane of the screen. The intersection region is shown enlarged in Figure 3 with the intersection angle and the wave length greatly exaggerated for clarity. The wavefronts of one beam, #1, are parallel to the screen; the other beam, #2, forms an angle with the first beam. Each solid wavefront line represents a crest, or the maximum

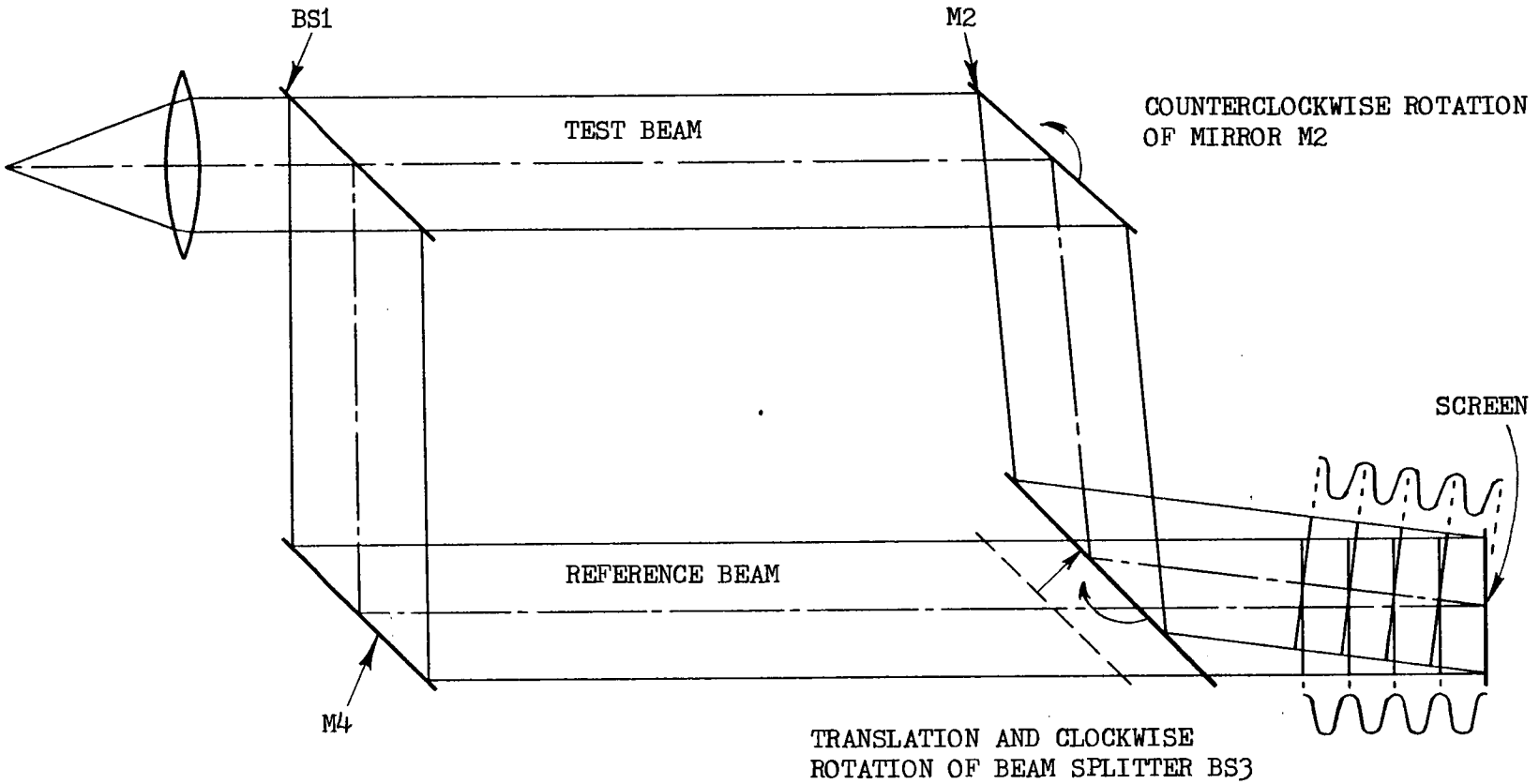


Figure 2. Optical arrangement for wedge fringe formation.

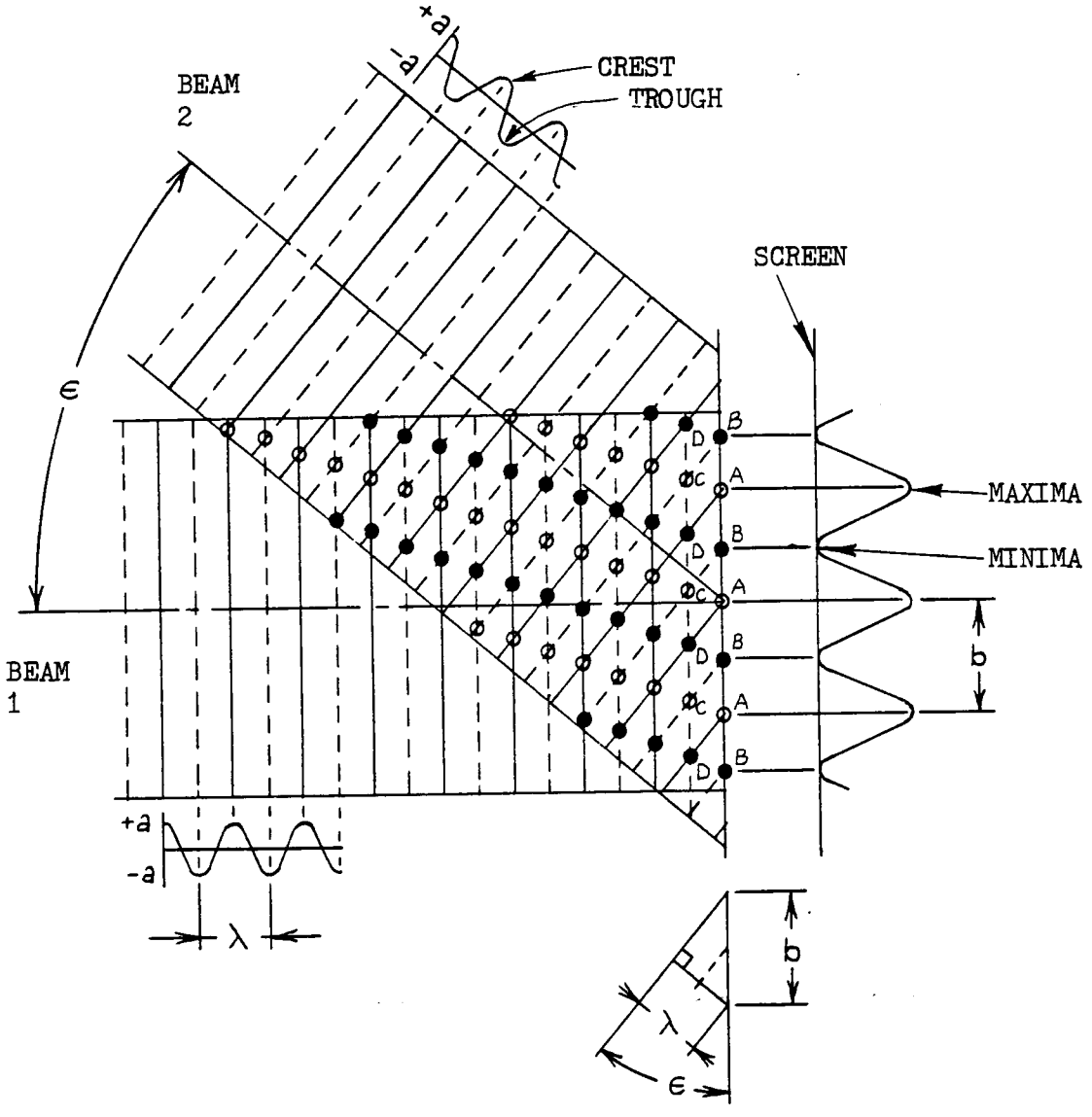


Figure 3. Enlargement of the beam intersection region of Figure 2.

positive amplitude of the light waves, while each dashed wavefront represents a trough, or the maximum negative amplitude of the waves.

For the instant shown in the figure, a crest of beam 1 is at the screen while a crest of the central ray of beam 2 also intersects the screen. At points labeled A in the figure, two wave crests are superimposed; hence, constructive interference occurs and a bright region is seen. At points labeled B, a crest and a trough are superimposed; thus, destructive interference occurs and a dark region is formed on the screen. At intermediate points between A's and B's, the brightness varies smoothly from maximum to minimum. At points labeled C, two troughs intersect; thus constructive interference again occurs. At points labeled D, a crest and a trough intersect and destructive interference again produces a dark region.

As the wavefronts of the two beams march toward the screen, the wavefront intersections at points C move along lines intersecting points A; simultaneously, the wavefront intersections at points D move along lines intersecting points B. As the trough of beam 1 approaches the screen, the wave amplitude at the screen varies from +a to -a. Similarily, as beam 2 advances by a half wavelength, its amplitude at points A varies from +a to -a and that at points B from -a to +a. Thus, as the wavefronts approach the screen, the resultant wave amplitude at points A varies

between -2a and +2a. The intensity or brightness perceived by the eye is proportional to the wave amplitude squared; thus, at points A, the intensity varies from 0 to $4a^2$. Since the eye receives about 10^{16} light pulses per second from points A, these points appear continuously illuminated and of greatest brightness. These points are referred to as "maxima." At points B, the two beams continuously cancel each other as they approach the screen; hence, points B are points of continual darkness. These points are referred to as "minima." In Figure 3, the construction to the right of the screen illustrates the intensity variation with the wavefronts in the position shown. Of course, when the wavefronts advance a quarter of a wavelength, the maxima points will be at zero intensity.

The maxima and minima are also referred to as "fringes," that is, as bright fringes or dark fringes, respectively. The fringe spacing (the distance between two light or two dark fringes) may be determined from the geometry of the beam intersections. From the inset, the fringe spacing b is

$$b = \frac{\lambda}{\sin \epsilon}$$

For an example, the wavelength of helium-neon (He-Ne) laser light is 6328 X 10^{-10} meter. If the fringe spacing is taken as 1 millimeter which is "medium fine" in MZI work, then the beam intersection angle $\epsilon = 0.036^{\circ}$. For such

small angles, one may assume $\sin\epsilon = \epsilon$; thus

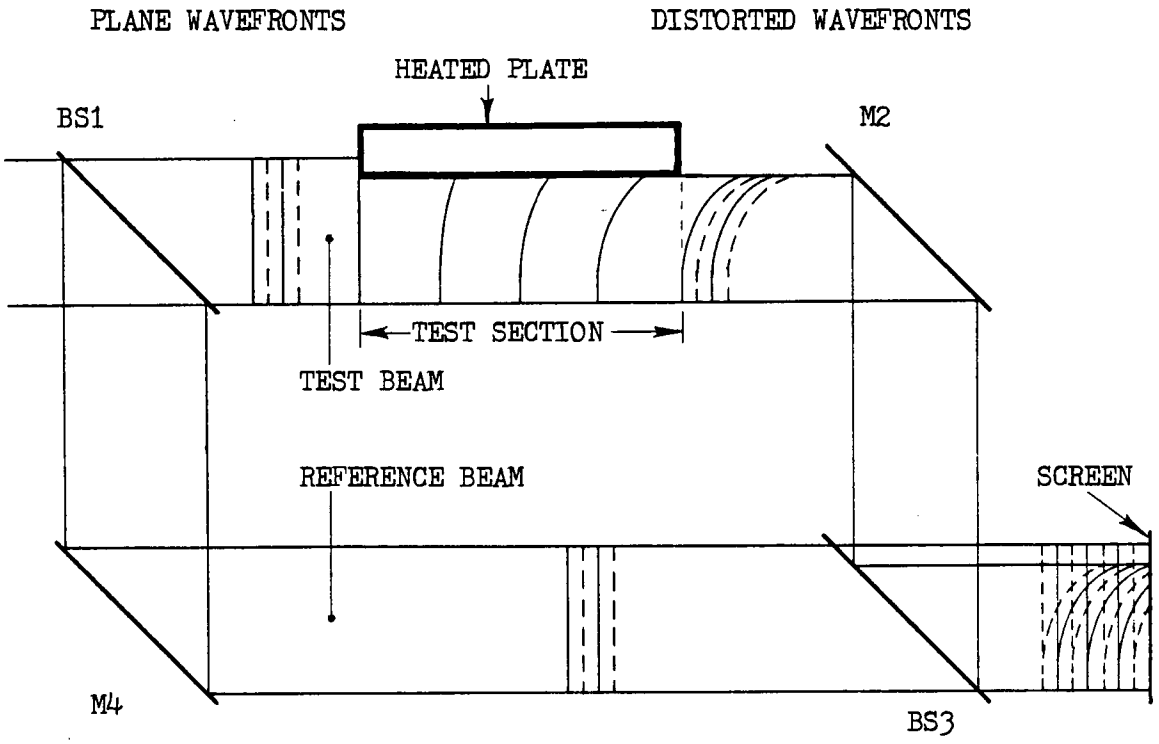
$$b = \frac{\lambda}{\epsilon} \qquad [4]$$

Note that as ϵ approaches zero, b approaches infinity. Thus, the arrangement illustrated in Figure 1, where the two output beams are parallel, is referred to as the infinite fringe adjustment. The arrangement in Figure 2 where parallel, evenly spaced fringes are present is referred to as the wedge fringe adjustment; this is the type of field that would occur if a wedge shaped optical element were placed in the test beam of an interferometer initially in the infinite fringe adjustment.

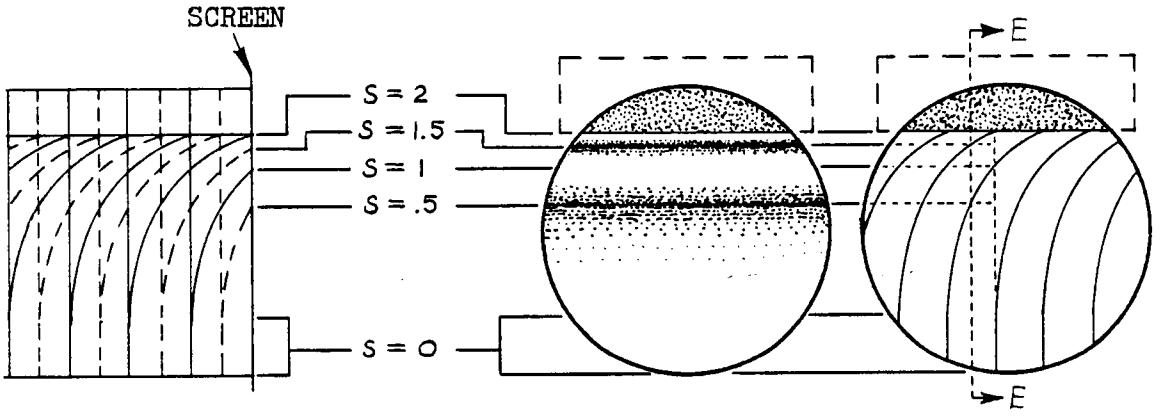
The term interference (constructive or destructive) has been used in referring to two intersecting light beams. As pointed out by Wilkie and Fisher, light beams do not actually interfere or interact with each other; they pass undisturbed beyond the region of intersection. One may only say that the principle of superposition holds within the intersection region. Nevertheless, since the term interference is always used, it will continue to be used in this paper.

As mentioned previously, the MZI's main use in heat transfer studies is the determination of temperature distributions. The scheme by which temperature variations influence the fringe pattern is illustrated in Figure 4.

The MZI layout shown in Figure 4A is assumed to have



A. Interferometer layout.



B. Beam intersection region.

C. View on the screen for infinite fringe adjustment.

D. View on the screen for wedge fringe adjustment.

Figure 4. Fringe formation due to the effects of a heated plate in the test section.

been initally adjusted to the infinite fringe position. A flat plate is partially interposed in the test beam and is maintained at a uniform temperature higher than that of the surrounding fluid which is assumed to be air. Heat conducted out of the plate heats the surrounding air; to simplify the drawing, the air temperature in the direction normal to the paper is assumed uniform.

In the figure, plane wavefronts are split into a test beam and a reference beam by BS1. Upon entering the test section (the region about the heated plate) the plane wavefronts are distorted due to the presence of the higher temperature air about the plate. Heating the air decreases its density; as its density decreases the effective speed of light through the air increases. Since the speed of light through the heated air near the plate is greater than the speed of light through the lower temperature air farther from the plate, the wave fronts are distorted into a shape that is characteristic of the temperature distribution. It may be seen in Figure 4A that as the wave fronts pass through the test section, they are increasingly distorted out of the planar shape. The wavefronts in the reference beam remain planar, of course, since the reference beam passes through undisturbed, and therefore isothermal, air.

The two beams are combined as usual by BS3 and are projected upon a screen. An enlarged view of the beam

intersection region at the screen is shown in Figure 4B, plus a view of the resultant fringe pattern that would be seen on the screen is shown in Figure 4C. Superposition of the two beams results in regions of constructive interference and regions of destructive interference precisely as described earlier in reference to wedge fringe formation, except in this case, the curved wavefronts result in unevenly spaced fringes. In Figure 4, the symbol S, called the "fringe number," is introduced to quantify the fringe shifts. At S = 0, the reference beam wavefronts interfere with the undisturbed part of the test beam wavefronts; that is, there is no change from the original infinite fringe condition. At the S = 0.5 location, there is a 0.5 wavelength difference between the test and reference beams; here crests and troughs intersect and form a minima. Similarily, at S = 1, the test beam wavefronts have advanced one wavelength ahead of their corresponding reference beam wavefronts; here constructive interference results in the formation of a maxima. This explanation extends on to the higher number fringe shifts.

It was assumed that the interferometer of Figure 4A was in the infinite fringe adjustment. It may also be used in the wedge fringe adjustment for determining temperature distributions. Note that the infinite fringe case may be considered to exist in a direction parallel to the wedge fringes. Figure 4D illustrates what happens to wedge

fringes due to a nonisothermal test section. Before the plate was heated, the fringes were straight and normal to the plate, as they still are in the S = 0 region. After heating the plate, the fringes bend into a curve characteristic of the temperature distribution. In going from S = 0 to S = 2 in Figure 4C, two (bright) fringes are crossed. Likewise, along a line normal to the plate in Figure 4D, two fringes (either bright or dark) are again crossed in going from S = 0 to S = 2. Figure 4B is valid for illustrating fringe formation for the wedge fringe case if it is taken to represent a cross section of the beam where a maxima is located in the S = 0 region of Figure 4D, such as Section E-E. In later sections, advantages and disadvantages of the infinite and wedge fringe cases will be pointed out, so that one can select the better arrangement to use with a given experimental setup.

Although the fringe shift is labeled at only certain discrete locations in this example, it actually varies continuously from zero to the maximum value. Only certain shift values, however, may be easily and accurately located. The brightest points of a maxima locate a whole number of fringe shifts (0, 1, 2, 3, etc.) while the darkest points of a minima locate whole plus half fringe shifts (0.5, 1.5, 2.5, 3.5, etc.). For the example shown in Figure 4, it was contrived to have a maximum fringe shift of exactly two at the heated plate. In general, the

fringe shift at a particular location (such as a wall boundary) will not be known, unless it happens to be located exactly on a maxima or minima.

The magnitude of the fringe shift is a function of the optical and physical properties of the medium, the test section length, the wavelength of light, and the temperature difference. Later in this chapter, a formula will be developed that gives air temperature as a function of fringe shift as well as the other quantities above. This formula allows the temperature at locations of known fringe shift to be calculated; thus, the temperature profile about a heated plate may be interpolated from the temperatures at discrete locations.

The interferometer descriptions given above were for the case of "ideal" interferometry; that is, the assumptions presented resulted in the simplest optical layout and simplest description of fringe formation. A listing of the assumtions made for ideal interferometry is found in Hauf and Grigull [4, pp. 203-204]. Briefly, these assumptions are: (1) The mirrors and beam splitters are exactly parallel and their midpoints form an exact planar parallelogram. This arrangement is termed the "geometric basic position" and results in the infinite fringe condition. (2) The mirrors and beam splitters are perfect planes and the beam splitters have no thickness. (3) The light source is a pure point source and is strictly

monochromatic. (4) The light rays within each beam remain exactly parallel while traversing the interferometer's optical path. (5) The interference pattern is influenced only by the refractive index through the test section length and the refractive index through an equal length within the reference beam. That is, the refractive index is constant along a given ray, except for a step change upon entering and leaving the test section.

The Real MZI

Various complicating factors separate an ideal interferometer from a "real" interferometer. These factors will now be described and their influence on the design of the MZI will be illustrated.

The light source for the ideal interferometer was a monochromatic point source. All real sources have some wavelength spread and they all have a finite size, although some real sources from the practical standpoint are essentially ideal. The light sources most frequently mentioned in the literature for use with an MZI are a mercury vapor lamp and a He-Ne gas laser.

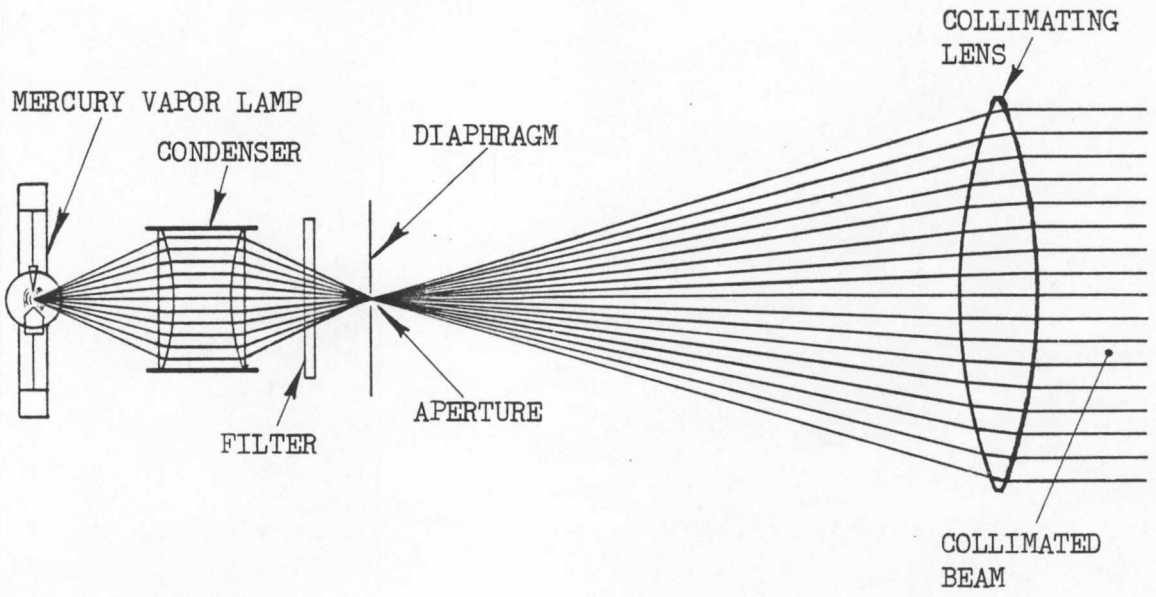
A mercury lamp produces light from an arc between two electrodes through mercury vapor; the vapor is contained within a quartz envelope. The spectral content of mercury vapor illumination is composed primarily of certain bright bands plus a continuous background spectrum. In use, a

filter is often installed in the light path; it passes only a narrow band of wavelengths within the green region of the spectrum. The wavelength of this filtered light is taken to be 5461 X 10^{-10} meter.

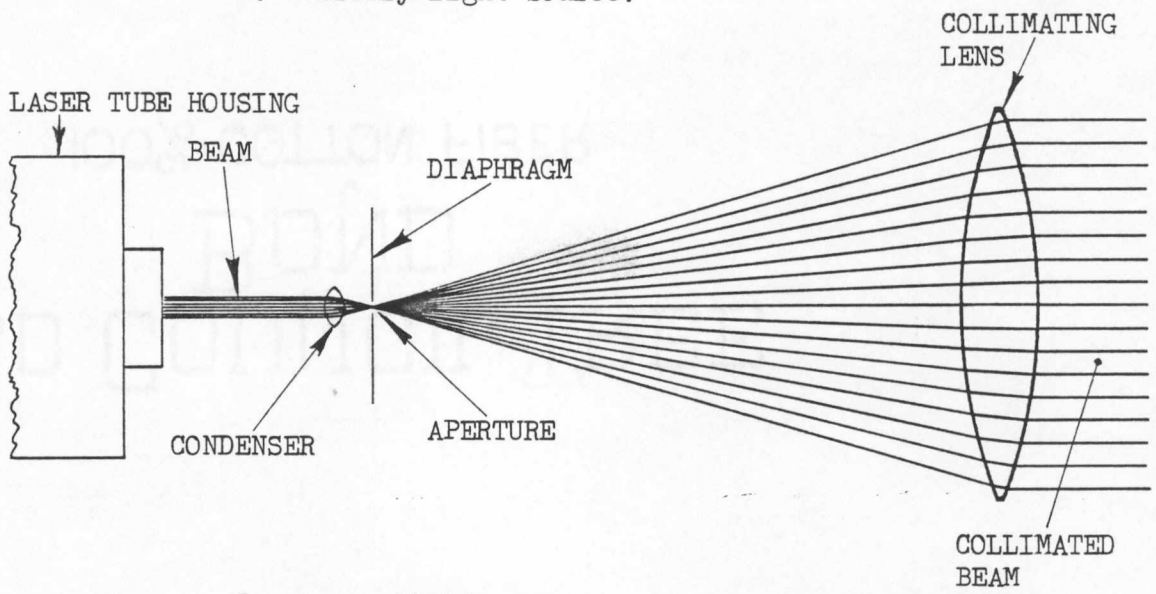
The layout of a mercury light source for an MZI is diagrammed in Figure 5A. Light is emitted by the mercury vapor arc in all directions; the condenser lens is placed relatively close to the lamp to collect as much light as possible and to bring it to a focus. The aperture is located at this focus. Since this is the point of greatest light intensity, the maximum amount of light will pass through the aperture and on to the rest of the system. The light rays radiate from the aperture and fall on the collimating lens which deflects the rays so that they exit parallel to each other. For this to occur, the focal point of the collimating lens must coincide with the location of the aperture.

The light emitted by a gas laser originates from atoms of gas that are excited by a high voltage electrical discharge. The light emerges as a narrow, relatively intense beam from one end of the discharge tube. The wavelength of He-Ne laser light is 6328 X 10^{-10} meter.

The layout of a laser light source for an MZI is diagrammed in Figure 5B. The basic arrangement is seen to be similar to that of the mercury light source. One major difference between the two sources is the function



A. Mercury light source.



B. Laser light source.

Figure 5. Light source arrangements for the Mach-Zehnder interferometer.

performed by the aperture. In the laser light source, the aperture acts primarily as a "spatial filter"; that is, it has a smoothing effect on the intensity of the light brought to a focus by the condenser. If the laser were used without a diaphragm, the collimated beam would suffer from severe brightness variations over its area. With a very small aperture (about 10^{-5} meter diameter) in place, diffraction effects smooth out the brightness so the emergent cone of light is uniform in brightness except for a regular decrease from the center to the edge.

The aperture in the mercury light source primarily serves to limit the physical size of the source; that is, the aperture can reduce the source more nearly to a point source. With a diaphragm in place, light emanates from all points of the aperture as if there were an infinite number of point sources within the area of the aperture. These point sources possess different phase relationships to each other; plus, the light from each source originates from a different spatial location. A detailed discussion of the influence of aperture size on interferometer performance is presented by Hauf and Grigull [4, pp. 221-230]. To summarize, the fringe contrast (brightness difference between maxima and minima) is an inverse function of aperture size; thus, when the aperture size is decreased, fringe contrast is enhanced. During inital set-up of an MZI, the aperture may be omitted to allow the maximum

amount of light to pass for ease in observing the beams' locations. If, during an experiment, relatively large fringe numbers are encountered, a small aperture may be needed; else, the contrast could be so poor as to make the fringes invisible.

Other assumptions of ideal interferometry are that the midpoints of the mirrors and beam splitters form a parallelogram and the beam splitters have no thickness. These properties assure that the test and reference beams will have equal optical path lengths. (Uniform optical properties of the medium traversed by the light is implicitly assumed, except for the test section, of course.) Two beams have equal optical path lengths if they contain the same number of wavelengths. Referring to Figure 1 again (p. 4), the wavefront that has just left the collimating lens is marked by an arrowhead at one end. This wavefront is split into halves by BS1. After traversing the interferometer's optical path, the same two halves are then reunited by BS3. Since the two halves of the wavefront are exactly identical when they are reunited, perfect (constructive) interference is obtained. This result holds true even if the light is not monochromatic; that is, with equal optical path lengths, each wavelength in each separate beam bears the same phase relationship to the same wavelength in the other beam at the point where they are recombined.

It is possible to change the optical path length of only one beam (test or reference) of the MZI. Referring to Figure 1, assume that BS3 is translated parallel to the reference beam and toward M4. Mirror M2 will need to be rotated so that the reflected test beam still strikes BS3 centrally. This translation of BS3 serves to lengthen the distance from M2 to BS3 (lengthens the test beam) while the reference beam remains unaffected.

Now assume that the light source in Figure 1 emitts three wavelengths for the colors red, green, and blue. These, the three primary colors, add together (in the proper proportions) to appear as white. Thus, if a screen is interposed in the collimated beam just before BS1, the beam appears white to the eye. Similarly, the output beam past BS3 appears white if the interferometer is adjusted for equal optical path lengths. Now, let the test beam be lengthened by one half of green's wavelength. Total destructive interference occurs for green in the output beam; blue and red suffer partial destructive interference resulting in their apparent brightnesses being decreased. The output beam no longer appears white; blue and red add together to yield magenta.

This appearance of color from an initally white beam is used as a clue to distinguish when an interferometer has been adjusted for equal optical path lengths. An MZI with either a white light or an unfiltered mercury light source

may be adjusted to form wedge fringes as in Figure 2 (and magnified in Figure 3) so that several fringes (representing different optical path lengths) will be visible simultaneously. The region of equal optical path length is characterized by a bright white maxima fringe bordered on both sides by dark minima with the succeeding maximas on either side tinged with color and decreasing contrast for both maxima and minima at increasing distance form the central maxima. The decreasing fringe contrast is a result of the wavelength spread. Equation 4 (p. 13) shows that fringe spacing is proportional to wavelength. Each wavelength in a non-monochromatic beam forms its own fringe pattern which is superimposed on the fringe patterns of the other wavelengths. Contrast is decreased because maxima of some wavelengths begin to fall on top of minima of other wavelengths. A light source may have a sufficient spread of wavelengths such that only a few fringes on either side of the central maxima are visible before the contrast becomes so poor as to make the fringes invisible. This is why an MZI may need to be adjusted for equal optical path lengths. A laser light source is sufficiently monochromatic that it is impossible to locate the equal optical path length condition by the above method; thus, this condition need not be met when the laser is employed.

In use, an MZI would generally be adjusted for equal path lengths at the region S = 0 in Figure 4B. The maximum

value of S attainable with different light sources is discussed by Hauf and Grigull [4, pp. 218-221]. Typically, maximum S values of several tens to several hundreds may be reached (usually larger than maximum S values reached in typical experiments). If an experiment contains end windows that the test beam passes through, windows of equal thickness may need to be interposed in the reference beam to equalize optical path lengths. If the experiment contains water or other liquid between the windows, a similar cavity (but maintained isothermal) will probably have to be placed in the reference beam. This may be necessary even if laser light is employed.

The assumption of ideal interferometry that the light rays remain parallel while traversing the interferometer holds true in real interferometry for most of the optical path but not for the test beam after passing a nonisothermal test section. The test beam with distorted wavefronts as depicted in Figure 4 is fictitious because light rays propagate perpendicularly to their wavefront. Thus, the shape of the wavefronts continues to change after leaving the test section. A real interferometer employs a focusing lens in the combined beam past BS3; the viewing screen (or photographic film) is in an image plane that corresponds to an object plane usually within the test section. The focusing lens essentially recreates in the image plane the wavefront shape that was formed in the test

section [4, p. 243].

It is important that the proper location be chosen for the object plane; the reason for this will be explained with the aid of Figure 6. Nearly all diagrams of Mach-Zehnder interferometers in books and papers show the test beams and reference beams interchanged from that shown in Figure 1 or Figure 4. In order to simplify the drawing, Figure 6 was depicted in this way with the test beam in-line with the combined output beam. A thorough explanation of focusing effects is given by Hauf and Grigull [4, pp. 230-237]; the following explanation comes largely from this reference.

In Figure 6, two light rays, A and B, of a test beam are shown entering from the left. They enter initally parallel to the surface of a heated plate. Ray A enters a region near the plate that is assumed to have a constant refractive index gradient in the y direction (dn/dy = const) and a constant refractive index in the z direction. Ray B enters an undisturbed region beyond the thermal boundary layer. The boundary layer extends only between planes Q and P. A reference beam containing rays E, F, G, and H enters from below and is combined with the test beam by the beam splitter which is shown without its glass carrier. The combined beam enters the focusing lens which refracts the various rays.

For a given interferometer, the location of the

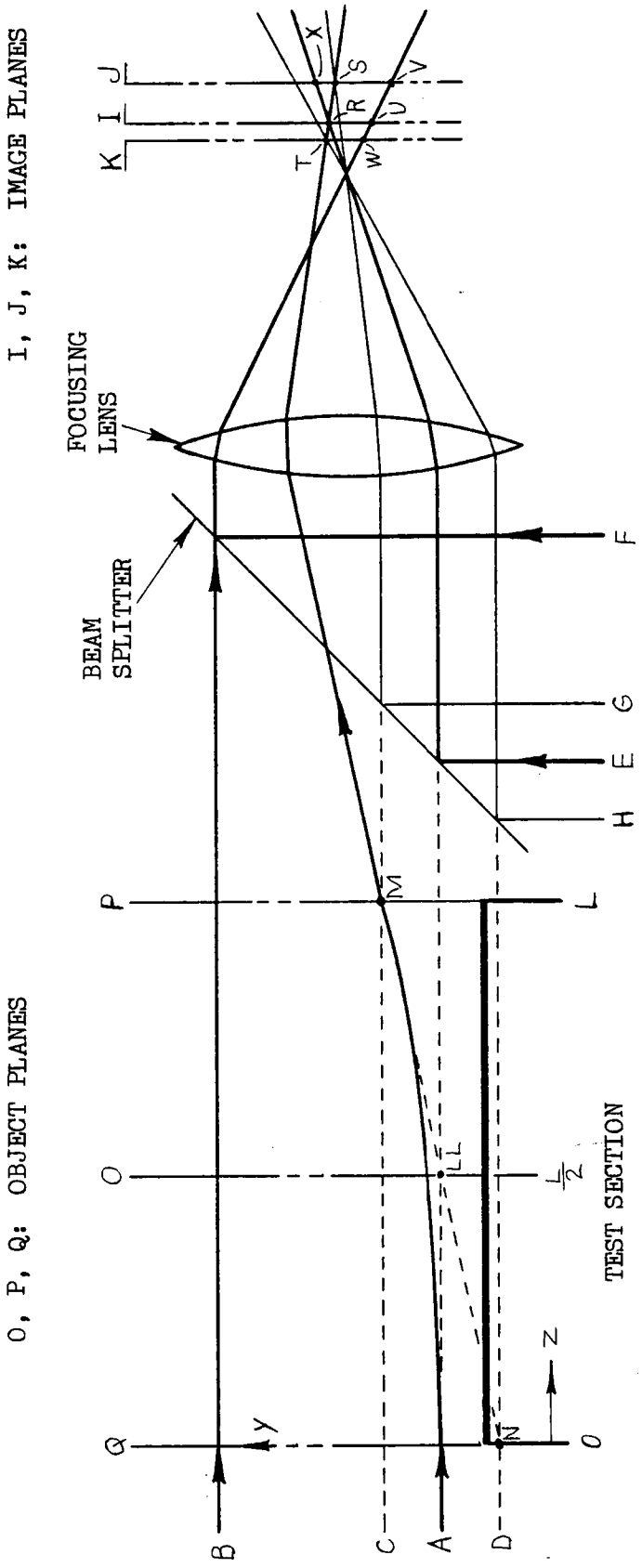


Figure 6. Effect of focusing on image formation.

focusing lens as well as its focal length are probably fixed; thus, an object distance and corresponding object plane is selected by choosing an image distance with corresponding image plane (the object distance must be greater than one focal length for real image formation, which is assumed in this example). In Figure 6, image planes I, J, and K correspond to object planes O, P, and Q, respectively.

As a result of the constant refractive index gradient in the test section (which could be caused by a linear temperature drop), ray A is bent into a parabolic path while within the test section. Beyond point M, ray A follows a linear path except when refracted by the lens. A line tangent to ray A at point M passes through point LL. Point LL is in object plane O which was contrived to be at the center of the test section. Point LL is also on the straight line path ray A would have followed if it had not been deflected by the thermal gradient. A parabolic curve (for ray A) has the property that regardless of the extent of deflection, a line tangent to ray A at point M will pass through point LL. Thus, viewing from points beyond plane P, ray A appears to have originated from point LL. Object plane O was chosen to be in the center of the test section for this reason. After being refracted by the lens, ray A intersects plane I at point R. Since ray A always appears to originate from point LL, it will always pass through

point R since R is in the image plane of point LL.

Ray E is the twin of ray A; that is, they are the two halves of a ray that was split by the first beam splitter. If ray A had not been deflected in the test section, it would have been joined with ray E at the beam splitter as it should have to ensure good fringe contrast. But ray E, after refraction by the lens, intersects point R in image plane I. Thus, rays A and E will always be joined when the object plane is located in the center of the test section.

Point LL, seemingly the source point of ray A, is the same distance from the wall (or distance from ray B) as ray A was upon entering; thus, the phase shift of ray A is indicative of the refractive index value along the line parallel to the wall containing point LL. The interference condition at point R, then, is indicative of the refractive index at point LL and remains so regardless of the extent of ray A's curvature. (The ray curvature in Figure 6 is an exaggeration. Actual curvatures are much smaller.)

Rays B and F, which are also twins, are joined by the beam splitter and intersect plane I at point U. Line segment RU contains the points intersected by all the rays from ray A to ray B. There is a one-to-one correspondence between points on RU and points in object plane O and this correspondence is not affected by differing beam curvatures in the test section (as long as they remain parabolic).

Suppose that plane P is selected as the object plane;

then, plane J is the corresponding image plane. Ray A now appears to originate from point M. Ray A intersects plane J at point S; thus, the interference condition at point S is attributed to the refractive index at point M (along line C) rather than at point LL where it should be (since the ray originated on the line through point LL). Another item, albeit minor, is that ray A now interferes with ray G which is not its twin; this could degrade fringe contrast.

Now suppose that the refractive index gradient is eliminated so that ray A follows a linear path through the test section. It will combine with ray E and intersect plane J at point X, which is a displacement from its former intersection point, S. Thus, there is no consistent point to point correspondence between points in plane J and points in plane P. If plane P were selected as the object plane for a determination of the refractive index profile, the location points measured in plane J would be incorrect. This displacement of image points is referred to as "displacement error."

This same argument could be extended to cover object plane Q and image plane K. Then, ray A would appear to originate from point N with the resulting effects similar to those described above.

Thus, it is clear that if a light ray follows a parabolic path within the boundary layer, the displacement error may be eliminated by proper focusing. However, it is

unlikely that light rays in a real experiment will follow an exact parabola. In order to study a realistic situation, Hauf and Grigull present a detailed description of ray deflections and focusing effects for the case of a laminar forced convection thermal boundary layer [4, pp. 250-262]. They consider three examples; one is an extreme case (reaching 20 fringes per millimeter at the wall) but two other cases are more typical (reaching 2 and 6 fringes per millimeter at the wall).

The location of the object plane for "correct" focusing is defined as that position such that the ray nearest the wall will be focused with no displacement error. For a parabolic ray, this is at 0.5L (as in Figure 6). For the extreme case of a thermal boundary layer, the object plane should be at 0.493L, and for the typical cases, the plane should be at 0.496L. Thus, locating the object plane at 0.5L would cause negligible error. The location of correct focusing as defined above is correct only for the ray nearest the wall and for rays outside of the boundary layer (which are always correctly focused). Rays at intermediate locations suffer a displacement error. There is no single plane for correct focusing of all rays in a boundary layer. The displacement error remains very small for rays up to about 4% of the boundary layer's thickness from the wall; beyond that, the error increases rapidly until it reaches a maximum at a distance of about

25% to 30% of the boundary layer thickness from the wall. For the extreme case, the maximum displacement error is just under 1% of boundary layer thickness; for the typical cases, it is just under 0.02%. From its maximum value, the displacement error decreases steadily to zero at the edge of the boundary layer. Thus, if the object plane is located at the center of the test section, the displacement error for all rays is negligible.

Other researchers have reported a different location for the object plane in order to minimize the displacement error (also called "refraction error"). Mehta and Black [5] have analyzed the refraction error for an MZI having both air and water in a test cavity. They report that the error is eliminated for an object plane at 2L/3 for both the air and water cases. Wilkie and Fisher [3] concur with this value. It is not clear why this value differs from that of Hauf and Grigull. The difference is not very important if the test fluid is air, but an unacceptably large displacement error could be generated if the test fluid is water or some other fluid with a large refractive index.

The effects of the thick glass carrier of the beam splitter in Figure 6 were ignored. In reality, the thick glass of the splitter or of an end window of an enclosed test cavity creates an astigmatic error in the distorted wavefronts of the measuring beam. Hauf and Grigull [4,

pp. 263-264] estimate this error and find it to be several orders of magnitude smaller than errors due to focusing effects; however, a significant change in object plane location may be needed if a test cavity has a thick glass end window [4, p. 235]. The astigmatism due to the thick beam splitter may be entirely eliminated if the MZI employs the optical arrangement of Figure 1 where the measuring beam does not traverse the second beam splitter.

Relationships Between Fringe Shifts and Temperature Changes

The MZI has some utility for qualitative studies such as making visible thermal boundary layers; however, because of the relative ease with which the data may be reduced, its main use is in quantitative studies. To use this instrument, the relationship between fringe shifts and temperature changes will now be developed. This explanation is condensed primarily from that of Hauf and Grigull [4, pp. 287-293].

The optical path length between two points (some physical length apart) is defined as the integral of the refractive index along a path connecting the two points. Thus,

$$\text{Optical Path Length} = \int_1^2 n(z)\, dz \qquad [5]$$

Using the assumption of ideal interferometry that the

refractive index along a ray's path is constant except for a step change upon entering and leaving the test section (boundary layer), then, over a test section of length L and with a refractive index of n_m, the integral in Equation 5 reduces to n_mL. Similarly, the optical path length over the same physical path length, L, but outside the boundary layer where the refractive index is n_r is n_rL. Two light rays, one traversing the boundary layer where $n = n_m$ and the other remaining outside the boundary layer where $n = n_r$, will differ in optical path lengths by an amount $n_rL - n_mL$ (where it will be assumed that $n_m < n_r$ implying that $T_m > T_r$). This optical path length difference may be set equal to some number, S, of a particular wavelength, λ. Thus,

$$n_rL - n_mL = S\lambda \qquad [6]$$

This equation is known as the "interferometer equation of ideal interferometry." S is the number of wavelengths difference between a point on a test beam wavefront and the corresponding point on a reference beam wavefront, as it was defined in Figure 4 (p. 14).

Variations in refractive index are related to variations in density, ρ, by the Lorentz-Lorenz equation:

$$[(n^2 - 1)/\rho(n^2 + 2)] = \text{const} = \bar{r} \qquad [7]$$

The constant, $\bar{r}$, is termed "specific refractivity" and is a

function of the particular substance through which the light is passing and the particular wavelength considered. The refractive index of most gases is near unity (for normal room air it is about 1.0003); for this case, Equation 7 may be simplified to the Gladstone-Dale equation:

$$[2(n - 1)/3\rho] = \bar{r} \qquad [8]$$

Inserting the ideal gas equation of state, $\rho = P/RT$, for ρ in Equation 8, one obtains

$$(n - 1) = \frac{3\bar{r}P}{2RT} \qquad [9]$$

or

$$(n_\infty - 1) = \frac{3\bar{r}P}{2RT_\infty} \qquad [10]$$

Here, n_∞ and T_∞ are the reference conditions where S = 0, and n and T are at some location where the fringe number is S. The pressure, P, is assumed constant; thus, only temperature differences influence fringe shift (for a given experimental arrangement). Inserting these equations into the interferometer equation, one obtains the expression used by Hauf and Grigull [4, p. 293]

$$T = \frac{T_\infty}{1 - aS} \qquad [11]$$

$$a = \frac{2\lambda R T_\infty}{3L\bar{r}P} \qquad [12]$$

Note that the quantity "a" remains constant for a

particular experimental setup, so that the temperature at a point is a function only of the fringe number at that point.

For some experimental studies such as internal cavity flows, there may not be any unaffected region to use as a reference. In this case, the air immediately adjacent to a heated wall of known temperature may be used as the reference. Thus, S is set equal to zero at the wall temperature, T_w, and increases with either increasing or decreasing temperature away from the wall. If the temperature increases away from a wall, then Equations 11 and 12 are used with T_w in place of T_∞ (this is the same case as the temperature increasing from the field reference temperature). If the temperature decreases away from a wall, then the following equations for the temperature result.

$$T = \frac{T_w}{1 + aS} \qquad [13]$$

$$a = \frac{2\lambda R T_w}{3L\bar{r}P} \qquad [14]$$

The End Effect Error

The previously stated assumption that the refractive index (or temperature) exhibits a step change at the ends of the test section is, of course, not usually realistic. If a heated plate is suspended in air, one would expect

that a region of heated air would extend beyond the ends of the plate. This situation is illustrated in Figure 7. Here, the assumption has been made that the isotherms above the plate will follow circular arcs about the plate's corner and down its end. This heated air beyond the end of the plate will introduce a phase shift into a ray of the measuring beam in addition to that shift occuring over the length, L, of the plate. Thus, if the geometric length of the plate is inserted in Equation 12 and Equation 11 is used to calculate the temperature associated with a particular fringe, then the temperature value obtained will be erroneously large.

This "end effect error" may be compensated for in the following way (from Hauf and Grigull [4, pp. 265-266]). At a particular fringe location (as viewed on an interferogram) the actual fringe number or fringe shift (S-number) is known (this is S_{actual}). S_{actual} is comprised of a fringe shift along the length L of the test section (S_{ideal}) plus a fringe shift in the affected region beyond the ends of the test section (S_{end}). Thus,

$$S_{actual} = S_{ideal} + 2\, S_{end} \qquad [15]$$

assuming symmetrical conditions at the ends of the test section. S_{end} may be estimated by making a suitable assumption for the temperature distribution from the end of the test section to the unaffected field.

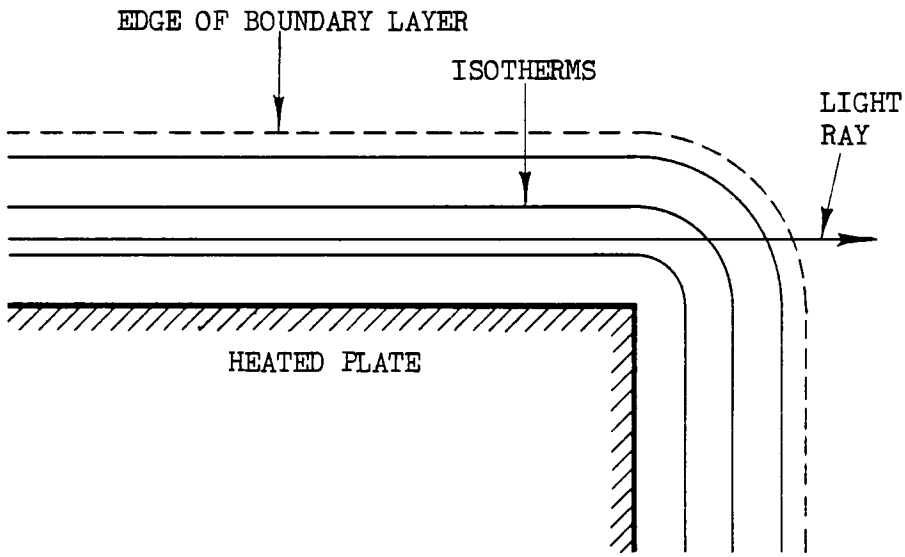


Figure 7. A possible assumption for the end effect about a plate in free air.

Possible assumptions concerning end effects are shown in Figure 8. In the arrangement shown (a heated plate in free air), an isotherm is assumed to extend from above the face of the plate, along a circular arc about the corner, and along the end of the plate. This isotherm is assumed to lie at the same y-location as a fringe (on the image of the plate). A first approximation of this isotherm's temperature is available from Equation 11 with the plate's geometric length inserted in Equation 12. Other isotherms may be drawn in at other fringe locations. The temperature distribution along the "end effect length," that is, the line in Figure 8 that extends from an isotherm location above the end of the plate to the edge of the boundary layer, may be interpolated from the temperatures at the discrete locations where the line would cross the other isotherms. A much easier technique is to simply assume some temperature distribution along this line. The temperature could be assumed to drop linearly from the isotherm temperature to the field temperature at the boundary layer's edge, or, perhaps better, a parabolic distribution could be assumed. Alternatively, the mean temperature between the isotherm and field could be assumed along the line. In any case, the assumed temperature distribution would be inserted in Equation 9 which would be substituted for n in the following equation:

$$S_{end} = n_r \frac{\delta'}{\lambda} - \frac{1}{\lambda} \int_o^{\delta'} n \, dz \qquad [16]$$

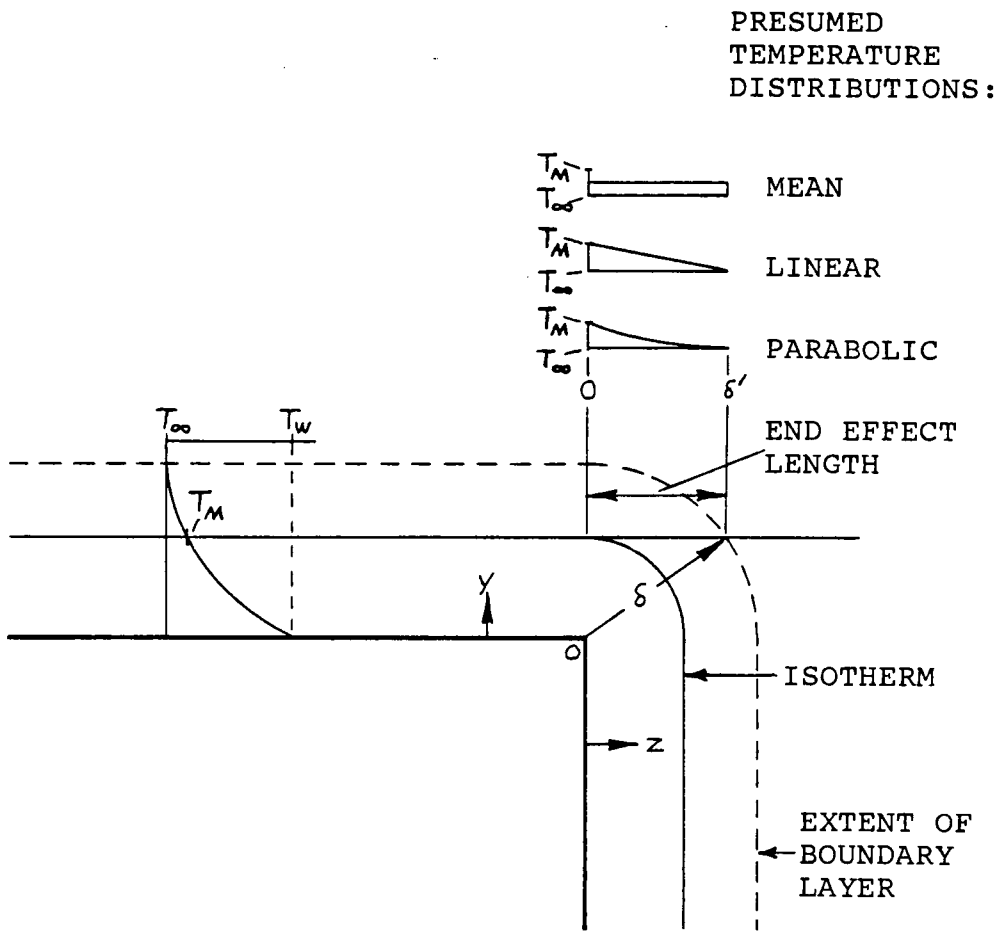


Figure 8. Notation for correction of end effect error.

where δ' is defined as the end effect length. Then, the temperature associated with a fringe would finally be found by inserting S_{ideal} from Equation 15 into Equation 11.

For an example, assume that the temperature distribution follows a parabolic curve as shown in Figure 8. This problem is worked in Appendix A; the resulting end effect correction (for one end) is

$$S_{end} = \frac{3\bar{r}P}{2R\lambda}\sqrt{\delta^2 - y^2}\left[\frac{1}{T_\infty} - \frac{1}{\sqrt{\Delta T\, T_\infty}}\tan^{-1}\frac{\Delta T}{\sqrt{\Delta T\, T_\infty}}\right] \qquad [17]$$

where

$$\Delta T = T(y) - T_\infty$$

If a mean temperature is assumed, the correction is

$$S_{end} = \frac{3\bar{r}P}{R\lambda}\sqrt{\delta^2 - y^2}\left[\frac{T(y)}{T_\infty\left(T(y) + T_\infty\right)}\right] \qquad [18]$$

The boundary layer thickness, δ, should be visible from the fringe locations or displacements on the interferogram.

An alternative technique for the end effect correction is employed by Kennard [6]. Instead of modifying the fringe number as by Equation 15, the plate length in Equation 12 (or 14) is modified by using

$$L = L_o + \Delta L \qquad [19]$$

where L_o is the plate's geometric length and ΔL is a correction obtained by some means.

Kennard considered the case of a heated plate in free

air. For this case, the wall (plate) temperature can be determined two ways: by direct measurement (as by thermocouples) and by counting fringes to the wall from a measured field temperature and calculating from Equation 11. The two wall temperatures can be made equal by the proper choice of ΔL in Equation 19. For a particular example, Kennard found that ΔL should be 5 millimeters (at the wall) where L_o was 103 millimeters and $T_w - T_\infty$ was 118 C^o. The value of ΔL would be expected to decrease from a maximum at the wall to zero at the undisturbed field. Kennard considered four cases for the variation of ΔL with distance, y, from the wall. They were (in millimeters):

1. $\Delta L = 5$
2. $\Delta L = 25 - y^2$
3. $\Delta L = 5 - y$
4. $\Delta L = 0$

A plot of temperature profiles about the heated plate employing the four cases above is presented in Kennard's paper. For the first three cases, the curves virtually coincide; they are just noticably different over their middle regions. For the fourth case (no correction), the profile curve rises above the other curves as the wall is approached; it predicts a wall temperature 5% greater than that measured.

The method just presented has a potential disadvantage in that the calculated temperature profile is forced to

terminate at the measured wall temperature. With the first correction method presented, this is not a requirement, and the discrepancy between the calculated and measured values of the wall temperature (which there surely will be) can serve as a simple check on the accuracy of the interferometric method. Of course, once confidence is gained with the interferometer, the method of Kennard could be employed.

The Refraction Error

In the previous discussion concerning focusing effects, it was explained that a light ray follows a curved path through a non-isothermal test section. The curved path is a different length than the straight line path of ideal interferometry; hence, the light ray following a curved path will undergo a (slightly) different phase shift than the equivalent ideal ray. Hauf and Grigull [4, pp. 246-250] analyzed this situation and derived the following equation

$$S = (n_\infty - n)(L/\lambda) - \Delta S_1 \qquad [20]$$

Thus, the actual fringe shift, S, visible on the interferogram can be analyzed in terms of an ideal fringe shift with an additional correction term, ΔS_1. For a parabolic ray path, the correction is

$$\Delta S_1 = \frac{n_o \lambda L}{12 b^2} \qquad [21]$$

where $n_w < n_o < n$ and b is the fringe spacing (distance between adjacent fringes). This error will be referred to as "refraction error" (not to be confused with what Mehta and Black [5] termed "refraction error"). The use of these end and refraction error corrections will be demonstrated in CHAPTER IV when specific examples are considered.

B. The Mach-Zehnder Interferometer of Aerolab, Inc.

The basic design layout and operating principles of a Mach-Zehnder interferometer have been presented. The details of setup and inital adjustment will now be described for a real interferometer.

General Description

The MZI owned by the Mechanical and Aerospace Engineering Department at the University of Tennessee, Knoxville, is a commercially manufactured instrument purchased from Aerolab Inc. of Laurel, Maryland. The following discussion as well as other interferometer descriptions apply specifically to this instrument.

Figure 9 shows a pictorial representation of the Aerolab interferometer. The basic optical design is the same as that in Figure 1 with the laser light source of Figure 5 added to it. A difference is that the Aerolab interferometer utilizes parabolic mirrors for collimation

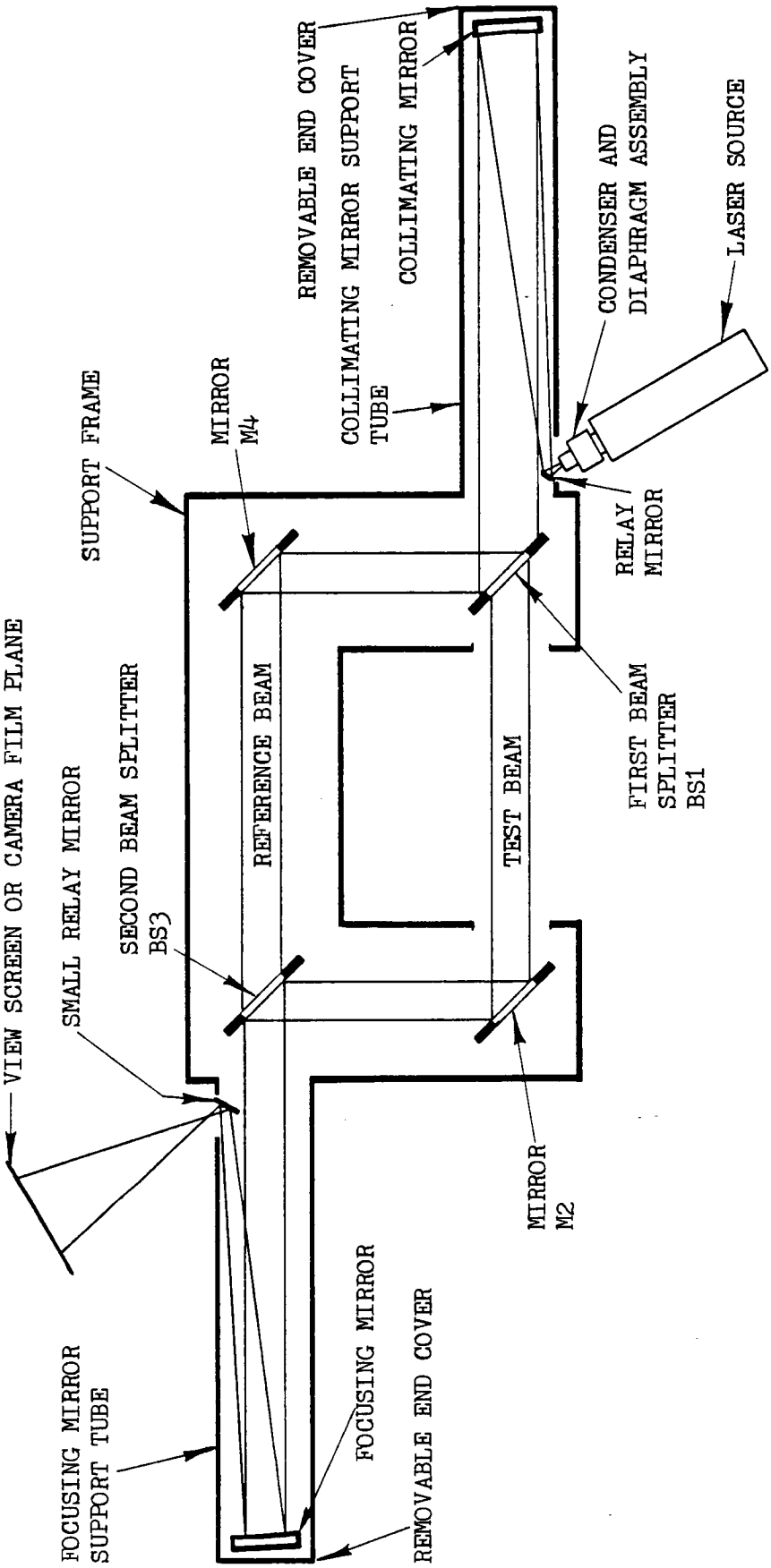


Figure 9. Layout of Aerolab, Inc. Mach-Zehnder interferometer.

and focusing instead of lenses. There is no difference, in principle, between lenses or mirrors (for present purposes); only the optical layout must be changed. The major optical elements (beam splitters and flat or curved mirrors) of the interferometer are 6 inches in diameter and about one inch thick. Thus, since the splitters are at a 45° angle to the light beam, the test and reference beams are of elliptical shape with about a 6 inch major axis. Some light is lost around the edges of the beam due to the thickness of the splitters. The major axis of the ellipse is usually vertical (that is, the cross-section of the interferometer shown in Figure 9 usually lies in a horizontal plane); however, the frame of the Aerolab interferometer may be rotated 90° so that (say) a horizontal wind tunnel could extend through the gap in the "C" frame.

The interferometer was supplied with two light sources: a mercury arc source and a He-Ne laser source. The mercury or laser sources mount on an L-shaped rod that would be underneath the laser source shown in Figure 9; only one source at a time can be mounted and adjusted for use.

The Mercury Arc Light Source

The optical arrangement of the real mercury source is very similar to the schematic of Figure 5. The lamp is

held within a metal housing which mounts on the L-rod. A pair of condenser lenses is mounted within a tube which can slide for focusing in or out of a hole in the housing. As originally supplied, no provision was made for having a diaphragm in the optical system; however, a diaphragm holder was designed and partially constructed. It consists of a round rod attached to the lamp housing with an attachment on the rod that holds the diaphragms. The location of the aperture is adjustable in all directions. The diaphragms are aluminum discs an inch in diameter and are interchangable with a different aperture size to each disk. For inital trials, apertures of about 2, 1, and 0.5 millimeter diameter were intended to be made and used. Another rod on the lamp housing supports the filter which is interposed between the condenser and the aperture. The mercury light source with the diaphragm holder and the filter in place is shown in Figure 10.

To set up the mercury source for use, the lamp housing is first attached to (slid onto) the L-rod and clamped at any convenient location. For inital trials, at least, the tube holding the condensing lenses should protrude about 1 to 1.5 inches from the lamp housing. The mercury lamp should be started (consult the instruction sheet provided by Aerolab regarding starting the lamp) and the diaphragm moved back and forth until the aperture is at the point of brightest focus. A collar on the round rod allows the

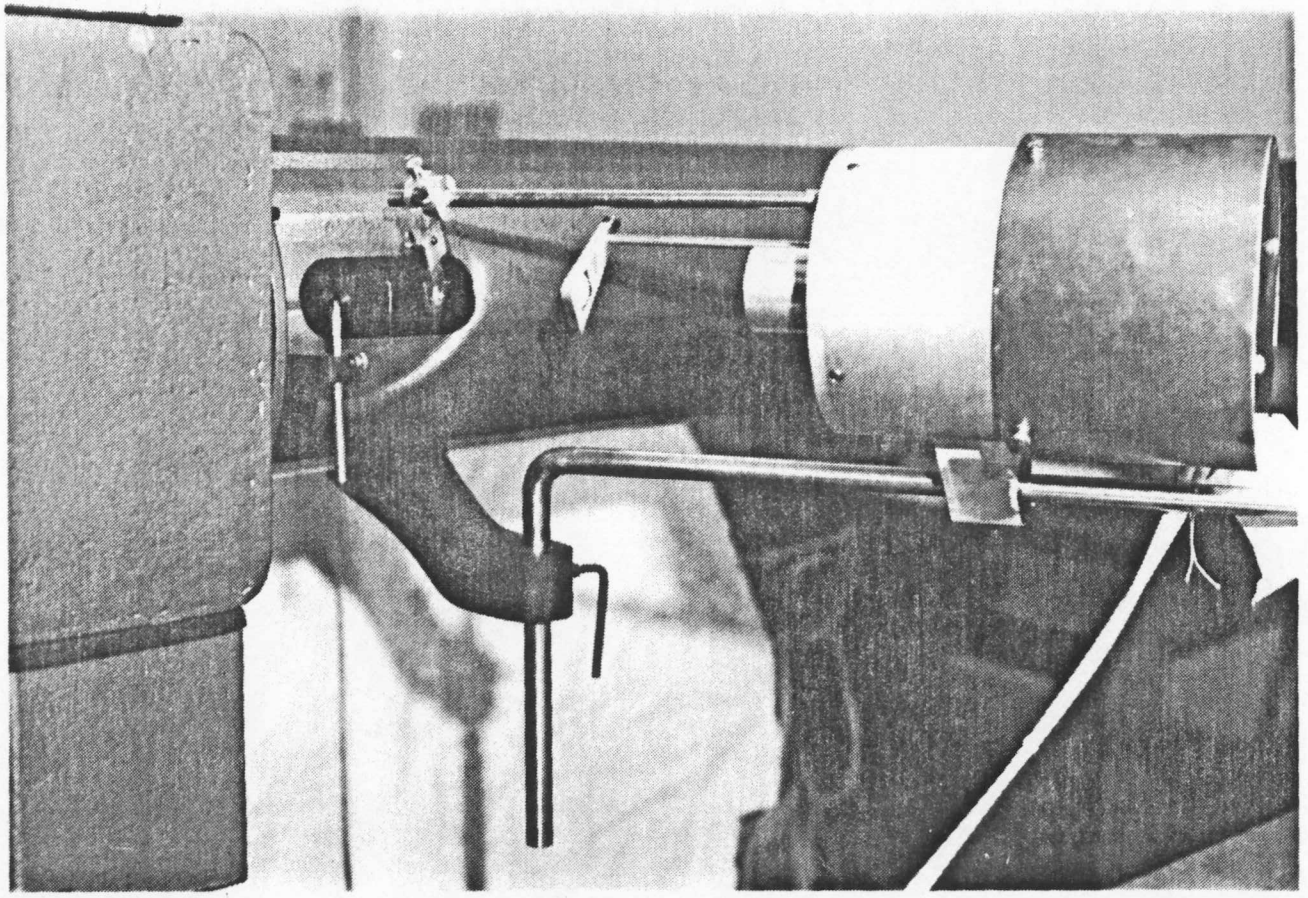


Figure 10. The mercury arc light source mounted on the interferometer.

diaphragm holder to rotate without slipping along the rod. The filter probably should be in place while focusing, since it affects (though slightly) the location of the focal point; it can be removed to let more light pass for further adjustments.

The Helium-Neon Laser Light Source

The laser light source provided consists of a 5 milliwatt (nominal light power) He-Ne laser with a condenser and diaphragm holder attachment screwed onto the laser's accessory mount. In Figure 11, the laser and diaphragm holder assembly are shown mounted on the L-rod and adjusted for use. As mentioned previously, the diaphragm, when used with the laser, has a very small aperture and serves primarily as a "spatial filter," that is, a device to make more uniform the brightness of the expanded laser beam. Without the aperture, the expanded laser beam would suffer severe brightness variations over its area due to the presence of dust and dirt particles on the condenser lens surfaces (the dust and dirt particles are large compared to the size of the unexpanded laser beam). The small aperture serves to "smooth out" the brightness of the beam. The adjustment of the aperture to the focus of the condenser is rather delicate; the process will be explained with the aid of Figure 12.

In Figure 12, certain parts of the diaphragm holder

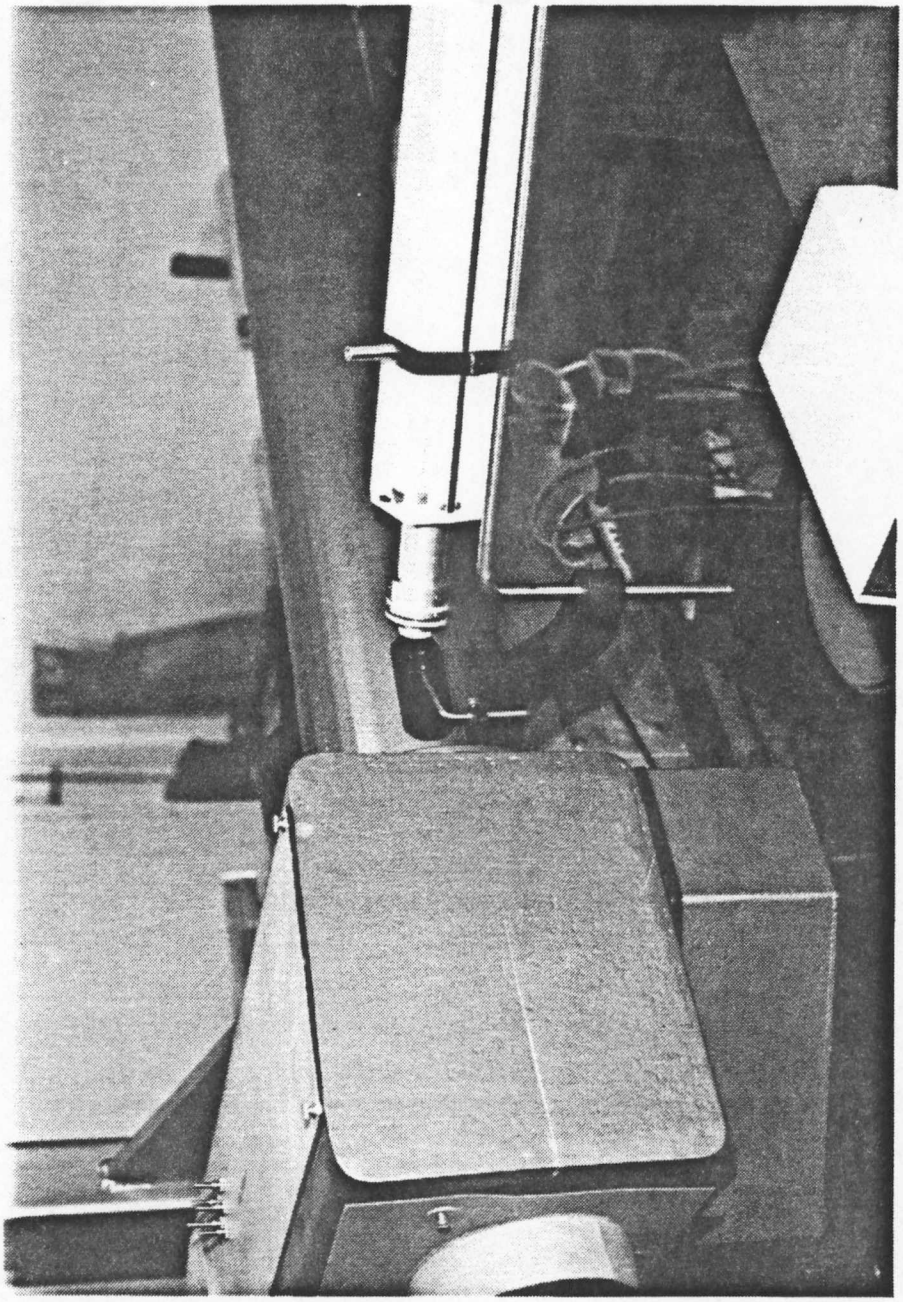


Figure 11. The laser light source mounted on the interferometer.

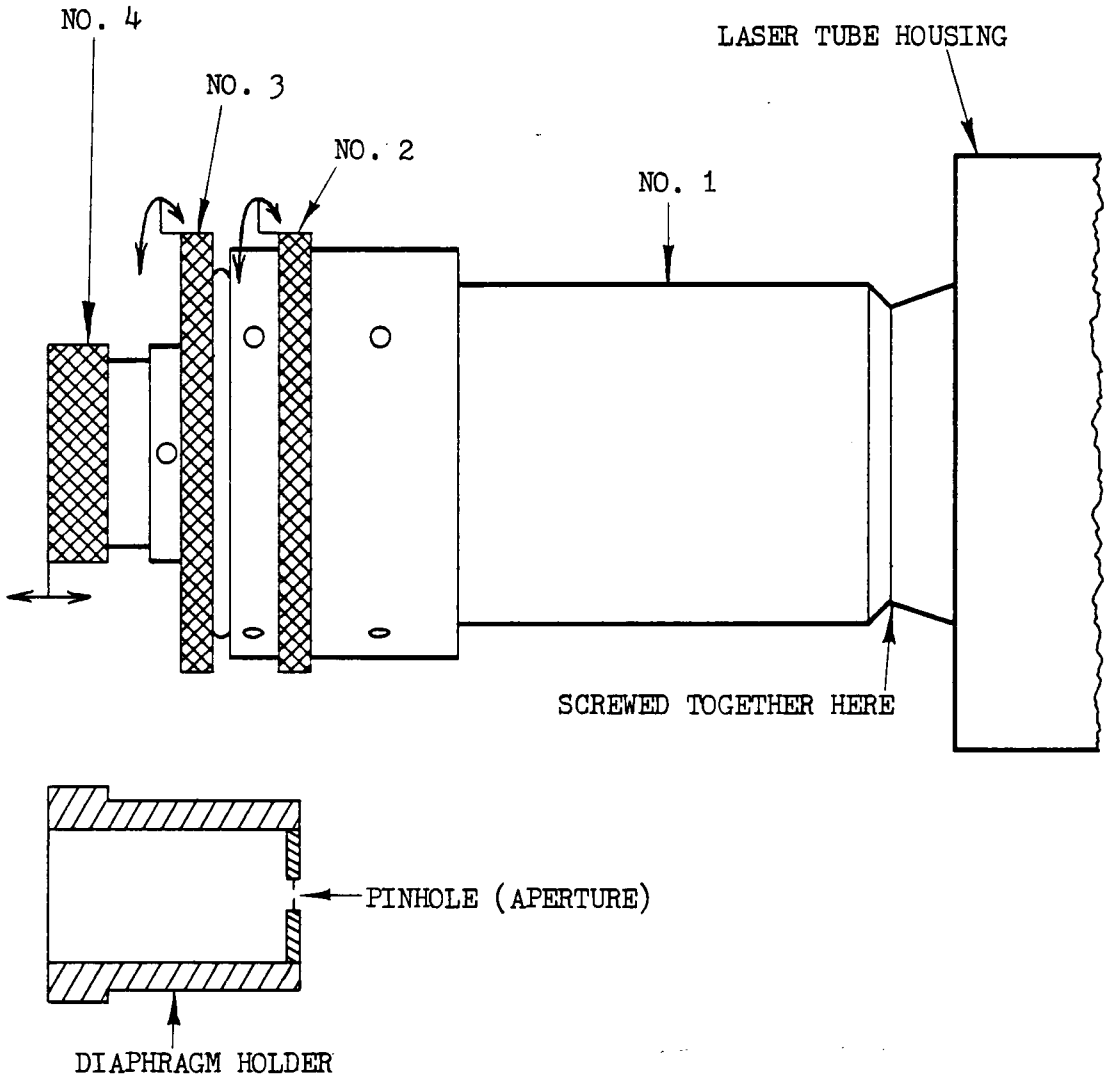


Figure 12. Condenser and diaphragm assembly for the laser light source.

assembly are numbered for clarity of explanation. Part No. 1, the main body piece, screws into the accessory mount of the laser. Part No. 2 is free to rotate; when No. 2 is rotated the higher numbered parts rotate with it. Part No. 3 can be rotated relative to No. 2. Part No. 4 is for in-and-out (focus) adjustment.

The aperture, or pinhole, has a diameter of 10 microns (10^{-5} meter) and is carried by the diaphragm holder, No. 4. This pinhole is too small to be seen by the naked eye and could, thus, easily be obscured by a particle of dirt. Careful attention to cleanliness is, therefore, in order when dealing with this optical assembly. The condenser is a microscope eyepiece; its location is not adjustable.

Certain parts of the diaphragm holder assembly were machined so that the parts would be (slightly) eccentric with respect ot each other. By rotating either part No. 2 or part No. 3, the pinhole will trace a circular path. By rotating both of the parts, the pinhole can be brought to any point within a circular area. This movement, plus the in-and-out motion of No. 4, is used to bring the pinhole to the focus of the condenser.

In practice, the laser assembly should be set up on a table with a white screen about a foot from the diaphragm holder assembly. With the room blacked out, the screen can be examined for light emitted from the pinhole. Adjustment is mainly a trial-and-error procedure. Part No. 2 may be

rotated through 360°; if no light is seen, part No. 3 may be rotated a small amount relative to No. 2 and No. 2 rotated again. This process may be repeated; if no light is seen, No. 4 should be moved in or out and the process started over at the beginning. Once a spot of light emission is found, the various parts may be oscillated back and forth to make the spot as bright as possible. The focus adjustment of No. 4 is particularly sensitive and troublesome.

The first reasonably bright spot found will, almost invariably, not be the brightest spot attainable, though it may be adequate. Occasionally, an extra bright spot will be seen to flash by on the screen; a fair amount of time and tinkering will be needed to capture one of these bright spots. Properly, a photodetector of some type should be used to give an objective measure of the brightness of the light; this possibility has not been investigated. Once the pinhole is adjusted, care should be taken that the diaphragm assembly is not touched or otherwise disturbed; however, it should be covered to exclude dust. The six setscrews in part No. 2 hold the parts together; the tightness of the screws sets the freedom of rotation of the parts.

Alignment of the Aerolab MZI

Adjustment of the two light sources has been

described; the following procedures are basically the same regardless of which source is utilized.

The light radiating from the aperture must be reflected off of the relay mirror and onto the collimating mirror. Two relay mirrors (only one of which is used at a time) are provided for the light source side of the MZI (another relay mirror is on the output side); these mirrors are mounted on small L-shaped rods. One, which has a horizontal arm about 3.75 inches long, must be used with the laser source; the other, with an arm about 2 inches long, can be used with the mercury source. The mirror with the 2 inch arm cannot be used with the laser. Its shorter arm places it so far from the collimating mirror that the laser's diaphragm cannot be brought close enough to this mirror to reach the focal point and achieve collimation. The mercury source, since it was initally supplied without a diaphragm, can use a relay mirror farther from the collimating mirror. The mirror with the longer arm can probably work with either light source.

The relay mirror selected should be vertically centered in the slot in the collimating mirror's support tube. The mirror must be placed far enough inside the tube so that the light reflected from it will not be blocked by the edge of the tube (the end of the slot), but not so far inside that it blocks much of the light reflected toward the beam splitter from the collimating mirror. Some

blockage of the beam will not hurt, since the sides of the beam will be blocked by the beam splitter anyway.

The relay mirror should be turned to an angle so that the light from the aperture will strike the collimating mirror. The light source should then be positioned so that the cone of light is centered upon the relay mirror. It is found convenient to have the L-rod supporting the light source at roughly 70° from the support tube. The location where the light strikes the relay mirror can be seen by looking closely at the mirror. A faint patch of light can be seen on the mirror's surface. The light source can then be given a fine adjustment so that the light centrally strikes the mirror.

Next, the relay mirror must be adjusted so that the cone of light is centered upon the collimating mirror. To do this, a piece of paper or a screen should be set in the MZI's optical path just before the first beam splitter. Now, either the relay mirror or the collimating mirror or both must be adjusted to show a circle of light on this screen. The relay mirror is adjusted by manual rotation. The collimating mirror is in a mount that is adjusted by turning any of three nuts that are available when the tube's end cover is removed. The cone of light from the aperture (of either light source) is not totally uniform in brightness; it is brightest at the center with a decrease toward the edge. To center the cone of light on the

collimating mirror, the relay mirror should be adjusted until the brightest part of the circle of light on the screen is at its center; that is, the circle of light should be symmetrical in brightness.

The major optical elements of the interferometer should already be in correct primary alignment; that is, the light path through the instrument should already be established (this was done at the factory). Fine adjustments are another consideration to be covered later. With the previously mentioned screen removed from the light path, the light, if adjusted to hit the first beam splitter, should pass through all the elements to the focusing mirror. Since there will be a small amount of misalignment of the elements (the light beam will not hit them all symmetrically), the collimating mirror should be fine-adjusted so that the (elliptical) beam strikes the focusing mirror squarely (since the focusing mirror is the element most distant from the collimating mirror). Some astigmatism may be avoided if the center of the beam reflects from the center of the focusing mirror. To achieve this adjustment, the end cover on the focusing mirror support tube should be removed and a white screen placed on the wall of the room where light missing the mirror can exit the tube and strike the screen. By fine adjusting the collimating mirror, the beam may be made to miss the focusing mirror and show up on the screen. The

collimating mirror should be adjusted back-and-forth until the beam seems centered on the focusing mirror. The beam should then appear to be approximately centered on the other optical elements.

Next, the light beam must be collimated. Experience has shown that the best test for collimation is to interpose in the light beam two fine parallel wires whose separation distance has been carefully measured. Then, the separation of the wire's shadows is measured as far down the optical path as possible, and the aperture adjusted toward or away from the collimating mirror until the shadow's separation equals the wire's separation. A collimation tool consisting of a frame of heavy steel wire forming a 7.5 inch square was constructed and is shown in Figure 13. It holds two wires stretched across two of the sides plus a third wire across the other two sides. The wires, which have a diameter of 0.0063 inch, can be slid to different locations along the sides of the tool. The wires are attached to small springs to maintain tension. Two "fingers" on the tool's frame allow it to be suspended vertically from a top opening of the interferometer's frame (with the cover removed) as shown in Figure 14. In practice, the two parallel wires must first be located so that they are in the light beam when the tool is hung on the interferometer; they must also be adjusted to be approximately parallel and to be at the selected

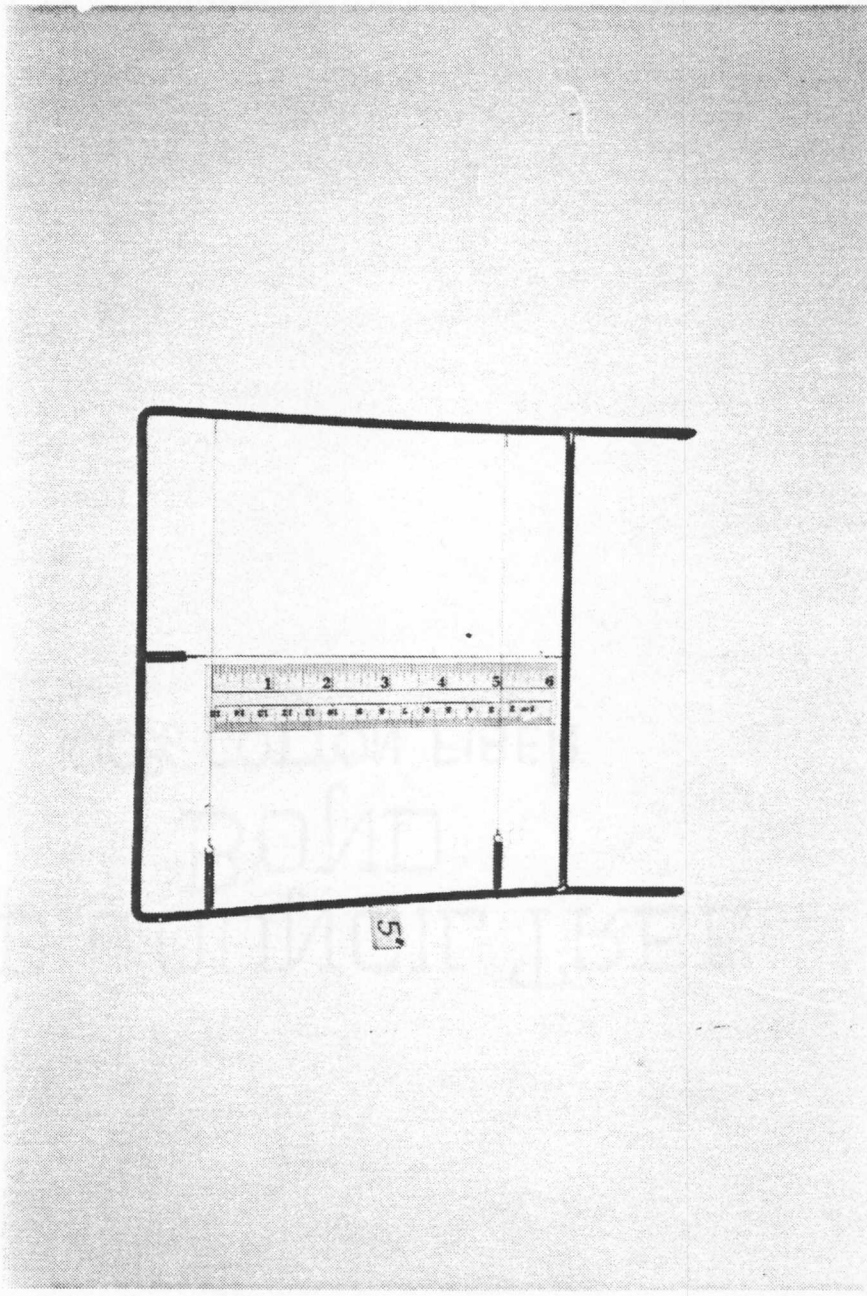


Figure 13. The collimation tool used with the interferometer.

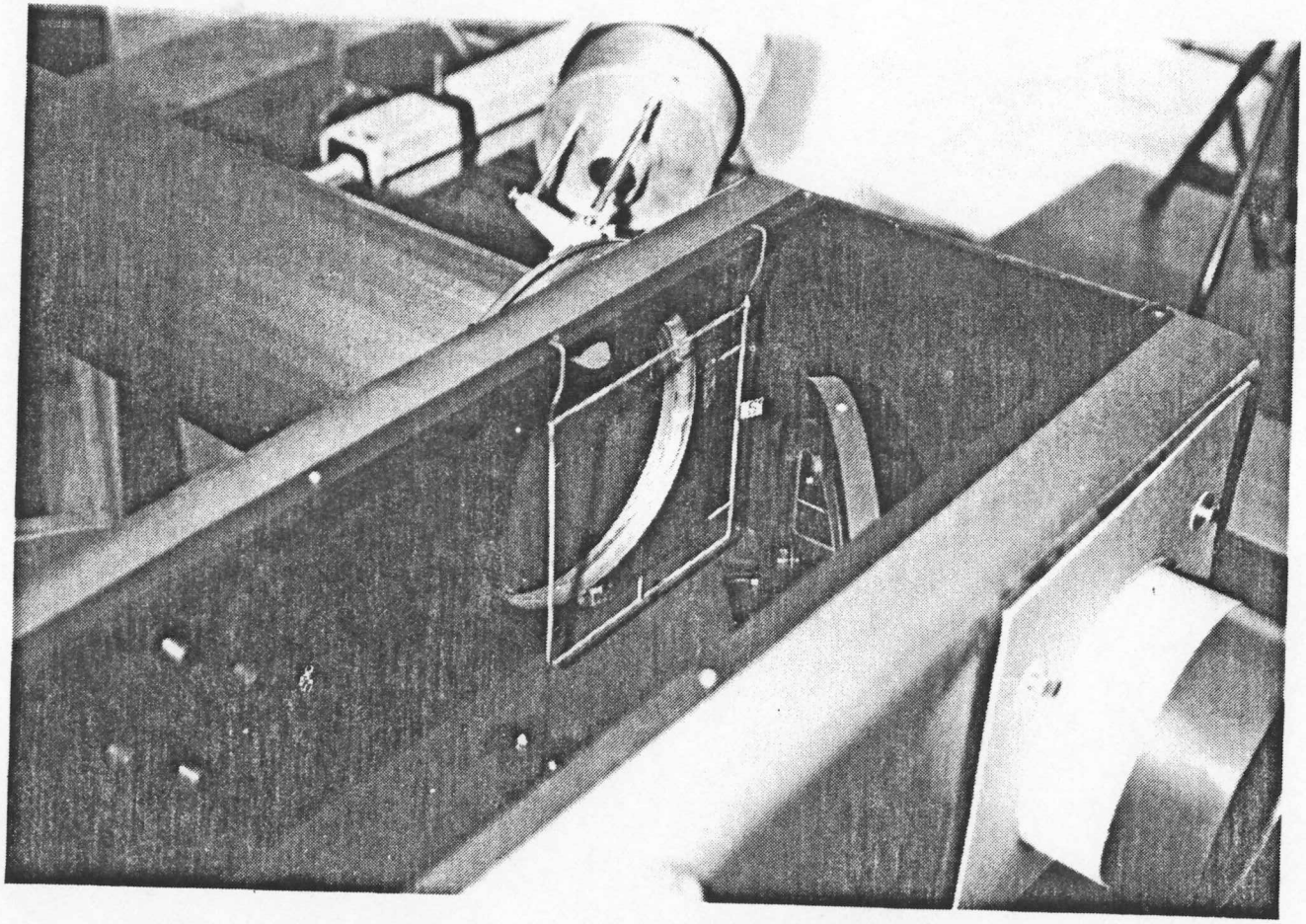


Figure 14. The collimation tool in use suspended inside the interferometer.

separation. A larger distance, such as 4 or 5 inches, will give greater sensitivity than smaller separations. The separation should be measured at the location where the third wire crosses the other two, as shown by the scale in Figure 13. This way, the two wires do not have to be made precisely parallel. A convenient way to measure the separation is to use a transparent plastic scale held just above the wires. The ends of the wires can be (carefully) slid back and forth to achieve the desired separation.

The collimation tool is hung from the interferometer's frame in the light path just before the first beam splitter. This is the closest a tool can be placed to the collimation mirror without it being inside the support tube where it would be hard to adjust. The wires cast shadows that follow the light path. To measure the shadow's separation at the greatest distance down the optical path, the focusing mirror must be removed thus allowing the light beam to fall on a screen (a card) attached to the wall of the room. The mirror mount should be marked so it can be replaced in its original orientation. The mount does not fit the support tube well (or vice versa) so some difficulty will be experienced in its removal and replacement. If an outline of the beam is drawn on the screen, then, after collimation, the beam can be replaced to its original adjustment (centered on the focusing mirror). One of the beam halves, either test or reference,

should be blocked during collimation, since the two halves, most certainly, will not be exactly superimposed at the screen.

The collimation tool should be set so the wires' shadows are centered in the beam's image on the screen. The shadows will be easily visible in a totally darkened room. The shadows will not be sharp; they will be fuzzy since there are no image-forming elements in the light path. Especially when the laser source is used, the shadows will consist of a relatively wide central dark region bordered by alternate bright and dim lines. One method of determining separation is to mark with a pencil on the screen the upper boundary and lower boundary of each central dark shadow (where the dark and bright merge near the crossing of the third wire). Next, with the room lights on, the separation of the upper bounds and the lower bounds for each shadow should be measured, preferably with the same scale used to set the wires. This way, an average separation can be obtained. Alternatively, a card with two parallel lines drawn on it at the set separation, or the scale itself, can be held against the wall in the beam's path, and the drawn lines compared with the shadow's separation. In any case, if the shadow's separation is greater than that of the wires, then the aperture of the light source is inside the focus of the collimator, and the light source must be moved farther away (along the optical

path) from the collimating mirror (this can be done by sliding the light source outward on the L-shaped rod). Likewise, if the separation is too small, then the aperture is outside the focus and must be moved closer to the mirror. As the light source is moved in or out, care should be taken to keep the light path maintained as it was before; that is, the beam should be kept symmetrically illuminated and centered on the focusing mirror's location. The process of checking the separation and adjusting the light source should be continued until satisfactory agreement is reached. It is not known just how accurate collimation needs to be; this process should be carried out until there is no readily detectable difference between shadow separation and wire separation.

Another method sometimes reported for checking collimation is to hold a card in the light path with a circle drawn on it the same diameter as the collimating lens or mirror. The beam is collimated if the circle of light just fills the drawn circle. Experience has shown that this method is not suitable for the Aerolab MZI except as a rough check. In Appendix B, this collimation technique is further described and is compared to the previously described technique.

With collimation achieved, the focusing mirror may be replaced and, if necessary, the light beam finally centered upon it. Now, the focusing mirror must reflect a cone of

light to the second relay mirror and from there be projected away from the interferometer to the camera or viewing screen. Adjusting the mirror to get the cone of light to hit the relay mirror might be troublesome; one has to look inside the support tube or hold a card partially in the optical path in order to find the spot of light from the mirror. Once the reflection is found, it must be centered on the relay mirror which should be turned so that the beam is projected out of the interferometer at about a 70^{o} to 90^{o} angle from the support tube. The location where the spot of light hits the mirror can, as mentioned previously, be seen by looking closely at the mirror's surface. This relay mirror is larger than the others because some light rays, in traversing a nonisothermal test section, are deviated from the path of the collimated light; the mirror must be larger in order to capture these deflected rays.

It is convenient to have the output beam parallel to the floor. This may be done by measuring the height above the floor of the spot of light on the relay mirror. This height may be marked on the wall or on a screen; the relay mirror may be tilted until the centerline of the light beam matches this line.

The interferometer is now aligned and its output may be viewed on a screen or recorded photographically.

Viewing and Recording the Output of the Interferometer

Originally provided with the interferometer was a viewing screen supported by a heavy adjustable stand plus a 4X5 view-style camera minus its lens, lens board, and bellows. The viewing screen is made of frosted plastic. An image on it is best seen in rear projection; that is, one should look at the screen on the side opposite from where the light is striking. The stand that supports the screen allows for vertical and tilt adjustments. This viewing screen and its stand are shown in Figure 15. The camera was apparently intended to be supported by a separate tripod, not provided by Aerolab. An adapter was designed and constructed to allow the camera to be supported by the screen's stand. The camera attaches to a slider that mates with a dovetail track on the adapter; this allows a linear travel of about 9 inches for focusing. The massive stand provides more rigidity than a regular camera tripod. Figure 16 shows the camera mounted on its stand.

The camera provided with the MZI, a Speed Graphic, was apparently chosen because of its focal plane shutter, that is, a shutter adjacent to the film plane and with an opening of the same size as the film. The lens and lens board were removed from the camera to keep from blocking the cone of light from the focusing mirror (which takes the

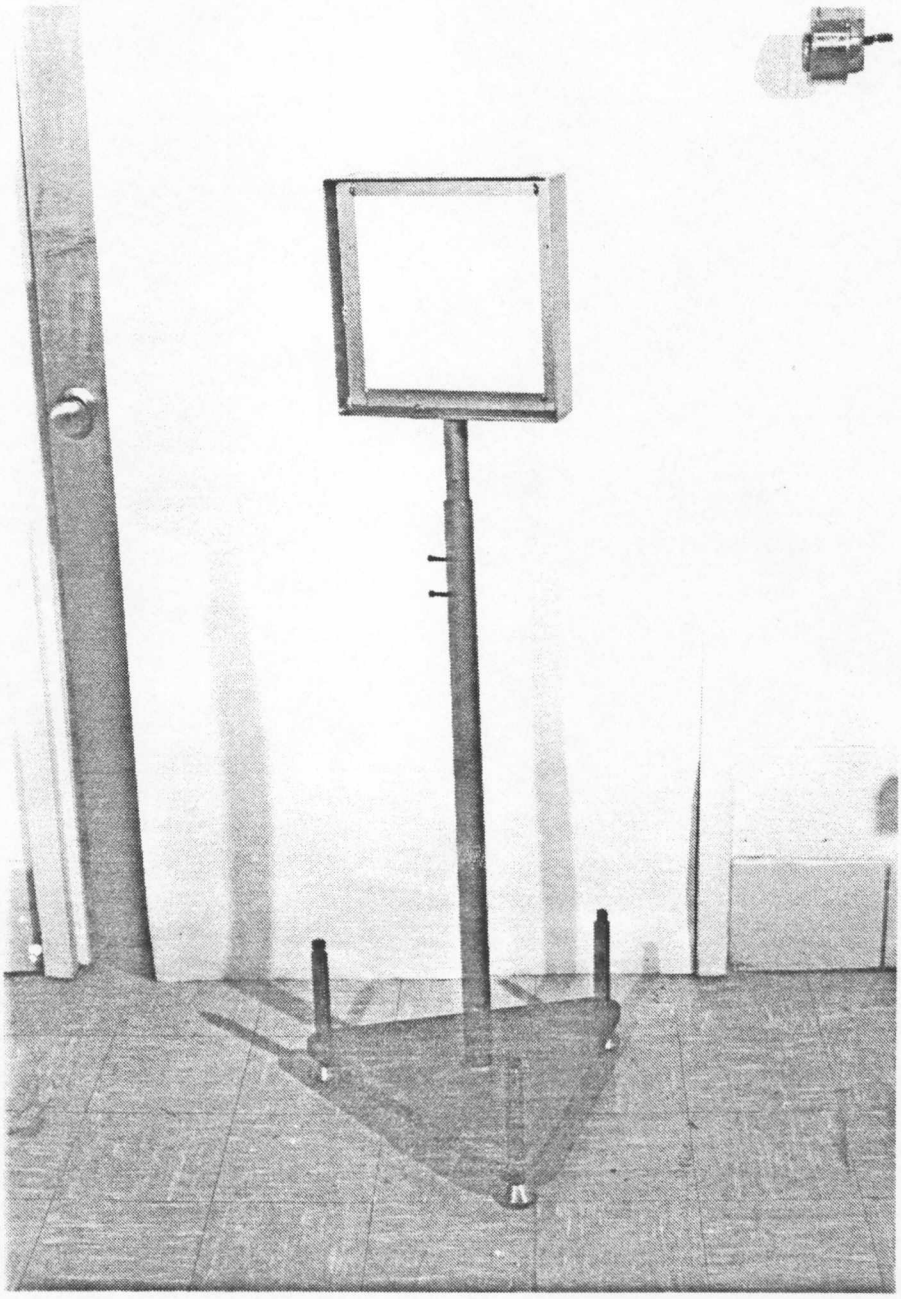


Figure 15. The viewing screen and its stand used with the interferometer.

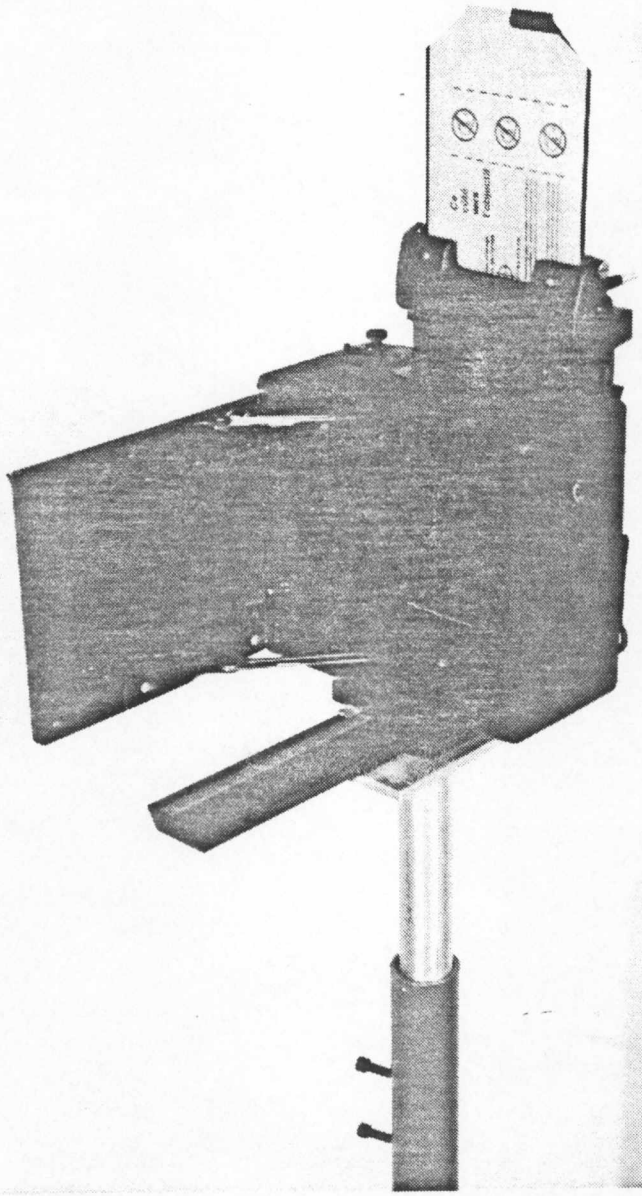


Figure 16. The camera and its focusing track on the stand as used with the interferometer.

place of the camera's lens). The camera accepts standard plates for 4 inch by 5 inch sheet film; an adapter for using Polaroid (self developing) sheet film was provided, thus obviating the need for darkroom services. The camera's shutter has several self timed settings plus a "Time" setting. Exposure is set by two knobs on the camera's side: a larger wing-shaped one and a smaller knurled one. The shutter curtain contains openings of various widths, selected by the larger knob, that slip by the film, thus exposing it. The smaller knob sets the speed at which the curtain travels. The "Time" setting allows the curtain to be held open indefinitely; it is timed by the operator. Exposure times needed are generally determined by trial-and-error.

A ground glass screen on the camera's back is used to view images for focusing (with the shutter held open on "Time"). This screen may be used in place of the other viewing screen; it gives a sharper image due to the finer grain of its ground glass.

The camera's film plane should be adjusted to be perpendicular to the centerline of the output light cone. To assist this adjustment, an alignment tool (labeled "Camera Alignment Tool") was designed. This tool attaches simply by friction fit to the "apron," or the part where the original lens board attached, of the camera as shown in Figure 17. In place, this tool, of thin sheet metal, looks

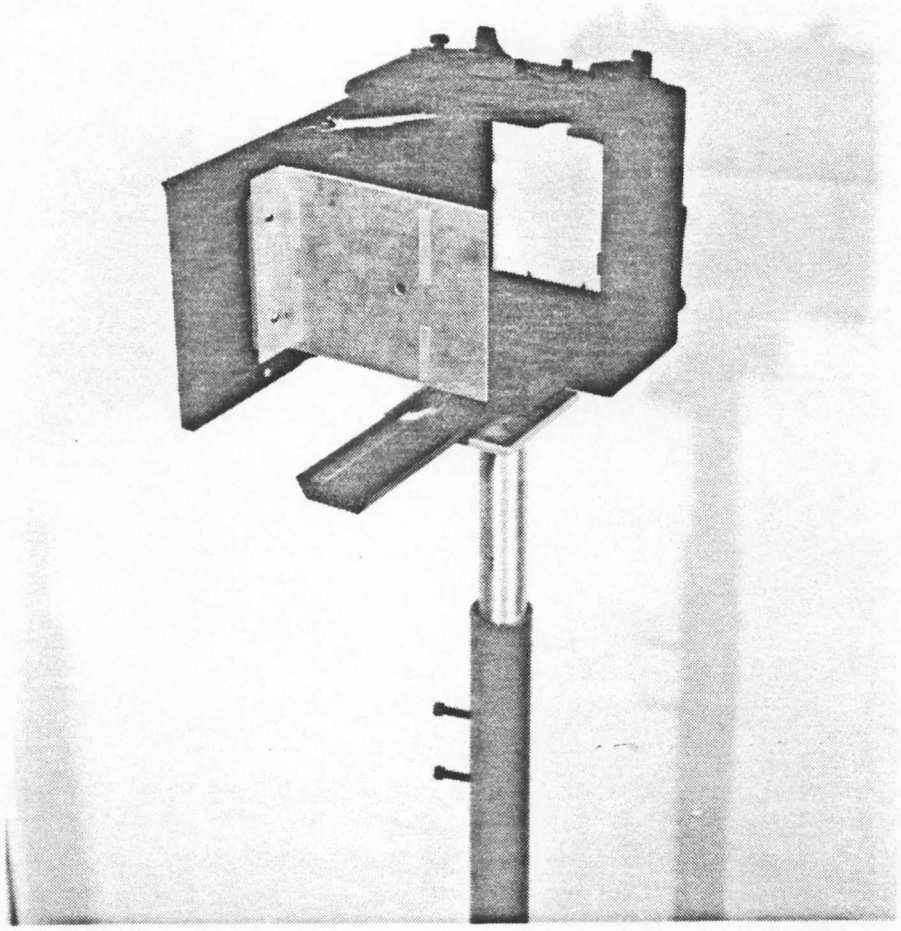


Figure 17. The "camera alignment tool" mounted on the apron of the camera.

much like a lens board standing in front of the film holder and shutter assembly.

In aligning the camera to the beam, the camera is first adjusted so that the elliptical image of the beam is symmetrically centered on the ground glass. An "X" mark has been drawn on the camera's ground glass to mark its center. With the image centered, the centerline of the beam should be hitting the penciled "X". The alignment tool centains a hole that was located on a line passed through the "X" and perpendicular to the ground glass. Thus, with the alignment tool in place on the camera, the camera stand is tilted or twisted until the light passing through the hole in the tool is centered on the "X" on the ground glass. After adjusting the tilt, it will be necessary to remove the tool and recenter the image again. This process should be repeated until the camera is in good alignment to the beam.

As discussed previously, the camera (film plane) must be focused to an object plane usually within the test section. In addition, it is also necessary to know the scale factor or magnification of the the image. (Magnification equals the ratio of an image distance to the corresponding object distance.) These two operations can be combined by placing an object such as a transparent plastic scale in the test section at the appropriate object plane, moving the camera in and out along the output light

beam until the scale appears in focus, photographing the scale, and measuring the scale's image and, if necessary, the scale itself to yield the magnification. The use of a transparent scale is recommended since it allows use of the interferometer's light source for illumination. An opaque object requires front lighting which, experience has shown, must be very intense to yield an image of adequate brightness. With an intense light source, the entire laboratory will be brightly lit, which would fog the photographic film if a photograph was desired. Even the relatively dim laser source produces a conveniently bright image for focusing. The interferometer's reference beam should be blocked during focusing since interference effects tend to blur the image.

When focusing the camera, a magnifier should be used to view the image. A very convenient magnifier to use is the one provided with the laser anemometer system. The magnifier is designed to be placed in contact with the object to be viewed, plus it has its own focus adjustment. In use, the magnifier should be held against the ground glass screen and initally focused on the pencil marks on the screen. Now, the image of the scale may be viewed, and the camera adjusted until the markings appear sharpest. It was found convenient to make very fine scratches on the measuring scale and to focus on these. The dovetail that the camera slides on has a graduated scale; several

focusing trials should be made and the resulting scale readings recorded. The average reading of these trials should be used as the correct focus location.

Focusing results in considerable eyestrain. After a short time, it may be found that the image appears blurred at all locations. If this occurs, one should temporarily abandon the attempt; otherwise, the wrong focusing location may be selected.

With focusing completed, a photograph may be taken of the scale's image. A measuring microscope was purchased for use in the Natural Convection Laboratory for measuring photographic images. The photograph may be examined under the microscope, and the distance between two selected graduations (preferrably a relatively long distance apart) on the image may be measured. Since an inexpensive plastic scale is used, the scale itself should be measured for the actual distance between the corresponding graduations. Thus, the magnification is obtained from the ratio of these two distances.

Note that although alignment of the camera to the output beam was discussed before focusing, the camera should be rough focused first, so that the camera stand will be in the correct general location before alignment. After alignment, it may be carefully focused.

Establishment and Alignment of the Desired Fringe Pattern

The output beam of the interferometer is composed of two superimposed beams. The appearance (or nonappearance) of fringes in the image, however, has not been mentioned since they do not influence the previously discussed adjustments. The fringe pattern, of course, contains the desired information concerning the test section; thus, one must initally locate and adjust the fringes to some particular state before beginning an experiment.

The wedge fringe and infinite fringe conditions have previously been described. These conditions are achieved by the appropriate orientation of the beam splitters or flat mirrors. One or another of the optical elements must be rotated about vertical or horizontal axes to achieve the infinite fringe condition or to form wedge fringes of some particular spacing and orientation. In addition, one element must be translated to achieve the required equal optical path length when using the mercury light source. The Aerolab interferometer meets these needs by supporting the splitters or flats in micrometer adjusted gimbal mounts. Two of the mounts, for elements M2 and BS3 as labeled in Figure 1, have electric motor drives and are controlled from a console that can be located near the viewing screen, thus greatly facilitating the instrument's adjustment by allowing the operator to view and adjust

fringes simultaneously. The other two mounts, for elements BS1 and M4, are not normally disturbed from their factory set adjustments.

Operation of the control console should be more or less self explanatory from the diagram and labels on it. It has switches for controlling the pitch and yaw (rotation about horizontal and vertical axes) of M2 and BS3, plus there is a switch for the translation of BS3. The control circuit contains a rheostat which controls the voltage fed to a servo motor when a switch is pressed. This allows the optical elements to be moved relatively rapidly when a gross change is needed and moved slowly when a fine adjustment is desired.

Returning to the matter of locating fringes, if the laser light source is being used, then fringes should be visible in the image, since the interferometer has previously been used for experiments and the fringe pattern should be unchanged from the last setting. If no fringes are visible, the fringes may be so fine (the spacing so close) that individual bright and dark fringes are invisible and the image appears continuously illuminated. This was the case when the interferometer was initally tried after receipt from the factory. Checking the image with a magnifier may reveal the fringes.

If fringes are visible, they may be adjusted as desired using the pitch or yaw controls. Depending on

whether the fringes are closer to vertical or closer to horizontal, one of the controls, either pitch or yaw, will affect the fringe spacing while the other control will affect fringe orientation (i.e., angle from vertical or other reference). As a change in fringe orientation approaches 90°, the effect of the pitch and yaw controls on the fringes becomes interchanged; that is, if the pitch control formerly affected fringe spacing, it will increasingly affect fringe orientation as the orientation change approaches 90°. It is just as effective to use trial-and-error in adjusting the fringes as trying to remember which control affects what aspect of the fringes. Adjustments of BS3 or of M2 seemingly have the same effects on the fringes. Differences between the two will be pointed out below.

If the mercury light source is being used, then it is highly unlikely that fringes will be initally visible due to the stringent requirement for equal optical path lengths. The instruction sheet provided by Aerolab suggests checking for fringes during the first few seconds after the lamp is turned on. Apparently, the light is closer to monochromatic at this time. This suggestion indeed proved helpful when the interferometer was set up with the mercury light.

If, with either light source, fringes are not visible, then one of the techniques used for inital (factory)

adjustment must be tried. The technique described in Aerolab's instruction sheet seems about as good as any of the numerous other techniques described in the literature. For another technique that is conceptually simple, consult Panarella [7].

The technique described in the Aerolab paper is referred to as a modification of the "near and far crosshair" technique. With this method, a crosshair is first inserted in the collimated beam just before the first beam splitter. The collimation tool with its fine, crossed wires is perfect for this task. The crosshairs cast shadows that are split and follow the test and reference beams. The screen in the output beam should be located so that the crosshairs are in-focus. The goal of this alignment technique is to get the output extensions of the test and reference beams parallel and superimposed, or, in other words, to get close to or reach the infinite fringe condition. This may be done by adjusting the optics so that the spots of light on the relay mirror from each beam coincide and so that the shadows of the crosshairs also coincide. The method may be better understood by referring to Figure 2 (p. 9). Although no focusing mirror is shown in the figure, its presence in the real interferometer does not materially affect this explanation.

Assume that, in Figure 2, the centerline of the beams represents the shadow of a vertical (perpendicular to the

paper) crosshair located just before BS1. For the case shown, the output beams are not parallel but do coincide at the screen. Thus, only one shadow of a crosshair will be seen on the screen since the two overlap. If either M2 or BS3 is made to yaw, then the output test beam will be deflected and the shadows will no longer coincide at the screen, giving two separated shadows of the single crosshair. In general, this will be the case when the real interferometer is initally examined. In a manner similar to the way in which the test and reference beams intersect BS3 at different locations in the figure, two spots of light on the real relay mirror may be discerned when the two beams do not coincide at the mirror's location. In practice, this is a difficult criterion to check, since the spots on the mirror are very dim and have fuzzy edges. Nevertheless, this alignment technique is being described to provide understanding of MZI alignment principles. If two spots are visible on the mirror, then they should be made to coincide by adjustments of M2. Likewise, if the shadows are not superimposed, they should be brought together by adjustments of BS3. An iterative procedure is necessary; after adjusting the shadows to coincide, one must adjust the spots of light again. The reason for selecting M2 to adjust the spots and selecting BS3 to adjust the shadows should be obvious from Figure 2 when one examines the effect of rotations of either optical element

on the beam path. From the figure, it appears that the easiest way to reach the infinite fringe condition is to rotate M2 until the two beams are superimposed at BS3 and then to rotate BS3 until the beams are superimposed at the screen (a rotation of BS3 has little effect on how the beams intersect at BS3).

If, with the laser source in use, the crosshair shadows coincide and the light spots seem to coincide (as well as can be discerned), then fringes should be visible unless they are too fine to be seen. If none are seen, then one must drive one of the optics (M2 would probably be best since the shadows are already aligned) in one direction and then, if no fringes are found, in the other direction.

Once fringes are found, then alignment of the output beams becomes relatively easy. The beams are parallel when the infinite fringe condition is reached; in the infinite fringe condition and with the shadows aligned, the output beams will be both parallel and superimposed, which is a good starting point for adjusting the fringes to the wedge fringe case, if desired. Remember that the beams should be made to coincide so that a ray in each beam will interfere with its other half or, more often, with a ray very close to its other half, so as to give best fringe contrast. From examining Figure 2, it can be seen that the best procedure to use to reach the infinite fringe condition

from wedge fringes is to rotate BS3 until the infinite fringe condition is reached and then rotate M2 until the shadows are aligned, which produces some wedge fringes again. The procedure is then repeated starting again with BS3.

Once the infinite fringe condition is reached (with the shadows in reasonable alignment), the interferometer may be used to reveal approximate isotherms in the test section. It will be found from working with the instrument, that the infinite fringe condition is very difficult to achieve to good satisfaction and also somewhat unstable with time. This is to be expected since the infinite fringe condition is a special case of the more general wedge fringe condition, and also since relatively small movements of the optics have rather large influences on the fringe pattern at and near the infinite fringe condition. Also, imperfections in the MZI's optics themselves (mainly due to nonperfect flatness of the splitters and mirrors) become obvious as nonstraightness and distortion of the fringes as the infinite fringe is approached.

For these reasons, unless one particularly wants isotherm fringes, it may be best to use the wedge fringe adjustment when gathering data. As described previously and illustrated in Figure 4D, when using this scheme, the fringes are initally adjusted to be parallel to the axis

along which the temperature distribution is desired to be determined.

Wedge fringes may be formed by rotating either M2 or BS3, but recall that the two beams should coincide at the screen (as illustrated in Figure 2), so both M2 and BS3 should be adjusted to form the fringes. This is the reverse of the procedure described above for reaching the infinite fringe adjustment. M2 is first rotated (in either pitch or yaw, depending on the desired orientation of the fringes) to form some wedge fringes. Then BS3 is rotated until the shadows are aligned, which will then reduce the fringe density. The procedure is repeated until the desired fringe density is attained. The problem associated with this technique is that the screen must now be located at the test section focus, which results in the crosshairs being considerably out of focus and, thus, difficult to accurately align. Practical experience seems to indicate that especially accurate adjustment is not needed (at least with the laser source) so the alignment attainable with the fuzzy shadows may be considered acceptable.

The above fringe manipulation instructions were primarily oriented to the case of laser source utilization. They can be extended to the case of mercury source usage by adding the requirements of establishing and maintaining equal optical path lengths. As described previously in the section dealing with non-monochromatic light sources, the

equal optical path length condition is recognizable by the appearance of a bright white maxima (this marks the location of equal lengths) between maxima tinged with color and both maxima and minima of decreasing contrast.

Assume that the crosshair shadows and the spots on the mirror are aligned. If, during the first few seconds after the lamp is started, fringes are seen, the translation control should be pressed (in either direction) to change the path lengths. If the fringes are excessively fine, then they should first be made more readily observable before beginning the translation. Translation of BS3 causes an apparent movement of the fringes perpendicular to themselves across the image. This movement must be continued even if the fringes fade out as the mercury bulb warms up. If, after a few minutes of translation in one direction, no fringes are seen, then the translation should be reversed for a longer period. This is continued until the fringes become visible with the lamp hot, and the zero order fringe is located. The fringes may then be manipulated as described above, always keeping the zero order fringe in the field of view. After adjustment is complete, the filter can be placed in the light path to narrow the light's bandwidth.

C. Laser Doppler Velocimeter

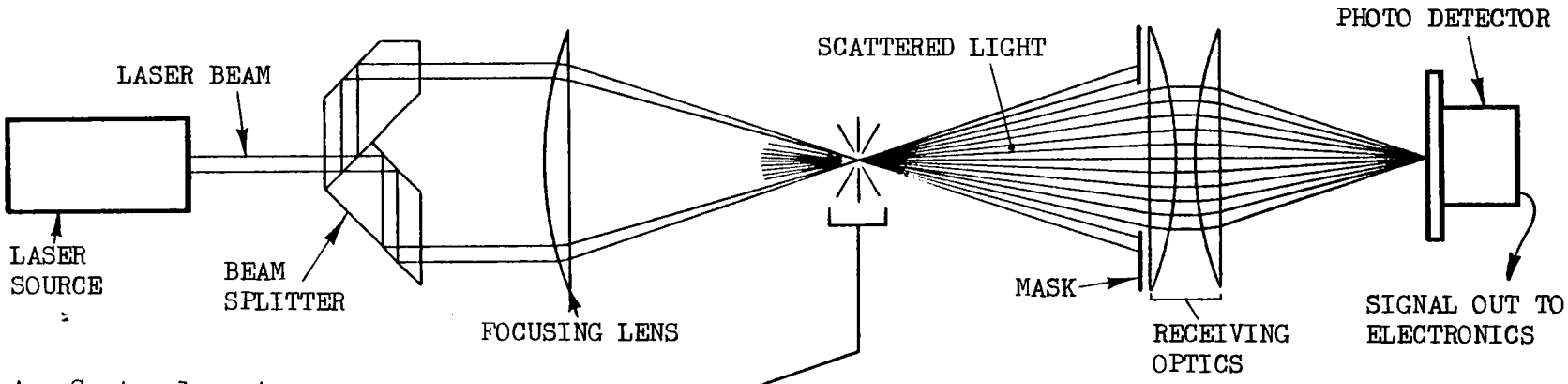
The Laser Doppler Velocimeter (abbreviated as LDV) is

of relatively late invention; an LDV was first described and constructed by Yeh and Cummins in 1964 [8]. As its name implies, this instrument provides a completely optical technique for measuring the velocity of a flowing fluid. This technique is particularly advantageous in natural convection flows where the introduction of a physical probe could produce disturbances of the same order of magnitude as the undisturbed flows.

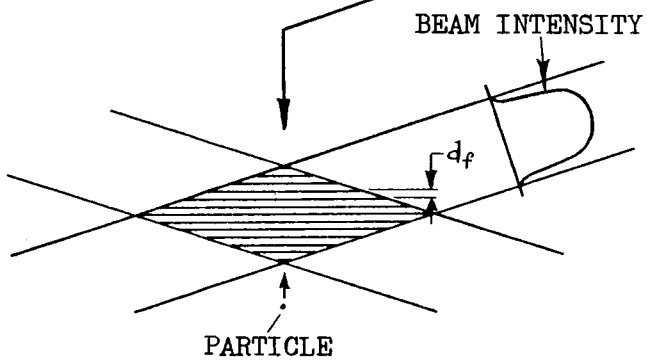
Principles of Operation

An LDV may operate in one of three primary modes or optical arrangements: reference beam, dual beam, or dual scatter. The reference beam mode was the first to be used. This mode is most easily understood in terms of a Doppler shift of light (hence the inclusion of Doppler in the instrument's name). Only the dual beam mode will be considered in this paper; it is the easiest of the three modes to implement and provides the best signal-to-noise ratio. Its operation is most easily explained in a way that does not make use of Doppler shift.

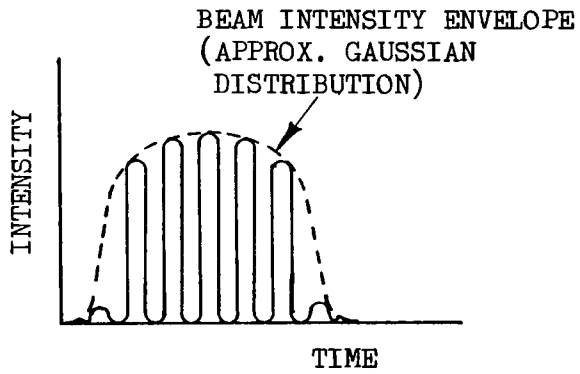
Figure 18A shows a schematic of an LDV system operating in the dual beam mode. A laser light source emits a beam of coherent, monochromatic light that is split into two equal intensity beams by a beam splitter prism. The two beams are separated and leave the prism parallel to each other. The beams strike a focusing lens which



A. System layout.



B. Enlargement of beam crossing region showing light and dark fringes.



C. Light intensity at photodetector for a particle crossing test volume.

Figure 18. Schematic of the Laser Doppler Velocimeter in dual beam, forward scatter mode with details illustrating the principle of operation.

deflects the beams until they cross. Besides being made to cross, the beams are focused to a smaller diameter at the crossing region. (Due to its wave nature, a beam of light will not focus to an absolute point.) Optical interference between the two beams of light results in the formation of a fringe system within the crossing volume. Details of this fringe formation can be understood from Figure 3 (p. 10) and its associated explanation (previously covered). The fringes, both light and dark, form parallel planes that are stacked upon each other, as illustrated in Figure 18B, throughout the roughly ellipsoidal beam crossing region.

After crossing, the beams continue on as though they had not intersected. Also on the optical centerline of the system (as shown in Figure 18A) are a pair of focusing lenses, referred to as the receiving optics, and a photodetector of some type. The photodetector is located at the focus (of the lenses) that is associated with the beam crossing region. Thus, any light emitted from the crossing region and striking the lenses will converge at the detector. The output of the photodetector is an input to some type of signal processing device. For explanatory purposes, one may assume that the signal is displayed on an oscilloscope.

The LDV of Figure 18 is assumed to be surrounded by an optically transparent fluid. Now assume that a small

(about one half or less of fringe spacing in size) piece of particulate matter in the fluid enters and moves continuously across the beam crossing region (Figure 18B shows such a particle). When this particle is within a bright fringe region, light rays, which normally would have continued on a straight path, will be scattered by the particle. This light will be scattered in all directions from the particle's location. Some of this light will be collected by the receiving optics and focused at the photodetector. Note that the laser beams past the crossing point are blocked by a mask; thus, the scattered light is the only light reaching the detector. With this light input, the detector signals an output to the electronics. When the particle enters a dark fringe, little or no light is scattered and the light input to the photodetector reaches a minimum level resulting in a minimum output signal. As the particle moves continuously through the fringe system, the detector's output oscillates in a manner similar to that shown in Figure 18C. The velocity of the particle, V, can be calculated from the fringe spacing, d_f, and the frequency, f, at which it crosses the fringes (equal to the frequency of oscillation of the detector's output). Velocity equals distance traveled (one fringe spacing or one light-dark cycle) divided by the time to traverse this distance (the reciprocal of the frequency, f). Thus,

$$V = \frac{\partial f}{\frac{1}{f}} = f\, d_f \qquad [22]$$

The fringe spacing may be derived from the geometry of the wave fronts of the light. The relationship can be shown to be

$$d_f = \frac{\lambda}{2\sin\frac{\phi}{2}} \qquad [23]$$

where λ is the wavelength of the light and ϕ is the intersection angle of the two beams. Thus, velocity measurement requires only wavelength of the laser, which is known, the beam intersection angle, which can be calculated from the lens' focal length or measured directly, and the oscillation frequency of the scattered light (often called "Doppler frequency"), which is the output of the special electronics package. The fringe system is formed only where the two beams cross; thus, this is the only region where velocity measurement can occur.

Note that it is the particle velocity that is actually being measured, not the fluid velocity. Thus, the flow must be "seeded" with appropriate particles whose velocities can then be measured. The need for seed particles is one of the major limitations of the LDV velocity measurement technique. In some flow situations, it may be difficult or undesirable to introduce particles. In other cases, a flow may possess large accelerations which, due to the particle's inertia, cause their

velocities to be significantly different from the fluid velocity. Fortunately, the LDV technique lends itself well to many measurement situations, particularly where the tradeoff of measuring particle velocity instead of fluid velocity is compensated for by the need to have only light beams (as opposed to solid object probes) within the test space. The absence of a physical probe is especially welcome for the relatively weak natural convection flow within a small enclosure to be considered later in this paper.

A typical fringe spacing, d_f, for an LDV system is about 3 microns. Thus, a suitable seed particle should be about a micron in diameter. Rays of light encountering particles in this size range are scattered primarily about the direction the rays were originally traveling. This is referred to as "forward scatter." The LDV setup of Figure 18A is arranged with the receiving optics on the optical centerline to take advantage of this highest intensity scattered light. The direction of the second most intense scattering is that directly opposite to the inital ray's direction. This is referred to as "backscatter." Figure 19 shows an LDV system arranged to operate in the dual beam, backscatter mode. Scattered light from the test volume is collected and collimated by the focusing lens. An additional lens brings the light to a focus at the photodetector after a reflection from a plane mirror. The

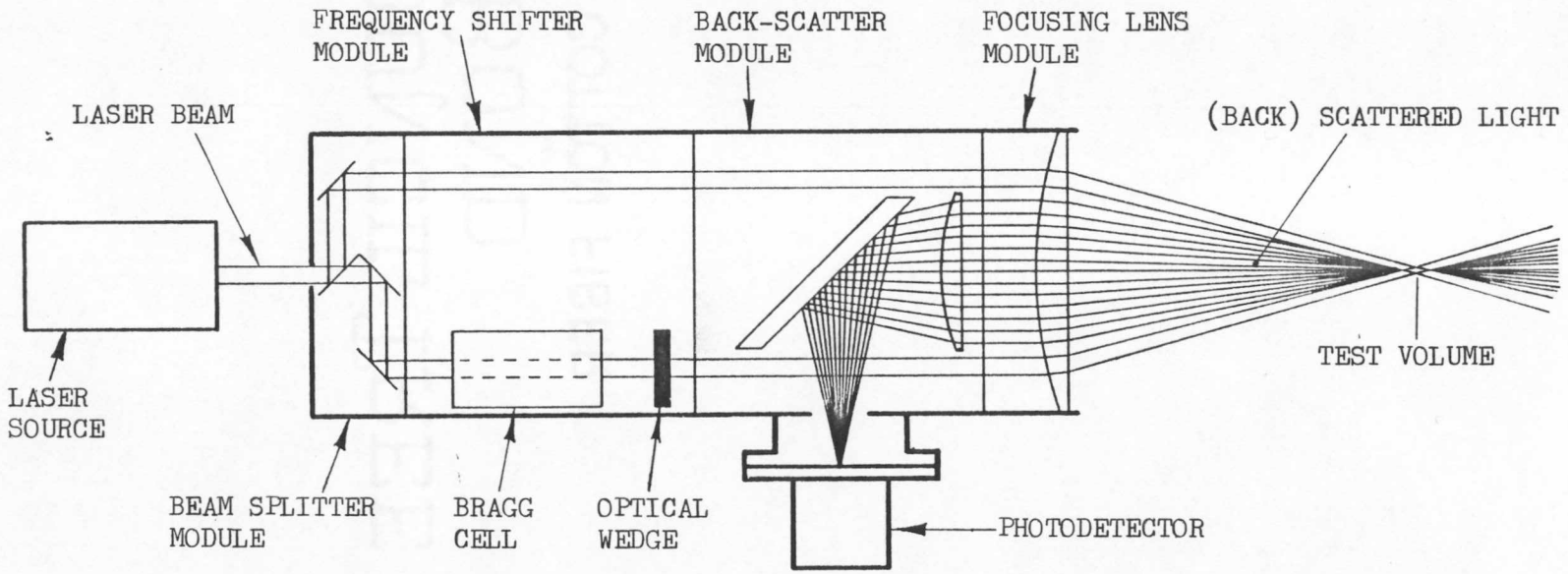


Figure 19. The Laser Doppler Velocimeter system in dual beam, back scatter mode with the optional frequency shifter in place.

intensity of backscattered light is roughly one to three orders of magnitude weaker than the corresponding forward scattered light; thus, the forward scatter mode is generally preferred unless this system's "straight through" optical arrangement prevents it from being used with a particular experiment. In this case, the backscatter mode would probably be used, although the receiving optics assembly (that used for forward scatter) may be located to collect the scattered light from any angle.

The LDV systems discussed measure only that component of velocity that is perpendicular to the fringes within the test volume. It should be apparent from Figure 18B that motion parallel to the fringes cannot be detected. The component sensed is that normal to the optical centerline and in the plane of the two beams. Further, the sense or direction of motion of the particle velocity cannot be detected. Motion across the fringe system in one direction is indistinguishable from motion across the fringes in the opposite direction.

To resolve this ambiguity, a frequency shifting device may be interposed in one of the dual beams between the beam splitter and the focusing lens. Such a device is illustrated in the LDV system in Figure 19 and could be added to the system in Figure 18. This "frequency shifter" employs a "Bragg cell" along with a compensating optical wedge to shift or change the frequency of the beam of light

by a chosen amount. The Bragg cell is a block of glass that is excited with high frequency acoustic (ultrasonic) waves. The laser beam entering the cell is shifted in frequency by an amount equal to the ultrasonic frequency (a typical value might be 40 MHz). Additionally, the beam is diffracted into several "orders," or different beams, that leave the cell at different angles. Only one of these beams is wanted for intersection with the unshifted beam. The optical wedge deflects the orders so that the one desired beam is once again parallel to the unshifted beam (for clarity and simplicity, the multiple orders were omitted from Figure 19). Fortunately, the Bragg cell assembly may be adjusted so that the one desired order contains most of the power of the entering beam.

Shifting the frequency of one beam of the dual beam pair effectively results in a moving fringe field; that is, the fringes move perpendicularly to themselves across the depth of the test volume. Thus, even if a particle is stationary within the test volume, an output signal (a frequency) will be produced by the photodetector and electronics package. Using the previously given value of 40 MHz for the ultrasonic frequency, a stationary particle in the test volume would have an indicated velocity (by the frequency output of the photodetector) equivalent to 40 MHz. If, however, the particle moves in the same direction that the fringes move, then the indicated Doppler frequency

would decrease from the 40 MHz value. The frequency to be inserted in Equation 22 is the difference between the indicated Doppler frequency, f, and the frequency shifter's frequency, f_o. Thus, Equation 22 must be modified to read

$$V = | f - f_o | d_f \qquad [24]$$

Similarly, if the particle moves opposite to the direction of movement of the fringes, then the indicated Doppler frequency increases above f_o. Thus, the sense of the particle's motion can be determined by knowing whether the indicated frequency is greater than or less than the ultrasonic frequency, f_o, and by knowing the direction of motion of the fringes (this information may be available from markings on the optical wedge in the frequency shifter module.

As mentioned previously, use of a frequency shifter results in an output signal even when a particle is stationary within the test volume. Thus, even when the motion of particles in a flow undergoes a change of direction, a continuous output signal will be available. Conversely, if the shifter is not used, then at the zero flow velocity point no output signal is available, resulting in a discontinuity in the measurement. Furthermore, the electronics package that displays the fluid velocity requires a minimum frequency input for operation, resulting in a "no data available" region about

the zero velocity point. Use of a frequency shifter to provide continuous data at and near zero velocity is especially important with natural convection flows, since the velocities in these flows are relatively low and flow direction reversals are always present in completely enclosed natural convection flows.

A General Description of the Thermo-Systems, Inc. LDV System

The Mechanical and Aerospace Engineering Department's LDV is a commercially produced system made by Thermo-Systems Incorporated (TSI), of Saint Paul, Minnesota. The parts comprising this LDV system will be described, followed by instructions for setting-up and operating the system. This material is included here for the sake of completeness. The illustrated and detailed manuals provided by TSI, Inc. should be regarded as the primary references for the TSI LDV system.

TSI's laser velocimeter is layed out in a manner very similar to that shown in the schematics in Figure 18 and Figure 19. (The latter figure best illustrates the component modules into which the system is divided.)

The actual laser source is a Spectra-Physics He-Ne gas laser of 15 milliwatts nominal light power output. The laser tube's housing is attached by adjustable mounts to a 45 inch long channel-section frame. The laser beam exits

the housing and enters any component modules which may be attached at one end of the frame. These modules are 3.25 inch diameter tubes that may be joined together as suggested by Figure 19.

The beam splitter module contains the splitter prism which is in a rotary mount; thus, the prism may be rotated to select the desired velocity measurement direction. The mount has detents at 45° increments. The beam enters the splitter module through the aperture of a removable diaphragm plate. The two halves of the split entering beam exit parallel to each other and with a separation (center to center) of 50 millimeters, which is the standard separation for a TSI laser velocimeter. The module is supported by a base that is clamped to the channel frame.

If the frequency shifter and back-scatter units are not used, the focusing lens may be attached directly to the splitter module. The modules are all held together by pairs of knurled screws and may be easily attached or removed. Three pairs of lenses are included in the system. The pairs have nominal focal lengths of 120, 250, and 600 millimeters. One lens of a pair is the focusing lens of the sending optics, while the other lens is the collecting lens of the receiving optics (when forward scatter is used). Often, lenses of the same focal length will be used for both the sending and receiving ends; this simplifies alignment somewhat and has other optical advantages, but is

not an absolute requirement. The three focal lengths are included to provide flexibility for different measurement situations. Since the test volume is about one focal length from the sending lens, a range of relatively small to relatively large experiments may be accomodated. Additionally, a shorter focal length lens causes a closer fringe spacing which gives increased measurement sensitivity as well as a smaller test volume; whereas, a longer focal length lens causes wider fringe spacing which provides a higher maximum velocity measurement (relatively unimportant for natural convection studies).

If either or both the frequency shifter or back scatter modules are used, they are attached between the beam splitter and focusing lens as illustrated in Figure 19. Since these units are relatively long, an additional support ring is provided. This support would be used between the frequency shifter or the back-scatter module and the lens. The support has a base similar to the beam splitter module that is clamped to the channel frame.

An "angle reducer" accessory is also available. It is a module that contains a pair of prism assemblies that reduce the separation of the (parallel) laser beams from 50 millimeters to 22 millimeters; this smaller separation may allow the beams to enter a test cavity too small to accept beams at the 50 millimeter separation. This accessory, when used, mounts just before the focusing lens.

The receiving optics assembly is attached to a support plate. This plate is 23.5 inches long by 5 inches wide and rests on three adjustable support screws. A pair of lenses is held by a support ring that is usually clamped at one end of the plate. The first lens is the collecting lens and is one of the 120, 250, or 600 millimeter focal length pairs. If the collecting lens is placed one focal length from the test volume, which is the usual case, then the light exiting the lens will be approximately collimated (this is the scattered light from the test volume). The second lens (no alternate focal lengths are provided) then brings the collected light to a focus. The photodetector is located at this focus.

Two photodetectors are available from TSI: a photodiode and a photomultiplier. The UT system includes only a photomultiplier which has greater sensitivity and bandwidth than the photodiode. The photodetector attaches to a mount that has 3-axis adjustments. For movement perpendicular to the optical axis (that is, movement in the x and y directions), two thumbscrews allow fine adjustment of the photodetector's location. The mount attaches by a dovetail to the base plate. This dovetail provides longitudinal, or z-axis, movement for locating the photodetector at the lens' focus. This assembly is manually adjusted; no screw adjustments are provided.

The photodetector has a diaphragm plate with a 0.01

inch aperture through which the collected light must enter. This diaphragm is for limiting the area from which light may enter the detector; it allows the detector to "see" only part of the test volume (thus blocking as much extraneous light as possible). If the same focal length receiving lens as focusing lens is used, then the detector will be able to "see" about 70 per cent of the test volume's nominal diameter.

A special alignment tool, TSI Model 10096, is provided. The photodetector is removed and this tool substituted in its place when the system is initally being aligned. This tool has a frosted plastic screen on which crossed "target" lines are printed. A 7X magnifier is provided for observing this screen. The Model 10096 aids alignment in the following way: when scattered light from the test volume is focused onto the crossed lines, the photodetector's mount is in the proper location so that the collected light will pass through the aperture when the alignment tool is replaced by the detector. Use of this tool will be further explained when a detailed discussion of alignment is presented below.

A special power supply, the TSI Model 965, is provided for the photomultiplier. A knob on the supply adjusts the voltage that powers the detector. The setting of this voltage level will be discussed later.

The signal output from the photodetector goes by

coaxial cable to a signal processor, a TSI Model 1090 "tracker." This is a relatively sophisticated electronics package that does signal amplification, noise rejection, data validation, and signal output. The tracker uses a frequency-to-voltage converter so that the Doppler frequency is actually output as a voltage. In addition, a sample-and-hold circuit holds a voltage level until a new measurement is validated; this is necessary because the frequency readings are obtained discontinuously. The tracker includes an analog voltmeter for measurement output. An external meter, such as a digital voltmeter, may also be connected to the tracker. Again, more details will be provided later.

If the frequency shifter is being used, then another electronics module is added to the system. This is the TSI Model 985 "Bragg Supply/Signal Mixer." The Model 985 includes an oscillator which provides the 40 MHz signal for the Bragg cell; the signal is fed through a coaxial cable to the shifter module. Often, a 40 MHz shift is undesirably large. Thus, the 985 also contains a "downmix" circuit so that the effective frequency shift will be less than 40 MHz. In use, the signal line from the photodetector to the tracker is input to the 985 instead. The 985 provides an output for the tracker. The effective frequency shift is set by a knob on the front of the 985; available shifts are 10 KHz, 20 KHz, 50 KHz, 100 KHz,...,

20 MHz. For a shift of 40 MHz, the photodetector's signal goes directly to the tracker.

Alignment and Operation of the TSI LDV System

The documentation provided by TSI for the velocimeter system is very thorough compared with that provided for the interferometer. TSI provides the following manuals: "Instruction Manual, 900 Series Laser Optics"; "Instruction Manual, Model 1090 Tracker"; and "Instruction Manual, Model 980."

A detailed description of the setup and operation of the LDV system will now be provided. This text should be regarded as an accompaniment to the instruction manuals listed above.

The bases that the LDV's optics units are mounted on provide very little height adjustment--only small leveling screws are attached. To adjust the height of the LDV so that the test volume may be placed within the experiment, a pair of support bases was assembled for the sending and receiving optics units. These bases are of 45 inch by 8 inch by 0.5 inch aluminum plates with two scissor action laboratory jacks attached to each. Each jack has a 6 inch by 7 inch platform that can be raised or lowered by turning an adjustment knob. The jacks are spaced to fit under the support screws of the sending or receiving units. The

jacks provide continuous and relatively fine height adjustment over a 9 inch range.

Since the LDV has been previously operated several times, the sending unit (the base, laser source, and optics modules) may already be set for immediate use. If, however, the laser or optics modules have been removed from the base, then more extensive alignment and adjustment will be necessary.

A mount at each end of the laser's housing attaches it to the base. Four cap screws, one at each corner, secure the laser mounts to the frame; if these screws are loosened or removed, the housing is free to be moved. Side-to-side or up-and-down motion is effected by the setscrews at each corner of the housing. If the laser housing has been removed and then replaced on the base, it should be located parallel to the base and on its centerline. To get the housing on the centerline, a straightedge can be held (vertically) against the side of the base, and a measurement made from the straightedge to the side of the laser housing. This measurement should be the same from end to end and side to side. A measurement from the base to the top of the housing at each end serves to check for parallelism. It should be noted that the laser tube may not be accurately parallel to its housing, so that some later adjustments of the housing may be needed. A bubble level should also be used to level the base and then to

level the laser housing, so that the housing will not be twisted.

The sending optics modules are clamped down at one end of the frame by screws that fit in threaded holes in the channel frame. The optics modules to be considered in this paper (in order of assembly) are the beam splitter, the frequency shifter, the support or mounting ring, and the focusing lens. The beam splitter module and the mounting ring are attached to bases that are clamped to the frame. The clamping arrangement allows a limited amount of sideways travel of the modules for adjusting them properly in the path of the laser beam. They have no vertical adjustment; only the laser has vertical travel.

The centerline of the optics modules must be made to coincide with the laser beam. The beam splitter end of the optics assembly is correctly aligned when the laser beam cleanly enters the aperture in the diaphragm plate. Some caution should be exercised here. The brightest part of the beam should symmetrically enter the aperture; the dim edges of the beam, which will be visible on the diaphragm, may not be symmetrical with the central bright spot. Furthermore, the laser should be allowed to throughly warm up before checking alignment. To help align the other end of the optics assembly, TSI provides a special alignment tool. This tool, a Model 904 Alignment Mask, is attached to the mounting ring in place of the focusing lens (it

attaches in the same manner as the lens). In place of a lens element, however, this tool has a frosted plastic screen with radial (center) lines and two circular lines printed on it. One circle has a 50 millimeter diameter to match the standard beam separation; the other circle has a 22 millimeter diameter for use with the angle reducer accessory. In use, correct alignment is achieved when the (two separated) beams strike the intersection point of the appropriate circle with the radial lines. The beams can be in either a vertical or horizontal plane for this operation. As mentioned previously, with the clamp-down screws loosened, the optics assembly is simply slid sideways as needed to achieve alignment. If enough travel is not available, then the laser will have to be moved. Also as mentioned, only the laser can be moved to achieve vertical alignment.

The frequency shifter module, which is mounted between and supported by the beam splitter and the mounting ring, may be rotated to the desired angle when the four attachment screws are removed. For the alignment described immediately above, the Bragg cell itself should be rotated out of the beams, or, if desired, the cell may be left in a beam but the cell must be energized (the shifter's power supply turned on) and the proper order selected for alignment. As mentioned previously, the Bragg cell diffracts an incident beam into several orders which leave

the cell at different angles. An optical wedge then deflects the beams. With the cell unenergized, only a single beam leaves the cell; it is deflected by the wedge so that it is not parallel to the other beam. With the cell energized, one of the diffracted orders will be parallel to the unaffected beam. This is the order to use for alignment, and the beam crossing point of this order with the other beam is the one to be focused on by the receiving optics assembly. The correct order may be located by viewing the beams on a card placed several feet from the optics assembly with the focusing lens removed. The desired order is simply the one that is 50 millimeters from the unaffected beam (or 22 millimeters if the angle reducer follows the shifter module). As described in the "Instruction Manual, Model 980", the Bragg cell has a "tilt" adjustment which affects the beam intensity of each diffracted order. Of course, the one desired order should be at maximum intensity. This adjustment was performed, and the shifter may continue to be correctly set. If, however, the shifted beam appears to be considerably dimmer than the unshifted beam, then the tilt adjustment should be checked.

Another adjustment to consider is that of the compensating optical wedge. This wedge may be rotated through 360°. The mounting ring holding the wedge has an arrow engraved on it; the direction this arrow points is

the direction that the fringes effectively move (of course, the arrow must be more or less within the plane of the two beams). The direction the arrow points may be chosen to suit the flow measurement situation, or it may be arbitrarily set. The wedge requires a fine adjustment so that the two beams exactly overlap at the beam crossing region. (Rotating the wedge causes the beam passing through it to be deflected by a relatively small amount.) A method for fine adjusting the wedge will be presented after setup of the receiving optics is presented. However, it should be verified that the beams do cross; holding a card at the beam crossing region should disclose whether or not they do cross.

As described previously, the LDV's optics kit includes three pairs of lenses with nominal focal lengths of 120, 250, and 600 millimeters. Each lens is marked with the lens' actual focal length and the resulting beam intersection angle, $\emptyset$ (not valid when the angle reducer is used).

With the desired lens clamped to the mounting ring, setup of the transmitting optics should be complete. If an angle reducer is desired, it is clamped between the ring and the lens, turned so that the prisms are in the beams.

The next step in assembling the system for operation is to position the transmitting optics or the experiment package so that the (correct) beam intersection is located

to measure the desired velocity component. The details of doing this for a particular experiment will be presented in CHAPTER III; for present purposes, it will be assumed that the two transmitted beams may freely enter an experimental device and cross and that the forward scattered light may freely exit the experiment.

For practice in setting up the LDV system without the added burden of handling an experimental device, a "scatter plate" may be set up at the intersection point. This scatter plate, supplied by TSI, is simply a piece of frosted plastic sheet that may be held by an alligator clip mounted on a cast iron base. The frosted plastic takes the place of the seeded fluid and scatters the light. Of course, the velocity of the scatter plate is zero, but with the frequency shifter functioning, it will register an apparent velocity.

The support base and the receiving optics assembly should be set up along the optical centerline defined by the transmitting optics assembly. Briefly, alignment of the receiving optics assembly consists of locating the assembly the proper distance from the beam crossing point, centering the lenses on the optical centerline, and fine adjusting centering and focus so that the collected light is focused at the photodetector's aperture. For the following discussions, the frequency shifter, if used, must be energized and the one correct shifted order of the group

selected for alignment purposes. If the shifter is not used, it must be removed or rotated so that neither of the beams enters the Bragg cell.

The receiving optics assembly is located so that the collecting lens is one focal length's distance from the beam crossing point. The focal length of the collecting lens chosen may be dictated by the size of the experimental device. If not, then a focal length equal to that of the focusing lens of the transmitting optics should be chosen, at least for inital practice. A shorter focal length collecting lens gathers more scattered light than a longer focal length lens; thus, if the scattered light is weak, the shortest focal length that can be accomodated by the experiment should be tried.

The receiving optics may be set by measuring with a scale a distance of one focal length from the crossing point to the collecting lens. Good accuracy is not really needed here. A mask may then be placed over the collecting lens. (Two masks are available; one is for use without the angle reducer, and the other is for use with it. If the frequency shifter is used, a mask that blocks all of the orders should be used.) These masks are similar to the plastic dust covers that protect the lenses when they are stored; however, they have cutouts shaped so that the scattered light may pass to the lens while the two laser beams are blocked. (Remember that the two beams, after

crossing, are of no further interest, except for purposes in this alignment procedure.) Each mask has a line scribed upon it along one of its centerlines. Assume that the laser beams are in a vertical plane. The mask should be mounted so that the scribed line is vertical (judged by eye). With nothing blocking the beams (the scatter plate removed), the collecting lens may be centered on the optical centerline by moving the optics assembly sideways so that the beams strike the scribed line and adjusting the support jack vertically so that the beams appear centered on the face of the mask (again judged by eye). The mask may need to be rotated slightly so that the scribed line intersects both of the beams. Vertical centering is relatively easy to achieve by observing whether the two spots of light on the mask appear to be equidistant from the mask's edge. This procedure centers only one end of the receiving optics assembly; the other end is centered next.

The second lens of the receiving optics assembly, the focusing lens, and the mask must be removed. With this lens removed and the collecting lens one focal length from the crossing point, the laser beams exiting the collecting lens will be parallel. Further, the beams will also be at the original beam separation, 50 millimeters (or 22 millimeters with the angle reducer). The photomultiplier's support stand has on its face a circular groove of 50

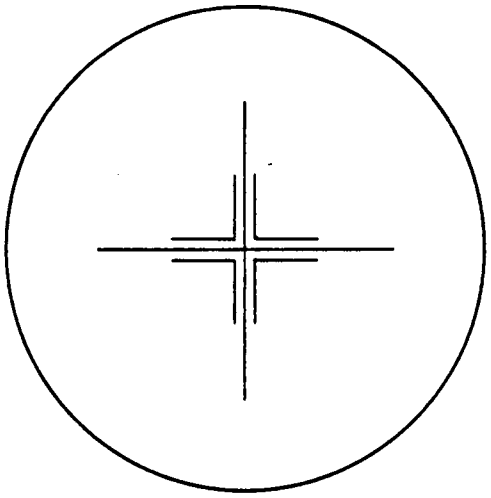
millimeters diameter. Thus, alignment of the optics assembly is achieved by adjusting the back end of the assembly so that the beams (in a vertical plane) intersect the groove (demonstrates vertical centering) and appear horizontally centered (relatively easy to judge by comparing the beam intersections with the adjustment screws in the stand, which define horizontal and vertical centerlines). Instead of setting the one focal length distance of the collecting lens from the crossing point by use of a measuring scale, the distance could just as well be set by adjusting the optics assembly so that the two beams simultaneously strike the circular groove. Thus, centering and distance setting can be combined into one operation. After centering the back end of the assembly, another iteration of the centering procedure should be performed, since adjusting one end slightly affects the other end of the assembly. (If the 22 millimeter angle reducer is employed, then the 50 millimeter groove should be ignored. The edge of the center hole through the photodetector mount is used for the alignment in this case.)

The next adjustment is focusing and fine adjustment of the photodetector mount. This mount is composed of a vertical plate attached to a base that slides on a dovetail track attached to the optical assembly's base plate. This upright (which has the 50 millimeter diameter groove on it)

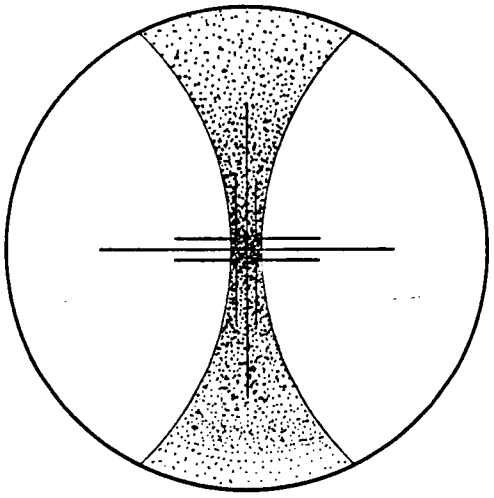
supports the photodetector's mounting plate, which is a circular plate free to move by means of screw adjustments over a very limited range in the x and y directions. Inital adjustment is performed with the photodetector removed from the mount.

Before starting the alignment procedure, the detector mounting plate should be centered within the limits of its travel. This is easily done by eye and by feel. Also, the second focusing lens must be reattached behind the collecting lens and the mask removed. The Model 10096 alignment tool is now attached in place of the photodetector. This tool, as previously described, has a frosted plastic screen with lines printed on it. Figure 20A represents a view of the screen through the 7X magnifier, with the text on the screen omitted. (The magnifier has a focus adjustment; each user should adjust it so that the lines on the screen are sharp.) The ⌋⌊-shaped marks on the screen are 0.01 inch apart; thus, they mark the boundaries of the 0.01 inch diameter aperture of the photodetector. These lines aid centering and focus adjustment of the image on the screen.

The light rays in the laser beams that travel through and beyond the beam crossing volume are similar to the scattered light in that they both appear to have originated from within the test volume and they both exit radially from the crossing region. Thus, if the photomultiplier



A. The focusing screen and center lines.



B. At optimum focus of beam crossing.

Figure 20. The view through the magnifier of the Model 10096 alignment tool.

mount is adjusted so that the two beams converge at the crosshairs on the alignment tool, then the scattered light will converge to the same point. The laser beams, being much brighter than the scattered light, are much easier to use for coarse focusing and alignment.

While viewing the alignment tool without the magnifier, the photodetector mount should be moved back and forth along the dovetail until the two laser beams appear to converge to the same spot on the screen. Then, with the magnifier in place, the intersection of the beams on the screen may be closely checked. The laser beams are very bright and will dazzle the eye; however, the beam spots may be closely observed after the eye has adjusted to the brightness. A filter, such as a 4X neutral density photographic filter, can be attached in front of the beam splitter to make the viewing more comfortable (or a filter could be worn in front of the eye). The beams should intersect to form a single circular spot, when properly focused. Undoubtedly, the beams will not intersect at the crosshairs. The back end of the mounting plate may be adjusted (moved horizontally or the jack moved vertically) so that the intersection spot will be at or near the target point. The fine adjustment screws may be used to move the photodetector mounting plate for the finest adjustment.

The setting of the compensating wedge in the frequency shifter may be checked at this point. With the beams in a

vertical plane, rotations of the wedge cause the shifted beam (the several orders) to shift horizontally. The wedge is correctly set when the two beams are merged. Alternatively, the alignment tool can be set up directly at the crossing volume, and the alignment checked the same way as given above.

Now the mask may be placed over the collecting lens to block the beams. To observe the scattered light on the alignment tool, the scatter plate must be placed at the beam intersection point, or, if an experimental apparatus is used, the fluid under study must be seeded. Positioning of the scatter plate is rather critical; with the shorter focal length lenses, the test volume is rather small and careful adjustment of the plate is needed. The plate is located to the intersection point by moving the plate until the spots of the beams merge, precisely as the alignment tool was focused.

The image of the scattered light on the alignment tool will differ depending upon whether the scatter plate is used or if an actual seeded fluid is used. Figure 20B is a rather idealized drawing of the focused scattered light observed when a seeded fluid is used. The beam crossing volume is the region of greatest light intensity and is centered on the crosshairs (since both beams are contained in the crossing volume, this region appears at about double the brightness of the other regions of the beams). As the

laser beams extend away from the crossing point, their images on the screen are increasingly out of focus (since the screen is focused onto a plane through the crossing point). Thus, the laser beam images grow larger and dimmer away from the crosshairs, as seen in the figure. Another fine adjustment of the mounting plate may be needed to get the bright spot representing the crossing volume centered in the target lines. The focus adjustment may also be tried, though it usually is not needed. To optimize focus, the brightest spot should be made as small as possible and kept centered within the lines.

If the scatter plate is used, the image will not appear as in Figure 20B since the laser beams do not extend beyond the plate but will appear simply as a bright spot on the screen. The mount should be adjusted so the spot is centered on the lines and is of minimum size.

This procedure, observing the scattered light image on the alignment tool and adjusting it to the target lines, is probably the most troublesome aspect of the LDV's alignment. In many flow situations, the image will be rather indistinct, making it hard to identify the spot representing the crossing point. Only by practicing with the actual system can such problems be overcome.

After finally adjusting the alignment tool to the scattered light, the tool may be (carefully) removed and the photodetector installed. Two cables connect the

detector to its power supply. Another cable, for the output signal, connects the detector to the tracker or to the frequency shifter's control box (the Model 985) if the shifter is used. The voltage adjustment knob on the power supply, for inital trials at least, should be turned so the mark on the knob is near the one o' clock or the two o' clock position. One of the instruction manuals warns that if the voltage is turned too high, the tube may saturate and loose the signal; if turned too low, the tube will cease to operate.

The Model 1090 Tracker

The Model 1090 tracker will now be described along with the details of its operation.

The front control panel of the 1090 is illustrated in Figure 21. The tracker shares an enclosure with a power supply and an analog voltmeter, not shown. The signal from the photodetector or from the Model 985 enters the tracker through the BNC connector labeled "1" in the figure. The signal is then amplified. The gain of the amplifier is variable, by turning the GAIN knob, "2," so as to suit the strength of the input. Too much gain is indicated by the OUT OF RANGE light, "4," turning on. With a signal applied and the light initally off, the GAIN knob is rotated clockwise until the light turns on, then turned back counterclockwise until the light just turns off. Of

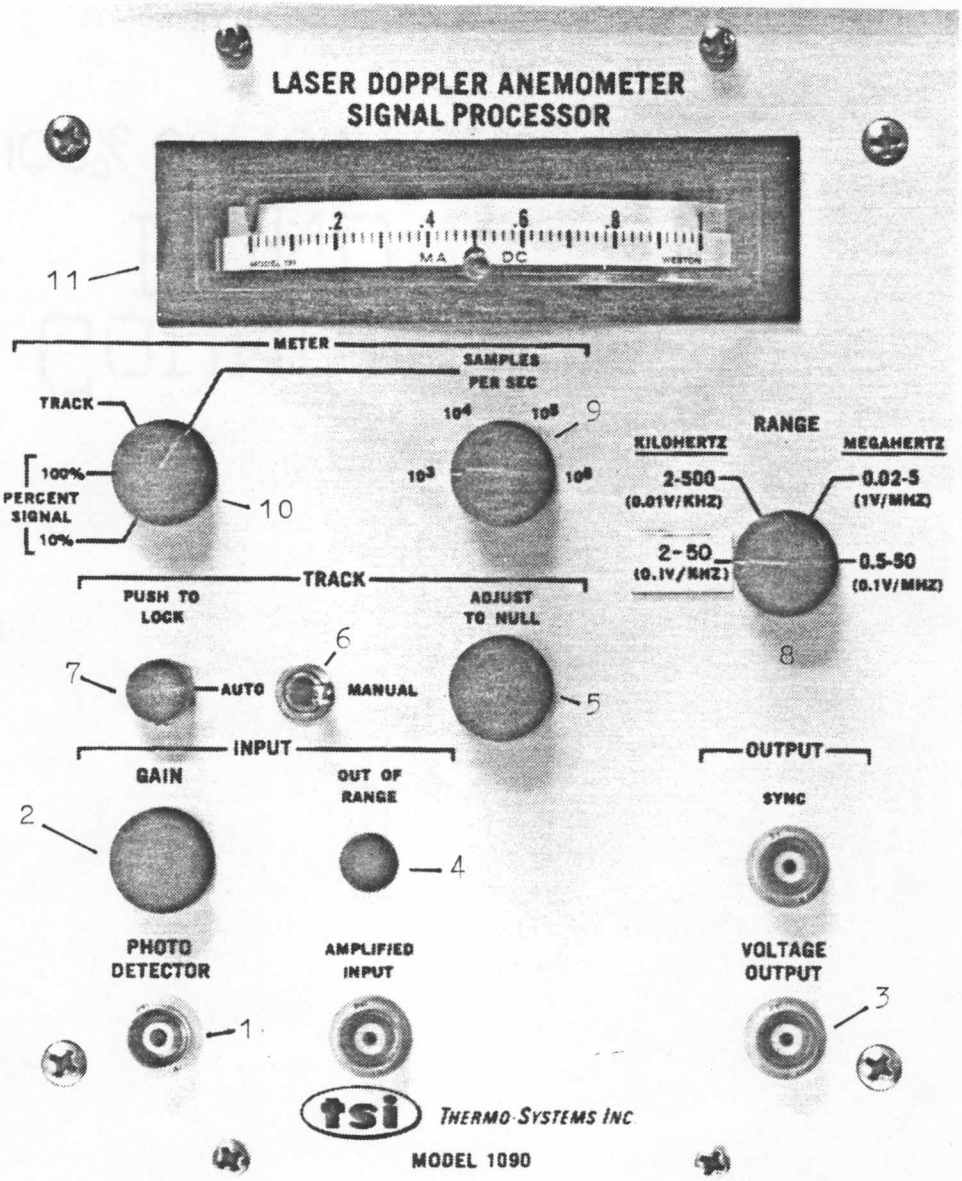


Figure 21. The Thermo-Systems, Inc. Model 1090 Tracker.

course, if the light is already on, the knob is turned counterclockwise until the light extinguishes. The light can be expected to flicker occasionally. The input signal, after amplification, is available as an output at the BNC connector, labeled "3" in the figure. The primary purpose of having this signal available is so that it may be viewed on an oscilloscope, allowing the nature and quality of the signal to be seen. (A low impedance termination box, a TSI Model 10098, should be connected to the oscilloscope's input to receive the signal from the 1090.) Using the oscilloscope provides feedback so that the components of the LDV system can be adjusted for an optimum signal.

The RANGE knob, labeled "8," sets the frequency range over which the tracker will function with a Doppler frequency. The Model 1090 tracker in the University of Tennessee Natural Convection Laboratory has had added to it a special higher sensitivity lowest frequency range. This frequency range, 2-50 KHz, has a sensitivity of 0.1 volt per KHz, (the output of the frequency to voltage converter) which is 10 times the sensitivity of the lowest range normally provided, 0.01 volt per KHz. Only the 2-50 KHz range will be used for the experiments described in this paper; this apparently is the most useful setting for natural convection studies. Obviously, the downmix frequency set on the Model 985 will have to match the frequency range of the tracker. Thus, the 10 KHz, 20 KHz,

and 50 KHz settings will be most used.

The instruction manual for the Model 1090 provides a detailed explanation of its principle of operation. The following simplified description should provide enough information for a user to satisfactorily operate the instrument.

Within the input frequency range setting, such as 2-50 KHz, there is a narrower frequency range or "window" within which a Doppler frequency will be admitted. This pass window may be positioned anyplace within the larger range. If an input Doppler frequency falls within the limits of the window, then it will be "tracked" or "locked onto" by a phase-locked-loop circuit. (Actually, it is the difference between the Doppler frequency and an internally generated frequency that is tracked.) When the system is tracking, a frequency-to-voltage converter produces a signal that varies with the positioning of the pass window. Thus, for the output voltage to be proportional to the Doppler frequency, the window must be properly positioned. This positioning may be done automatically by the instrument or adjusted and checked manually by the user.

A Doppler frequency "burst" (a sequence of cycles from a given particle as it passes through the fringe system) must pass a validation check to be accepted by the instrument. The phase-locked-loop must remain in-lock for eight Doppler cycles of a burst for the burst to be

considered valid. After being validated, the output of the frequency-to-voltage converter is reproduced by a sample-and-hold circuit. The circuit's previously held voltage is lost; a given output is held until a new Doppler burst has been validated. The output of the sample-and-hold is the Model 1090's final data output.

The setting of the toggle switch, labeled "6" in Figure 21, determines whether the positioning of the pass window will be done automatically or manually. Turning the switch to AUTO and depressing the PUSH TO LOCK pushbutton switch, "7," causes the tracker to search across the selected frequency range for a Doppler frequency and lock onto the signal if one is found. With the switch placed in MANUAL, the window is positioned by turning the ADJUST TO NULL knob, labeled "5." The knob is turned throughout its range until the instrument begins tracking the signal. Whether the unit is tracking or not may be checked in three ways corresponding to the three function settings of the meter function switch, labeled "10." The most important criterion is the number of data values validated per second. This data rate is observed by switching the meter function switch to SAMPLES PER SECOND and reading the rate from the meter, labeled "11." The SAMPLES PER SECOND knob, labeled "9," determines the full scale reading of the meter. It is generally best to start at the most sensitive setting, 10^3, and go to a higher range if the indicator

goes off scale. The absolute number of samples per second is generally of no particular interest. What is desired is the maximization of the sample rate. While observing the sample rate, the various components of the LDV system may be fine adjusted until their optimum settings are found. This will be discussed further below.

As previously stated, once the system begins tracking, the pass window must be properly positioned. Positioning is checked by switching the meter function knob to the TRACK position and observing the meter reading. The window is properly set (by turning the ADJUST TO NULL knob) when the meter reads zero (it is nulled). As the -NULL knob is turned back and forth through the null setting, the meter will be observed to swing in the positive or negative directions (only a very limited range of motion is available in the negative direction before the limit of travel is reached). The meter will also read zero when the system is not tracking a signal. If the TRACK switch is turned to the AUTO position, the instrument will perform this nulling operation automatically. Further, if the Doppler frequency changes, the window will need repositioning. In the AUTO mode, the Model 1090 will continually readjust itself to maintain the null condition (as long as the rate of change of the frequency does not exceed the instruments' ability to follow it). Set to MANUAL, the -NULL knob will require readjustment each time

the Doppler frequency changes. For reasons that are obscure, depressing the PUSH TO LOCK button does not result in the Model 1090 automatically finding and locking onto the signal when it is set to the lowest frequency range, 2-50 KHz, although this feature does function with the other range settings. Thus, in this range setting, the signal will always have to be manually located but may then be automatically held in track.

The third setting of the meter function switch is that labeled PERCENT SIGNAL. This is an indication of the percentage of time that the phase-locked-loop is tracking a signal. Two ranges are available; full scale on the meter can represent 100% or continuous tracking, or it can represent 10% of continuous tracking. If a scatter plate is used in the test volume, the system will indicate 100% tracking time; lower values are attained for a seeded fluid.

Thus, one can be reasonably confident that the Model 1090 is correctly tracking a valid signal if there is a distinct samples per second reading, if the meter is nulled, and if a nonzero percent signal value is observed as the meter is checked for the three functions. As previously stated, a samples per second indication is the most important; the function switch should be at this setting as the -NULL knob is turned through its range. Occasionally, as the -NULL knob is turned, a significant

samples per second reading may be discovered but the percent signal remains zero. In this case, the instrument is obviously not tracking and the -NULL knob should be turned elsewhere. When turned to the TRACK function, the meter will indicate zero when the system is not tracking; however, this case is distinguishable from the tracking-and-nulled case because, for the latter, small changes in the -NULL knob will drive the meter pointer positive or negative.

The Model 1090's voltage output, that representing the Doppler signal, may be read from the analog voltmeter supplied with the system, or it may be read out on a separate instrument, such as a digital voltmeter. The output voltage is available at the BNC connector labeled "13" in Figure 21. The SYNC output, labeled "12," provides an output pulse each time a new frequency burst is validated. This feature is generally used only in automated data acquisition and recording systems.

Now that the Model 1090 has been described, some information and recommendations concerning its use will be presented.

As mentioned previously, the photodetector may be fine adjusted to its optimum location by observing its output (as presented by the Model 1090) on an oscilloscope or by observing the data rate. If a scatter plate is used, then the output of the photodetector as seen on the oscilloscope

will be a very clear and distinctive sine wave. The fine screw adjustments on the photodetector's mount may then be turned until the sine wave's amplitude is maximized. The quality of the signal is also a function of the scatter plate's exact location. Tiny movements of the plate can greatly affect the signal (this problem does not occur with a seeded fluid, since the fluid is continuous throughout the test volume). The signal produced by a seeded fluid when observed on the oscilloscope is much less distinct and is more ambiguous than that from the scatter plate. This author, for the LDV experiments to be described in this thesis, did not find the oscilloscope to be a very useful tool for fine adjusting the system. Instead, the system was adjusted by maximizing the SAMPLES PER SECOND indication. The technique used to perform this adjustment was to turn the fine adjustment screws on the photodetector's mount in one direction until the data rate decreased to some particular value, then to turn the screws in the other direction until the rate increased and then decreased to the same lower value again. Then the screws were simply turned to the mid position between these two extremes. The focus may also be adjusted in the same way. However, since there is no screw adjustment available, pencil marks were made on the dovetail track at the two ends of the mount's travel where the same lower data rates were obtained. Then the mount was placed at the mid

position. (Before moving the mount, a mark should be made to show its original position. This will help in regaining the signal if it should be lost.)

As an example, for an experiment of the type described later in this paper, the data rate, indicated on the meter, oscillated in the range of 0.4 to 0.8 (X 10^3) counts per second. The adjustment screws were turned in both directions until the rate dropped to about the 0.1 level. There was a one-half turn difference for the screws between these extremes. The focus adjustment required about a one-half inch travel between the 0.1 data rate extremes. Thus, at least for this experiment, a confortable adjustment range was available within which the data rate remained high, so that extreme care in adjustment was not required. The photomultiplier's voltage setting can also be checked by observing the data rate. The voltage should be changed in any direction that increases the sample frequency, but not turned so high as to saturate the tube. (Changing the voltage will require adjustment of the tracker's gain level.)

If the aperture of the photodetector is covered over (one of the black plastic lens covers works well) and the gain of the Model 1090 increased to the near out-of-range level, a signal generated by the Model 985's downmix circuit will feed through at a level that the Model 1090 can track. This signal, if observed on an oscilloscope,

looks like a very clean sine wave. As explained previously, use of the frequency shifter results in an apparent velocity reading even at zero particle velocity. Thus, the voltage output of the Model 1090, when tracking this signal from the Model 985, represents the zero velocity frequency, f_o, to be inserted in Equation 24. Due to inaccuracies in the various instruments, the output voltage does not correspond exactly with the downmix frequency set by the Model 985. For an example, when the Model 985 was set for a 20 KHz shift, the tracker's output should have been exactly 2 volts (20 KHz X 0.1 V/KHz = 2 V). However, the actual output (as indicated by a digital meter) was 1.96 volts. Thus, this offset voltage should be subtracted from the indicated voltage of a velocity measurement to give the voltage attributable to the particle's velocity. For actual data reduction, Equation 24 was modified to the form

$$\text{Velocity} = \left| \frac{V - V_o}{S.F.} \right| d_f \qquad [25]$$

where V is the indicated voltage, V_o is the zero velocity offset voltage, S.F. is the "Scale Factor" (e.g., 0.1 V/KHz), and d_f is the fringe spacing, as before. Using the actual output voltage of the tracker at zero velocity rather than the nominal voltage is especially important when flow velocities at and near zero are encountered, since the relative size of the error is greatest at zero

velocity.

Details of the alignment of the test volume to an experiment and on data reduction will be explained when an actual experiment is presented in CHAPTER III.

CHAPTER II

DESIGN OF EXPERIMENTS

A. Introductory Remarks

The experiments to be considered in this thesis were performed to support a specific research project. This project is concerned with natural convection flows within a two dimensional enclosure. The enclosure consists of an isothermal vertical heated wall (the "hot wall"), an isothermal cooled wall (the "cold wall"), and adiabatic top and bottom surfaces. The aim of the research is to find shapes for the cold wall such that the heat transfer rate across the cavity by natural convection is maximized or minimized for a given length (greater than the vertical height) of the cold wall. The wall shapes are to be predicted analytically and the predicated shapes tested experimentally. In the course of analytically predicting the wall shape, the fluid temperature and velocity distributions as well as the total heat transfer rate are determined. The accuracy of the analytical solutions can be checked by comparison with experimental measurements. Thus, the MZI was to be used to determine the fluid temperature and heat flux distributions and the LDV used to measure the fluid velocity distribution. An experimental apparatus containing a test cavity approximating the ideal

cavity was designed and constructed. Since the MZI and LDV were relatively new additions to the Natural Convection Laboratory, it was necessary to gain proficiency in their use and confidience in their output data. Therefore, a series of experiments was performed using only a plane vertical cold wall in the test cavity. The plane wall is designed to be replaced with a curved shape to fulfill the original intent of the research. In this chapter, the apparattuses used for these preliminary experiments will be described and their operation explained.

B. The Two-Dimensional Enclosure Experiment

Basic Design Features

A cross-sectional view of the internal enclosure test apparatus is shown in Figure 22. The actual test space is defined by two vertical plane walls made of copper, two horizontal insulating surfaces made of balsa wood and styrofoam, and (not shown in the figure) glass windows to seal the two ends of the enclosure.

The spacing between the two vertical walls is variable. This allows the aspect ratio (height/width) of the cavity to be changed. The height of the cavity was chosen, somewhat arbitrarily, to be 40 millimeters (1.575 inches). It was desired to keep the wall size relatively small to help alleviate potential difficulties in manufacturing the curved wall and also to allow the length

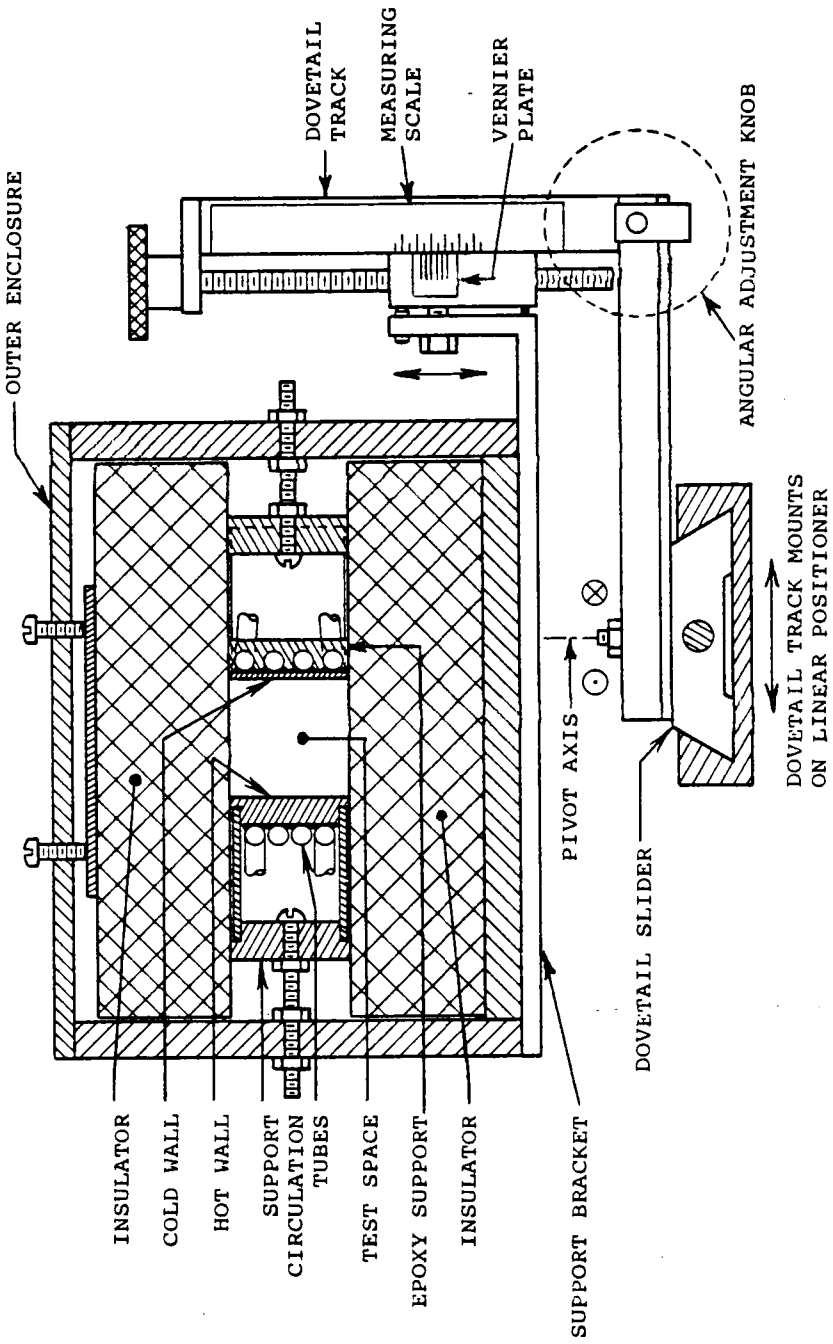


Figure 22. Cross sectional view of the test enclosure and the support arrangement.

of the cavity (its dimension normal to the paper in Figure 22) to be fairly large relative to its height or width. This helps to minimize the magnitude of the end effects that disturb the flow from the original idealized assumption of two-dimensionality. The length of the walls is 244.5 millimeters (9.625 inches). However, the distance between the glass windows, allowing a space for gaskets, is approximately 250 millimeters (9.84 inches). The aspect ratio was variable from approximately 0.6 to infinity (vertical walls touching). For the experiments presented in this thesis, only the square enclosure (aspect ratio of one) was utilized.

Design of the Vertical Walls

The vertical walls, since they ideally were to be isothermal, were constructed of copper because of its high thermal conductivity. The two walls are of different designs because it was intended that the hot wall would be permanent while a different cold wall would be needed for each different shape. Each of the walls is part of an assembly that also includes plexiglas "support pieces" the same height as the copper walls and other plexiglas pieces attaching the walls and supports together. Both walls have four 1/4 inch diameter copper tubes soldered to their back faces. These tubes are connected in parallel to headers at each end of the walls. The walls are heated or cooled by

circulating heated or chilled water from either of two Haake Model NK22 "constant-temperature circulating baths" available in the laboratory. The water enters and leaves from diagonal corners of each wall. It was expected that, due to the relatively high flow rate of the water and the relatively small heat flux at the wall, the temperature along the length of the walls would be nearly constant.

The hot wall is 3/8 inch thick and the plexiglas support parallel to it is 1/2 inch thick. As can be seen in Figure 22, the wall and support were milled away on their edges and plexiglas "attachment pieces" were screwed to each to make a rigid assembly. The tilt of the hot wall is adjustable over a small range so that it can be set square to the cavity. The circulating water enters or leaves through two copper tubes (partially shown) that extend through holes in the support piece and through the outer enclosure wall. Plastic hoses connect these tubes to the constant-temperature baths. In retrospect, this method is seen to be poor because these extended tubes are liable to receive strong bending forces during handling of the apparatus which could cause them to bend or break off.

The cold wall is of 1/16 inch thick copper. At the time it was designed, it was not known just how a curved wall shape would be formed. It was hypothesized that a combination of bending of a relatively thin sheet along with finish milling would be used. This wall differs from

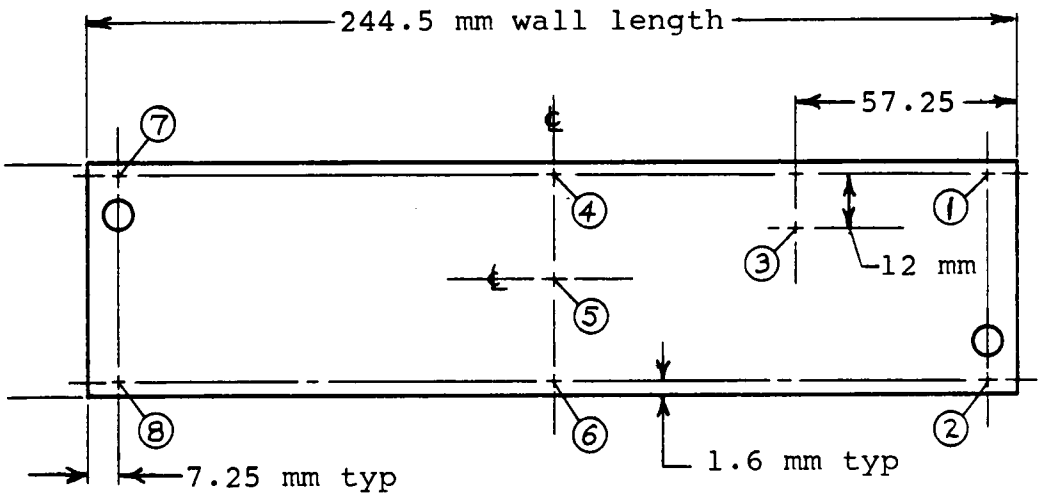
the hot wall in that the attachment pieces (two plexiglas rectangles) are in a vertical plane and are attached to the extreme ends of the cold wall. It was thought that the pieces would eventually be cut to fit the different wall shapes. The cold wall circulating tubes, as can be seen in Figure 22, could be located closer to the top and bottom of the cavity than those in the hot wall. Instead of using the long copper tubes to carry circulating water to and from the cold wall, only short tubes were soldered to the headers. Rubber hoses are attached to these tubes and extend through holes in the wall support pieces and the outer enclosure. Outside the enclosure, the hoses are spliced to the tubing from the circulator.

It was felt that the thickness of the cold wall should be built up to keep the wall from making deep impressions in the relatively soft insulators. This was done by casting a thick slab of epoxy resin onto the back side of the wall. This was accomplished as follows: The copper plate, with the tubes and headers soldered onto it, was placed face down on a flat surface. Two angle irons, with a "release agent" smeared onto their sides, were placed against the long sides of the wall and clamped in place. The plexiglas support piece with the two attachment pieces screwed to its ends was placed in position above the wall (the two attachment pieces touched the extreme ends of the plate). Thus, a "dam" was formed by the two angles and two

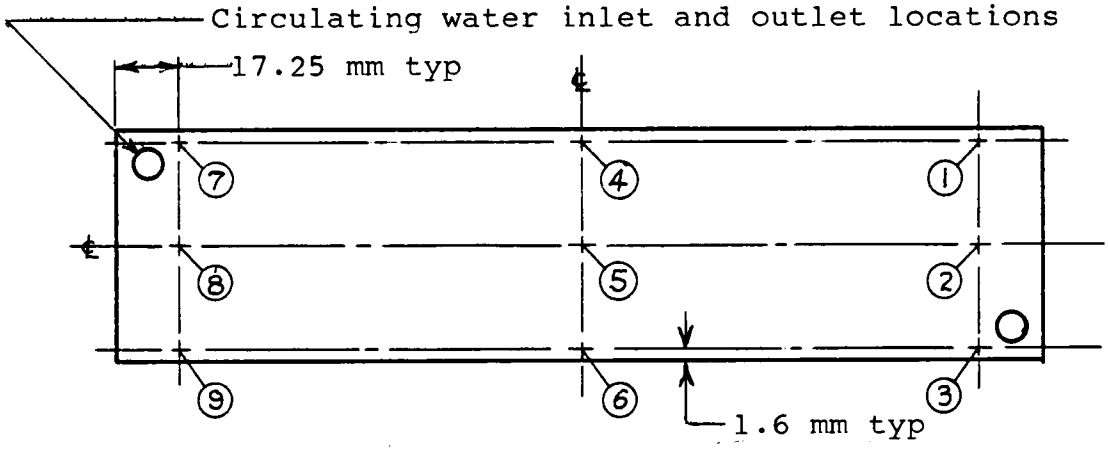
attachment pieces. Epoxy resin was poured over the back of the wall and allowed to harden; this epoxy is what holds the attachment pieces to the wall. The copper plate, as well as the attachment pieces, were thoroughly cleaned and degreased with solvent before the epoxy was poured. With the epoxy, the wall is approximately 1/2 inch thick.

The Thermocouple System

In order to measure the temperatures of the walls and to check for uniformity of temperature, numerous thermocouples were attached to the hot and cold walls. The locations of these thermocouples along with their reference numbers are shown in Figure 23. The thermocouples are made from 36 gauge copper-constantan wire. A number 60 drill bit (0.040 inch) was used to drill from the back sides of the walls to within about 0.75 millimeter of the wall faces. The couples were attached by dipping them into cyanoacrylate adhesive and then inserting and holding them in the holes for the few seconds it takes for the adhesive to set. Some of the holes, particularly in the cold wall, were then covered over with epoxy cement. The couple wires extend through holes in the support pieces and through the outer enclosure. The leads are about 8 feet long and terminate in plug-in connectors. The connectors are plugged into sockets in a thermocouple reader panel which was assembled in the Natural Convection Laboratory. The



A. Hot wall, view from back side



B. Cold wall, view from back side

Figure 23. Thermocouple locations on the hot and cold walls and their identifying numbers.

panel has 48 input connector sockets and a switching arrangement so that any one of these sockets can be selected for reading. Temperatures can be read directly from an Omega Model 200 digital thermometer, reading in Celsius degrees to a resolution of 0.2 degree, or a separate potentiometer can be connected for the actual voltage measurement. The panel has connections available for a reference junction which was needed when using the potentiometer. An Omega Model TRC "ice point reference cell," a thermoelectric refrigeration device, is also available for conveniently maintaining the reference junction at the ice point. All thermocouple wire, connectors, switches, the digital meter, and the ice point cell were obtained from Omega Engineering, Inc.

The potentiometer used for the thermocouple potential readings is a Leeds and Northrup Millivolt Potentiometer, Model 8686 (serial number 1726393). It is graduated to 0.005 millivolt, but a resolution of 0.0025 millivolt was generally maintained for all readings.

Design of the Horizontal Walls

The insulators forming the top and bottom surfaces of the test enclosure are formed from styrofoam blocks with a thin layer of balsa wood glued to the sides that face the test space and to two ends. These blocks are approximately 1 13/16 inch thick. The insulators were initally intended

to be solid balsa, but styrofoam was chosen since the thermal conductivity of styrofoam is roughly 0.6 that of balsa. The styrofoam blocks were cut to size on a hot-wire type cutter that was constructed specifically for this project. The balsa sheets, of 1/32 inch thickness, were glued to the foam to provide a smooth surface and give greater strength to the face of the blocks. The porous balsa was given several coats of "balsa fillercoat dope" (a product usually used in model aircraft construction) to which had been added some talc (baby powder). The balsa was sanded smooth between coats. After the wood was well sealed, several coats of flat black polyurethane paint were applied to the blocks, again sanding the surface smooth between coats.

After constructing and finishing the insulators, it was found that they had warped such that the sides with the balsa facing were distinctly concave. An attempt was made to sand the surfaces until they were flat, but it was found that the insulators, when pressed against the wall assemblies by the compression screws in the top of the outer enclosure, flatten out nicely against the rigid wall assemblies. (The compression screws were turned only finger tight, and the stress was relieved when the cavity was to sit idle for an extended period.)

A brass fill or drain tube of about 5/32 inch diameter was glued into a hole drilled through each of the

insulators. The tubes were made flush with the finished faces of the insulators and are about 3 inches long so that they extend (through holes) to outside of the outer enclosure. The tubes are 1 inch from one end of each insulator and on its centerline. The tube in the upper insulator is designated the "fill tube" and that in the lower insulator the "drain tube". They are oriented to be at opposite ends of the cavity. Smoky air, for the LDV, or a liquid can be introduced through the fill tube, and the fluid removed from the drain tube.

Design of the Support Structure and End Windows

The outer enclosure, which supported the wall assemblies and insulators, has sides and a bottom of 1/2 inch thick aluminum plate and a top of 1/4 inch thick plate. As shown in Figure 22, the walls are held in position by two long screws attached to each of the plexiglas supports with a given spacing maintained by two nuts tightened against the enclosure's side pieces. As previously stated, the cavity is sealed at its ends by glass windows. A detail of the mounting scheme for the windows is illustrated in Figure 24, which represents a cross sectional view through one of the cavity's ends. Large pieces of plexiglas, one inch thick, completely cover the end faces of the cavity assembly; these endpieces were

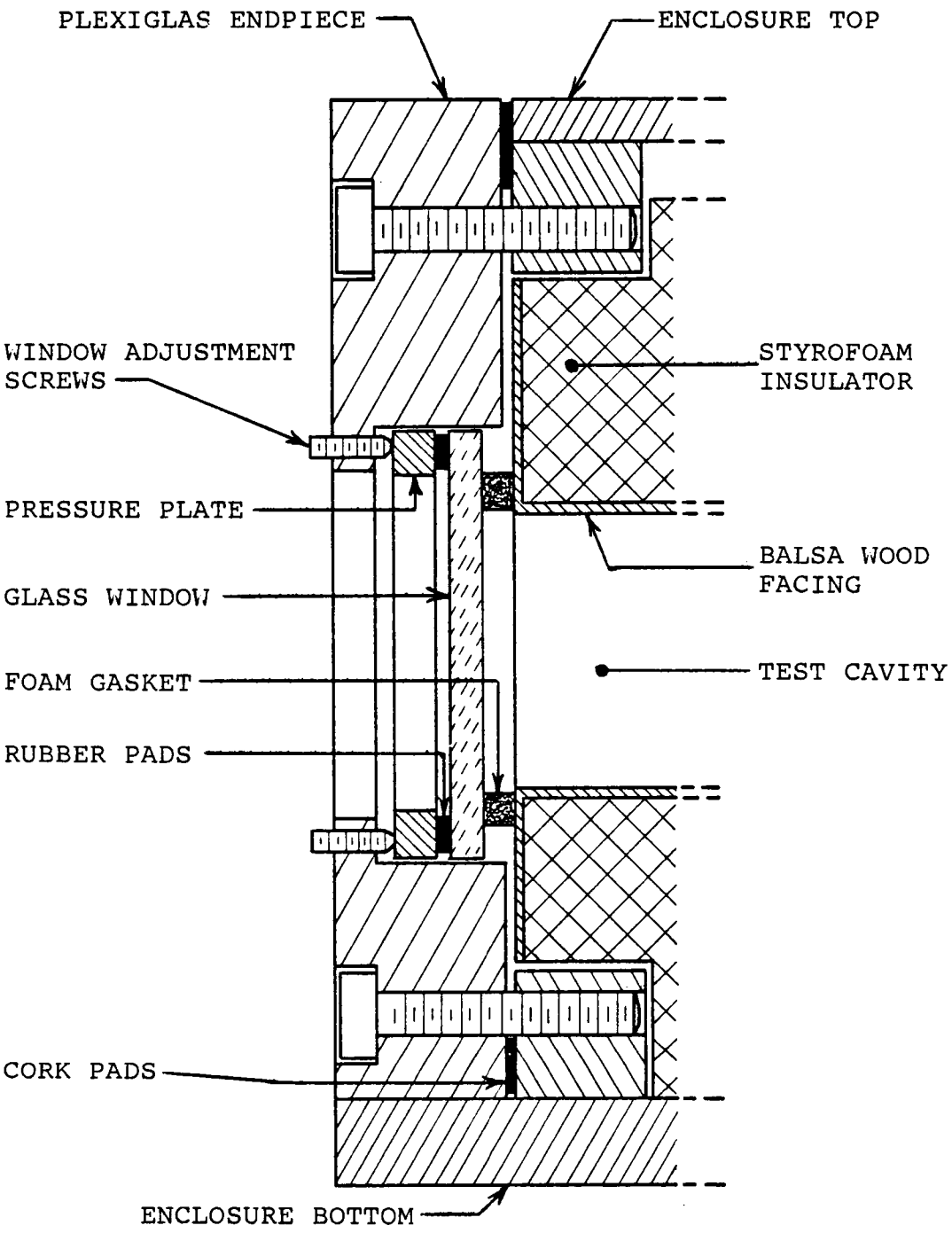


Figure 24. Cross section of the test enclosure illustrating details of the end windows.

held in place by 4 cap screws. Due to small manufacturing defects, parts of the wall assemblies or the insulators needed to extend slightly beyond the ends of the outer enclosure. To keep the plexiglas endpieces from pushing against any protruding parts, four small cork pads were attached to the ends of the enclosure to bear the compression force and provide a clearance gap.

The glass window fits into a 2 1/2 inch high by 4 9/16 inch wide cutout in the plexiglas; the window is slightly smaller than these dimensions to allow free movement within the space. A gasket of easily compressible 1/4 inch thick foam rubber extends around the outside face of the test cavity and seals the cavity to the glass. The gasket is not allowed to protrude past the edge of the cavity so that it does not obstruct any light passing through the cavity. Vacuum grease (a silicone grease) was smeared onto the gasket to seal and to initally hold the gasket in place during attachment of the endpiece.

A steel "pressure plate" of 1/4 inch square cross section transfers the force of the compression and adjustment screws to the glass window. Pads of silicone rubber attached to the pressure plate are intended to uniformly distribute to the window the force applied to the plate. The pads were formed in the following manner. A plexiglas endplate was placed flat on a horizontal surface with the side that normally faces the enclosure facing

upward. The adjustment screws were extended so that the pressure plate, when placed in the cutout, rested on the screws. Next, three small spacers of 1/16 inch diameter wire were placed on the pressure plate at three approximately equidistant locations. Beads of silicone rubber sealer material were then applied over the surface of the plate but did not touch the spacers. The window, with a release agent smeared on its surface, was placed in position in the cutout and pushed downward, spreading out the silicone rubber, until the glass touched the spacers. The assembly was left for the rubber to harden. Later, the assembly was taken apart and the spacers removed. This method of forming the pads ensures that the contact pressure between the pressure plate and the glass is as uniform as possible over the contact area.

Certain aspects of the window and its assembly are relatively important and should be further explained. When a test cavity is inserted into the test beam of the interferometer, the light rays that pass through the cavity will undergo a phase shift (relative to the reference beam) from traversing the end windows and (possibly) from traversing the test cavity length. If the two faces of each window are perfectly parallel, then the phase shift due to the windows will be the same over the area of the cavity and only a constant value will be added to the shift due to the length of the cavity. The absolute fringe shift

at one point (of the cross section) is of no particular interest. It is the fringe shift difference between two locations that is important and is used in Equation 11 or Equation 13 to calculate the temperature distribution. Thus, with the windows introducing a uniform shift, no error is introduced due to this shift. If the window glass is not of uniform thickness, then a variable fringe shift will be added to that due to the test fluid. Properly, this shift should be separately determined (such as when the cavity is isothermal) and later subtracted from the total shift. In practice, this is a difficult and troublesome operation to perform. It is generally considered much better to use windows of sufficient flatness so that this effect can be neglected. Just how flat the glass should be, of course, depends upon the accuracy desired in a particular experiment as well as the accuracy of the MZI's own optics. The size of errors in an optical surface is usually expressed as the equivalent number of wavelengths of light, presumably in the wavelength of greatest interest. An "interferometric quality" test window for a typical experiment might be 1 inch or more thick (for rigidity) and polished flat to within 1/4 wavelength and cost roughly $500 or more. For preliminary experiments, at least, it would be highly desirable to use a much less expensive and more expendable piece of glass. For the experiments involving the test

cavity described in this paper, end windows of ordinary "float" window glass were used. The glass was readily available and could be cut to size (by one vendor) only in 3/32 inch, 3/16 inch, and 1/4 inch (approximate) thicknesses. Pieces of the glass were held in the test beam of the MZI when it was adjusted for wedge fringes, and the straightness of the fringes examined in the output image. No numeric evaluation of flatness was made, but the 1/4 inch thickness glass was judged to be relatively "poor" while the 3/16 inch thickness was considered to be "suprisingly good." Since the 3/16 inch thickness was judged acceptable, the 3/32 inch glass was not considered for use because of its relative fragility.

Since the 3/16 inch thickness is relatively thin, only light pressure should be exerted upon it. The gasket joining the glass to the cavity is cut from a piece of easily compressed foam rubber intended for use as a door seal. The gasket has to conform to the irregularities present when the two walls and two insulators are joined. Solid rubber and cork gaskets were judged absolutely unacceptable.

There are three window adjustment screws; one bears on the top leg of the pressure plate and the other two bear on the bottom leg. The screws are turned until the window is "snug" against the gasket.

For some experiments, it may be desired to have the

cavity airtight. Airtightness of the cavity can be determined by checking whether it will hold a slight positive pressure. A plastic tube can be run from the cavity drain tube, and its end submerged a small distance in a vessel of water. A squeeze bulb air pump can be used to pump air into the cavity fill tube. The air will bubble out of the submerged tube end. If the water surface within the tube remains below the level in the vessel after pumping is stopped, then the cavity is reasonably airtight. If it is not, tightening the window adjustment screws may help. A "leakproof" enclosure is really not essential if the test fluid is simply air.

The two windows need to be adjusted so that they are perpendicular to the cavity's axis in order to make the physical path length between the windows the same over the entire cross-sectional area of the cavity. This requirement ensures that any fringe shifts will be due only to temperature variations and not to physical path length differences (assuming that the glass is flat). This adjustment is particularly critical if fluids of high refractive index, that is, liquids, are used in the cavity. A method for checking for adjustment of the windows will be presented when setup of the experiment is presented in CHAPTER III.

Design of the Positioning System

During the inital trials with the cavity assembly, it became obvious that some convenient means was needed whereby the cavity could be positioned within the MZI's test beam and then easily repositioned along the optical axis of the LDV. Present within the laboratory is a "vibration isclation table." It is a table with a 40 inch wide by 80 inch long by 4 inch thick granite top. This top, which normally rests on a steel frame, can be "floated" on gas bags inflated from a high-pressure nitrogen bottle. The inertia of the granite slab plus the "softness" of the gas bag supports tend to isolate whatever is supported on it from the vibrations always present within a building structure. It seemed that, with the table adjacent to the MZI and with its long axis parallel to the MZI's optical axis, the LDV system could be set up along the length of the table, and the cavity could simply be translated a distance of about 2 feet between the optical axes of the two instruments. To translate the cavity this distance, a "linear positioner" or "track" with a "carriage" on it was designed and constructed. This track is shown in Figure 25. It consists of a channel-shaped aluminum frame, 44 inches long, with two 0.75 inch diameter round-ways, 40 inches long, attached to it. A 6 inch by 8 inch "carriage" supported by four linear motion ball bearing pillow blocks, support an experiment

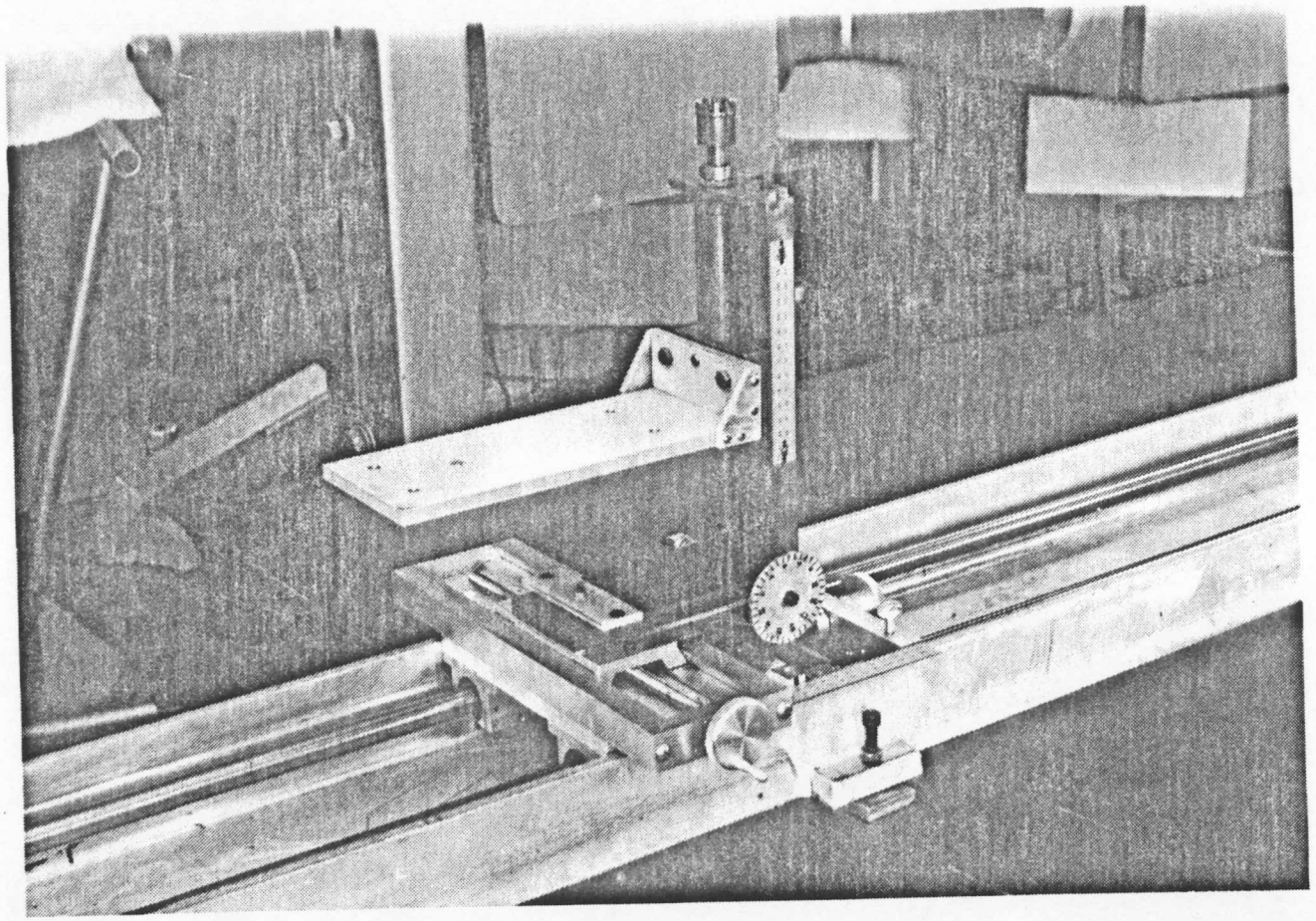


Figure 25. The "linear positioner" or "track" with the "carriage" for supporting and transporting the experimental device.

and allow it to be moved along the length of the track. To reach the test section of the MZI, part of the track is cantilevered over the edge of the table. The track rests on three leveling or adjustment screws, two on either side of the channel frame near the table's edge next to the MZI and the other in the frame's center at its other end.

As stated previously, the LDV system is rather large and divided into two separate parts. Thus, it is more practical to leave the probe volume stationary and to move the experiment about relative to it than to move the LDV relative to a stationary experiment. A dovetail track and slider, shown in cross section in Figure 22, was purchased and attached to the carriage. This slider allows the cavity to be translated in the direction that is parallel to the optical axes of the instruments (the "z-direction"). Also shown in the figure is a vertical dovetail which provides height adjustment of the cavity. Horizontal motion of the cavity is effected by moving the carriage along the track. A fine adjustment screw device was added to the carriage to aid in positioning the cavity.

Since it is necessary to know the position of the LDV probe volume relative to the cavity, measuring scales were attached to the three linear positioning devices. The scale attached to the vertical dovetail is shown in Figure 22. The scales are 150 millimeters long and are graduated to 0.5 millimeter. A vernier plate attached to the

vertical dovetail's slider allows reading the scale to 0.02 millimeter. The vertical scale is attached by two screws in slots at its ends; it can be moved over a small range for "zeroing" onto a whole number on its scale. The scale attached to the z-axis dovetail is simply attached with double-sided tape. A pointer attached to the slider indicates position (no vernier is used). The third scale is attached to the channel frame by special holders that clamped onto one of the flanges. A bracket attached to the carriage supports another vernier plate for reading this scale.

It is important that the enclosure be easily rotatable about a vertical axis. This was not so important for use with the LDV (which can itself be moved about fairly easily), but the enclosure's walls have to be adjusted closely parallel to the light rays when in the MZI's test section (the MZI cannot be moved about easily). Thus, an "angular adjustment" was added to the assembly. The arrangement to provide this adjustment is (partly) shown in Figure 22. A thin aluminum plate is rigidly attached with screws to the z-axis dovetail slider. A small screw extends upward from a hole drilled in the plate at the center of the top surface of the slider. A thicker steel plate rests upon the thinner aluminum plate and contains a hole to pass the extended screw, which acts as a pivot axis. The vertical dovetail is attached to the end of this

thicker steel plate which, thus, supports the enclosure assembly. The length of the steel plate was chosen so that the center of gravity of the enclosure and support assembly would be located approximately along the pivot axis, for ease of rotation. An "angular adjustment knob," shown in dashed outline in Figure 22, was attached to a screw that, when rotated, causes the steel plate and the cavity to rotate (this screw is threaded through a piece attached to the end of the thin aluminum plate, and the screw bears against the steel plate). The adjustment knob is graduated each 10° so that a chosen angular position can be relocated. This will be further explained when set-up of the cavity is described.

C. The Vertical Flat Plate Experiment

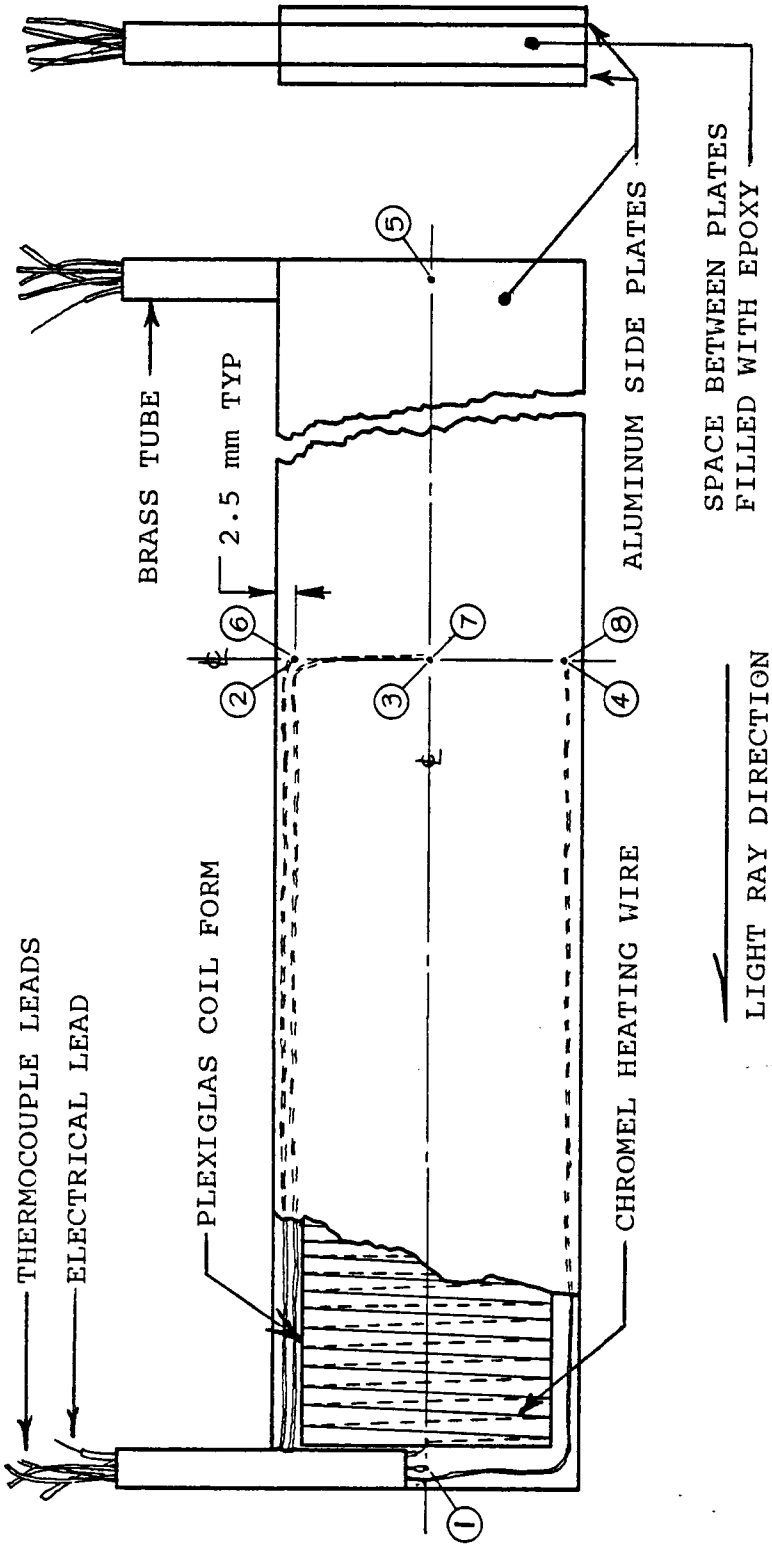
As previously stated, the wall heat fluxes were obtained by differentiation of the temperature profile measured with the MZI. Taking the derivative of experimental data, however, generally results in an increase of the percentage error (over that percentage error in the undifferentiated data). Thus, values of heat flux obtained from the MZI were considered to be the least accurate data to be obtained from this instrument. In order to check the instrument's accuracy, an electrically heated wall or plate was constructed. The electrical power input to this plate can be measured with good accuracy, and

the radiative heat loss estimated. The difference between these two quantities is the convective heat loss. Only the convective heat loss is measured by the MZI. Thus, the optically measured value can be compared with the directly measured (and calculated) value of heat transfer.

This plate, which is illustrated in Figure 26, was made the same height and length as the hot and cold walls and was intended to be inserted into the test cavity (thereby forming two test cavities); however, inital measurements with this plate indicated that a "very significant" heat loss from the plate was occuring from its top and bottom into the "insulators" (the indicated error was about 40%). No further measurements were made with the plate within the test cavity; the plate was used suspended in free air only.

At the center of the plate is a plexiglas form with chromel resistance wire wound on it with a 0.1 inch pitch. This coil is contained between two aluminum side plates that had been accurately milled to the proper dimensions. Pieces of paper are used to insulate the wire from the aluminum plates.

Each plate has four thermocouples attached to it. The numbering scheme for these couples (the way the plug-in connectors were numbered) is shown in Figure 26. Couples numbered 1, 2, 3, and 4 are attached to the near side-plate in the figure; couples numbered 5, 6, 7, and 8 are attached



Note: Couples 1 to 4 are in the near side-plate; couples 5 to 8 are in the far side-plate.

Figure 26. Cutaway view of the electrically heated vertical plate.

to the far side-plate. This numbering scheme is valid when the plate is turned so that the test section light rays are traveling in the direction indicated by the arrow. The couples that are near the edges of the plate are in 0.040 inch diameter (No. 60 drill) holes drilled 2.5 millimeters from the edges and drilled to about 0.75 millimeter from the plate's faces. It would have been desirable to install more couples, but only eight were used because of the difficulty of routing the wires. The thermocouple wires and the heating wire leads exit from the plate through brass tubes at each end of the plate.

The parts making up the plate assembly were sandwiched together and held by clamps. Then the interior of the plate was poured full of epoxy resin; this was done to hold the parts together as well as to improve the heat transfer between the heating coils and the aluminum plates. It should be apparent that, since plexiglas and paper and epoxy were used in the construction of the plate, the plate temperatures should be kept at moderate levels.

CHAPTER III

ASSEMBLY AND OPERATION OF EXPERIMENTS

A. Preliminary Remarks

The electrically heated vertical plate and test enclosure represent typical external and internal natural convection flows, respectively. In an external natural convection flow there is a heat transfer between an object and a fluid that is very large in extent compared to the object, while in an internal natural concection flow, the fluid is completely surrounded by solid surfaces. The plate experiment was originally built only to check the heat flux measurement accuracy of the MZI. It is, however, important in itself since it is a different flow situation from the cavity and can be used to illustrate a different data reduction technique.

The setup and operation of the heated plate within the MZI will now be described.

B. The Heated Vertical Plate Experiment

Introduction

The heated plate was used for five experimental "runs." As previously mentioned, one experiment was performed with the plate in the enclosure while the remaining experiments were performed in free air. The final test run should have been the most representative

one, since knowlege that was gained during the previous runs was available for guidance on the final run. The following discussion describes the procedures followed for the last experimental run with the plate, though many parts of the procedure were common to all of the runs.

Preparation of the Plate

It had been noticed that the sides of the plate were not particularly flat; evidently they had been warped when clamped together during inital construction. An attempt was made to flatten the sides by rubbing the plate against a piece of sandpaper placed on the granite table. After grinding both sides for a while, the plates were checked by placing a steel straightedge on each of the sides at various locations, both parallel to the edges of the plate as well as on each diagonal. It was found that a 0.001 inch thick shim could not be slipped under the straightedge at any point on one side of the plate and could be slipped under on the other side only within a small region. This was considered to be an adequate measure of the flatness of the plates.

During the first four experimental runs, the aluminum sides of the plate had been left "shiny" (they had been sanded smooth). The calculation for radiative heat loss requires a value for the emissivity of the surface. The value of this property can vary by a factor of 2 or more

for a shiny surface. Thus, it was desired that for this final experimental run, the emissivity value should be more dependably known. It was, therefore, decided to coat the wall with a layer of lampblack, whose emissivity value is rather consistently reported as about 0.95. Some attempts at coating the wall were judged unacceptable. The technique that was finally used was to collect lampblack from a piece of steel held within a candle flame. This was mixed with alcohol in a minature, improvised ball mill for a few hours, and then painted onto the wall. The resulting coating had poor adhesion; however, since the wall was generally not touched, it was adequate.

Mounting the Plate

For all of the experimental runs made in free air, the plate was suspended within the test beam by use of two, approximately L-shaped pieces of steel rod that were attached to the top of the test cavity's outer enclosure. This is illustrated in Figure 27. The shorter leg of the "L" was bound, by loops of wire, to the upright brass tubes at the ends of the plate; the longer leg of the "L" was clamped down by the compression screws in the top of the enclosure. Thus, with the plate mounted off of the cavity, the cavity's range of motions, expecially the angular adjustment, were available to the plate.

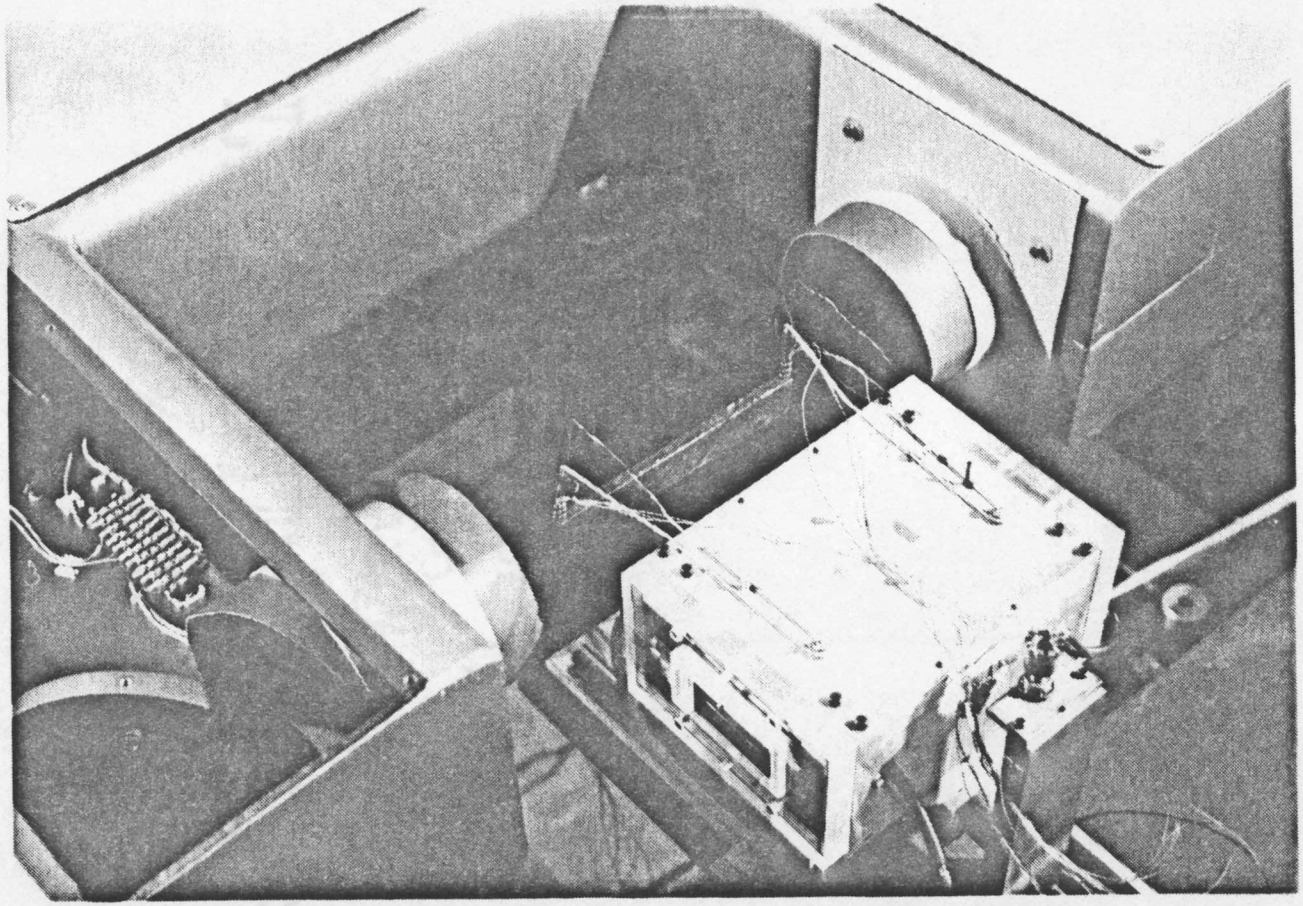


Figure 27. The vertical plate mounted on the enclosure package and within the test beam of the interferometer.

Power Supply

A regulated direct current power supply, a Lambda Model LPD-422A-FM, was used to supply power to the plate. Its output potential is continuously adjustable from 0-40 volts; while its maximum output current is 1 ampere. Current flow was measured with a Weston AC or DC ammeter (Model 370, No. 8639). Its measurement ranges are 0-1 and 0-2 amperes, and it is graduated to 0.01 ampere on the 0-1 scale.

Approximately 4 foot lengths of relatively heavy copper wire were used to connect the plate's leads to the power supply (and to the meter). A pair of "5-way" binding posts was clamped onto the plate's leads for the connection. The copper wires were taped to the L-rods to keep them from pulling on the plate.

Camera Alignment and Focusing

The small output relay mirror on the MZI was adjusted so that the centerline of the output cone of light was parallel to the floor. Then the camera's stand was adjusted so that the camera was at the proper height for the output beam, and the camera and stand were adjusted so that the film plane was perpendicular to the centerline of the output light cone (using the "Camera Alignment Tool").

The plate was moved into the test beam, turned into approximate alignment with the beam, and centered within

the beam (with the camera correctly positioned, the X-mark on the ground glass marked the center of the beam).

Next, the camera was focused. The technique described in CHAPTER I was used. A piece of cardboard, holding a transparent plastic scale, was "saddled" over the plate at the plane that was to be in-focus. As explained in CHAPTER I, Hauf and Grigull [4] report that the correct focusing plane is at L/2; whereas, Mehta and Black [5] and Wilkie and Fisher [3] conclude that it should be at 2L/3. For the previous experimental runs, the camera had been focused at L/2. For the run described here, however, the 2L/3 focusing location was used. Thus, the scale holder was placed at 163 millimeters from the end of the plate that was nearest the light source. The camera was moved back and forth on the dovetail track while the image of the scale was viewed on the camera's ground glass screen through the 7X magnifier. The reference beam was blocked during focusing. The best focus point was found to be at 25.8 on the dovetail's scale. A photograph made with the scale holder in position is reproduced in Figure 28. This photograph could be measured to determine the scale factor of the image.

The photographs for all experimental runs were made with Polaroid Type 55 Positive-Negative film. This film, besides providing the usual positive print, also provides a "recoverable" negative. This positive-negative film was

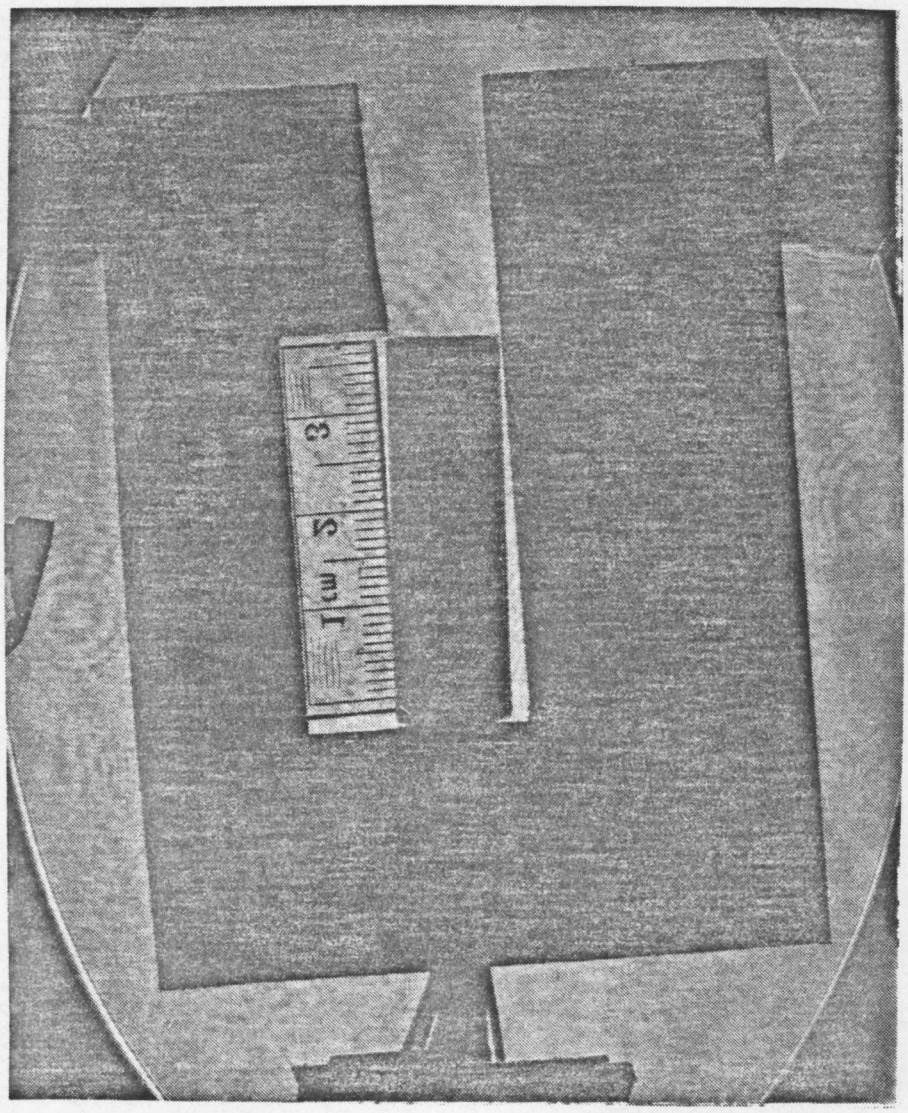


Figure 28. Exposure for scale factor determination and to illustrate focusing.

used because the resolution of the negative is about 6 to 7 times better than that of its print (and presumably better than that of a print from any print-only film). All measurements or data values were obtained from negatives. Information on the operation of the camera is presented in Appendix C.

Plate Alignment

After the focusing step, the plate was adjusted so that its sides were vertical. A plumb line was used for this adjustment. A very fine copper wire was attached to one end of a metal bar that was placed on top of the interferometer's frame. At the other end of the wire was attached a piece of steel, a plumb bob, which was suspended near the floor. The plumb line could be moved about within the test beam, and its shadow could be viewed on the camera's screen.

The plumb line was placed as close to the z = L end of the plate as possible (the plate's and the line's supports kept the line a short distance from the plate's end). Then, the line was moved (in the y- or normal-direction to the plate) close to one side of the plate. The camera was moved to the end of its travel on the dovetail so that the plumbline would be nearly in focus. Now, with the line very close to the plate, the image on the screen was examined, using the magnifier, to see how nearly parallel

the plate was to the plumb line. (The plumb bob was suspended within a beaker of water to dampen its oscillations.)

For a coarse adjustment to plumb, the plate was gently pushed in one direction or the other (its method of attachment to the support rods allowed for some play). For a fine adjustment, the adjustment screw at the end of the track was turned. This caused the whole track and cavity, as well as the plate, to be rotated about a horizontal axis. The process of adjusting the plate and examining the image was continued until the side of the plate did not deviate noticeably from parallelism with the plumb line.

After adjusting the plate to vertical, it was moved (the dovetail or the carriage was moved) until its shadow was again centered on the X on the ground glass.

Next, the plate was carefully adjusted to be parallel with the light rays of the test beam. The method used to test for this adjustment will generally be referred to as the "reflection-off-the-wall" method. This method is suggested by Hauf and Grigull [4, p. 267] who state that it can be as good as more elaborate techniques.

This alignment method works as follows. If the test plate is turned to a (relatively small) angle with the light rays, then the rays that hit one side of the plate (the other side will be in a shadow) will reflect off of the plate and thus be deflected at an angle with respect to

the other light rays. If a screen is placed in the light beam on the other side of the plate from the light source, then a bright streak of light will be observed where the deflected rays strike the screen. As the plate is turned toward parallelism with the rays, the bright streak will approach closer to the shadow of the plate on the screen. Thus, the plate is turned until the streak merges with the (shadow) edge of the plate, at which point parallelism is achieved.

The problem with this technique is that as the light streak approaches the wall, it becomes narrower and finally disappears just as the plate reaches parallelism. Thus, some judgement is needed in deciding when to stop turning the plate or wall.

Clearly, the plate (and later the cavity) must be aligned in two directions; that is, by rotations about two axes. Alignment of the (vertical) sides of the plate requires a rotation about a vertical axis. This rotation is available by turning the angular adjustment knob, which was described in the last chapter. Also, the top and bottom of the plate must be aligned, which requires a rotation about a horizontal axis normal to the test beam. This adjustment was effected by turning one of the two track adjustment screws that was on the track's side and, hence, caused primarily a rotation about the horizontal axis parallel to the track (and approximately normal to the

test beam). This screw had no angle scale attached to it since the accuracy of its setting was not considered to be as important as that of the other angle adjustment.

In aligning the plate, two variations of this reflection-off-the-wall technique were used. With one technique, the dust cover was removed from the top of the MZI frame and a piece of paper (the screen) was suspended from a small rod within the MZI's test beam between mirror M2 and beam splitter BS3. This is shown in Figure 29. With the screen at this position, one person could clearly observe the screen while simultaneously turning the angle adjustment knob or the track adjustment screw (the two were close together). Thus, one would get immediate feedback as to the effect of a movement of the adjustment knob or screw on the bright streak's location relative to the plate. This is important since one has to estimate just when the streak merges with the wall.

The other variation of the alignment technique made use of a special alignment tool that was designed for this purpose. The operation of this tool is illustrated schematically in Figure 30. This tool consists of a thin metal plate, 1 foot square, from which extends perpendicularly a metal strip nearly 1 foot long. Attached to this strip is a bracket that holds a first surface mirror at a 45° angle from horizontal. This tool is shown in position on the interferometer in Figure 31.

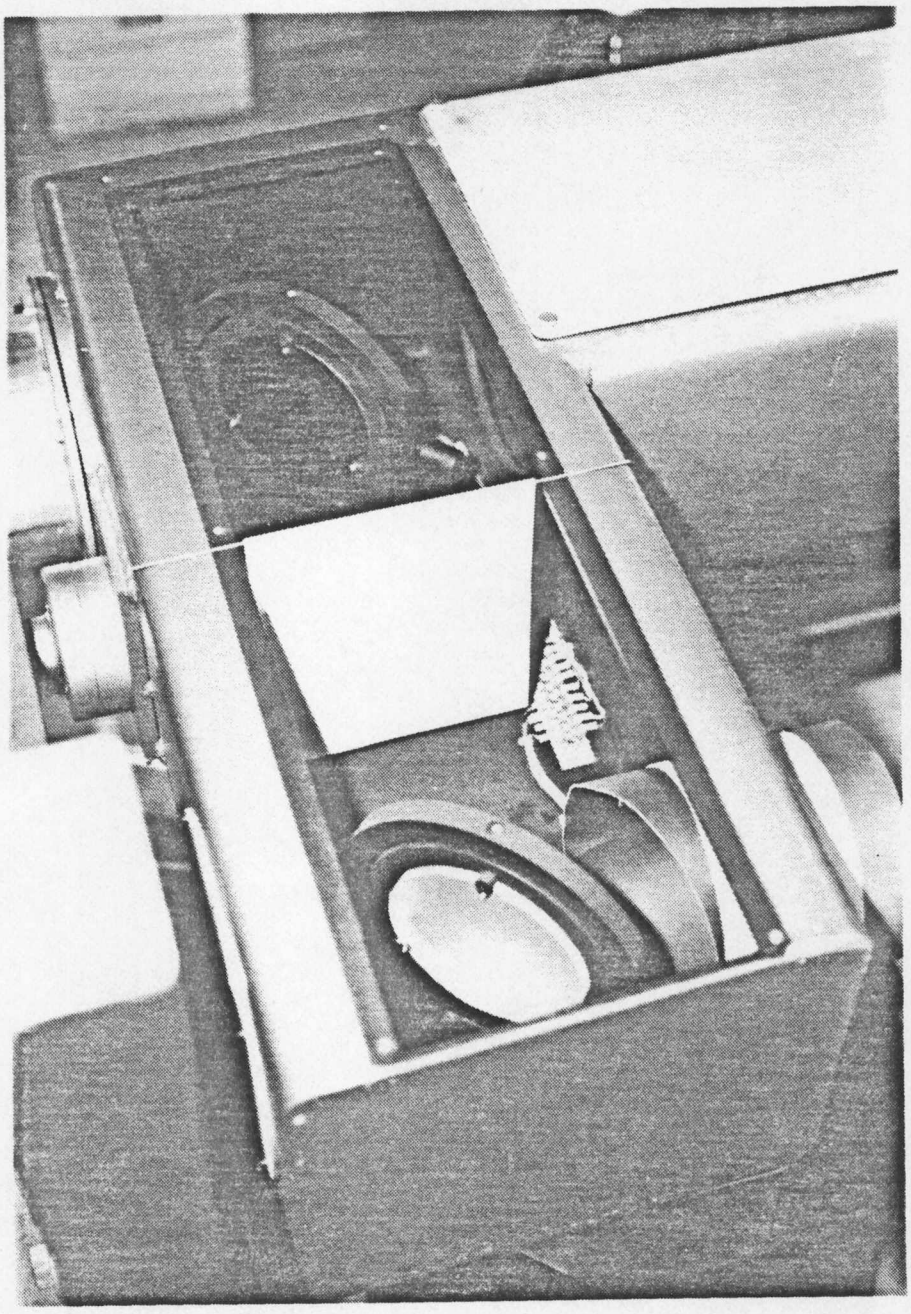


Figure 29. The viewing screen in place in the interferometer for alignment of the experiment with the test beam.

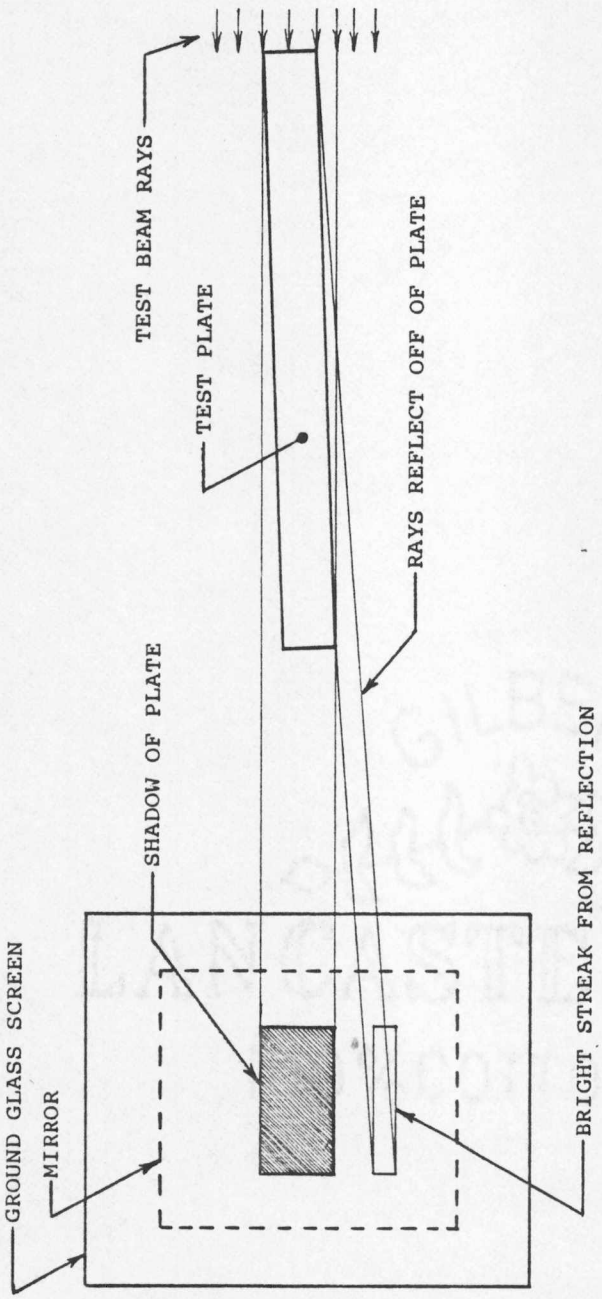


Figure 30. Schematic of the "reflection-off-the-wall" alignment technique and the alignment tool.

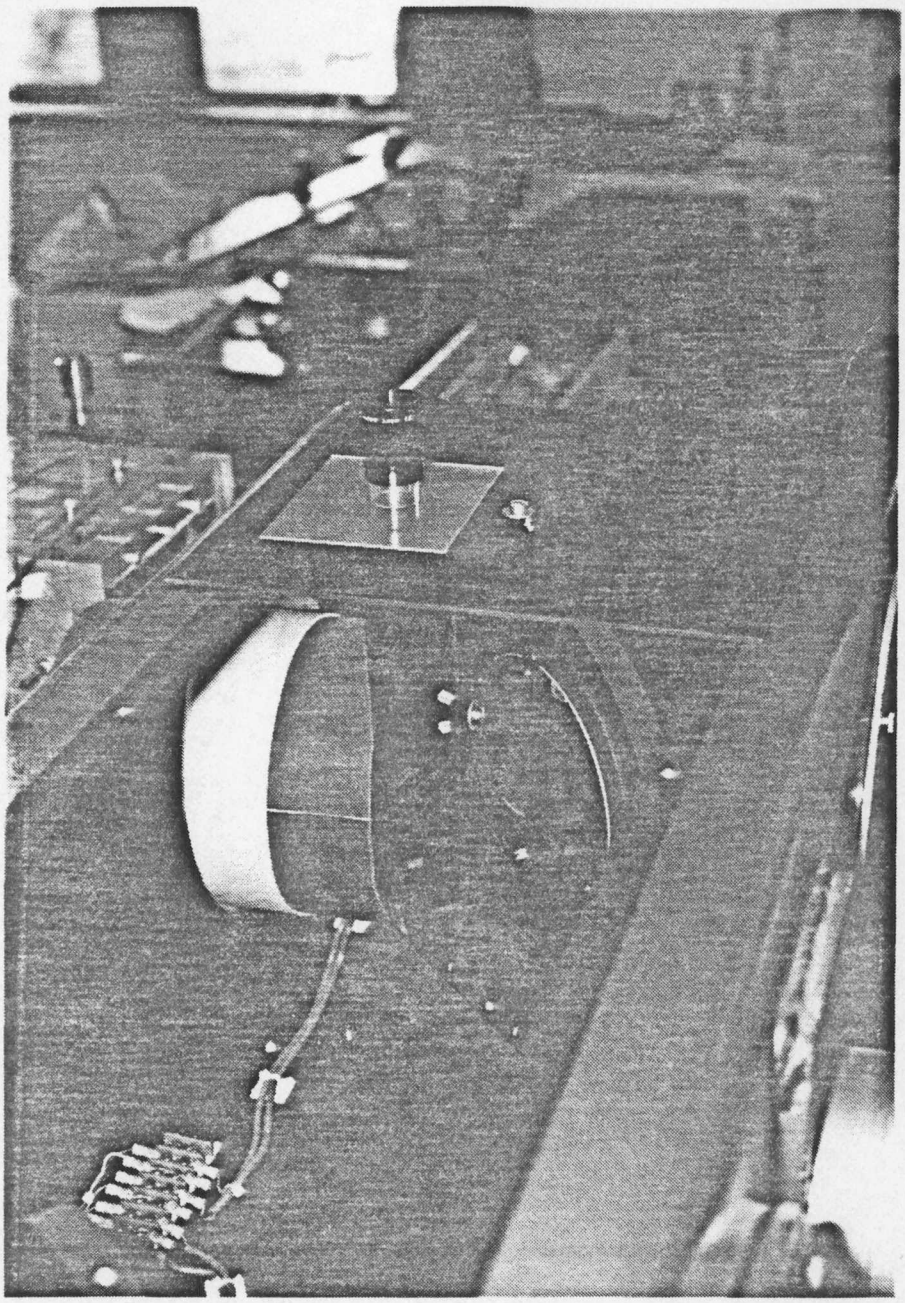


Figure 31. The "alignment tool" in place in the interferometer for alignment of the experiment with the test beam.

In use, the metal plate sits on top of the interferometer's frame near M2 with the perpendicular strip extending down into the frame. The tool is positioned so that the mirror is in the test beam and intercepts the shadow of the test plate (the mirror can be moved up or down on the metal strip to put it at the proper height). Light rays hitting the mirror are reflected upward to the plate, which has a rectangular hole cut in it to pass these rays. A ground glass screen is placed over the hole to view the light reflected by the mirror. (When positioning this tool, one should be very careful not to touch the reflective surface of mirror M2, since the tool must be located very close to this component). The view seen on the screen of this alignment tool is identical to the one seen on the paper screen used in the previous alignment technique, except it is seen in rear projection whereas the latter is seen in front projection. The possible advantage of this tool is that a magnifier, such as the 7X magnifier already used, can be placed on top of the ground glass screen to give a much closer view of the light streak as it approaches the wall.

In Figure 30, the test plate, which is turned at an angle, casts a shadow onto the glass screen. The light rays are shown reflecting off of the side of the plate, traveling away from it, and intersecting the screen where they form a bright streak.

The alignment of the plate to the light rays should be done with relative care. The usual assumption is that the temperature at a given distance from a plate (constant x and y locations) is constant along the length of the plate. Obviously, a light ray should travel parallel to the plate so that the ray's phase shift will be attributable to a single temperature in the test section. However, as explained in CHAPTER I, a light ray traveling in a fluid bends in an arc when a thermal gradient is present in the fluid. Hauf and Grigull [4, p. 266] explain that there is an angular tolerance within which the plate may be aligned with the light rays and within which the error due to the ray traversing regions of different temperature is minimized. Using Figure 6 (p. 28) as a reference, the plate may be aligned parallel to a ray as it first approaches the plate (in the figure, the plate is parallel to ray A at plane Q), or the plate may be parallel to a ray where it leaves the test section (the plate could be parallel to ray A at plane P), or the plate could as well be turned to any angle between these two extremes without incurring more than the minimum error.

In Appendix D, a calculation is presented by which the allowable tolerance is determined. When the values associated with a previous experimental run were used in the calculations, a tolerance of 4 increments of the angle adjustment knob was obtained. That is, there is a 4

increments of rotation difference between the plate being parallel to an incoming ray and parallel to an exiting ray (for rays just grazing the wall). This is for a wall temperature of about 48°C and a room temperature of about 23°C, which were the approximate values expected to be encountered on the present experimental run.

The following procedure is used in aligning the plate. As stated above, the sides of the plate and its top and bottom have to be aligned to the beam, but a rotation of the track adjustment screw (used to align the top and bottom surfaces) would cause a slight rotation of the plate about a vertical axis. Thus, the plate is first rough aligned for its sides, then carefully aligned for its top and bottom, and finally fine aligned for the sides.

For the rough alignment of the sides, the angle adjustment knob is turned so that the light streak is obviously visible on one side of the plate. Then, using either alignment tool, the knob is turned back until the light streak seems to just reach the wall.

For the alignment of the plate's top and bottom, an allen wrench is used to turn the track adjustment (cap) screw. Instead of using an angle scale to indicate location, the orientation of the wrench (such as being at the 9 o'clock position) was observed and noted. The procedure of moving the light streak away form the wall and then moving it back until it just reaches the wall is tried

several times for both the top and bottom. There seems to be a different position of the screw that is best for top alignment and for bottom alignment. The screw should be left at the average of the top and bottom alignment positions.

For the fine alignment of the plate's sides, the value of the angle scale at which the streak reached the wall was recorded for several trials on each side of the plate. For the plate's right hand side (RHS, viewed looking into the test beam) and using the alignment tool, the angle values obtained were: 7.5, 9.5, 10, 8.5, 8, 9, 7.5, and 8. The mean of these values is 8.5. When the alignment was tried using the simple screen in the beam, the values obtained were: 8, 7.5, and 9. The mean of these is 8.2. Thus, the two methods seem to give essentially the same result, though the method using the magnifier is generally trusted more. It was decided to use a value of 9 as the best alignment position; for the plate's RHS, an increase in the scale value turned the plate in the same direction that a light ray near the plate would turn, if the plate was heated.

For the left hand side (LHS) of the plate, the alignment values obtained using the alignment tool were: 1, 2, 2, 3, 0.5, 2, 4, and 2. The mean is 2. The alignment was quickly checked with the simple screen and a value of 2 seemed best. The value 1.5 was chosen as best

alignment for the LHS. Here, a decrease in the scale value turned the plate the same way a light ray near the plate would turn, if the plate was heated.

It is not clear why the alignment values for the two sides differ by so much. Some of the difference may be due to the plate's sides not being closely parallel; however, this factor does not seem to be sufficient to account for all of the rather large difference in alignment values. The main factor may be the observer error in estimating just when the light streak reached the wall.

(When the alignment procedure is being performed, one must be careful not to touch forcibly or to lean against the interferometer; this could introduce a significant error into the alignment if the interferometer and the experiment are separately mounted, since the interferometer can be deflected relatively easily.)

Adjustment of the MZI

The next major step in the experimental run (after again centering the plate in the beam) is to adjust the optical elements of the MZI so that wedge fringes are properly formed. The reference beam is unblocked, and the collimation tool is hung in the light path just before BS1. The interferometer is then adjusted to the infinite fringe condition and also adjusted so that the (two sets) of crosshair shadows from the tool are superimposed. (The

technique for doing this is described in CHAPTER I.) The ground glass screen that is used with the wall alignment tool is suspended in the MZI's output beam at the location where the crosshairs are in-focus, so that the image of the hairs can be clearly viewed (the camera's track is not long enough to reach this point, otherwise the camera's screen could be used). It is recommended that the interferometer be adjusted to this condition (that is, infinite fringe with crosshairs superimposed) before each use. If it is not, after the instrument has been used several times and the optics driven around in various directions, the optics may come to be rather far out of proper adjustment.

Next, the wedge fringes are formed. Since the vertical sides of the plate possess most of the plate's area, it was desired to determine the temperature profiles about the sides of the plate; hence, the fringes were desired to be perpendicular to the plate's sides.

The fringes are formed by the method given in CHAPTER I. With the previously mentioned ground glass screen removed and the camera at the 25.8 setting for focus on the plate, mirror M2 is adjusted in pitch so that some (horizontal) fringes are formed. The crosshair shadows become noticably misaligned. Then, beam splitter BS3 is adjusted in pitch such that the fringe density decreases; this is continued until the shadows seem to be in alignment again (remember that the hairs are out of focus and, hence,

fuzzy at all times). This alignment is reached before the infinite fringe is reached. This process is repeated, first forming the fringes with mirror M2, and then spreading them apart with beam splitter BS3 until the crosshair shadows are again superimposed. As the fringes become finer, it becomes harder to estimate the position of best shadow alignment. It comes to be noticed (with increasing fringe density) that when the shadows are badly misaligned, each shadow by itself is so faint as to nearly disappear. Thus, beam splitter BS3 is adjusted back and forth until the shadows seem to be at maximum density. This fringe formation process is carried out until the fringes reach a density of approximately 2 per millimeter.

For all the other experimental runs, the optics were not adjusted as herein described; instead, they were adjusted to the infinite fringe point, and then wedge fringes were formed by a rotation of beam splitter BS3 only. For reasons described in CHAPTER I, it is best if the two output beams intersect at the camera screen, which they will not do if the method of adjusting only beam splitter BS3 is followed.

After the fringes are formed, they are made perpendicular to the sides of the plate. A small clear plastic triangle, intended for drafting use, is cut to form a square of about 50 millimeters on each side. This square is very carefully taped onto the camera's ground glass with

one side of the square aligned to the plate's right side. Then, the "tilt" of the fringes is adjusted using beam splitter BS3's yaw control until the fringes are parallel to the other side of the square. A magnifier is used to view the square and the plate and the fringes to maximize the accuracy of the adjustment. It was noticed that when the square is viewed along a line parallel to its edge (its thickness), the square seems to disappear except for a very fine line just at its edge. This is used to check for best alignment.

Next, a photograph was made with the plate at room temperature. It is reproduced here as Figure 32; note that the crosshairs of the collimation tool are visible in the picture. The relatively faint concentric circles visible on this and most of the other photographs are probably interference fringes formed from light that scatters off of dirt particles on the optical elements. If mercury light was used, the circles probably would not exist since the requirement for equal optical path lengths would not be met. Thus, exposures made using mercury light are likely to be "cleaner" than those made using laser illumination. For reasons given in CHAPTER I though, only the laser source was used for the experiments described in this paper.

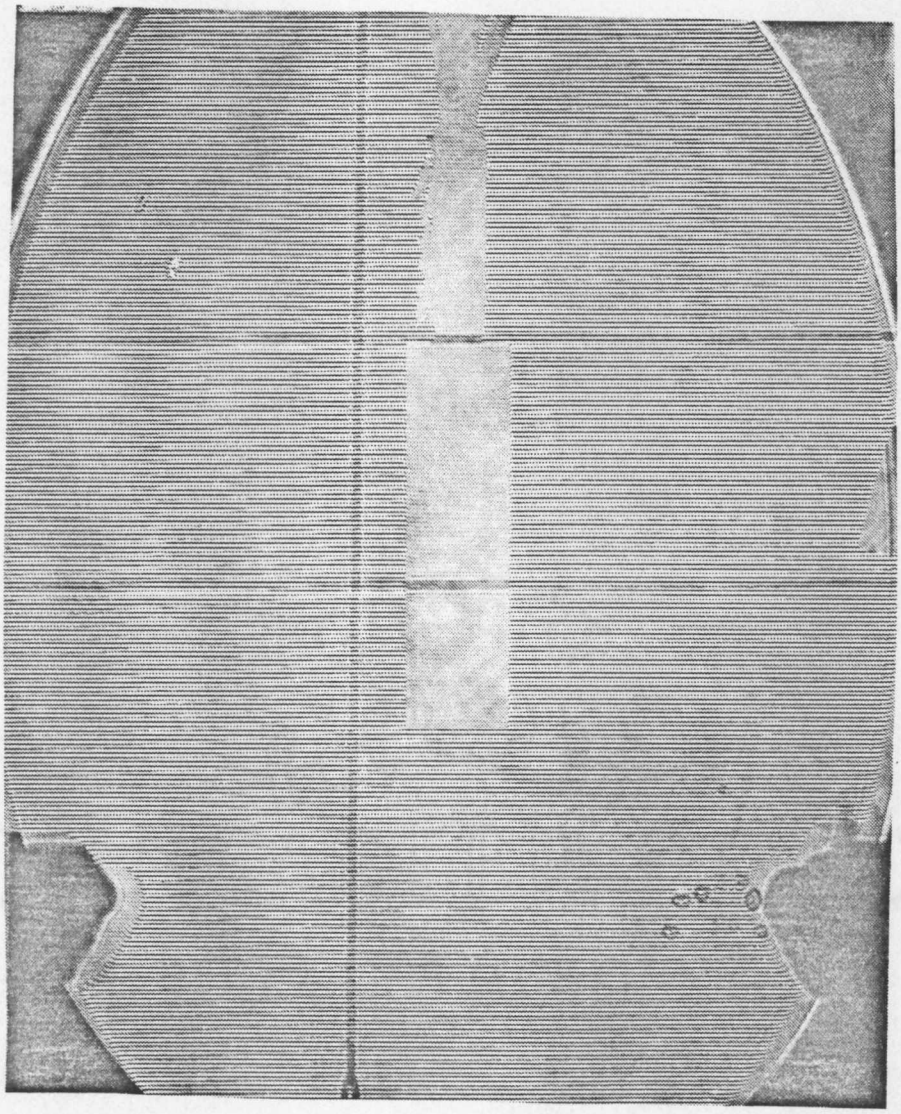


Figure 32. The test plate at air temperature showing straight wedge fringes along with the shadows of the wires of the collimation tool.

Performance of the Experiment

Since the plate was open to the room air, it was desired that the air should be as still and uniform as possible. Thus, the air circulating fans in the air conditioning units in the laboratory were turned off prior to the test (the interferogram exposure). The fans were stopped at 8:05 P.M. on the day the experiment began (this time was actually before the fringe setting process described above was begun). At approximately 12:30 A.M., the electric power to the plate was turned on. The current was set at about 0.8 ampere until the plate warmed up to nearly 52 ^{o}C (as indicated on the digital panel meter (DPM)). This required just about 5 minutes. Then, the current was turned down to 0.48 ampere. Soon, the plate's temperature was observed to be still increasing, so the current was again turned down to 0.45 ampere, where it remained for the duration of the experiment (it was checked occasionally to be sure that it had not changed).

The plate's temperature was measured with its eight internal thermocouples; the free air temperature was measured with three thermocouples. One thermocouple was placed approximately 8 centimeters beneath the center of the plate. A second thermocouple was opposite from the RHS of the plate, at its center and half way up the side. It was protected by an aluminum foil radiation shield, which is just visible to the right in all of the photographs of

the plate. The third thermocouple was taped to the back of the thermocouple reader, away from the plate, with the junction in free air. A mercury-in-glass thermometer was hung from a string in free air at the same height above the floor as the plate and about 1 meter from the plate.

For an experiment of the type described here, it was necessary that the heat loss from the plate be equal to (as closely as practical) the electrical power input to the plate. This means that the plate had to be given sufficient time to reach the steady state condition. So, the temperatures indicated by two of the thermocouples, one (TC #3) in the plate and the other (TC #24) in free air, were recorded at various times. The temperature indicated by the thermocouple which was in the center of the plate on its RHS (TC #3) was of greatest interest; the room air temperature was not controllable.

The following temperatures were observed, as indicated by the DPM.

Time:	TC #3:	TC #24:
1:00 A.M.	53.8 °C	27.0 °C
1:15	54.0	27.0
1:30	54.0	27.0
1:50	54.0	27.0
4:45	53.0	27.0

Thus, since the plate temperature was observed remaining constant for 35 minutes (from 1:15 to 1:50), it was considered to be sufficiently close to steady state so

that the current setting would not need readjusting (the first exposure was not made until 2:35 A.M.). The measurement at 4:45 was made after all of the exposures had been made. Needless to say, it would have been preferrable if the temperature had not changed so much.

The room temperature remained remarkably constant. This may have been because the experiment was performed very late on a July night, when the outside temperature had cooled down to approximately what the inside temperature had been before the air circulators were turned off. If the experiment had been performed during the day, the room would have continued to warm up as long as the circulators were off.

Next, the exposures were made, and the temperature data was taken. The following procedure was used. First, potentiometer (millivolt) readings were recorded for all of the thermocouples along with the time of the reading. The filmholder was prepared but not inserted into the camera. The room was darkened and the camera screen was watched for a period (sometimes several minutes) to observe the steadiness of the air about the plate. Unsteadiness of the air can be clearly detected by the movements of the deflected fringes within the boundary layer about the plate. It was observed that the fringes would remain apparently stationary for a short period (on the order of tens of seconds) and then a disturbance would move through

the fringe pattern. (This observer was careful to keep his own movements to a minimum while watching the fringes.) When it appeared that the fringe motions had died out and a steady period reached, the camera shutter was cocked, the film holder was inserted, and the exposure was made. Then, the film was extracted, developed, and the negative retrieved, cleared, and put in wash water. Finally, the thermocouples were read again, marking the beginning of the next exposure sequence. The couples were read five times for four exposures.

The first exposure was made with the angle scale set at 9, so that the plate's RHS would be in best alignment; this exposure is reproduced here as Figure 33. The second exposure was made with the angle scale at 1.5 so that the plate's LHS would be in best alignment. This exposure is not reproduced here since it is not obviously different from Figure 33.

It was decided that the fringe spacing for the two previous exposures might be too fine. This was suspected since a blurred region existed on both of the previously made photographs along the left side and near the bottom edge. Thus, the interferometer was readjusted to give a wider fringe spacing.

The next exposure was made at this wider spacing. For this case, the angle scale was set to 5.25, which is the average between the 1.5 and 9 settings. This exposure is

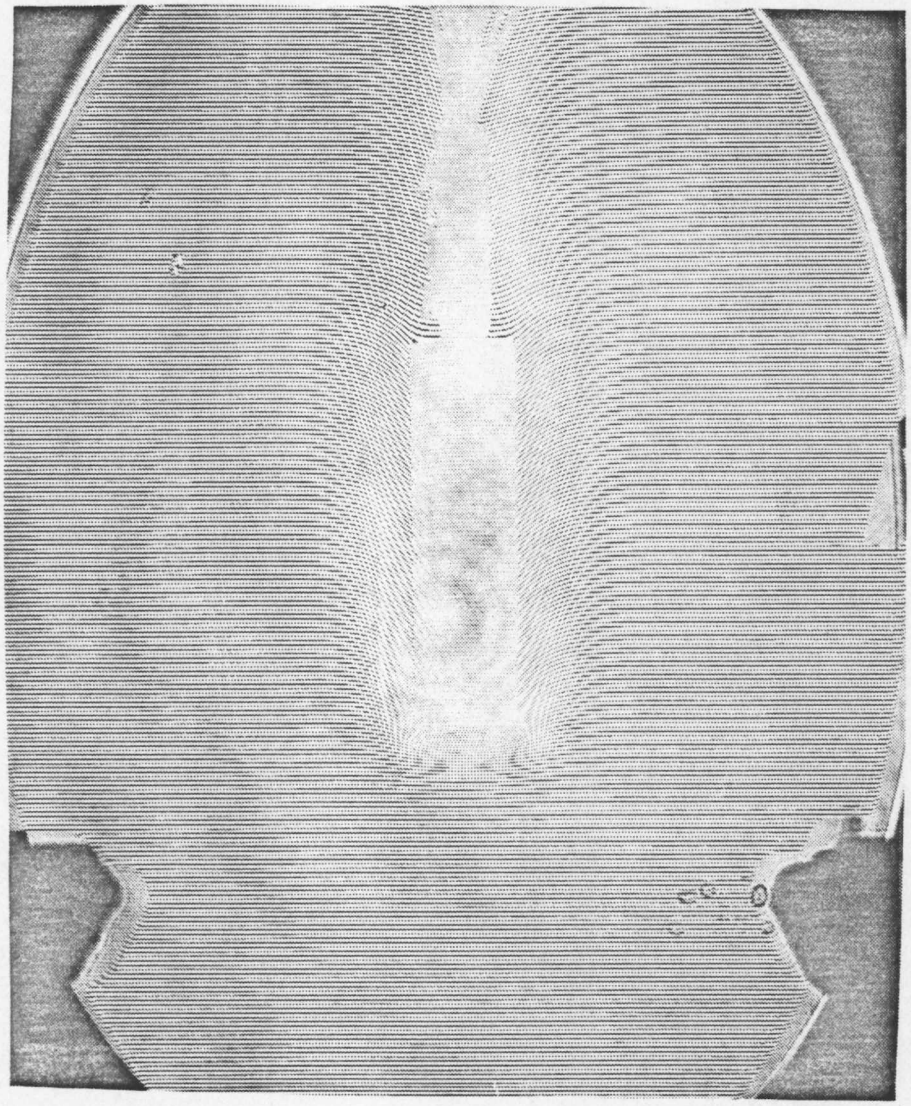


Figure 33. Exposure of the heated plate with the RHS in "best" alignment (angular adjustment knob at 9).

reproduced here as Figure 34.

For the final exposure, the interferometer was adjusted (approximately) to the infinite fringe setting with the angle scale set at 5.25. This photograph is reproduced here as Figure 35. It can be seen that the upper right region of the field is noticably dark; it is virtually impossible to get the field uniformly bright, that is, to reach the exact infinite fringe condition over the entire field.

As stated previously, the current flow through the plate was set at 0.45 ampere (indicated by the ammeter). The potential across the connections to the resistance wire was indicated as 13.75 volts by the DMM. But this includes the voltage drop across the chromel wire leads that extend from the plate; so, the leads were shorted out (on the side opposite the plate) in such a way that the voltage drop in the leads to the plate could be estimated. At 0.45 ampere and with the leads shorted, the potential was 0.4 volt. Therefore, the potential across the plate and excluding its leads was 13.75 - 0.40 = 13.35 volts.

The mercury thermometer that was suspended in air indicated 80.4 ^{o}F (26.9 ^{o}C) during the tests.

After the last exposure was taken, the mercury barometer in room 206 of Dougherty Hall was read. It indicated 743.2 millimeters of mercury at 22 ^{o}C.

The temperature values obtained from thermocouples by

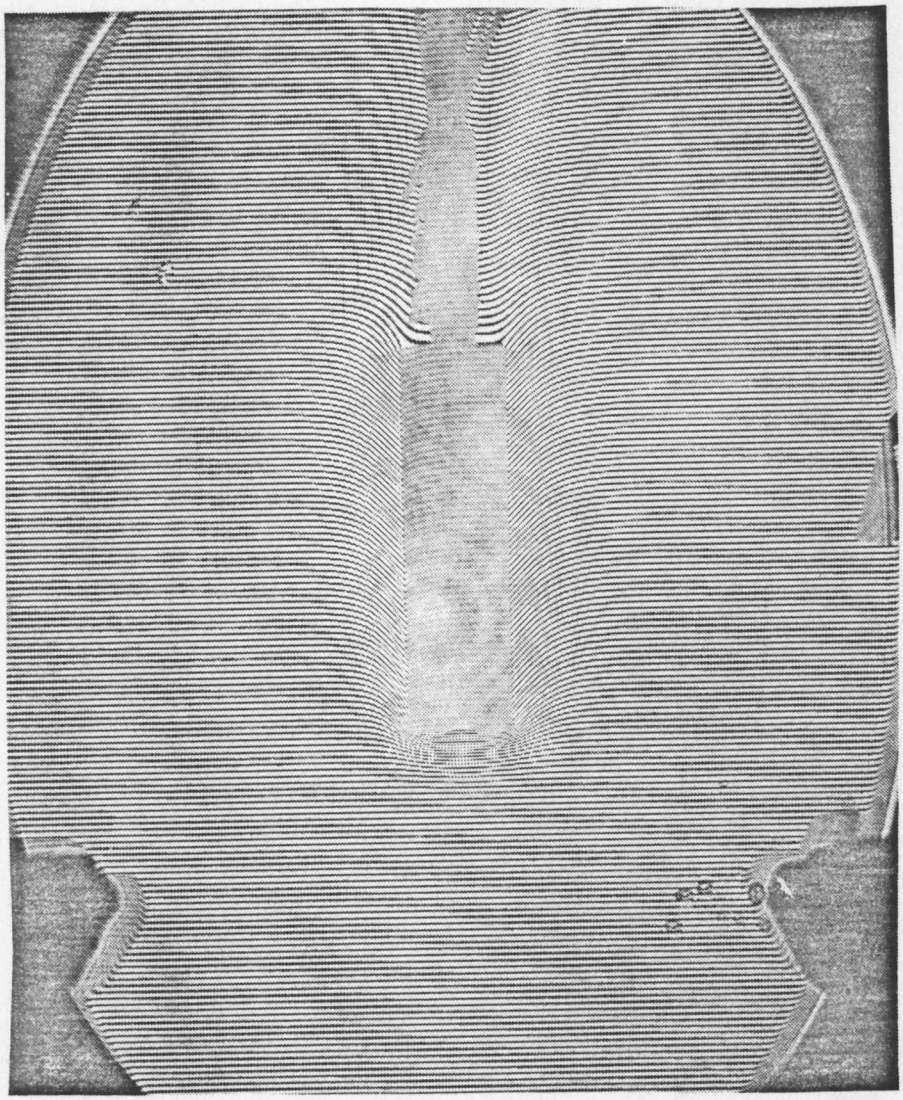


Figure 34. Exposure of the heated plate at a wider fringe spacing than the previous figure and adjusted for average alignment of the two sides.

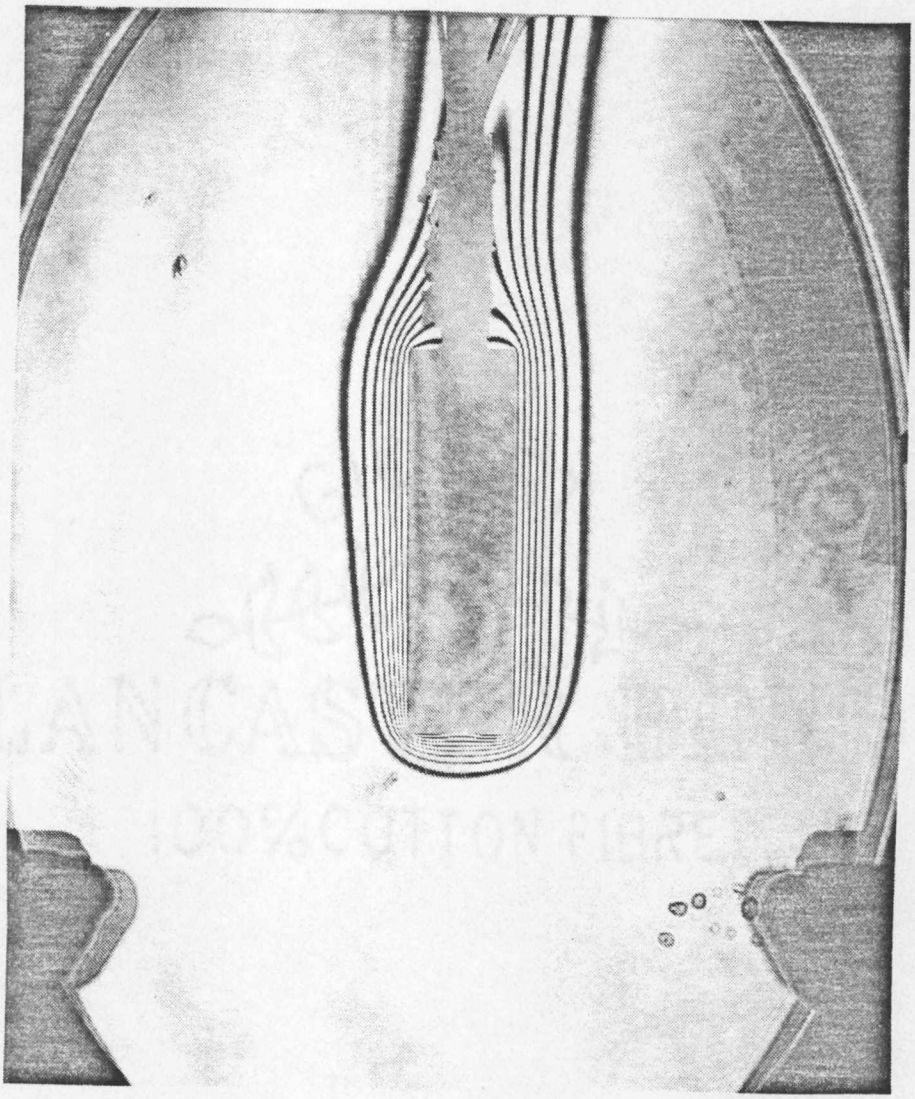


Figure 35. Exposure of the heated plate with the MZI in the infinite fringe setting showing isotherm fringes.

simply using the standard millivolt versus temperature tables are not especially accurate (plus or minus 1 C^{o} is the standard error bound for the type of couples used in the experiments described in this paper). Thus, it was considered desirable to calibrate the thermocouples; that is, their millivolt readings would be recorded when the couples were at a "known" temperature. The difference between a couple's "actual" temperature and the temperature indicated by the millivolt-temperature table at the recorded millivolt reading is the error and can be used to correct temperature readings near the calibration temperature.

After the experiments with the plate in the test section were completed, the plate was removed from the MZI and inserted into one of the constant temperature circulator's tanks. The machine was turned on (its discharge was shorted back to its suction) and the thermoregulator was adjusted until the millivolt readings of the couples in the plate were of the same approximate values as those values obtained during the experiment with the MZI (the operation of the baths is described in Appendix E). The data so obtained are listed in Appendix F. Two identical mercury thermometers graduated to 0.2 F^{o} were used to determine the "actual" temperature of the water bath and, hence, that of the couples. When inserted into the bath near the plate, both thermometers indicated

126.0 °F (52.2 °C).

As a check on the accuracy of the thermometers, they were inserted into a beaker of water at room temperature along with a thermometer (serial number 3J7968) that was taken from a bomb calorimeter and which has a calibration certificate. The calorimeter thermometer indicated 28.160 °C, and the correction was -0.012 C°; so the water temperature was 28.148 °C (82.67 °F). The thermometers being checked both indicated 82.63 °F or 28.13 °C (estimated, using a magnifier to view the graduations). Thus, the apparent error was only about -0.02 C° (-0.04 F°) which was assumed to be negligible; therefore, no correction factor was applied to the thermometer's readings.

Thermometer #1 was also checked. It indicated 82.60 °F or 28.11 °C, which indicates an error of -0.04 C° (-0.07 F°) which is still only about 1/3 of the graduation size and also will be ignored. This thermometer also indicated "precisely" 32 °F (0 °C) when checked in an ice water bath.

C. The Enclosure Experiment

The sequence of steps that comprise an experiment with the two-dimensional enclosure will now be described.

Thermocouple Calibration

The first step in preparing for an experiment is to

calibrate the thermocouples that are in the hot and cold walls. This is done by inserting the walls into the water tank of one of the constant temperature circulating baths, operating the bath at a fixed temperature, recording the millivolt output from a potentiometer for each thermocouple, and recording the water temperature indicated by one or more mercury thermometers. These operations are further described and the resulting data are presented in Appendix G.

Preparation of the Vertical Walls

It had been noticed when holding a straightedge against the hot and cold walls that they deviated noticably from flatness; the hot wall was slightly convex while the cold wall was concave. An attempt was made to sand the surfaces flat by placing a piece of sandpaper on the granite table (which was first checked and found to be relatively flat over the region used) and rubbing the walls back and forth upon it. This was continued until the walls, when checked by the straightedge, were "acceptably" close to being flat (no measurements were taken). Any further improvement in the flatness of the walls would have required the removal of a rather extensive amount of copper.

Next, the wall support assemblies, which had been removed for the sanding operation, were reattached and the

whole assemblies were placed with the copper walls vertical onto the granite table. They were then checked for "flatness" and "squareness"; that is, an attempt was made to insert a 0.001 inch thick shim between the wall or support piece and the table top all around the wall assembly. In addition, a combination square was held against the two walls and the table top to determine whether the wall was square with the surface. The shim could not be inserted at any point under either assembly, which indicated good "flatness." As stated in the previous chapter, the "tilt" of the hot wall was adjustable over a small range; it was adjusted so that it was precisely square with the table, as well as could be determined using the square. The cold wall, which was not adjustable, was found to be tilted somewhat. The top edge overhung the bottom edge by about 0.006 inch, as indicated by using feeler gauges.

It was decided to blacken the two copper walls. This would help (slightly) to absorb extraneous laser beam reflections when using the LDV. A chemical blackening solution, "Antique Black Immersion Finish (M-20)" made by Birchwood Casey Industrial Chemicals, was used. The copper walls were sanded bright with very fine sandpaper and then washed. They were then immersed, face down, into the M-20 solution which had been diluted with 3 parts of water to 1 part M-20. The walls were left in the solution for about 3

minutes, then they were removed and washed under running water and left for the black coating to dry. The solution produced a deep, dull black coating on the copper, but it rubbed off easily leaving a less black, but firmly attached grey coating on the copper. The blackening procedure was actually tried several times with variations (such as using longer or multiple immersions) but none of the methods yielded a hard black coating. Thus, the walls were left with the grey coat.

Assembly of the Enclosure

Next, the walls and insulators were mounted in the enclosure apparatus. The bottom insulator was placed into position, and then the wall assemblies were put into place and located so that the center of the cavity formed (of 40 millimeter nominal width) was approximately centered between the sides of the outer enclosure. The inside nuts on the screws that lock the walls into position, as shown in Figure 22 (p.127), were turned so that they just touched the walls. Then, the walls were removed, and vacuum grease (Dow Corning brand) was spread around the edges of the hot and cold walls. The grease was applied to seal any gaps between the walls and the insulators. The walls were replaced. Since the nut's locations had already been set, the walls could be placed into their proper positions without having to be moved back and forth across the

insulator and thereby smear out the grease. Next, the vacuum grease was spread on the top edge of the walls, the top insulator was put into place, and the aluminum pressure plate was centered on top of the insulator. The enclosure's top was set in position and attached with a cap screw at each corner (the enclosure's top and sides are marked and should be assembeled only in one way).

It was important that the two walls be accurately parallel. To accomplish this alignment, two spacers were made that could be inserted between the walls to set the gap. Two pieces of balsawood, each 1/2 inch square, were cut slightly longer than the desired wall spacing. The nominal spacing was chosen to be 40 millimeters (1.575 inch), but since the upper edge of the cold wall overhung the lower edge by about 0.006 inch (0.15 millimeter), the spacers were carefully sanded down until they were 0.003 inch oversize; that is, they were made 1.578 inches (40.08 millimeters) long, as measured by a vernier caliper, so that the average wall spacing would be 40 millimeters. Wooden spacers were chosen so that the walls would not be scratched.

It was explained in the previous chapter that the insulators were dish-shaped; they were slightly concave on the sides that were to form the horizontal surfaces of the enclosure. Thus, the nuts in the long screws that hold the walls in place should <u>not</u> be tightened against the

enclosure's sides before the compression screws in the enclosure's top are tightened, so that the wall assemblies will be free to move downward without binding as the insulators flatten out. With the nuts just touching the enclosure's sides, the compression screws were tightened (after shifting the insulators or walls so that they were as flush with the ends of the enclosure as possible), and the wall spacing was checked by inserting (or trying to insert) the spacers into the ends of the cavity. The compression screws were loosened to change the wall spacing. This process was continued until a spacer (actually, only one was used) could just be inserted into both ends of the cavity. After completing this process, the walls were considered to be sufficiently parallel.

The vacuum grease that was squeezed from the joints within the cavity had to be removed; a special tool was made to do this. It consisted of a light steel rod with a piece of cardboard attached to one end to act as a scraper. Tissue paper was wrapped about the cardboard and the tool was worked back and forth against the corners of the cavity to rub off the grease.

Alignment of the Enclosure and its Support and Transport System

To help clarify some of the following procedures, Figure 36, a schematic view of the cavity and its support

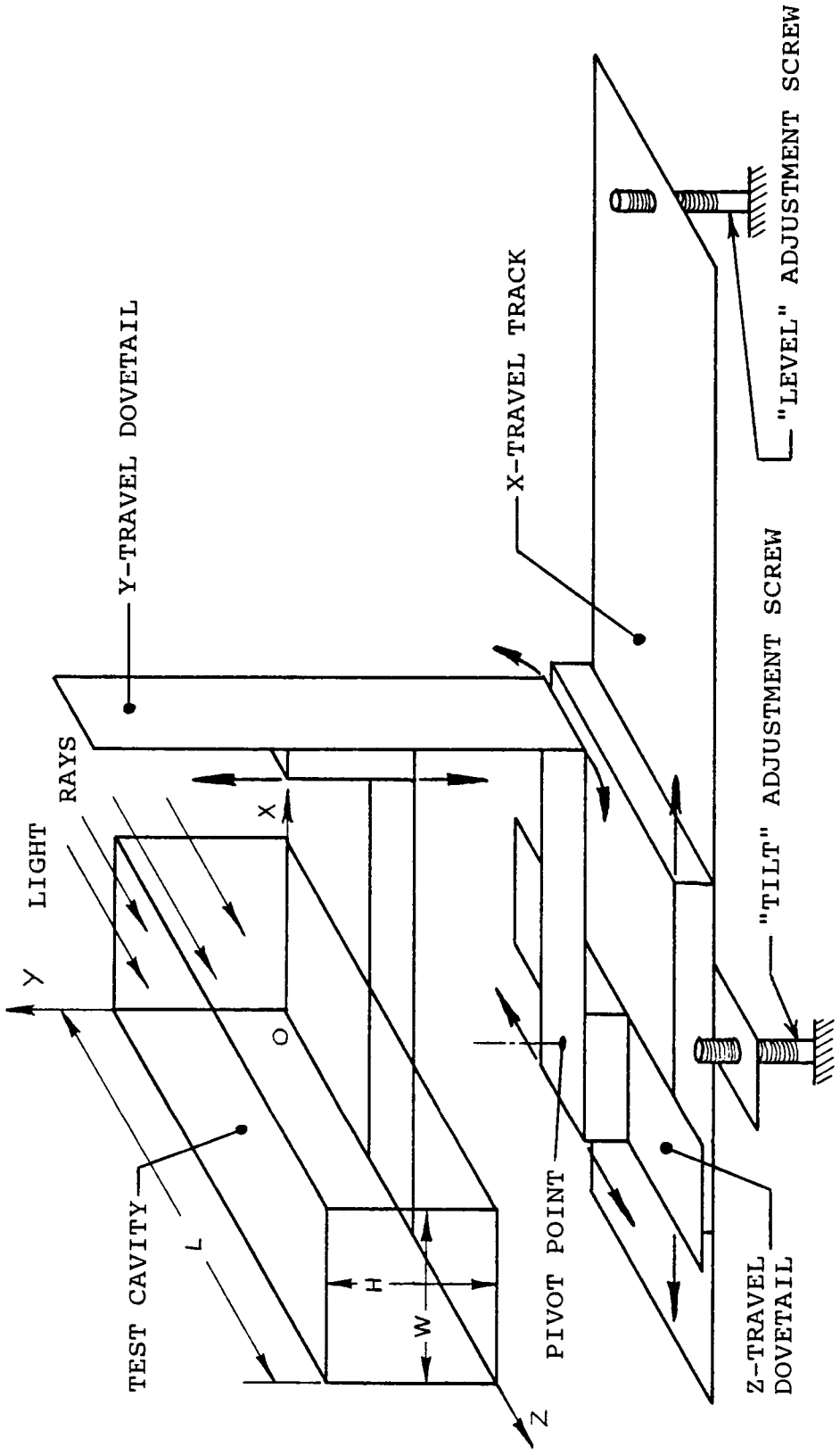


Figure 36. Schematic of the enclosure and mounting arrangement.

arrangement, is provided. As can be seen in the figure, the z-axis is parallel to the length of the cavity. This axis is generally made parallel to the optical axes of the MZI and LDV (which should be horizontal, or normal to the gravity vector). The x-axis extends across the width of the cavity perpendicular to the constant-temperature walls (this axis is generally desired to be horizontal), and the y-axis extends in a direction parallel to the constant-temperature walls (this axis is generally desired to be vertical).

The enclosure, when inserted in the MZI, did not need to be moved about after the inital setup, centering, and alignment of the x-, y-, and z-axes were completed. When used with the LDV, however, besides the above adjustments, the x-travel track needed to be made horizontal, and the y-travel dovetail needed to be vertical (or plumb). These alignments are required because, as explained in CHAPTER I, the cavity had to be moved about in order to effectively move the test probe volume about the cavity.

Since it appeared that there were a number of leveling jobs to be performed, a bubble type level was constructed in the laboratory to perform these jobs. The level consists of a block of balsawood, 1 inch square by 7 inches long, with a vial of the type intended as a replacement for a relatively sensitive machinists level attached to it by a pair of screws. The balsa block was sanded flat on its

bottom by rubbing it against sandpaper placed on the granite table. The level was adjusted by placing the instrument on a firm surface and adjusting the vial so that the bubble read either level or the same amount out-of-level as the level was turned 180°. Balsawood was used so that the level would be lightweight. It was considered undesirable to have a heavy cast iron or similar commercially made level which would, due to its own weight, deflect that which was desired to be leveled.

The cavity support and transport assembly was adjusted as follows.

The track's carriage was placed so that the cavity was approximately in the proper location for LDV measurements to be taken. Chalk marks were made on the track to indicate the carriage's location . The bubble level was placed on the side of the z-travel dovetail and the "tilt" adjustment screw on the track (identified in Figure 36) was turned so that the bubble was centered. Then, the carriage was pushed out of the way, the level was placed on top of the roundways (parallel to the x-axis) within the region of the chalkmarks, and the "level" adjustment screw on the track turned. It had been found that the roundways possessed a slight helical twist, so the track was leveled for the average between the two roundways.

The angle adjustment knob was turned so that the heavier steel piece that supported the vertical dovetail

was aligned with the thinner aluminum strip underneath it. The resulting scale setting was 25.

Next, the blade of a combination square was clamped against the back side of the vertical dovetail (the side away from the enclosure), and the bubble level was placed on top of the square head (on the horizontal leg) and checked for level. Then, the blade was clamped against the dovetail's side (facing the negative z-direction) and the bubble level was checked again. The dovetail was found to be closely vertical in both directions. This is fortunate since no convenient adjustments are built into the dovetail's attachment assembly. If it had been out of plumb, shims could have been put under the end of the dovetail to put it closer to plumb.

The L-shaped bracket that supports the cavity can be adjusted. This bracket is shown in Figure 37. The shorter leg of the L (which is vertical) is clamped by two screws to the slider. A metal rod of about 3/32 inch diameter is attached to the lower part of the shorter leg to hold it away from the slider and to act as a pivot. A setscrew at the top of the leg also holds it away from the slider. Thus, the bracket can be rotated about an axis parallel to the z-axis by adjusting the setscrew in or out and tightening or loosening the two clamp screws as needed. Further, since the two clamp screws fit into oversize holes, the bracket can be rotated about an axis parallel to

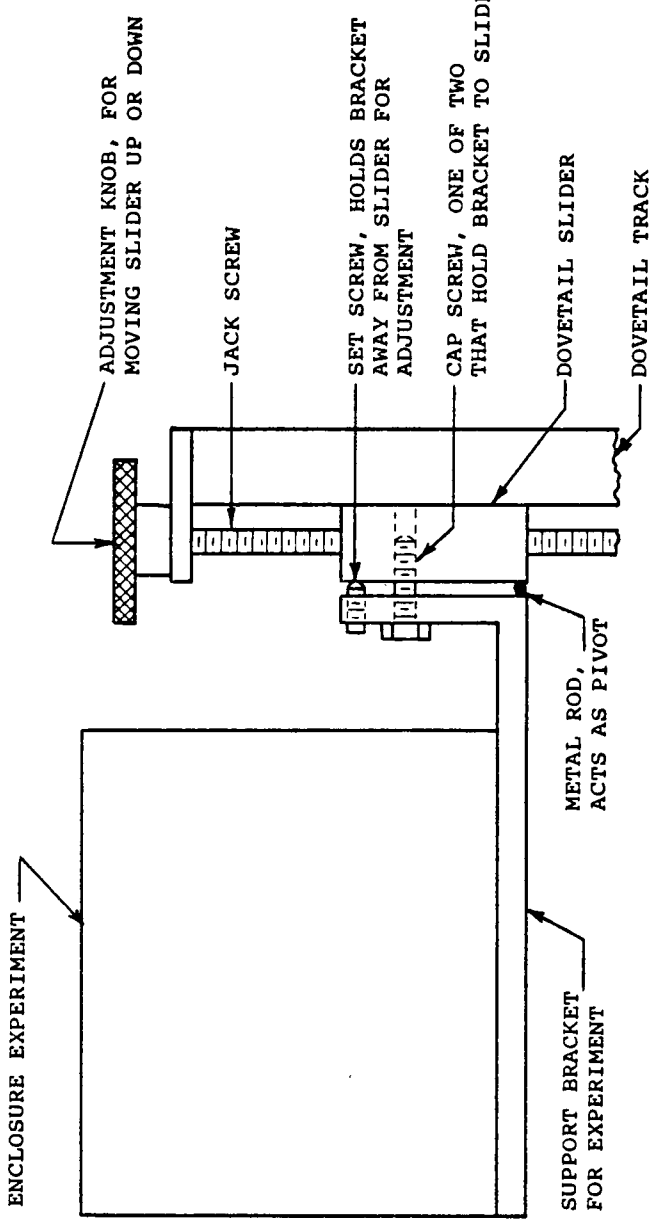


Figure 37. Detail of the support bracket's attachment to the vertical dovetail slider.

the x-axis, though this adjustment is rather inconvenient.

The L-bracket is adjusted by placing the level on the top of the enclosure parallel to the z-axis and turning the bracket about the x-axis (allowed by the slack in the oversize holes) until level is reached. Then, with the plexiglas endpieces sitting in place, the level is placed on the top of one of the endpieces (say the one at z = L) and the bracket is rotated about the z-axis (by the adjustment described in the preceeding paragraph) until level is reached. (For these alignment procedures, the endpieces should be in place (but not necessarily attached) so as to weight down the enclosure assembly as it normally would be weighted.)

It was wondered how close to parallel the cavity was with the top of the enclosure (since the level was placed on the top). A straightedge, the blade from the combination square, was placed on its edge on the bottom insulator through the length of the cavity, and a measurement was made from the top of the enclosure to the top of the straightedge at each end. The distance near the z = L end was found to be 0.018 inch (0.46 millimeter) greater than at the other end. It was decided to correct for this factor; this was done by placing a shim under the level toward the z = 0 end so that when the bubble indicated level the bottom of the cavity would be level. An 0.018 inch deviation over the 9.625 inch length of the

cavity corresponded to 0.013 inch over 6.75 inches, which was assumed to be the effective length of the level. Thus, a 0.013 inch shim was placed under the end of the level (near z = 0). Properly, the tilt of the support bracket should have been adjusted until the bubble was centered, but since this was a troublesome adjustment, instead, the tilt adjustment screw on the track was turned until the bubble centered. This probably caused a slight tilt of the vertical dovetail, but this was felt to be too slight to matter.

The cavity was moved into the test beam of the MZI, and the tilt of the track and the angular rotation of the cavity were adjusted until the horizontal and vertical surfaces of the cavity were in relatively good alignment with the test beam (using the reflection-off-the-wall method). The level on top of the enclosure (parallel to the z-axis) indicated that the cavity was out-of-level; however, since the MZI was relatively immovable and since it was rather important that the cavity be aligned to the beams, this out-of-level condition was ignored.

The level was placed on top of the plexiglas endpiece at the z = L end and the track's level adjustment screw turned until the bubble was centered. The plumb line (the one used with the plate experiment) was set near the hot wall and an exposure was made of the cavity, showing the plumb line passing through it. The negative was examined

in the measuring microscope; it was found that the distance from the hot wall to the plumb line was greater by 0.0057 inch (0.144 millimeter) at the top of the cavity than at the bottom (after accounting for the scale factor). This deviation corresponded to 0.024 inch (0.62 millimeter) over the assuumed effective length of the level. Thus, to make the hot wall plumb, a 0.024 inch thick shim was placed under the end of the level toward the cold wall side and the track's "level" screw again turned until the bubble was centered. This shim was also used under the level when the track was "leveled" with the cavity at the LDV end.

Alignment of the LDV System with respect to the Enclosure

Next, the LDV was aligned to the cavity; that is, with the cavity "leveled" or otherwise oriented as desired, the LDV's sending optics assembly was adjusted so that its optical axis was parallel to the cavity's z-axis and so that the test probe was at known x, y, and z locations.

The cavity was leveled in both directions (using the two shims under the level), and the angular rotation scale was returned to 25. The LDV sending optics assembly was first rough aligned to the cavity by adjusting the assembly so that the beams just grazed along the length of the hot wall when the (crossed) beams were in a vertical plane and just grazed the length of the cavity bottom when the beams were in a horizontal plane. The sending assembly was also

located so that the beams crossed approximately at the center of the cavity when the 250 millimeter focal length focusing lens was installed.

Since it was desired to make the velocity measurements in the z = L/2 plane, the position for the cavity so that the probe volume would be located at L/2 had to be found. The technique used to do this employed a frosted plastic screen held at the L/2 position. This screen and its holder are illustrated in Figure 38. This tool was made of 1/2 inch square balsa wood with a "stop" at one end and with two slots cut into the wood. In use, the tool is inserted into the cavity until the stop rests against the end of the insulator at the z = L end of the cavity. With this done, the two slots are located at the L/2 and 2L/3 positions. For the present operation, a small screen of frosted mylar had been placed in the L/2 slot. When looking into the cavity from the z = L end, spots could be seen on the screen where the laser beams struck it. As the slider of the z-travel dovetail was moved, the two spots could be seen to approach or to recede as the screen moved toward or away from the crossing point. The cavity was moved so that the screen was made to approach the crossing point from both sides and was stopped when the two spots seemed to just coincide. The z-axis scale reading, z', was recorded for both of these approaches and the average of the two was considered as representing the z = L/2 location

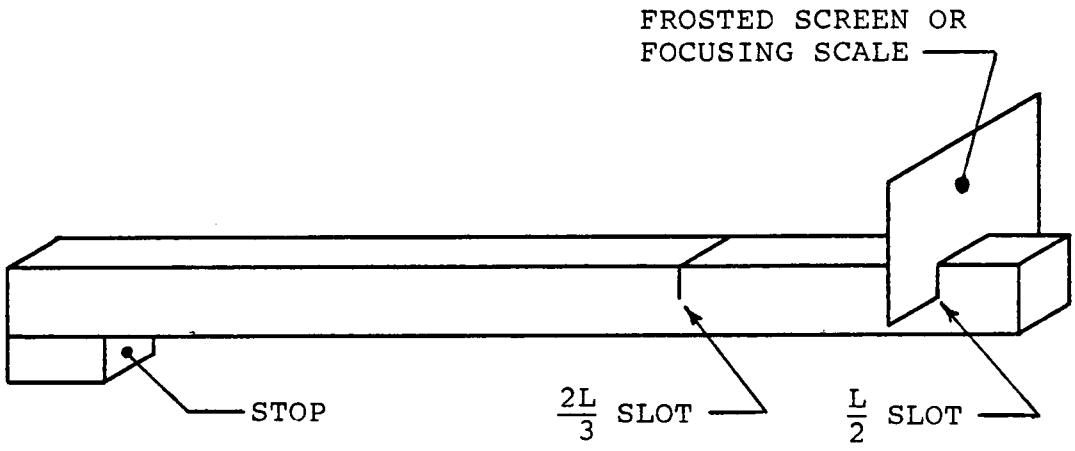


Figure 38. Alignment and focusing tool.

(for the test volume). It was found that z'(L/2) is at 62.5 (millimeters). The endpiece with the window had been set into place at the z = 0 end of the cavity for this operation, since the presence of the window influences the location of the test volume slightly.

At the time this alignment sequence was performed, it was considered desirable to do the alignment with the angle reducer as well as without it, even though the best data was expected to be obtained without the angle reducer (since using it reduces the sensitivity of the instrument). Thus, the above technique for finding z'(L/2) was repeated with the angle reducer in place; the scale reading for this case was found to be 42.75 (millimeters).

The 243 millimeter (actual) focal length lens was used with the transmitting optics for all of the alignments described herein. The 120 millimeter focal length was not long enough to reach the L/2 location in the test cavity, and the 600 millimeter focal length would have unnecessarily decreased the measurement sensitivity (compared with that of the 243 millimeter length) as well as needlessly increased the length of the optical system. Similarly, only the 243 millimeter focal length lens was used with the receiving optics.

Next, the laser beams were carefully aligned to the cavity's walls. Another "alignment tool" was created to assist in this operation. This tool is illustrated in

Figure 39. It consists of a 1/2 inch square balsawood block and a screen of frosted mylar attached to the block by two screws. The block and screen are slightly less than 40 millimeters high so that they will fit into the cavity. The screen has three fine, parallel lines drawn on it.

This tool was placed in the measuring microscope and the distance from the back side of the block to the middle line on the screen was measured at the top and bottom of the tool. With the two screws loosened, the screen can be moved relative to the block. The distance from the side of the block to the middle line at both ends was adjusted to be as close as possible to 20 millimeters (0.7874 inch). The tool was assumed to be ready for use when the indicated distance did not deviate by more than 0.01 millimeter from 20 millimeters at either end.

The alignment was performed as follows (remember that the cavity had already been "leveled" and the angular rotation scale returned to the 25 setting). The alignment tool was placed into the $z = 0$ end of the cavity with the side of the block against the hot wall and the laser beams in a vertical plane. The spring attached to the tool held it snugly against the wall. The carriage (and, of course, the cavity) was moved back or forth along the track until it appeared that the laser beams from the transmitting optics were centered on the middle line of the screen. A 10X hand-held magnifier was used to closely examine the

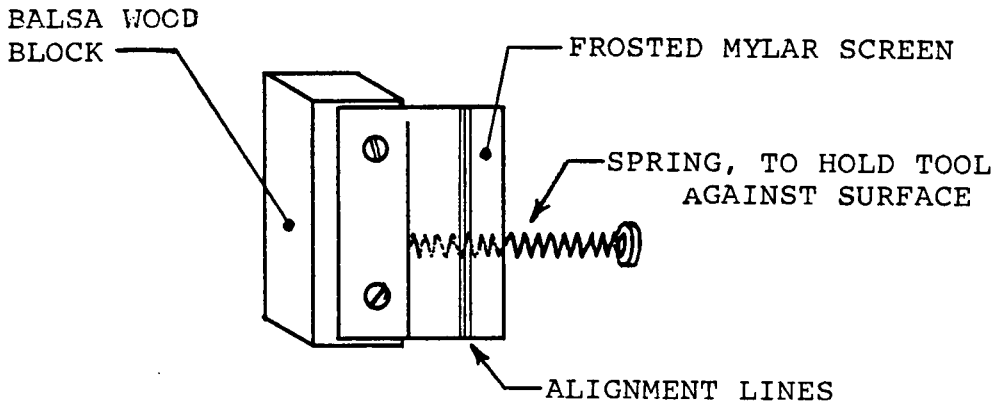


Figure 39. Tool for aligning laser beams to a surface.

intersection of the beams on the screen. (A 4X neutral-density photographic filter was usually installed against the diaphragm plate of the beam splitter module to reduce the glare of the laser spots on the screen during this step.)

Both of the laser spots could not be centered on the line simultaneously. Thus, the LDV assembly needed to be rotated about its optical axis. The leveling screws on the LDV's channel frame were adjusted to rotate the system. To accomplish this adjustment, the two screws at the end nearest the cavity were rotated (in opposite directions) by some amount. Then, the two screws at the other end of the frame were rotated, in the same corresponding directions, until each screw seemed to be of equal tightness; that is, they seemed to be supporting the same load (since the instrument has a four-point suspension, its weight is not self-dividing over the leveling screws). After adjusting the second set of screws, a downward force was applied to the center of the LDV assembly and it was shaken lightly from side to side. This was done to "seat" the instrument and the platform jacks, the latter of which contained a fair amount of "play."

After adjusting the leveling screws and the carriage until both spots were centered on the line, the alignment tool was removed and placed against the hot wall at the $z = L$ end of the cavity. Then, the end of the LDV assembly

(the aluminum plate supporting the assembly) farthest from the cavity was moved to one side or the other until the spots were centered on the line. The overall process was then repeated, beginning with the tool at the z = 0 end again.

After good alignment at both ends was obtained, the tool was placed against the cavity bottom, the laser beams were rotated to a horizontal plane, and the procedure was repeated. That is, when the tool was at the z = 0 end, the cavity was moved up or down (by the vertical dovetail) until the spots were centered on the lines (the whole LDV assembly had initally been raised to a "convenient height"). Then the tool was moved to the z = L end and the far end of the LDV assembly was moved up or down (using the support jack) until alignment was achieved. The process was repeated until good alignment was obtained with the tool at both ends. The LDV was <u>not</u> rotated about its axis during this portion of the alignment procedure. If both spots could not be centered, then the line was centered between the spots. The hot wall was thus considered to be a "primary reference." (It is believed that the hot wall is a flatter, and thus a better, reference than the insulator.)

When the alignment tool in the cavity was believed to be in best alignment to the beams, both horizontally and vertically, the scale readings, x' and y', were recorded

(the primed variables (x', y', and z') represented raw scale readings). Since these were the readings with the test probe at 20 millimeters from the reference planes, these readings were designated as x'_{20} and y'_{20}.

The procedure discussed above comprised the basic alignment sequence. Actually, it was more involved. It has already been explained that the frequency shifter would be used for all of the experiments. Thus, it was felt that the shifter should be in place for the alignment as it would be for the actual measurement. Therefore, when the beams were in a vertical plane, the shifter was turned to the vertical position, and when the beams were in a horizontal plane, the shifter was also turned to horizontal. The shifter was powered for all of the alignments. Also, since the relative intensity of the two beams is dependent upon the setting of the beam splitter prism, the prism had to be shifted against the two limits of its travel depending on whether the beams were in vertical or horizontal planes. Further, since, as already stated, it was desired to be able to use the angle reducer, the alignment was also accomplished with the angle reducer installed. When the reducer was installed, the z-dovetail slider was moved to the other L/2 focusing location (at $z' = 42.75$).

During some preliminary alignment trials, it was found that the z-dovetail has a slight twist in it. Thus, after

it was moved to either of the L/2 locations, the cavity was leveled again. This corrective leveling and the dovetail's twist cause the x'_{20} and y'_{20} readings to be slightly different depending on whether the angle reducer is installed or not. It was also discovered that the vertical dovetail possessed a slight bow (concave toward the cavity), but since no other dovetail was available, this imperfection was ignored.

In order to check for repeatability of the x'_{20} and y'_{20} values, the alignment sequence was performed several times and the associated values recorded. The sequence was performed as follows. With the angle reducer removed and the beams and frequency shifter in a vertical plane, x'_{20} was found. Then the beams and shifter were rotated to a horizontal plane, and y'_{20} was found. The angle reducer was then added, the cavity was translated to the other L/2 location, leveled, and y'_{20} was found (since the beams and shifter were already in a horizontal plane). Next, the beams and shifter were rotated, and x'_{20} was found. Then the angle reducer was removed, the cavity translated back to the first L/2 location and leveled, the beams and shifter rotated back to a vertical plane, and the process repeated. Obviously, the sequence could have been considerably shortened if it had been decided that the angle reducer definitely would not be used.

The results of the above sequence of alignments are

presented in Table I. Trials numbered 1 and 2 were performed, then the procedure was altered. The cavity was moved back and forth on the track and the angle knob was turned back and forth before the succeeding trials were performed. Only x'_{20} of trials numbered 3 and 5 were found, in order to shorten the procedure.

It can be seen from the table that the maximum variation of x'_{20} from one trial to another was 0.10 millimeter (0.0039 inch), and the maximum variation from the mean was 0.06 millimeter (0.0024 inch). The maximum variation between trials of y'_{20} was 0.12 millimeter (0.0047 inch), and the maximum variation from the mean was 0.08 millimeter (0.0031 inch). The effective diameter of the probe volume with the 243 millimeter focal length lens and no angle reducer is approximately 0.3 millimeter (0.01 inch). Thus, the anticipated maximum error in the probe's location was about 1/3 of the probe's diameter, which would seem to indicate that the method used for finding the probe's location was quite adequate.

Enclosure Alignment and Focusing for the MZI

Next, the cavity assembly was moved to the MZI and was rough aligned to the test beam, and the focusing operation was performed. The focusing tool illustrated in Figure 38 was used to hold a piece of a transparent plastic scale, and the camera, which had already been aligned to the

Table 1. Values of x'_{20} and y'_{20} readings for several alignment trials of the test cavity to the LDV's laser beams.

	Trial Number					
	1	2	3	4	5	Avg.
x'_{20}*	29.52	29.52	29.56	29.46	29.46	29.50
y'_{20}*	86.52	86.52	-----	86.40	-----	86.48
x'_{20}**	29.70	29.70	-----	29.68	-----	29.70
y'_{20}**	86.42	86.40	-----	86.44	-----	86.42

* Without angle reducer, z' = 62.50

** With angle reducer, z' = 42.75

output beam, was moved back and forth on the dovetail until the image on the screen appeared in best focus when the scale was in both the L/2 and 2L/3 locations. The best focus for L/2 was at 19.55 (millimeters) on the dovetail's scale and 15.55 for 2L/3 (z' was set at 90 millimeters). An exposure was made at each of these locations. The L/2 exposure is reproduced in Figure 40. In the figure, the hot wall forms the left side of the cavity and the top and bottom are correctly oriented. The scale was again intentionally mounted backwards. The plumb line can be seen next to the hot wall.

An exposure was made with the camera at the end of its travel on the dovetail so that the plumb line would be in best focus; this photograph was to be used to check for parallelism between the hot wall and the line. The reference beam was blocked for the focusing and exposures, since, as previously mentioned, interference effects tended to blur the image.

Final Assembly and Preparation of the Enclosure Including Window Alignment

The cavity was next moved to the LDV and was leveled to put the cavity into alignment with the beams. The glass end windows were cleaned, the dust was blown out of the cavity, the gaskets were coated with vacuum grease and put in place around the ends of the cavity, and the endpieces

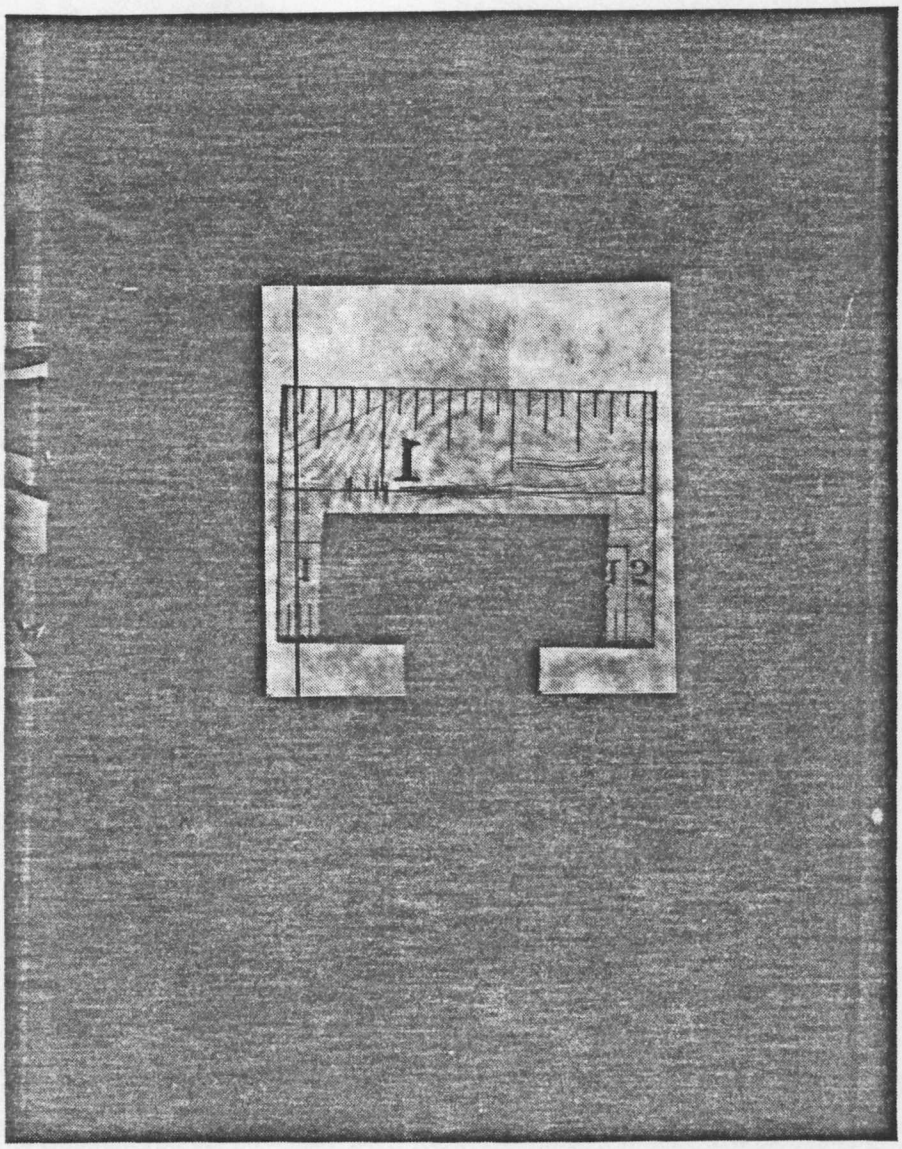


Figure 40. Exposure of the scale at the L/2 location for scale factor determination.

containing the windows were put into place and attached to the outer enclosure. The window adjustment screws were turned so that the gaskets were slightly compressed. During attachment of the windows, it was often found that the grease had oozed to where it could be seen when looking through the cavity and would block some light. When this occured, the windows were removed, the glass cleaned, and the assembly replaced with the gasket moved farther from the edge of the cavity.

The next step was to adjust the windows so that they were perpendicular to the axis of the cavity; the reason for doing this was given in CHAPTER II. This adjustment was performed using the "reflection-off-the-glass" technique, which is as follows. The focusing lens was removed from the sending optics of the LDV. Since the cavity and the LDV were previously aligned, each beam (with the lens removed) was closely perallel to the cavity's axis. The cavity was moved so that one of the beams could pass through the cavity (the beam separation was greater than the cavity's size). Next, a piece of paper with a hole cut in it about the size of the brightest part of the laser beams was placed where the focusing lens had been and was adjusted so that a beam passed through the hole and traversed the cavity. Upon striking the glass windows, a fraction of the beam is reflected from the glass surface. These reflected beams appear as spots of light on the piece

of paper. The window adjustment screws were turned so that the spots merged with the hole in the paper. Thus, the reflected beams were made parallel to the inital beam, which indicated that the windows were perpendicular to the beam which itself was parallel to the cavity's axis.

This setting of the windows was actually intended as a rough adjustment; the fine adjustment was to be done later after the cavity was aligned to the MZI's test beam. This rough adjustment step could, perhaps, have been omitted, but it was considered desirable to get the windows close to the proper setting before the fine adjustment was attempted.

The four hoses from the constant temperature baths were next attached to the hot and cold walls. The hoses were arranged so that they would not exert significant forces upon the cavity.

The cavity was moved back and centered in the MZI's test beam and was leveled (the hot wall made plumb). The cavity was then fine aligned parallel to the beam using the reflection-off-the-wall technique. Reflections off of both the top and bottom surfaces were examined when the cavity was rotated about the x-axis; the reflection off of the hot wall was given primary consideration in finding the setting for the angular rotation scale. Both the simple paper screen method and the alignment tool (with magnified image) method were used to examine the hot wall's reflection.

Sixteen trials were performed with each method and the resulting scale readings recorded. With the paper screen, the mean scale reading was 31 1/2, and with the alignment tool, the mean reading was 31 3/4 (which indicates good agreement between the two methods). The scale was set to 32 (since it is graduated in whole numbers).

The next step was the fine adjustment of the end windows. The parallel light rays of the test and reference beams strike the focusing mirror which causes the rays to converge to a small spot on the outside of the MZI's housing and a short distance from the second relay mirror. Similarly, if a light ray originates outside of the interferometer and passes through this focal point and then strikes the focusing mirror, it will be deflected into a direction parallel to the test and reference beams.

A small diaphragm was made from a thin piece of steel measuring about 45 by 55 millimeters. An aperture of approximately 1 millimeter (0.04 inch) diameter was drilled in the plate, and a piece of white paper was glued onto one side of the plate.

This aperture was located to be at the focal point of the focusing mirror. An arrangement of three small sliders allowing three axis motion is attached to the interferometer near the focal point. This device holds a knife edge that allows the MZI to be used as a schlieren system. The diaphragm was attached to the knife which

allowed it to be moved rather easily in all directions. As the light from the mirror was viewed on the paper surface, the diaphragm was moved back and forth until the circle of light reached its minimum size (indicating that the focal point had been found). Then the diaphragm was moved so that the aperture was just at the focus.

A 0.8 milliwatt He-Ne laser was available in the laboratory. It was set up on a tripod approximately on the centerline of the MZI's output cone of light. The laser was adjusted so that its beam was squarely centered on the aperture in the diaphragm plate. Thus, the beam passed through the focal point, struck the mirror, and was reflected back through the optical system parallel to the test and reference beams. This beam struck the cavity's end windows and, in the manner described previously, was partially reflected back towards its source. These reflected beams showed up as dim spots on the paper surface of the diaphragm. As before, the window adjustment screws were turned until the spots merged with the aperture. The optical arrangement of this reflection-off-the-glass technique is illustrated schematically in Figure 41.

The previous adjustment of the windows was considered as "rough" and this adjustment as "fine" because, in this latter adjustment, the reflected beams traveled a much longer distance back to the diaphragm than in the first method, which causes a considerable increase in the

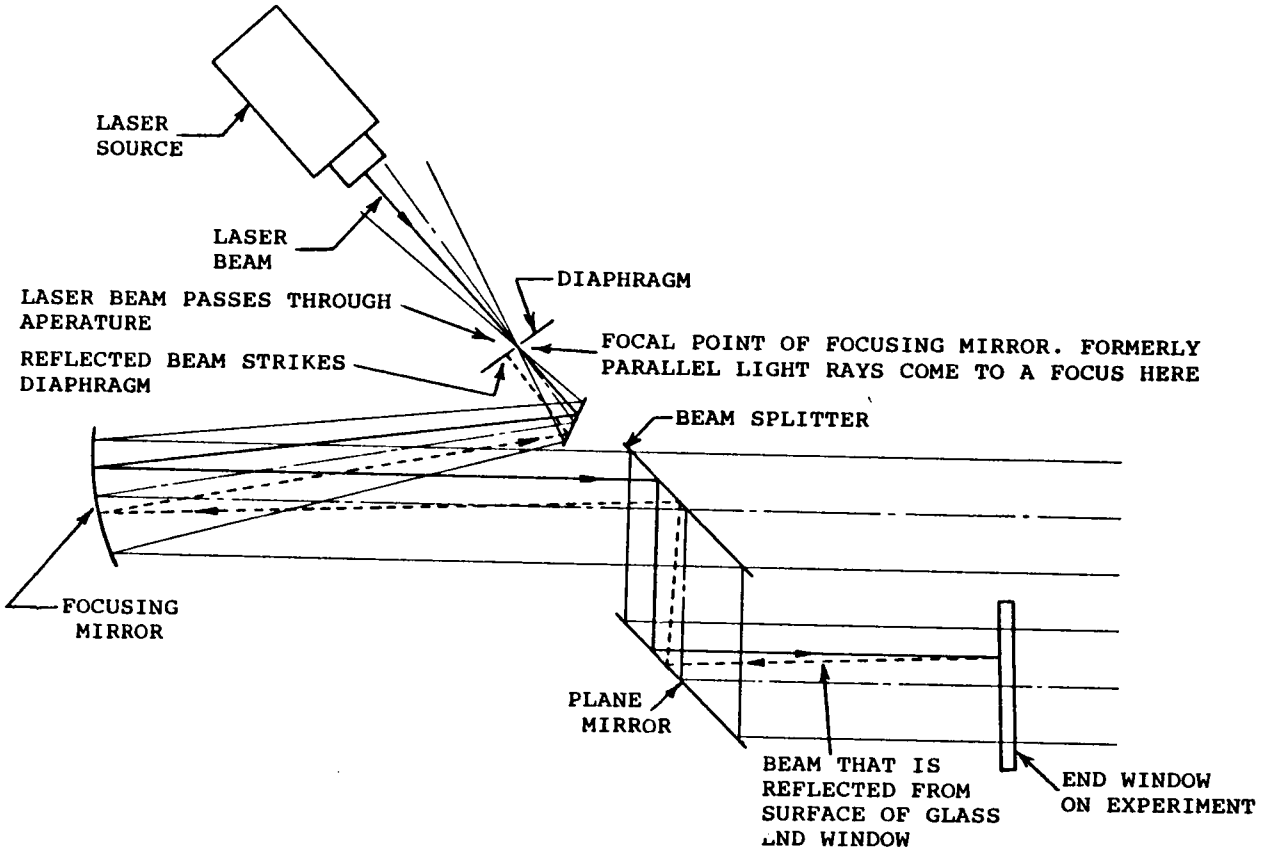


Figure 41. Schematic of the "reflection-off-the-glass" technique for aligning a glass end window to be perpendicular to the optical axis.

sensitivity of the adjustment. Actually, with only air in the cavity, this extra sensitivity may not have been needed, but this technique was developed for the applications in which it would be important.

It is unfortunate that the diaphragm of the MZI's laser light source is not accessable to viewing. If it was, then the reflection of the light off of the windows, after being focused by the collimating mirror, could be examined and adjusted to be coincident with the aperture. This would somewhat simplify the window adjustment operation.

With the alignment of the windows finished, the setup of the cavity was complete and preparations were begun for making exposures.

Performance of the Enclosure Experiment

It was decided to begin the experiment by making some exposures with the MZI in the infinite fringe setting. Thus, the reference beam was unblocked and the instrument was adjusted by the technique given in CHAPTER I to the infinite fringe condition. The cavity assembly was left within the test beam, so only that portion of the total cross-sectional area of the beam that traversed the cavity was examined for this adjustment. The image on the screen was watched and, after a slight inital adjustment, was observed to remain steady for approximately 20 minutes.

This was considered to be an adequate indication that the interferometer's setting was going to remain stable and that the experiment could proceed.

The circulating baths had already been started and had reached their set temperatures, but pinchcocks had been placed on all four of the hoses so that the cavity would remain isothermal. It was desired to have a "relatively large" temperature difference between the hot and cold walls to give a large fringe shift; plus, it was desired that the differences between the wall temperatures and the room temperature be approximately equal. Thus, it was decided to use a 30 C^{o} temperature difference between the vertical walls. Therefore, the circulating bath temperatures were set to approximately 15 C^{o} above and below the room temperature.

The pinchcocks were removed from the hoses allowing the water to circulate through the walls. Some air was blown into the cavity from a smoke generator assembly's air dryer (the smoke generator is described in Appendix H) so that dry air would be in the cavity, and the hoses on the cavity's fill and drain tubes were pinched shut.

The cavity was left to stabilize for approximately 1 1/2 hours before an exposure was made. The first exposure was at the L/2 focus position, and the second was at the 2L/3 position. The first exposure is reproduced here as Figure 42. The millivolt readings of the

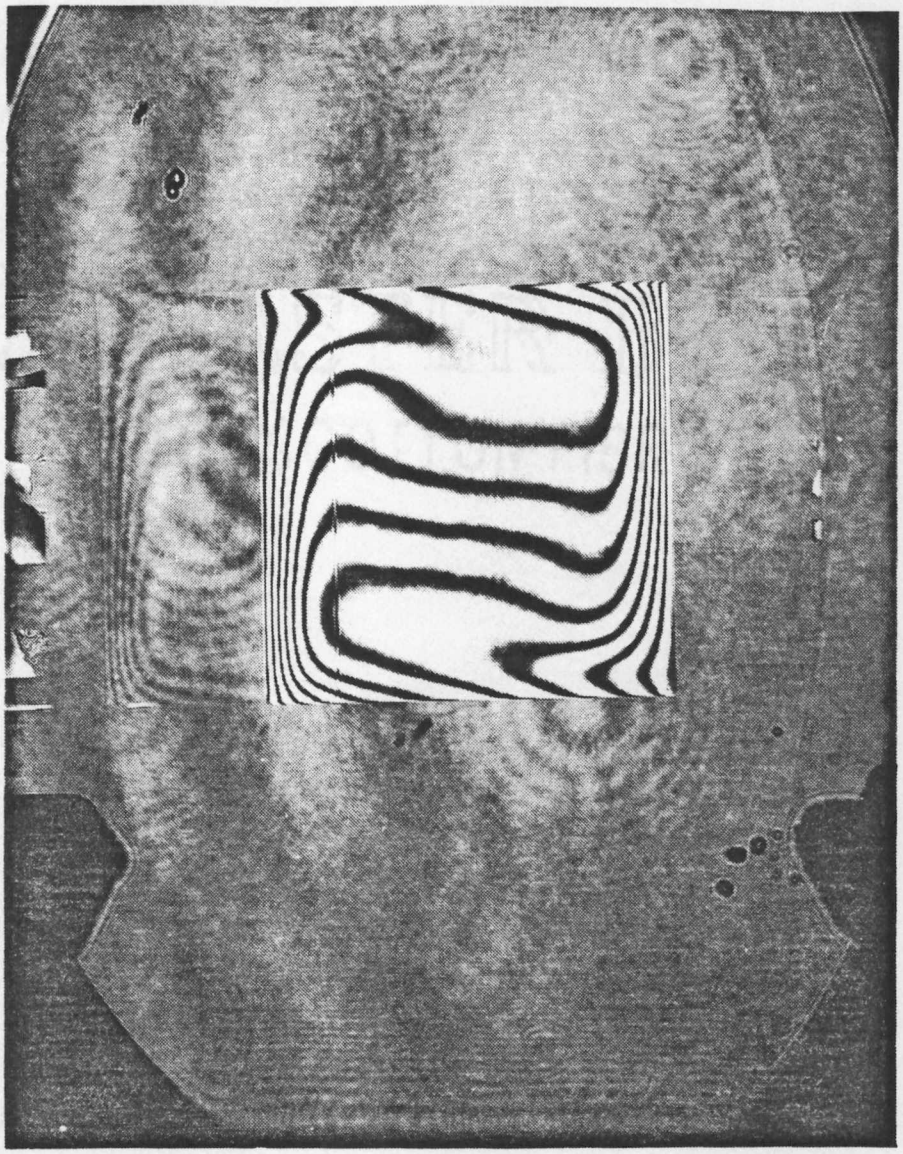


Figure 42. Exposure of the cavity at operating temperature showing approximate isotherm fringes.

thermocouples in the vertical walls were then recorded.

Next, it was desired to make interferograms with the MZI adjusted to give wedge fringes. Thus, the circulating baths were stopped and the cavity was allowed to sit until the wall temperatures had equalized. The wedge fringes were then formed. The plumb line was placed where it could be seen within the cavity; it is visible next to the hot wall in Figure 42. The transparent plastic square (that was previously described in the procedure for aligning the wedge fringes normal to the electrically heated plate) was again used to align the fringes within the cavity, except the square was aligned to the plumb line instead of the (hot) wall.

A pair of exposures were then made, one at L/2 focus and the other at 2L/3. The exposure at L/2 is reproduced here as Figure 43.

The circulating baths were then restarted, dry air was again blown into the cavity, and the assembly was left running for over 1 hour in order to give time to stabilize. An interferogram was then made at the two focus positions; the L/2 exposure is reproduced as Figure 44.

This was the last exposure to be made, so the experiment was concluded with the reading and recording of the barometric pressure from the mercury barometer.

At this point, the work with the MZI was finished, so the cavity assembly was moved to the LDV's test position

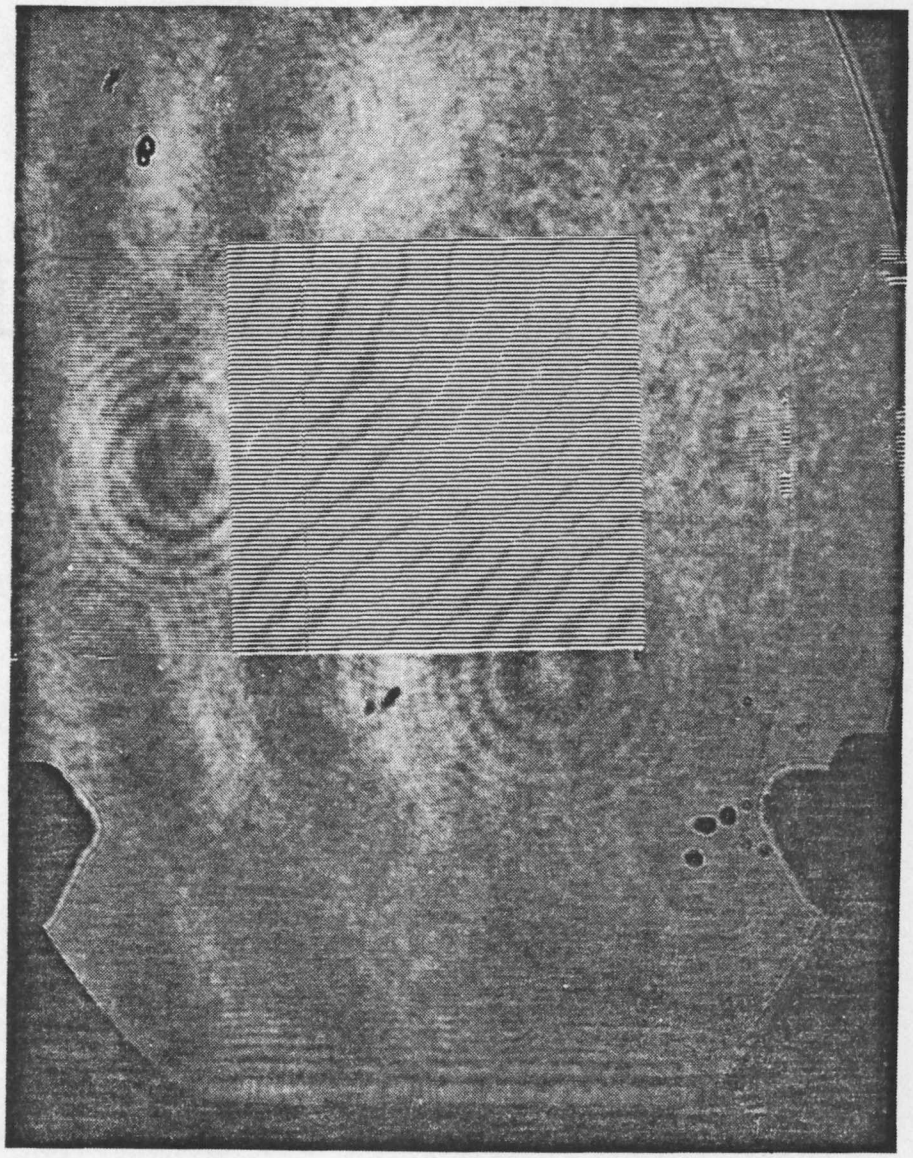


Figure 43. Exposure of the isothermal cavity with wedge fringes.

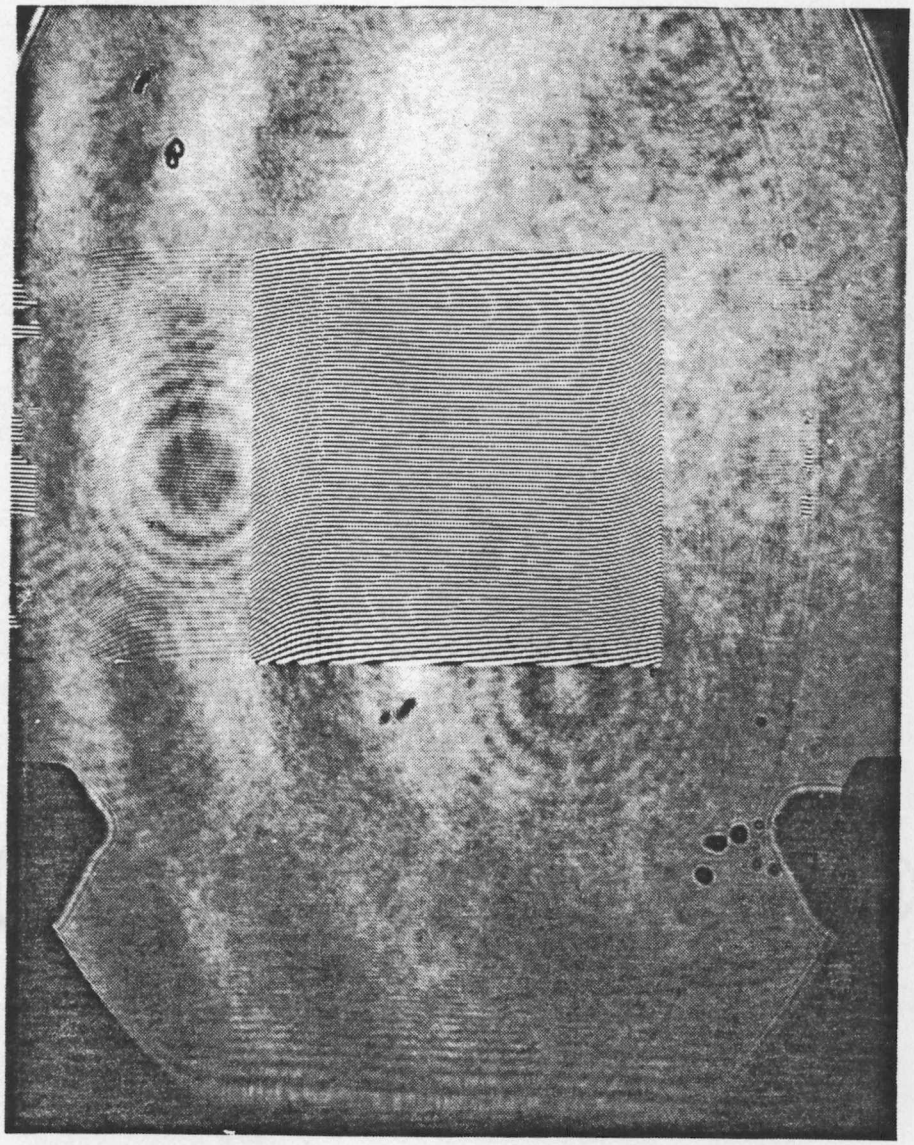


Figure 44. Exposure of the cavity at operating temperature with a wedge fringe field.

and was "leveled." The z-axis dovetail was set to the 62.5 millimeter location and the angle scale to 25.

It was previously explained that the x'_{20} and y'_{20} locations were 29.50 and 86.48 millimeters, respectively. The carriage and the y-dovetail were moved so that the zero marks of the x' and y' scale verniers were set to the x'_{20} and y'_{20} values. Then the scales were shifted (without moving the carriage or dovetail) so that the x'_{20} and y'_{20} values became 30.0 and 86.0 millimeters, respectively (for greater convenience).

As the value of x' increased, the value of x decreased; the following equation was used to relate these quantities.

$$x = x'_{20} + 20 - x' = 30 + 20 - x'$$

$$x = 50 - x' \quad \text{[millimeters]} \qquad [26]$$

As the value of y' increased, the value of y increased; these quantities were related by the following equation.

$$y = y' + 20 - y'_{20} = y' + 20 - 86$$

$$y = y' - 66 \quad \text{[millimeters]} \qquad [27]$$

The relation for z and z' varied as that of y and y', except the centerline value was 122 millimeters instead of 20 millimeters. Thus,

$$z = z' + z_o - z'_o = z' + 122 - 62.5$$

$$z = z' + 59.5 \quad \text{[millimeters]} \qquad [28]$$

The circulating baths were started and allowed to stabilize. The thermoregulators were not changed from their settings used during the MZI experiment. The LDV receiving optics assembly was set up and aligned.

The cavity was filled with smoky air from the smoke generator assembly, described in Appendix H. The smoke in the cavity appeared "relatively dense," but not so dense that the laser beams were completely attenuated by the scattering. After seeding the cavity, the fill and drain hoses were pinched shut, and the photodetector mount was fine adjusted onto the crossing volume.

A digital multimeter (DMM) was used for reading the output voltage from the 1090 tracker. The meter used was a Honeywell "Digitest," Model 333R (Tag 199950). It was used on its 10 volt range setting which provided a resolution of 0.01 volt. This corresponded to a velocity resolution of 0.32 millimeter/second. (This meter requires an approximately 30 minute warm-up period in order to stabilize. After warm-up, it should be checked for or adjusted to read zero with the signal input shorted to ground.)

The photodetector was blocked out and the zero velocity offset voltage, V_o, was determined. It was found to be 1.98 volts with the frequency shifter at 20 KHz and

4.98 volts at 50 KHz.

The cavity was left to stabilize for just over 1 hour from the time the smoke was blown in until data reading was begun.

The laser beams were in a vertical plane; the first "traverse," or movement of the cavity to obtain a sequence of velocity measurements, was made in the x-direction along the horizontal centerline beginning from x = 20 millimeters. The x' and Model 1090 tracker output voltage values were recorded each 2 millimeters when the voltage values were changing relatively slowly from point to point and were recorded each millimeter or 0.5 millimeter when the voltage was changing relatively rapidly.

The 10X magnifier was always used to observe the vernier and the scale to ensure accurate positioning. The frequency shifter was used in both the 20 KHz and 50 KHz settings. One or the other was selected so that the indicated voltage would either drop from the 5 volt level or increase from the 2 volt level, depending upon the sense of the flow. Fortunately, there was no discontinuity at the switch points.

The observed values of x' and voltage are presented in Appendix I. Also illustrated in the appendix are the forms that were made up to record the data.

After obtaining data across the entire horizontal centerline, the probe was located at x = 20 millimeters,

the beams were rotated to the horizontal plane, and a traverse was made (reading data) along the cavity's vertical centerline; these data are also presented in Appendix I.

The voltage (or velocity) indicated by the DMM was quite stable at each measurement location. Also, there was no apparent settling time needed when the cavity was moved from one position to another. At some locations, the voltage remained absolutely stable at a single value (to the 0.01 volt resolution of the meter) while at other locations, the least significant digit of the meter might oscillate back and forth between two numbers. Within about 1 millimeter of the wall, however, the readings usually became erratic and were probably not dependable (this was where the beams were partially striking the wall).

Each traverse required approximately 45 to 60 minutes to complete; by the time the second traverse was finished, the density of the smoke had decreased considerably, but it was still sufficient to give a good signal.

With the second traverse completed, this experiment with the cavity was finished.

CHAPTER IV

DATA REDUCTION TECHNIQUES AND RESULTS OF THE EXPERIMENTS

A. Introduction

The data reduction procedures will now be illustrated, beginning with an analysis of the interferogram for the heated plate and then covering analyses of the interferogram and LDV data for the internal cavity. Plots of the resulting data are then presented along with their physical interpretations.

B. Techniques for Reducing the Mach-Zehnder Data for the Heated Plate Experiment

Some of the basic principles of interferogram analysis have already been described. For example, Figure 4 (p. 14) illustrates an idealized interferogram of a heated plate in air. The temperature distribution normal to the plate could be determined by measuring the locations where the fringe shifts would be known (at S = 0, 0.5, 1, 1.5, and 2), calculating the temperatures associated with these fringe shifts from Equations 11 and 12, and using some type of interpolation to determine temperatures at intermediate locations.

Techniques for taking measurements from interferograms

will now be described. Measurements on interferogram negatives were made in the Natural Convection Laboratory by means of an EPOI (Nikon) "Shopscope" measuring microscope. Information on this microscope and its use is presented in Appendix J.

In CHAPTER III, it was explained that several exposures were made of the plate. The identification number and description of each interferogram follows:

071580-1: for scale factor determination

071580-2: plate unheated, for reference

071580-3: plate heated, RHS "best" alignment

071580-4: plate heated, LHS "best" alignment

071580-5: plate heated, average alignment, wider fringes than above

071580-6: plate heated, average alignment, infinite fringe field

Exposure 071580-1 was placed in the measuring microscope, and, after aligning the image of the edge of the scale to be parallel to the travel of the stage, a measurement was made from the "inside" side of the zero mark to the same side of the 3.5 millimeter graduation. The actual scale was then placed in the microscope, and a measurement was made between the same marks. The results were as follows.

Image Distance = 1.3216 inch

Object Distance = 1.3774 inch

Magnification = M = ID/OD = 0.9595

Distances measured on the other interferograms had to be divided by M to relate the image distances to the actual object distances.

In the hypothetical wedge fringe interferogram of Figure 4 (p. 14), the fringes in the undisturbed field were assumed to be perfectly straight, so there would be no difficulty in aligning the fringe with one of the travel axes of the microscope's stage and following the fringe's original path up to the plate. However, because of various optical defects, the fringe formed by a real MZI may not be straight even with an isothermal test section. As a "traverse" is made with the microscope from the field to the wall on an interferogram of a heated plate, the crosshairs should be moved along the line traced by the fringes when the plate was unheated, since the fringes locate points of constant phase shift (S-number) and to deviate from this path (of unheated plate fringes) is to introduce a phase shift not due to temperature effects alone.

A fringe at the horizontal centerline of the plate on interferogram 071580-2 was checked for straightness in the microscope. The negative was adjusted until the crosshairs remained centered on the fringe at two points, each one of which was near the extreme ends of the fringe, as the (6 inch travel) stage was moved. It was desired to select the

two points so that the same corresponding locations could be found on some of the other interferograms. The region near the extreme ends of the fringes was usually somewhat indistinct; thus, the reference points were chosen so that the extreme ends of the fringe would be just at the edge of the field of view through the eyepiece. That is, the reference points were one-half of a field of view from the extreme ends of the fringe (the 30X magnification was used).

In this discussion, the x-axis is taken as parallel to the wall face and the y-axis as normal to the wall; x = 0 is at the plate's bottom edge and x = H = 40 millimeters is at the top edge while y = 0 is at the wall. Values with a prime (x', y', H') are raw micrometer readings (or otherwise represent measurements made on the negative).

The results of the measurement on this fringe are presented in Table 2. The negative and stage were adjusted so that the two reference points were precisely at x' = 0.7100 and at y' = 0.4000 for the right hand point. (Two "zeroing" screws on the stage allowed the micrometers to be set to even numbers.) The "traverse" was made from the RHS to the LHS. The y' micrometer was turned (apparently causing the crosshairs to move along the chosen fringe) until the fringe seemed to be making a noticable deflection from the center of the crosshairs, at which point the y' micrometer was set to some even number and the

Table 2. Measuring microscope coordinate locations for the centerline fringe in exposure 071580-2 (unheated plate).

x' [in]	y' [in]	
0.7100	0.4000	RHS, 1/2 field from end of fringe
0.7102	0.6000	
0.7107	0.7500	
0.7114	0.9500	
0.7121	1.0500	
0.7127	1.2000	
0.7133	1.4000	
0.7133	1.6472	Wall, RHS
0.7121	2.0636	Wall, LHS
0.7121	2.3500	
0.7116	2.5500	
0.7108	2.7500	
0.7107	3.1000	
0.7100	3.3000	
0.7100	3.5750	LHS, 1/2 field from end of fringe

x' micrometer was turned until the fringe was again centered. One of the crosshairs was generally kept parallel to the fringe and centering of the hair on the fringe was for a local average (estimated by eye) near the crossing of the hairs.

The deviation of the x' value from 0.7100 represents the deflection of the fringe from straightness. It can be seen from the table that the fringe exhibited a "plateau" near its center; the maximum deviation was 0.0033 inch (an increase in the x' value represented a deflection toward the top of the plate). The fringe spacing (averaged over 10 fringes) was 0.0173 inch. Thus, the maximum deviation was by 0.0033/0.0173 = 20% of the fringe spacing. Fortunately, the fringe seemed to remain parallel to the reference line within a region of about 0.3 inch of the plate's sides.

A rough check was made of the straightness of other fringes; they all seemed to possess the "plateau." A fringe at about x = 0.9H had a 0.0025 inch maximum deflection from the reference while a fringe at about x = 0.1H had a 0.0030 inch maximum deflection. However, at a location above the plate, the maximum deflection was only about 0.0009 inch.

Interferogram 071580-3 was placed in the microscope and was aligned in the same manner as the previous interferogram and to the same fringe. The data associated

with this interferogram are presented in Table 3. It can be seen that the x' location of the fringe is again at 0.7100 inch at both ends (again, at one-half of the field of view from the fringe's ends) and the y' value was set to 0.4000 inch. It seemed best to make the traverse from the RHS to the wall and from the LHS to the wall. The x' locations of the fringe was checked at some of the same y' locations where it was checked on interferogram 071580-2. These values are indicated by the asterisk (*). In comparing the values of Table 3 to those of Table 2, it can be seen that the fringe is initally following approximately the same path in both cases. Within the boundary layer (B.L.), of course, no comparison is possible.

As the traverses were made from the field to the wall, the crosshairs were centered on each fringe where it was crossed. A scheme to compensate for nonstraightness of the original fringes could work as follows: With the crosshairs centered on a fringe, the y' value could be read and compared to the y' values in Table 2. From the table (or a graph of the data), an x' location could be determined (this would be of the original straight fringe) and the x' micrometer set to this value. Then, the y' micrometer would be fine adjusted to center the fringe on the hairs, and its value recorded. This "predictor-corrector" scheme was not needed, however, since practically all of the fringe shifts occured within the

Table 3. Measuring microscope coordinate locations for the centerline fringe and fringe intercepts in exposure 071580-3 (heated plate, RHS in "best" alignment).

x' [in]	y' [in]	y [mm]	S
0.7100	0.4000	32.894	0, RHS of fringe
0.7103*	0.6000		
0.7102*	0.7500		
0.7114*	0.9500		
0.7117*	1.0500		
0.7117	1.1120±	14.046±	0, edge of B. L.
0.7133	1.4076	6.221	1
0.7133	1.4684	4.611	2
0.7133	1.5076	3.574	3
0.7133	1.5377	2.777	4
0.7133	1.5646	2.065	5
0.7133	1.5889	1.422	6
0.7133	1.6129	0.786	7
0.7133	1.6372±	0.143±	8±
0.7133	1.6358±	+0.180±	Wall, RHS
0.7133	1.6494±	-0.180±	
0.7121	2.0492±	-0.113±	
0.7121	2.0577±	+0.113±	Wall, LHS
0.7121	2.0550±	0.041±	8±
0.7121	2.0828	0.777	7
0.7121	2.1069	1.415	6
0.7121	2.1304	2.037	5
0.7121	2.1555	2.701	4
0.7121	2.1846	3.472	3
0.7121	2.2218	4.457	2
0.7121	2.2762	5.897	1
0.7106*	2.5043±	11.935±	0, edge of B. L.
0.7109*	2.5500		
0.7108	2.7500		
0.7105*	3.1000		
0.7100	3.3000		
0.7100	3.5793	40.392	0, LHS of fringe

*Values required to center the crosshairs on the fringe when set to the adjacent y' values.

regions near the plate where the x' value was constant at either 0.7133 or 0.7121. Thus, the micrometer was set to these values where they are seen in Table 3.

The locations for the edges of the boundary layer were somewhat uncertain. A location was chosen where the fringe seemed to be just starting to move away from the crosshairs.

Also uncertain were the locations of the plate's walls. Two values were recorded for each wall. One value was the approximate location where the fringes started loosing their distinctness while the other value was the approximate other side of the indistinct region. In Table 3, the mean of the two wall locations was taken as the "true" wall location.

Even though the plate was supposed to be in best alignment on its RHS for 071580-3, the image showed a particularly wide indistinct region at the RHS wall. In Table 3, it can be seen that the indistinct region for the RHS was 1.6 times as wide as that for the LHS (0.360 millimeter versus 0.226 millimeter).

The third column in Table 3 lists the y value in millimeters for the various fringe numbers. The following equation was used to obtain these values.

$$y = | y' - y'_w | (25.4/M) \quad \text{[millimeters]} \quad [29]$$

Here, y'_w is the mean wall location, and M is the

magnification (the quantity 25.4/M was termed the "scale factor").

Interferogram 071580-4 was analyzed in the same manner as the previous interferograms. The resulting data are presented in Figure 45. This figure shows the form that was made up to assist recording of interferogram data. An x' or y' value was recorded in the upper line of a box, and the corresponding x or y value was calculated and recorded in the lower line. Row 1 (Trav. #1) lists the data from the RHS of the plate; the x' micrometer had been set to 0.7133 as before. Rows 3 and 5 list the data from the LHS of the plate. In row 3, the x' micrometer had been set to 0.7121 as before; however, the part of the fringe outside but near the boundary layer was observed to be a relatively long distance from the reference line. For the data in row 5, the x' micrometer had been set to 0.7161 inch, which was the fringe's location just outside the boundary layer. These two sets of data were made for comparison purposes.

The plate's LHS was supposed to be in best alignment for interferogram 071580-4; however, again it can be seen that the indistinct region for the image's LHS is about twice as wide as that for the RHS.

At the bottom of the form, the x' value of the plate's bottom edge (x_o), top edge (x'_H), and the difference of these two (H') was recorded. The x-location of the fringe was found from

From Interferogram No. 071580-4 Fringe Field: Wedge

Trav. #	X	BL Edge 0	1	2	3	4	5	6	7	8	Wall+	Wall−
		S										
1	.7133	1.075±	1.3333	1.4307	1.4801	1.5170	1.5464	1.5729	1.5989	1.6228±	1.6319±	1.6363±
RHS	19.837	14.801±	7.963	5.384	4.077	3.100	2.322	1.620	.932	.299±	.058±	-.058±
2	.496 H											
3	.7121	2.475±	2.2362	2.1926	2.1631	2.1373	2.1138	2.0902	2.0641	—	2.0554±	2.0449±
LHS	19.806	11.247±	4.925	3.771	2.990	2.307	1.685	1.060	.369		.139±	-.139±
4	.495 H											
5	.7161	2.4235	2.2525	2.2021	2.1704	2.1434	2.1192	2.0960	2.0730	2.0458±	2.0520±	2.0436±
LHS	19.911	9.946	5.449	4.085	3.245	2.531	1.890	1.276	.667	-.059±	.111 ±	-.111 ±
6	.498 H											
7												
8												
9												
10												
11												
12												
13												
14												
15												
16												
		Y										

x_o = −.0426"
x_H = 1.4816"
H = 1.5242"

$$SF = \frac{25.4 \frac{mm}{inch}}{.9595} = 26.472$$

JWJ Rev 2

Figure 45. Reproduction of a form for recording measuring microscope data from interferograms.

$$x/H = (x' - x'_0)/H' \qquad [30]$$

or

$$x = 40(x/H) \quad \text{[millimeters]} \qquad [31]$$

since the plate was 40 millimeters high.

Interferogram 071580-5 was also analyzed; its data are presented in Table 4. This exposure was of interest because the plate was set for the average of the RHS and LHS alignment values. The resulting image was relatively distinct for both sides. The indistinct region on the RHS extended from plus to minus 0.070 millimeter, which compares very favorably with any of the other ranges recorded, while the LHS wall boundary was sufficiently distinct that only one value was recorded. Thus, it appears that a test device should be tested for alignment on two oppositely facing surfaces and finally aligned for the average of the two positions. That is, the "best" alignment values should be found for two oppositely facing surfaces such as the two vertical sides or the top and bottom of a plate or the two vertical walls or the top and bottom of a cavity and the experimental device then aligned to the mean of the two "best" values so as to cancel out an apparent alignment bias that will be present in the two values.

It was mentioned in CHAPTER III that the fringe

Table 4. Measuring microscope coordinate locations for the centerline fringe and fringe intercepts in exposure 071580-5 (heated plate, average alignment).

x' [in]	y' [in]	S
0.9100	0.4000	0, RHS of fringe
0.9100*	0.6000	
0.9104*	0.7500	
0.9109*	0.9500	
0.9111*	1.0500	
0.9111	1.1500	0, edge of B. L.
0.9111	1.3936	1
0.9111	1.4611	2
0.9111	1.5033	3
0.9111	1.5353	4
0.9111	1.5635	5
0.9111	1.5893	6
0.9111	1.6143	7
0.9111	1.6382±	8±
0.9111	1.6403	Wall, RHS
0.9106	2.0615	Wall, LHS
0.9106	2.0794	7
0.9106	2.1013	6
0.9106	2.1243	5
0.9106	2.1483	4
0.9106	2.1760	3
0.9106	2.2104	2
0.9106	2.2604	1
0.9106	2.4750	0, edge of B. L.
0.9106*	2.5500	
0.9104*	2.7500	
0.9101*	3.1000	
0.9095*	3.3000	
0.9100	3.5595	0, LHS of fringe

*Value required to center the crosshairs on the fringe when set to the adjacent y' value.

spacing of interferograms 071580-3 and -4 was so close that a blurred region existed at the lower left corner of the plate, as can be seen in Figure 33. As reported above, the fringe spacing was 0.0173 inch, or 0.44 millimeter. For interferogram 071580-5, the spacing was 0.0246 inch or 0.62 millimeter. At this spacing, practically all of the blurring was eliminated.

Interferogram 071580-6 was analyzed, and the data are presented in Table 5. The negative was adjusted so that the RHS of the plate was parallel to the x-axis travel of the microscope's stage; the traverse to obtain the data was made at approximately the same x-location on the plate as the traverses for the previous interferograms. For this interferogram, the locations of the whole plus half fringe shifts were recorded. This was done because the interferometer was adjusted to give a bright (infinite fringe) field in the region outside the boundary layer. The dark fringes in the actual image indicated fringe shifts of a whole number plus one-half; these fringes became light or clear areas on the negative. These clear fringes were much narrower than the dark fringes so their locations could be more accurately determined.

Of course, it does not really matter whether the identified fringe shifts are of a whole number or of a whole number plus one-half. What does matter in this example is the fact that the fringe number of the field

Table 5. Fringe location measurements for interferogram 071580-6 (infinite fringe field).

y' [in]	y [mm]	S
1.2778	9.456	0.0±, RHS edge of B. L.
1.3557	7.394	0.5
1.4370	5.241	1.5
1.4832	4.018	2.5
1.5174	3.113	3.5
1.5460	2.356	4.5
1.5720	1.668	5.5
1.5970	1.006	6.5
1.6214	0.360	7.5
1.6350±	0.000±	Wall, RHS
2.0536	0.000	Wall, LHS
2.0549	0.034	7.5
2.0766	0.609	6.5
2.0992	1.207	5.5
2.1225	1.824	4.5
2.1480	2.499	3.5
2.1765	3.253	2.5
2.2140	4.246	1.5
2.2800	5.993	0.5
2.3300	7.317	0.0±, LHS edge of B. L.

Note: x' = 1.000 in (location of traverse)
x = 19.383 mm = 0.485H

x'_o = 0.2623 in
x'_H = 1.7847 in
H' = 1.5224 in

outside the boundary layer is practically indeterminable. As stated previously, the attempt was made to adjust the field to uniform and maximum brightness; however, that the field was not uniformly bright can be seen from Figure 35, where a dark region is apparent in the upper right side of the figure. Further, there is no way to be certain that the bright region is really at maximum brightness (indicating S = 0). (Hauf and Grigull mention that it is easier to adjust for a dark field than a bright one, since a relatively small deviation in the intensity of the field from darkness is more obvious than a small deviation from maximum brightness [4, p. 215].)

With wedge fringes, this problem does not exist, since the maxima and minima are adjacent, and one can be selected to follow in making a traverse toward the plate.

As shown in Table 5, only single values were recorded for the presumed wall locations. Actually, though the LHS wall was observed as being relatively distinct, the RHS wall was relatively indistinct. This could be expected when using the infinite fringe mode, since the fringe number just at the wall will be a more or less random value and the brightness of the fringe at the wall may nearly match the brightness of the wall. Here again, the wedge fringe adjustment can be expected to allow a better resolution of the problem, since the maxima and minima are next to each other and next to the wall, which is at an

intermediate brightness. With wedge fringes, even if the wall's location is not more distinct than with the infinite fringe mode, at least the extent of the region of indistinctness should be more obvious.

When using wedge fringes, it is possible to interpolate the fringe number at intermediate locations between fringe intercepts. The technique for doing this will be illustrated using Figure 46. In the figure, a reference line (dashed) is shown crossing a wedge fringe field. The fringe number is presumed to increase in going from right to left. Thus, the fringe number increases by one in going from A to D. Points B and C are representative points at which fringe number interpolations are being made. As can be seen in the figure, the distance x_1 is measured from the reference line to the "lower" fringe, and the distance x_2 is measured from the reference line to the "upper" fringe. The interpolated fringe value will be

$$S = S(A) + x_1/(x_1+x_2) \qquad [32]$$

It should be apparent that the fraction, $x_1/(x_1+x_2)$ varies from 0 to 1 in going from A to D .

This interpolation method suffers from the potential problem that measurements must be made to points off of the reference line, and the reference line is where the temperature profile is desired to be determined. As a

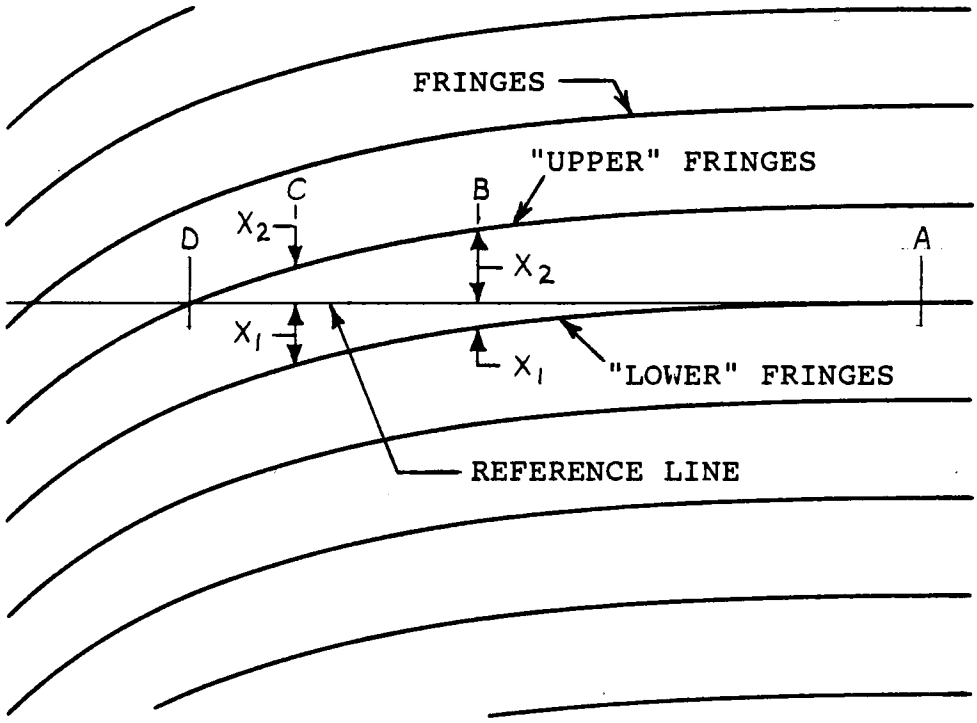


Figure 46. Distances X_1 and X_2 may be measured in order to interpolate the fringe number at intermediate locations between fringe intercepts.

practical matter, if the fringes are "relatively fine" and if no "very large" temperature gradients occur normal to the reference line, then no significant error is incurred by leaving the reference line.

As an example of interpolation, interferogram 071580-3 was again placed under the measuring microscope and was aligned to the extreme ends of the centerline fringe, as before. A traverse was made on the RHS of the plate; the data are presented in Table 6. For this measurement, the x' micrometer was initally set to 0.9100 inch instead of 0.7100 inch as before. Also, whereas before the x' value was increased by 0.0033 inch to account for nonstraightness of the fringe (see Table 3), this time the x' value was increased by only 0.0010 inch to 0.9110 which was the location of the fringe just outside of the boundary layer. The 0.9110 value represents the location of the reference line drawn in Figure 46. Fringe intercepts or crossings are marked by the entry of this value in the table. It can also be seen that whole number values are in the fringe number, S, column.

The x' values labeled "Upper" and "Lower" in Table 6 correspond to the locations of the upper and lower fringes as shown in Figure 46. The fringe shift values were calculated using Equation 32, where the fractional fringe shift was found from using the following x' values:

Table 6. Measuring microscope data for interferogram 071580-3 with interpolations between fringe intercepts.

x' [in] Ref. Upper	Lower	S	y' [in]		y [mm]
0.9110		0.000	1.1950		11.87
0.9263	0.9090	0.116	1.2750		9.76
0.9232	0.9061	0.286	1.3250		8.43
0.9182	0.9010	0.581	1.3750		7.11
0.9143	0.8977	0.801	1.4000		6.45
0.9110		1.000	1.4194		5.93
0.9253	0.9084	1.154	1.4300		5.65
0.9194	0.9022	1.512	1.4500		5.12
0.9110		2.000	1.4754		4.45
0.9195	0.9025	2.500	1.4954		3.93
0.9110		3.000	1.5130		3.46
0.9195	0.9025	3.500	1.5280		3.06
0.9110		4.000	1.5429		2.66
0.9200	0.9028	4.477	1.5550		2.34
0.9110		5.000	1.5688		1.98
0.9203	0.9030	5.462	1.5800		1.68
0.9110		6.000	1.5935		1.32
0.9200	0.9026	6.483	1.6050		1.02
0.9110		7.000	1.6172		0.70
0.9203	0.9029	7.466	1.6280		0.41
0.9110		-----	1.6370	(Wall+)	+0.17
0.9110		-----	1.6500	(Wall-)	-0.17

$$\text{Fractional Shift} = \frac{\text{Reference} - \text{Lower}}{\text{Upper} - \text{Lower}} \qquad [33]$$

The reduction from y' to y in Table 6 was done the same way as that in the other tables.

Figure 47 shows a reduced copy of a form that was made up to assist in the data reduction process. The RHS y and S data of Table 3 have been copied into Figure 47. In the lower section of the form are entered the necessary parameters associated with the experiment. The values for L and λ should be familiar. The value for P_∞ includes a temperature correction, a gravity correction, and an altitude correction since the barometer was one floor below the experiment. The value for refractive index, n, is found in Appendix K (the exact value is really not important here). The values for T_∞, θ_∞, T_w, and θ_w are found in Appendix F. (The symbol "T" was used for degrees Kelvin while the symbol "θ" was used for degrees Celsius.) The process of calculating correction factors and reducing data will now be explained.

A formula, Equation 21 (p. 44), was presented in CHAPTER I for calculating the refraction error. It is

$$\Delta S_1 = \frac{n \lambda L}{12 b^2} \qquad [34]$$

where b is fringe spacing. This formula is shown in the lower section of the form of Figure 47, where the n, λ, L, and 12 terms have been combined to yield 0.0129 (mm^2). The

Data from traverse # _____ Interferogram # 071580-3

x = ℄ RHS

S	y mm.	Δy = b	$\bar{b}$	ΔS₁	ΔS₂	S ideal	θ °C	Δ %
0	14.046			0	0	0	27.30	0
		7.825						
1	6.221		4.718	.001	.034	.967	30.25 30.35	.4
		1.610						
2	4.611		1.324	.007	.073	1.934	33.25 33.46	.8
		1.037						
3	3.574		.917	.015	.113	2.902	36.32 36.63	1.2
		.797						
4	2.777		.755	.023	.153	3.870	39.45 39.87	1.6
		.712						
5	2.065		.678	.028	.193	4.835	42.63 43.18	2.1
		.643						
6	1.422		.640	.032	.234	5.798	45.87 46.56	2.6
		.636						
7	.786		.640	.032	.276	6.756	49.16 50.01	3.3
		.643						
8	.143 ±			.032	.317	7.715	52.53 53.54	3.9
	0						53.28 54.33	4.0

Form for approaching heated wall from field.

L = .2445 m θ_w = 53.4 °C T_w = 326.55 °K

λ = 6328 × 10⁻¹⁰ m $\Delta S_1 = \frac{n_w \lambda L}{12 b^2} = \frac{.0129}{b^2}$

P_∞ = 739.5 mm Hg $S_{ideal} = S + \Delta S_1 - \Delta S_2$

n_∞ = 1.00025 $\theta = \frac{T_\infty}{1 - a S_{ideal}} - 273.15$

$\left.\frac{\partial T}{\partial y}\right|_w$ = −5.291

x = _____

T_∞ = 300.45 °K

θ_∞ = 27.30 °C $a = \frac{2}{3} \frac{\lambda R T_\infty}{L P_\infty} = .0060397 \frac{T_\infty}{L P_\infty} = .01004$

Figure 47. Reproduction of a form for recording and reuucing interferogram data.

refractive index value, n, could be determined for any temperature from that of the field to that of the wall. It is just as well to use 1 as the value of n since for air at near normal temperatures it is equal to 1 to about four significant figures.

The fringe spacing term, b, could be found by taking the difference between the y values for the fringe locations; these fringe location differences are recorded in the $\Delta y = b$ column of Figure 47. Hauf and Grigull use the technique of taking the mean value of adjacent b values and using this value as the fringe spacing at the fringe. This mean value is recorded as $\bar{b}$ in Figure 47; as can be seen, the ΔS_1 values are also recorded. The ΔS_1 value for S = 8 was not calculated but was estimated from the S = 6 and S = 7 values.

Two formulas for calculating the end effect correction, ΔS_2, are derived in Appendix A. The first formula, that for an assumed parabolic temperature distribution, is

$$\Delta S_2 = 0.3311 P_\infty \sqrt{\delta^2 - y^2}\left[\frac{1}{T_\infty} - \frac{1}{\sqrt{\Delta T\, T_\infty}} \tan^{-1} \frac{\Delta T}{\sqrt{\Delta T\, T_\infty}}\right] \qquad [35]$$

To clarify the use of this equation, it will be applied to the data of Figure 47 at S = 4.

The value for P_∞ is 739.5 (mm Hg). The value for δ is taken as the value of y at S = 0, that is, 14.046 (mm). The value for y is that value at which the

correction is being calculated, in this case, 2.777 (mm). The value for T_∞ is 300.45 (^oK). As shown in the appendix, $\triangle T = T_M - T_\infty$ where T_M is the approximate, uncorrected value for air temperature at the S-value under consideration. T_M is obtained from Equations 11 and 12 (p. 36), which are entered in the lower section of Figure 47 (with T replaced by θ). The value for "a" is shown in the figure as 0.01004. (See Appendix K for recommended values of $\bar{r}$ and R.)

Thus, at S = 4, $T = T_M$ = 313.02 ^oK (39.87 ^oC), and $\triangle T = T_M - T_\infty$ = 12.57 (K^o). Finishing the calculation, $\triangle S_2$ is found to be 0.153. (Programs were written for a programmable calculator to handle virtually all of the calculations in most of the data sheets and tables.)

The equation for refraction error derived by Hauf and Grigull (Equation 20, p. 44) is

$$S_{ideal} = S + \triangle S_1 \qquad [36]$$

where S_{ideal} replaces $(n_\infty - n)(L/\lambda)$. It has been explained in CHAPTER I that the end effect causes an additional fringe shift over that along the length of the test surface. Thus, for the present case, $\triangle S_2$ should be subtracted from S_{ideal}.

$$S_{ideal} = S + \triangle S_1 - \triangle S_2 \qquad [37]$$

For the present example, S_{ideal} = 4.000 + 0.023 - 0.153 =

3.870 with the resulting air temperature of θ = 39.45 °C.

In the θ column of Figure 47, two values are entered for each row; the upper value is the calculated air temperature with both corrections included while the lower value includes no corrections. The Δ column shows the relative difference between the corrected and uncorrected values; that is

$$\Delta = 100(\theta_{uncorr} - \theta_{corr})/(\theta_W - \theta_\infty) \qquad [38]$$

where $\theta_W - \theta_\infty$ = 26.23 C°. It can be seen that the corrections are relatively important, amounting to as much as a 4% relative difference. It can also be seen that the end effect correction, for the present example, was generally an order of magnitude greater than the refraction correction, and the refraction correction, it is now seen, could as well have been ignored.

The temperature values at y = 0 were obtained from those at S = 6, 7, and 8 by fitting a second order curve to the data and extrapolating to y = 0. Thus, using the corrected temperature values, the resulting equation is

$$\theta = 0.053y^2 - 5.291y + 53.285$$

At y = 0, θ = 53.28 °C, which is entered in the figure. Further, $d\theta/dy$ (at y=0) = -5.291 C°/mm. This thermal gradient at the wall may be used to find the total heat loss from the plate. To do this, the gradient at various

x-locations along the wall must be found, and the gradient integrated along the height and length of the wall to give the heat loss from the wall. Suitable calculations or assumptions must be made for the other wall, the top and bottom, and the ends. This will not be done here.

The estimated wall temperature by thermocouples is 53.53 ^{o}C versus 53.28 ^{o}C by interferometry. Thus, the indicated error is 53.28 - 53.53 = -0.25 C^{o} or -0.25/26.23 = -0.95%.

The data reduction procedure for the data that includes fringe number interpolations is nearly identical to the procedure just given. To illustrate, the y and S values in Table 6 were copied into Table 7. The values for ΔS_1 were calculated the same way that they were in Figure 47, with the exception that the values were calculated only at the rows of whole numbered S values. The fringe spacing, b, term is the difference between two y values over one wavelength (between two adjacent whole numbered S values). The intermediate ΔS_1 values in the table were simply estimated from the calculated values (an equation for direct calculation was not derived).

The ΔS_2 values in Table 7 were calculated exactly as they were for Figure 47, with the exception that a different value, 11.87 millimeters, was used for δ. In this case, there is no problem with the intermediate S values; ΔS_2 may be calculated for nonintegral S.

Table 7. Fringe number and temperature data for interferogram 071580-3 with fringe number interpolations.

y [mm]	S	ΔS_1	ΔS_2	S_{ideal}	θ [°C]
11.87	0.000	0.000	0.000	0.000	27.30
9.76	0.116	0.000	0.002	0.114	27.64
8.43	0.286	0.000	0.007	0.279	28.14
7.11	0.581	0.000	0.015	0.566	29.02
6.45	0.801	0.000	0.022	0.779	29.67
5.93	1.000	0.001	0.028	0.973	30.26
5.65	1.154	0.002	0.033	1.123	30.73
5.12	1.512	0.004	0.044	1.472	31.81
4.45	2.000	0.008	0.061	1.947	33.29
3.93	2.500	0.012	0.077	2.435	34.83
3.46	3.000	0.016	0.094	2.922	36.38
3.06	3.500	0.020	0.111	3.409	37.95
2.66	4.000	0.024	0.128	3.896	39.53
2.34	4.477	0.026	0.145	4.358	41.05
1.98	5.000	0.029	0.163	4.866	42.73
1.68	5.462	0.030	0.179	4.313	44.23
1.32	6.000	0.031	0.198	5.833	45.99
1.02	6.483	0.032	0.215	6.300	47.59
0.70	7.000	0.032	0.233	6.799	49.31
0.41	7.466	0.032	0.249	7.249	50.88
0.00				SOCF*:	53.21

*Second-order curve fit

The calculation of S_{ideal} and θ was the same for both Table 7 and Figure 47. The temperature at the wall, at y = 0, was calculated from a second order curve fit, as before. The estimated wall temperature was 53.21 °C and the thermal gradient was -5.788 C°/mm. The indicated error in temperature is (53.21-53.53)/26.23 = -1.2%.

The corrected and uncorrected temperature data of Figure 47 plus the (corrected) temperature data of Table 7 are plotted in Figure 48. It can be seen that the curve can be more accurately defined when fringe number interpolation is used. This is especially important in the region between S = 0 and S = 1, which is a relatively large gap.

For the data of Table 3 and Figure 47, S = 0 was taken to be at y = 14.046 millimeters; whereas, for the data of Tables 6 and 7, S = 0 was taken to be at 11.87 millimeters. This would appear to be a relatively large discrepancy; however, by glancing at Figure 48, the curves are seen to be so flat in this region that there is little real difference between the curves. At the wall, the difference between the (corrected) curves is (53.28-53.21)/26.23 = 0.3%.

C. Physical Interpretation of the Results of the Heated Plate Experiment

The temperature field about the heated plate is shown

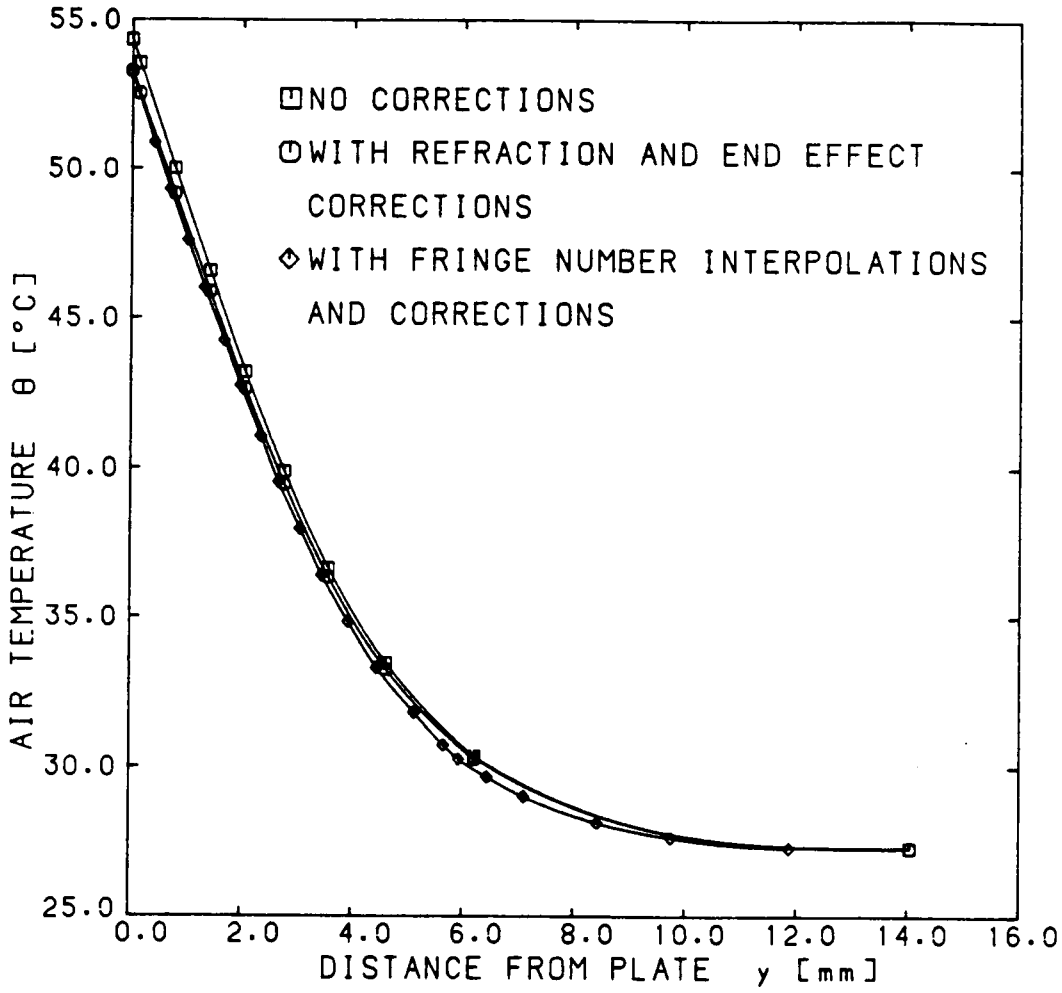


Figure 48. Temperature profiles about the heated plate.

quite vividly by the isotherm fringe pattern of Figure 35 (p. 180). The regular and concentric fringes indicate the presence of a laminar thermal boundary layer about the plate whose extent can be estimated to extend slightly beyond the outermost minima.

The equations for determining the temperature of a fringe results from some simplifications (from the Lorentz-Lorenz equation [7] to the Gladstone-Dale equation [8] and the use of the ideal gas equation) and some assumptions (the assumed temperature distribution and the extent of the boundary layer in the end effect correction equations). Nevertheless, errors of about 1% were achieved in comparing the interferometrically measured plate temperature to the "directly" (by thermocouples) measured plate temperature. That such low error values are obtained tends to confirm the validity of this (somewhat indirect) optical method of measuring temperature distributions.

D. Techniques for Reducing the Mach-Zehnder Data for the Internal Cavity Experiment

The process of data reduction for the MZI interferograms will now be described.

The interferograms to be considered here are:

121979-1: for scale factor determination

122079-4: wedge fringes, cavity isothermal

122079-7: wedge fringes, cavity operating

The magnification was determined in the same manner as that for the plate. The results were as follows.

Image Distance = 1.1435 inch

Object Distance = 1.2490 inch

Magnification = 0.9155

The "scale factor" is 25.4 (in/mm)/0.9155 = 27.744; when multiplied by the scale factor, an image distance in inches is converted to an object distance in millimeters.

Interferogram 122079-4 was placed in the measuring microscope and was aligned so that two points, one near each end of a fringe at approximately y = 0.25H, were aligned to be parallel to the x'-travel (the 6 inch travel) of the microscope's stage. Over the length of the fringe, its maximum deviation from straightness was found to be by 0.0010 inch.

Next, with the fringe at y = 0.25H still aligned to the stage, a fringe at approximately y = 0.5H was checked, and it was found that the right hand end of the fringe (the cold wall side) was lower or closer to y = 0 than the left hand end by 0.0008 inch over the width of the cavity. With the alignment unchanged, a fringe at approximately y = 0.75H was checked, and it was found that the right hand end was lower than the left hand end by 0.0018 inch. A rough check of other fringes showed that lower fringes (closer to y = 0) were better aligned than the upper fringes.

It was decided that when the measurements were to be

made on interferogram 122079-7, the stage-travel reference line should be parallel to the y = 0.5H fringe of interferogram 122079-4. This would be done to split the error between the top and bottom halves of the cavity (it was decided not to try to plot the path of the "straight" fringes and try to compensate as was done for the flat plate, since this was considered an "experimental" technique at the time).

With interferogram 122079-4 in the microscope, a fringe at approximately y = 0.5H was carefully aligned so that points near its ends were aligned to the x' stage travel. Measurements were made on the image of the plumbline in the interferogram, and it was found that the line's image at the cavity's top was 0.0028 inch to the left of its image at the cavity's bottom (actually, two fringes distance from the top or bottom). (One of the cavity's walls could have been selected instead of the plumbline for alignment.)

Interferogram 122079-7 was placed in the measuring microscope and was adjusted until the top of the plumbline was 0.0028 inch to the left of the bottom of the line. (It just happened to come out at precisely 0.0028 inch; a later check showed 0.0029 inch and after all measurements were completed, 0.0038 inch. There was no fine angle adjustment available on the microscope to position or to hold the negatives in place.)

It was decided to make the traverses at increments of 0.1H. Thus, the y' values for the cavity's top and bottom were determined, and the y' micrometer values corresponding to 0.1H, 0.2H, ..., 0.9H were calculated. The cavity top was taken to be at y' = 1.6455 inch and the cavity bottom at y' = 0.2125 inch. It was also decided to obtain approximately 20 data points for each traverse. About 10 fringe intercept points were expected, so about 10 fringe number interpolations were needed. At y = 0.9H, the hot wall was at x' = 1.6882 inch, and the cold wall was at x' = 0.2502 inch. The difference, 1.4377 inch, divided by 20 gives 0.0719 inch, which is equivalent to nearly 3 turns of the micrometer spindle. Thus, it was desired to obtain a data point for each 3 turns or fewer of the micrometer. Plus, it was desired to take measurements at x = 0.5L of each traverse. This would correspond to x' = (1.6882 + 0.2502)/2 = 0.9692 inch.

The y' micrometer was turned to the value corresponding to 0.9H, and then was adjusted so that the crosshairs were at the nearest fringe.

In analyzing the cavity interferograms, the technique used was that the reference line (the path of the center of the crosshairs) would originate where a fringe intersected the hot wall. Locating this intercept point is made difficult because the image of the wall boundary is fuzzy, and the fringe becomes "wavy," (oscillates up and down)

near the wall.

In analyzing interferogram 122079-7, the nominal wall location was taken to be at the end of the brightest part of the fringe (where it terminates at the hot wall). One of the crosshairs was aligned parallel to the wall, and then the x' micrometer was adjusted until this hair was at the nominal wall location. Then, the crosshairs were rotated and the y' micrometer was adjusted (moving the crosshairs up or down along the wall) until a hair (the hair nearer horizontal) was tangent to the fringe just outside of the fringe's "wavy" region at the wall. This extrapolated wall intercept point was defined as S = 0, and the micrometer values were recorded.

To help clarify the interferogram analysis procedure, an example using the traverse at 0.5H will be presented.

The nominal location for 0.5H was found to be at y' = 0.9694 inch; the y' micrometer was set to this value and then was adjusted to reach the nearest fringe. The hot wall and the S = 0 locations were found using the method described immediately above. The traverse's reference line was taken to be at y' = 0.9318 inch and the hot wall at x' = 1.6848 inch. The data obtained are listed in Table 8.

The x' micrometer was turned to make the traverse and was stopped and centered at the fringe crossings for S = 1, 2, 3, 4, and 5, and the corresponding x' values were recorded at these points.

Table 8. Interferogram analysis and temperature data of the y = 0.5H traverse for the internal cavity.

x' [in]	x [mm]	y' [in] Upper	y' [in] Ref.	y' [in] Lower	S	ΔS_1	ΔS_2	S_{ideal}	T [°C]
1.6848	0.00		0.9318		0.000	0.021	0.000	0.000	37.41
1.6556	0.81		0.9318		1.000	0.019	0.000	1.002	34.30
1.6258	1.64		0.9318		2.000	0.017	0.000	2.004	31.24
1.5925	2.56		0.9318		3.000	0.013	0.000	3.008	28.24
1.5525	6.67		0.9318		4.000	0.005	0.000	4.016	25.29
1.4805	5.67		0.9318		5.000	0.000	0.000	5.021	22.40
1.4030	7.82	0.9353		0.9196	5.223	0.000	0.000	5.244	21.77
1.3250	9.98	0.9342		0.9190	5.158	0.000	0.000	5.179	21.96
1.2250	12.76		0.9318		5.000	0.000	0.000	5.021	22.40
1.1500	14.84	0.9457		0.9309	4.939	0.000	0.000	4.960	22.58
1.0730	16.97	0.9447		0.9296	4.854	0.000	0.000	4.875	22.82
0.9694	19.85	0.9440		0.9289	4.808	0.000	0.000	4.829	22.95
0.9649	19.97	0.9436		0.9288	4.797	0.000	0.000	4.818	22.98
0.8500	23.16	0.9439		0.9282	4.771	0.000	0.000	4.792	23.06
0.7000	27.32	0.9431		0.9275	4.724	0.000	0.000	4.745	23.19
0.5500	31.48	0.9414		0.9258	4.615	0.000	0.000	4.636	23.50
0.4950	33.01	0.9418		0.9262	4.641	0.000	0.000	4.662	23.43
0.4261	34.92		0.9318		5.000	0.003	0.000	5.018	22.41
0.3660	36.59		0.9318		6.000	0.007	0.000	6.014	19.61
0.3302	37.58		0.9318		7.000	0.016	0.000	7.005	16.87
0.3018	38.37		0.9318		8.000	0.024	0.000	7.997	14.18
0.2776	39.04		0.9318		9.000	0.031	0.000	8.990	11.53
0.2553	39.66		0.9318		10.000	0.034	0.000	9.987	8.93
0.2450*	39.95		0.9318		------	-----	-----	-----	----

*Cold wall location

It can be seen from interferogram 122079-7 (Figure 44, p. 219), that the fringes near the center appear to curve upward from the hot wall and reach a crest, curve downward and reach a trough, and to curve back upward again before reaching the cold wall.

Along the traverse, as the crosshairs were advanced beyond the S = 5 fringe intercept, the fringe that was just beneath the one that made the S = 5 intercept was observed to curve upward only to reach the crest well below the center of the crosshairs. A fringe number interpolation was done at the approximate top of this crest. The y' values for the "upper" and "lower" fringes can be seen in Table 8. For this case, the interpolation equation was different from that given for the heated plate (Equation 33). The equation used for the data in Table 8 is

$$\text{Fractional Shift} = \frac{\text{Upper} - \text{Reference}}{\text{Upper} - \text{Lower}} \qquad [39]$$

(If one selects the wrong equation for calculating the fractional shifts, then the error should be apparent as discontinuities in the S-numbers along a traverse.) In the table, it can be seen that the crest was at S = 5.223.

From this crest, the fringes curved downward indicating that the S-number was decreasing. Another interpolation was made that yielded S = 5.158. Beyond this, the same fringe that yielded S = 5 previously was

crossed again to give another S = 5. In the table, it can be seen that the fringe number continued to decrease until it reached the trough, at which point S = 4.615. Beyond this, there was a continuous increase in S-value up to the cold wall.

It should be apparent that the ability to make fringe number interpolations was extremely important in this interferogram analysis. Without this ability, the sizes of the crest and trough and the general smoothness of the curve within the central region of the cavity could not be ascertained.

The x-values of Table 8 were calculated from the following equation

$$x = (x'_W - x')(27.744) \qquad [40]$$

where x'_W is the x' value at the hot wall (1.6848 for this example), and 27.744 is the previously determined scale factor.

The refraction correction term, ΔS_1, was calculated precisely as it was for the heated plate (with fringe number interpolations). The equation is

$$\Delta S_1 = \frac{n \lambda L}{12 \bar{b}^2} = \frac{.0129}{\bar{b}^2} \qquad [41]$$

As with the plate, only the x-values at whole numbered S-values were used in finding $\bar{b}$ (and thus, ΔS_1); the other ΔS_1 values were estimated.

The flow situation for this internal cavity is much more involved and complicated than that for the heated plate. The cavity contains six surfaces upon which boundary layers can be established and interact with each other. For this reason, determining an end effect correction for a cavity is a much more difficult task than finding one for a flat plate. Whereas before, an assumption for calculating the end correction for the plate seemed relatively obvious and reasonable, it is not at all obvious what assumptions to make concerning the cavity.

An estimate of the end effect error for the present cavity flow is presented in Appendix L. The maximum error in air temperature measurement relative to the hot-to-cold wall temperature difference was found to be about 1%. Thus, based on this relatively small error and the difficulty in properly correcting for end effects, the end effect correction, ΔS_2, will be assumed to equal zero, as shown in Table 8.

In the analysis leading to Equation 20 (p. 44) and Equation 36 (p. 247), the value of S was assumed to increase with increasing temperature. For the cavity, Equation 13 will be used to calculate temperature. In this equation, S increases with decreasing temperature. Thus, Equation 26 must be changed to read

$$S_{ideal} = S - \Delta S_1 \qquad [42]$$

(The analysis of Goldstein [9] produces this same equation.) But to use Equation 13, the S value at the wall must be zero. Therefore, the following equation was used for the data in Table 8:

$$S_{ideal} = S + (\Delta S_1)_W - \Delta S_1 \qquad [43]$$

where $(\Delta S_1)_W$ is the value at the hot wall. For the present example, $(\Delta S_1)_W = 0.021$.

As explained in previous chapters, there was a gap of approximately 3/16 inch (0.0048 meter) between the ends of the walls and the glass window. It was felt that better accuracy would be obtained if half the length of each end gap (or one gap's length) was added to the nominal length of the cavity (since the heating or cooling effect of each wall would extend into the gap). Thus,

$$L = 0.2445 \text{ m} + 0.0048 \text{ m} = 0.2493 \text{ m}$$

The temperatures of the hot and cold walls were taken as the mean of the corrected thermocouple readings. From Appendix G, the hot wall temperature, T_H, was 37.41 °C (310.56 °K), and the cold wall temperature, T_C, was 7.24 °C (280.39 °K). The mean temperature was 22.32 °C (295.47 °K), while the temperature difference, ΔT, was 30.17 C°. The room temperature, T_∞, was 23°C. The corrected atmospheric pressure was 744.3 mmHg. Thus, from Equation 14

$$a = .0060397\frac{T_w}{P_\infty L} = .01011$$

Temperatures were calculated from Equation 13 as

$$T = \frac{T_w}{1 + a S_{ideal}} - 273.15 = \frac{310.56}{1 + 0.01011 S_{ideal}} - 273.15 \qquad [44]$$

The data obtained from the interferogram are tabluated in Appendix M. Besides the traverses at 0.1H through 0.9H, traverses near the very top and bottom of the cavity were made. These traverses were made just outside of the fuzzy regions that border the images of the cavity's surfaces; the traverses were at 0.04H and 0.97H.

As in the case for the plate, the temperature at the cold wall was extrapolated from a second-order curve fit to the three points nearest the wall. For the example at 0.5H, the following curve was found

$$T = -0.185y^2 + 10.348y - 110.826$$

The cold wall on the interferogram was taken to be at 39.946 millimeters; this yields T = 7.65 ^oC. The indicated error is 7.65 - 7.24 = 0.41 C^o or 0.41/30.17 = 1.4%.

On four of the traverses, a fringe number interpolation was done just at the cold wall so that the temperature could be calculated "directly." This was done at 0.04H, 0.1H, 0.2H, and 0.97H; for three of the locations, the second-order curve fit and interpolation gave a wall temperature closer to the measured value (at

0.04H, 0.1H, and 0.97H).

The data of Appendix M have been plotted in Figure 49. For this plot, nondimensional variables were used: x was replaced by $x/L = x/40$, and T was replaced by $(T - T_C)/(T_H - T_C) = (T - 7.24)/(30.17)$.

E. Techniques for Reducing the LDV Data for the Internal Cavity Experiment

The data forms for recording the LDV data are presented in Appendix I. The raw scale and voltage readings are listed in the Axis' (x' or y') and Voltage columns in the order that the traverses were performed.

To assist in reducing the data, another form was made up. It is illustrated in Figure 50. For the LDV experiment, the 243 millimeter (actual) focal length lens was used, and the beam intersection angle, $\emptyset$, was 11.34° (these values were obtained from a tag on the side of the lens). In Figure 50, $\emptyset_R$, represents the value to use if the angle reducer is used (which it was not). (The C is a correction factor; for the 243 millimeter lens, it would have been 2.1.) The fringe spacing, d_f, was calculated as shown where λ was 6328×10^{-7} millimeter and $\emptyset$ was 11.34 ($\emptyset_R$ would have been inserted if the angle reducer had been used). The scale factor, SF, was found from the RANGE knob setting on the 1090 tracker. It was set to 0.1 V/KHz = 10^{-4} volt·sec. As explained in CHAPTER I, the offset

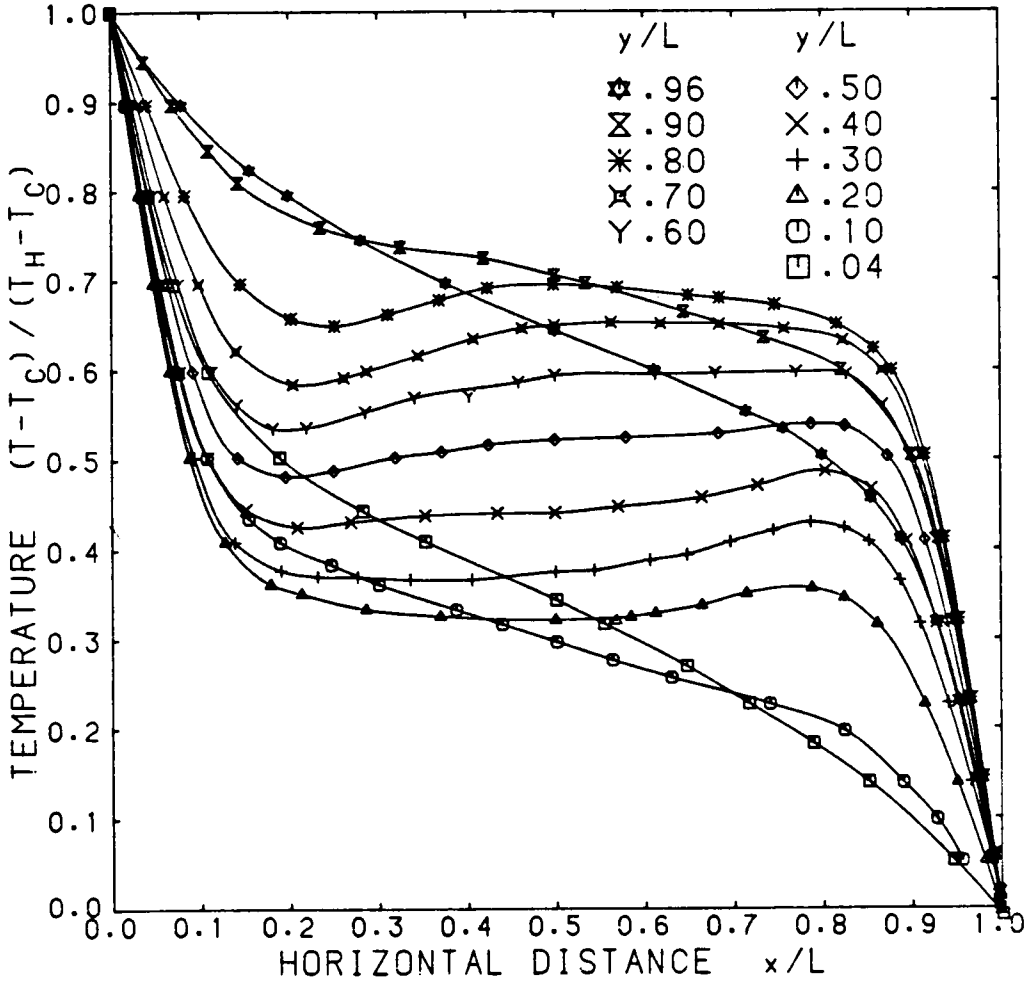


Figure 49. Horizontal temperature distributions within the cavity.

Form for LDV Data Experiment No. 2 Date 12-21-79

Lens F.L. = 243 mm.

ϕ = 11.34 ° $\phi_R = 2\tan^{-1}\left[\frac{11}{2S}+C\right]$ = ——— °

Nom. F.L	120	250	600
C	4.3	2.1	.9

Fringe spacing: $d_f = \frac{\lambda}{2\sin\frac{\phi}{2}}$ = .003202 mm.

Scale Factor, $SF = \frac{.1 \text{ Volt}}{1000 \text{ Hz}}$ = 10^{-4} Volt · sec

With frequency shifter: Offset Voltage, V_o = 1.98, 4.98

Velocity = $\frac{(\text{Voltage}) - V_o}{S.F.} \cdot d_f$ $\left[\frac{mm}{sec}\right]$

$x = x_o' + x_o - x' = 30.0 + 20.0 - x' = 50.0 - x'$ mm.

$y = y' + y_o - y_o' = y' + 20.0 - 86.0 = y' - 66.0$ mm.

$z = z' + z_o - z_o' = z' + 122 - 62.5 = z' - 59.5$ mm.

Wall: Hot

TC #	1	2	3	4	5	6	7	8	
Pot mV	1.50	1.4975	1.50	1.495	1.50	1.4975	1.4975	1.4975	
Temp. °C	37.3	37.25	37.3	37.2	37.3	37.25	37.25	37.25	
Corrected	37.45	37.4	37.45	37.35	37.45	37.4	37.4	37.4	

Wall: Cold

TC #	1	2	3	4	5	6	7	8	9
Pot mV	.27	.265	.2675	.2675	.275	.2725	.27	.2675	.2775
Temp. °C	6.9	6.8	6.85	6.85	7.05	7.0	6.9	6.85	7.1
Corrected	7.25	7.15	7.20	7.20	7.35	7.30	7.20	7.15	7.4

Room temperature = 23 ΔT = 30.17

Atm press. = $\frac{747.8 - 2.5 - .6 - .36 = 744.3}{20.5\,°C}$

Figure 50. Form for recording LDV data.

voltage, V_o, is the indicated output voltage due to the operation of the frequency shifter at zero actual velocity. With the frequency shifter at 20 KHz, the meter's output was 1.98 volts. At 50 KHz, it was 4.98 volts.

The next line in the form gives Equation 25 for the fluid (or particle) velocity.

The next three lines in the form, for x, y, and z, are equations that were explained in CHAPTER III. These equations are specific for the particular way that the cavity and the measuring scales were set up; whereas, most of the other lines are applicable to any experiment.

The next two sections of the form contain the thermocouple data for the walls. The millivolt readings from the potentiometer are recorded, the corresponding temperatures are recorded, and the corrected temperature values are entered. (Corrections are found in Appendix G.) The values recorded are the same as those for the MZI experiment (done the previous day). The thermoregulators on the constant temperature baths were left unchanged.

The atmospheric pressure was read from a mercury barometer (as explained in CHAPTER III). The raw reading was 747.8 mmHg. The 2.5, 0.6, and 0.36 values are temperature, gravity, and altitude corrections, respectively.

For an example of data reduction, on row #12 of traverse No. 1 in Appendix I, x' = 45.0 and Voltage = 3.12.

The value for x is obtained from x = 50.0 - x' = 50.0 - 45.0 = 5.0 millimeters. For velocity, Vel = $((3.12-1.98)/10^{-4})(0.003202)$ = 36.50 mm/sec.

The equation given in Figure 50 for velocity does not contain absolute value symbols whereas Equation 25 does. The absolute value symbols were removed so that the sense or direction of the flow would not be lost. For the present cavity and LDV arrangement, the equation in Figure 50 yields the correct sign; that is, a voltage increase over V_o represented a velocity in the assumed positive directions. As in the example above, at 5 millimeters from the hot wall, the velocity was found to be 36.50 mm/sec (positive, therefore, upward as would be expected). For other experimental situations, one may need to take the negative of the values obtained.

A plot of the centerline velocity profiles is presented as Figure 51. A listing of the data selected for this plot is in Appendix I.

Figure 51 was plotted using dimensionless variables; that is, the x and y distances were nondimensionalized by plotting x/LP= x/40 and y/H = y/40. The velocities u and v were nondimensionalized by plotting uL/α or vH/α where $\alpha = k/C_f \rho$

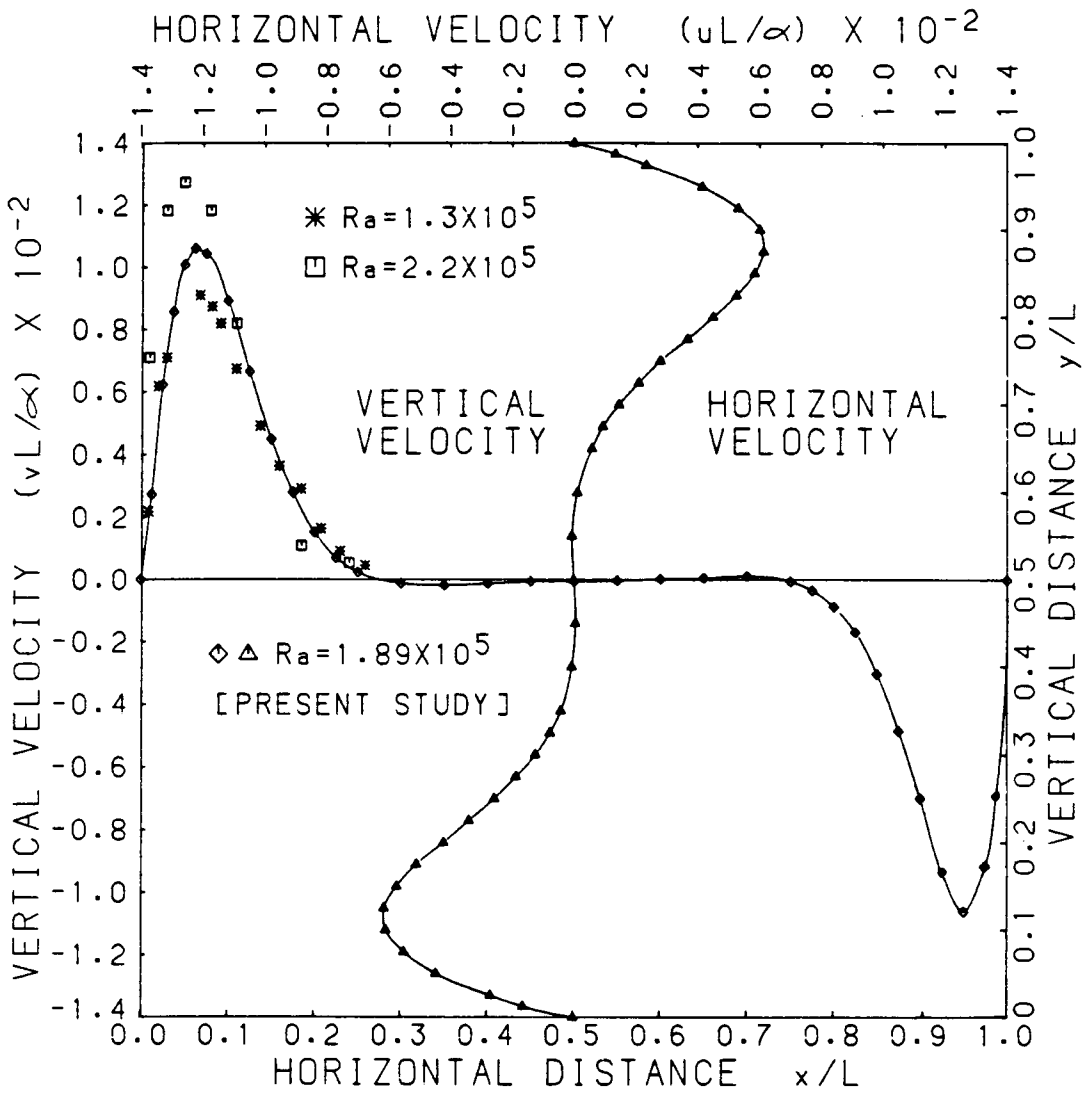


Figure 51. Centerline velocity profiles within the cavity.

The velocities at x/L = 0.0 and 1.0 and at y/L = 0.0 and 1.0 in the plot were not measured. These velocities were taken to be zero (due to the no-slip condition) in order to complete the curve.

F. Physical Interpretation of the Results of the Internal Cavity Experiment

The presence of thermal boundary layers on the vertical walls of the cavity can be seen in Figure 42 (p. 216), though the situation is not as clear as that for the heated plate in free air. Taking the hot wall for consideration, the isotherm fringes near the hot wall are farther away from the wall toward the top of the cavity, which indicates the presence of a thermal boundary layer that thickens toward the top of the cavity. The presence of a boundary layer can also be inferred from the curves of Figure 50. Considering the temperature profile curves from near the bottom of the cavity to the top, the slopes of the curves near the wall are seen to decrease (except for the two curves that pass through the relatively stagnant region in the lower corner).

Simple visual inspection of the profile curves of Figure 50, shows considerable symmetry among the curves. For example, the curve representing y/L = 0.96 looks identical to the curve of y/L = 0.04 (after a 180° rotation, of course). Indeed, the flows about the hot and

cold walls should be symmetrical except for relatively small differences due to fluid property variations with temperature. The isotherms of Figure 42 also show a large degree of symmetry, though this does not have to be the case. If beam splitter BS3 was translated (while the isotherm fringes were formed), then the interference condition at any given point would change and the fringes would seem to move (perpendicularly to themselves). Thus, an "off center" fringe pattern could be formed even if the temperature distribution is exactly symmetrical.

It can be seen from Figure 42 or Figure 50 that thermal stratification of the air in the central region of the cavity is present. This is further shown in Figure 52, which is a plot of the (nondimensionalized) air temperature along the vertical centerline of the cavity. It can be seen from this plot that the thermal gradients at the top and bottom of the cavity are not zero. This can also be seen from Figure 42, since the fringes are not perpendicular to the top and bottom surfaces. Thus, the ideal of having adiabatic top and bottom cavity surfaces is not realized.

The presence of velocity boundary layers on the hot and cold walls is shown by the velocity profile curve of Figure 51. Note the relative "sharpness" of the curves next to the vertical surfaces. The data of Linthorst et. al. [10] are included in the figure for comparison.

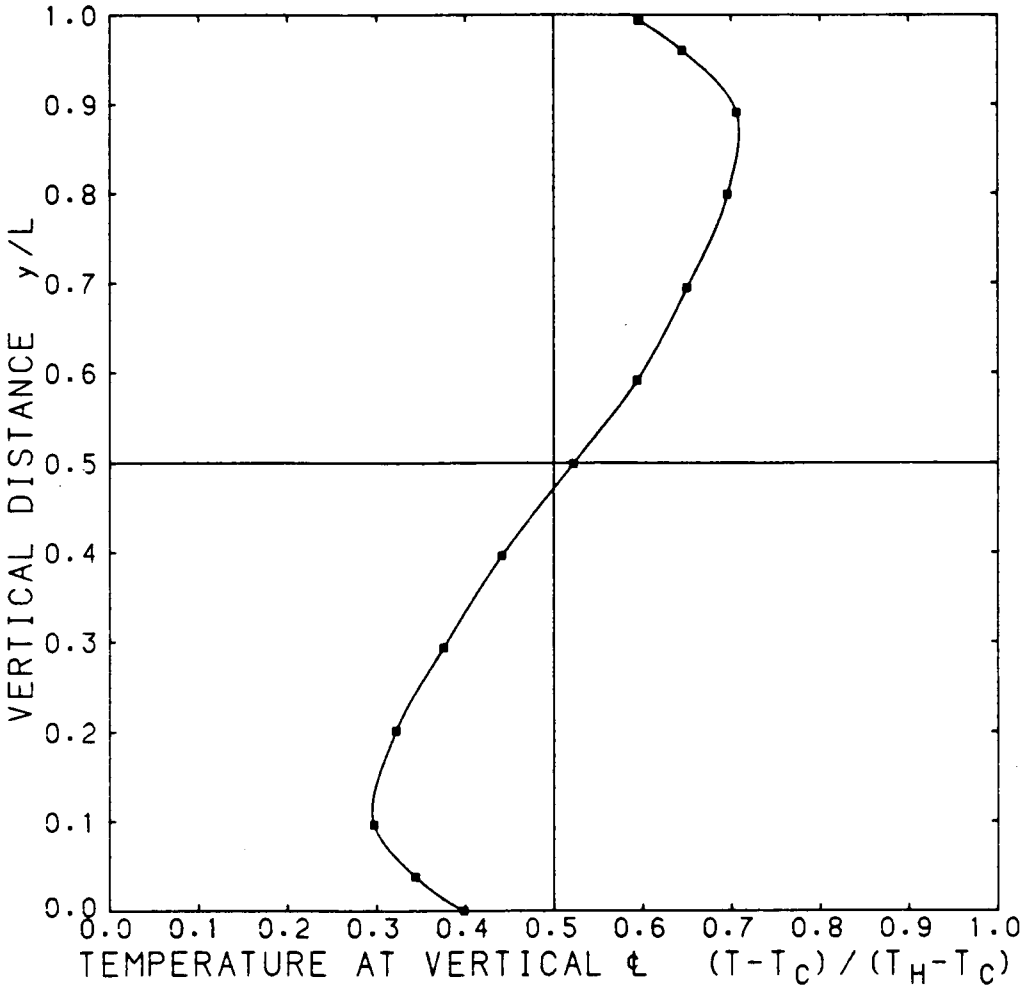


Figure 52. Temperature profile along the vertical centerline within the cavity.

These data were obtained from LDV measurements on air in a square enclosure at Rayleigh numbers of 1.5 X 10^5 and 2.2 X 10^5. The present study has a Rayleigh number of 1.89 X 10^5, and the plot is seen to lie mostly within the bounds of the data with the other Rayleigh numbers, as would be expected.

CHAPTER V

ERROR ANALYSIS

A. Introduction

In this chapter, estimates of the uncertainties in the MZI and LDV data will be made. With the MZI, only the internal cavity data will be considered.

B. Uncertainty Analysis of the MZI Data for the Cavity Experiment

It is desired to obtain a value for the possible error in the air temperature values obtained with the interferometer. This possible error value is usually termed "uncertainty." This analysis will generally follow the technique described by Kline and McClintock [11].

The equation used to calculate temperature is

$$T = T_W/(1 + (CT_W/P_\infty L)S) \qquad [45]$$

where T_W is the hot wall temperature in ^oK, P_∞ is the air pressure in mmHg, L is the wall length in meters, S is the fringe number, and $C = 2\lambda R/3\bar{r} = 0.0060397$ when the above listed units are used. (This is Equation 13 with the data values associated with the cavity experiment inserted.)

Let it be assumed that the uncertainty in the resultant temperature, T, is due to uncertainties in the

quantities T_W, P_∞ , L, and S. That is, the uncertainty in $C = 2\lambda R/3\bar{r}$ is expected to be of less significance in the resultant temperature than the uncertainties in the above listed four quantities.

The equation recommended by Kline and McClintock for determining the uncertainty, applied to the present problem, is

$$\Delta T = [(\frac{\partial T}{\partial T_W}\Delta T_W)^2 + (\frac{\partial T}{\partial P_\infty}\Delta P_\infty)^2 + (\frac{\partial T}{\partial L}\Delta L)^2 + (\frac{\partial T}{\partial S}\Delta S)^2]^{1/2} \qquad [46]$$

where ΔT is the resultant uncertainty in temperature and ΔT_W, ΔP_∞, ΔL, and ΔS are the uncertainties in T_W, P_∞ , L, and S, respectively.

Upon performing the partial differentiations on the equation for temperature, the results are

$$\partial T/\partial T_W = 1/D - (CS/P_\infty L)T_W/D$$

$$\partial T/\partial P_\infty = (CS/P_\infty^2 L)T_W^2/D^2$$

$$\partial T/\partial L = (CS/P_\infty L^2)T_W^2/D^2$$

$$\partial T/\partial S = -(C/P_\infty L)T_W^2/D^2$$

where

$$D = 1 + (CT_W/P_\infty L)S$$

Substituting the quantities T_W = 310.56 ^oK, P_∞ =

744.3 mmHg, L = .2493 meter, and S = 0 or 10 (the minimum and approximate maximum values of S):

	S = 0	S = 10
$\partial T/\partial T_W$	1.0	0.825
$\partial T/\partial P_\infty$	0.0	0.0348
$\partial T/\partial L$	0.0	104
$\partial T/\partial S$	3.14	2.59

Thus, at S = 0

$$\Delta T = [(1.0\,\Delta T_W)^2 + (3.14\,\Delta S)^2]^{1/2} \qquad [47]$$

and at S = 10

$$\Delta T = [(0.825\,\Delta T_W)^2 + (9.348\,\Delta P_\infty)^2 + (104\,\Delta L)^2 + (2.59\,\Delta S)^2]^{1/2} \qquad [48]$$

It remains to determine reasonable values for the uncertainties of the four quantities. This will be done, beginning with ΔT_W.

Whenever the thermocouples were read during the calibration procedure and during the experiment, a resolution of 0.05 C° was maintained. During the experiment, the hot wall was found to be isothermal to a variation of 0.1 C°. The principal thermometer used during calibration had a resolution of 0.2 F° (0.11 C°). A calibration check of this thermometer (discussed in CHAPTER III) showed that it was in error by 0.04 C° at room temperature. Thus, on the basis of this information, it

will be assumed that $\Delta T_W = 0.15\ C^o$.

The barometer was read to a resolution of 0.1 mmHg. Corrections for temperature (-2.5 mm), gravity (-0.6 mm), and vertical height (-0.36 mm) were applied. Thus, assume that $\Delta P_\infty = 1.0$ mmHg.

In CHAPTER IV, the effective value for L was taken to be 0.2445 + 0.00476 = 0.2493 meter where half the length of each endgap (between the end of the walls and the glass window) was added to the length of the wall. For this case, assume that the uncertainty is equal to one endgap. Thus, $\Delta L = 0.00476$ meter.

The uncertainty in fringe number, ΔS, will now be estimated using several different methods. Some of the methods will require a value for the fringe spacing. When interferogram 122079-4 was examined in the microscope, it was found that the fringe spacing, when averaged over 10 fringes, was 0.0166 inch (on the negative).

As previously stated in CHAPTER IV, interferogram 122079-4 was aligned in the microscope to the ends of the fringe at y = 0.25H, and the deviation of the fringe from the reference line was checked. The maximum deviation was by 0.0010 inch; related to fringe shifts, this is ΔS = 0.0010/0.0166 = 0.060.

The fringe at y = 0.5H was checked at its ends, and it was found that the fringe was inclined relative to the reference line by 0.0008 inch. The relative fringe shift

is $S = 0.0008/0.0166 = 0.048$.

The fringe at $y = 0.75H$ was checked the same way, and it was found to be inclined by 0.0018 inch; the resultant shift is $\Delta S = 0.0018/0.0166 = 0.108$.

When interferogram 122079-7 was analyzed, it was aligned the same way interferogram 122079-4 was aligned so that the endpoints of the $y = 0.5H$ fringe would be parallel to the reference line. Thus, the fringe shift due to the angling of the fringes should be zero or minimal near $y = 0.5H$ and should rise to a maximum shift near the top and bottom of the cavity. This maximum shift would probably be about 0.10 (it would increase from zero at the hot wall to its maximum value).

Also as stated in CHAPTER IV, the top of the plumbline's image on 122079-7 was aligned to be 0.0028 inch to the left of the bottom of the line. After all measurements had been taken, the alignment was checked again, and it was found that the difference was now 0.0038 inch. Thus, the possible fringe shift due to gross misalignment of the negative is $\Delta S = 0.0010/0.0166 = 0.060$. As in the above case, the fringe shift due to this misalignment would be zero at the hot wall and reach its maximum value at the cold wall.

It was desired to take S-number measurements on 122079-7 at the $x = 0.5L$ locations; a value for $x'(0.5L)$ was calculated and a number of data values were taken at

this location. Then, a better value for x'(0.5L) was calculated and repeat measurements were made at this point on several of the traverses. Of course, different S-values were obtained at these two x'(0.5L) locations. However, since the measurements were made so close together, they should be a good indication of the repeatability of S-number measurements. The data are listed in Table 9. The ΔS value in the table is the S-value at the higher number x-location minus the S-value at the lower number x-location. The mean of the absolute values of the ΔS values is 0.006; this should be a reasonably good estimate of the repeatability of the fringe number measurements. This contribution to the overall uncertainty in the fringe number measurement seems relatively insignificant compared to some of the other figures obtained.

For another estimate of uncertainty, when the traverse at y = 0.4H was being started, the y' micrometer was adjusted to find the S = 0 location by the technique described in CHAPTER IV. After selecting a y' location for S = 0, the y' micrometer was then turned until the crosshairs just seemed to be missing the "correct" location. The difference between these two micrometer readings was 0.0006 inch. In terms of fringe shift, ΔS = 0.0006/0.0166 = 0.036. This is an indication of the accuracy with which the S = 0 point was located.

On the basis of the ΔS-values obtained above (0.060,

Table 9. Values obtained for repeated measurements at the x = 0.5L location along with the S-value differences, ΔS.

y/H	x	S	ΔS
0.04	19.95	6.713	-0.004
	20.02	6.709	
0.1	19.95	7.210	0.009
	20.01	7.219	
0.2	19.95	6.939	0.005
	19.98	6.944	
0.7	19.89	3.468	0.007
	19.95	3.475	
0.8	19.90	3.019	-0.006
	19.94	3.013	
0.97	19.95	3.534	-0.003
	19.97	3.541	

0.048, 0.108, 0.060, 0.006, 0.036), for this analysis the uncertainty will be taken as: $\Delta S = 0.12$.

The end effect correction was considered to be negligible in the calculation of temperatures within the cavity. The maximum end effect fringe shift, calculated in Appendix L, was found to be approximately 0.080. Thus, $\Delta S = 0.12 + 0.08 = 0.20$.

Using the uncertainty values for ΔT_W, ΔP_∞, ΔL, and ΔS estimated above, Equation 47 yields

$$\Delta T = [0.0225 + 0.394]^{1/2} = 0.65\ C^o$$

while Equation 48 yields

$$\Delta T = [0.0153 + 0.0012 + 0.245 + 0.268]^{1/2} = 0.73\ C^o$$

It can be seen that the uncertainties in L and S are much more significant than those in T_W and P_∞. The uncertainty relative to the temperature difference across the cavity is 0.73/30.17 = 2.4%.

Another estimate of uncertainty may be made by comparing the interferometrically measured cold wall temperatures to the value obtained from the thermocouples. The data are listed in Table 10. The temperature values listed under the "T" column are those interpolated from a second-order curve fit to the three points nearest the cold wall with the wall location taken to be where it was observed on the interferogram. The differences between

Table 10. Cold wall temperature, T, obtained by interpolation from second-order curve fits, and measurement error, $T-T_C$, where T_C = 7.24 °C.

y/H	T [°C]	$T-T_C$ [C°]
0.04	7.02	-0.22
0.1	5.58	-1.66
0.2	7.14	-0.10
0.3	7.58	0.34
0.4	7.77	0.53
0.5	7.65	0.41
0.6	7.74	0.50
0.7	7.73	0.49
0.8	7.81	0.57
0.9	7.70	0.46
0.97	7.29	0.05

these interpolated wall temperatures and the temperature measured by thermocouples, T_C = 7.24 ^oC, are listed. These could be called errors rather than uncertainties. The mean of the absolute values of these errors is 0.48 C^o. The relative error is 0.48/30.17 = 1.6%. This value compares favorably with the estimated uncertainty, 2.4%.

C. Uncertainty Analysis of the LDV Data for the Cavity Experiment

The uncertainty in the values obtained for flow velocity will also be computed using the same technique developed by Kline and McClintock [10].

The equation used to calculate velocity is

$$Vel = ((V-V_o)/SF)d_f \qquad [49]$$

For this analysis, the equation will be used in this form

$$Vel = (f-f_o)d_f \qquad [50]$$

where f is the indicated frequency at some velocity, f_o is the indicated frequency at zero velocity, and d_f is the fringe spacing.

The uncertainty in velocity, ΔVel, will be found from

$$\Delta Vel = [(\frac{\partial Vel}{\partial(f-f_o)} \Delta(f-f_o))^2 + (\frac{\partial Vel}{\partial d_f} \Delta d_f)^2]^{1/2} \qquad [51]$$

Upon performing the partial differentations and substituting the values $f-f_o = (V-V_o)/SF = 1.80/10^{-4} =$

18000 Hz (approximately the value at peak velocity) and d_f = 0.003202, one obtains

$$\Delta Vel = [(0.003202\,\Delta(f-f_o))^2 + (18000\,\Delta d_f)^2]^{1/2} \qquad [52]$$

An experiment was performed on the 1090 tracker to check the accuracy of its frequency-to-voltage conversion. The sine wave output of a signal generator was input to both the signal (photodetector) input of the tracker as well as that of a frequency counter. The frequency counter was used to indicate the output frequency of the signal generator so that it could be set very accurately. The analog voltage output of the tracker was read from the same digital voltmeter that was used in the LDV experiments. The tracker's RANGE knob was set to the 0.1 V/KHz position, and the tracker was adjusted to "lock onto" the signal from the generator. (Note that this is actually a test of the tracker-voltmeter system rather than just the tracker since any error due to the voltmeter will also show up in the output.)

The data collected are:

Frequency Input [KHz]	Potential Output [Volts]
10	0.97
20	1.97
30	2.96
40	3.96
50	4.955

(At the 50 KHz setting, the indicated voltage oscillated between 4.95 and 4.96. The incertainty in these frequencies is estimated at about 4 Hz. This is about 0.04% or less.)

Over the 18 KHz range of the experiment, the error in indicated potential is 0.01 volt which corresponds to an error in frequency of $0.01\ V/10^{-4}\ V/Hz = 100\ Hz$.

In an error analysis of LDV data performed by Hess and Miller [12], the uncertainty in measurement of two laser beam's intersection angle was given as 0.05^{o} out of 12^{o}; this same value will be used here. Using the equation for fringe spacing, $d_f = \lambda/2\sin(\emptyset/2)$, one finds that a variation of 0.05^{o} in the angle $\emptyset$ (from 11.34^{o} to 11.39^{o}) results in a variation in d_f of 0.000014 millimeter, which will be taken as the uncertainty, $\triangle d_f$.

Thus,

$$\triangle Vel = [((0.003202)(100))^2 + ((18000)(0.000014))^2]^{1/2}$$

$$\triangle Vel = [0.103 + 0.0635]^{1/2}$$

$$\triangle Vel = 0.41\ mm/sec$$

This is the uncertainty in the peak velocity. As the magnitude of the indicated velocity approaches zero, this uncertainty should approach zero. The minimum value of uncertainty would be expected to be the change in velocity equal to a change in $V-V_o$ of 0.01, the resolution of the meter. This value is $\triangle Vel = 0.32$ mm/sec. Adding this

value to the above value gives $\triangle$Vel = 0.41 + 0.32 = 0.73 mm/sec. Relative to the peak velocity, approximately 60 mm/sec, this uncertainty amounts to 0.73/60 = 1.2%.

There are some other contributions to measurement error besides those uncertainties above. For example, since the velocity probe volume of the LDV is finite in size and since velocity gradients exist in the flow, the indicated velocity will be something of an average over the probe's width. For an estimate, the velocity gradient next to the hot wall, estimated from the two measured velocities nearest the wall, is (34.26-15.05)/(1.0-0.5) = 38 mm/sec·mm. The nominal diameter of the probe volume as stated in CHAPTER III was 0.3 mm; thus, (38)(0.3) = 11 mm/sec velocity difference across the probe. There does not seem to be an obvious method for estimating how much this velocity gradient across the probe volume would affect the indicated velocity. There apparently should be an effect, since there should be more particles passing through the probe on the higher velocity side than the lower velocity side in a given time, which would result in their being tracked more often and thus weighting the output toward a higher velocity.

Another source of error is that due to the deflection of light rays away from the hot wall and toward the cold wall. This was discussed previously as the displacement error and focusing effects as they relate to the MZI. For

the present case, light beams within the x/L = 0.0 to 0.1 region (near the hot wall) will be deflected away from the wall which will put the test volume in a higher velocity region (all probe locations given are from a scale outside the cavity and from an alignment performed with the cavity isothermal). The extent of this deflection can be estimated using Equation 74 for beam deflections as derived in Appendix D:

$$y = (dn/dT)(dT/dy)(1/2n)\ z^2$$

For P = 744.3 mmHg and T = 310.56 ^oK, dn/dT = 8.07 x 10^{-7} $1/K^o$. The gradient dT/dy can be estimated from the MZI data for the two points nearest the wall at y = 0.5H: dT/dy = (37.41-34.30)0/.81 = 3.84 K^o/mm. The refractive index, n, is 1.0003 and z will be at L/2 or 122.3 mm. Thus, y(L/2) = 0.023 mm. Using the above calculated gradient, 38 mm/sec·mm, the uncertainty in velocity is $\triangle$Vel = (0.023)(38) = 0.87 mm/sec. At 25 mm/sec, the relative uncertainty is 0.87/25 = 3.5%. This uncertainty will be much smaller within the central region of the cavity where the temperature profiles are much flatter than in the boundary layers on the vertical walls of the cavity.

Adding the uncertainties obtained, one finds $\triangle$Vel = 0.41 + 0.32 + 0.87 = 1.60 mm/sec. Relative to the peak velocity this amounts to 1.60/60 = 2.7%. Thus, the relative uncertainty is about 3% near the peak velocity

regions, and the uncertainty will be about equal to the meter's resolution (0.32 mm/sec) within the central region of the cavity.

CHAPTER VI

SUMMARY AND RECOMMENDATIONS

A. Summary

As stated in the Introduction, this thesis is intended as a "users manual" for the Natural Convection Laboratory. For this reason, considerable effort has been expended in providing adequate detail regarding the principal instruments and their operation.

In CHAPTER I, the Mach-Zehnder Interferometer and Laser Doppler Velocimeter systems were introduced and their principles of operation explained. The practical details of setting up, aligning, and adjusting the instruments for operation were presented.

In CHAPTER II, two experimental devices were described: an electrically heated flat plate for use in free air and an internal cavity with heated and cooled vertical surfaces for an internal flow study. These two devices can be regarded as typical experiments; that is, their designs can serve as models for similar experimental devices.

The setup of the experiments and their alignment to the instruments are presented in CHAPTER III. The flat plate was used with the MZI only; whereas, the cavity was used with both the MZI and the LDV. The operation of the

experiments and the recording of data are described.

The processes of data reduction are explained and illustrated in CHAPTER IV. The flat plate experiment provides data to illustrate the MZI data reduction process for an external flow situation, while the cavity experiment provides data to illustrate the MZI data reduction process for an internal flow situation as well as for the LDV data reduction process (the data reduction process for the LDV is the same for internal and external flows). Examples detailing the calculation of specific data values are presented to help clarify the data reduction processes.

Error analyses are presented in CHAPTER V in which the technique of Cline and McClintock is used to estimate the uncertainties in the cavity air temperature and velocity values.

B. Recommendations for Future Research

Some recommendations for future research or techniques to be developed with regard to the Natural Convection Laboratory are presented below.

At the time the experiments with the electrically heated plate were performed, the plate data were considered important in order to test the accuracy of the interferometric technique. The plate, however, was found to be rather nonuniform in temperature during the tests. It would be desirable to repeat one or more tests with a

redesigned and more nearly isothermal test plate (using, perhaps, circulating water for heating or cooling). Such a plate has already been constructed and is available for performing these tests.

Since interferometer tests in free air are prone to be spoiled by stray currents of air that would disturb the delicate flow pattern about a test surface, it would be very useful to have a large box or perhaps an elaborate set of baffles to protect an experiment from undesired environmental influences. An enclosed box could also contain the seeded gas needed for LDV experiments.

It was stated in CHAPTER IV that, based on the uncertainty in wall locations as viewed on interferograms, the best way to align a wall to an interferometer beam is to set the wall to the average of the "best" alignment positions for the two oppositely facing surfaces (p. 235). It would be good to perform some experiments to check this recommendation, especially at different wall temperatures since the light rays curve away from a heated wall.

The interferogram analysis and data reduction processes described in this thesis are exceptionally tedious and time consuming. It would be highly desirable to develop an automated data reduction process. The interferograms could, for example, be optically scanned and digitized and the information stored in a computer's memory. Then a program could access the digitized

interferogram and automatically reduce it to the desired temperature data. This automation of the data reduction process could allow a researcher, say, to run a large number of experiments in which only one parameter at a time had been varied. Also, compensation for nonstraightness of the fringes in the isothermal field interferograms (that is, for optical defects in the system) could be carried out easily by digitizing the isothermal field interferogram and processing its data appropriately with the data from the interferogram made at test temperature.

In lieu of this automated process, the "conventional" data reduction process could be improved with the additions of a rotary table with a fine angle adjustment and a rotary eyepiece to the measuring microscope. The rotary table (only a small angular adjustment would be needed) would facilitate aligning the interferogram images to the stage travel. The rotary eyepiece would allow the reticle (containing the crosshairs) to be rotated without the center of the hairs moving in a circle. A set of general purpose data recording forms would also assist the reduction process.

A computerized data acquisition and logging system would be helpful for use with the LDV system, especially when unsteady or turbulent flows are studied.

It was estimated that the end effect error for the cavity was negligible. This result should be further

tested and, if needed, a correction equation derived. Considerable care should be exercised here, since, due to the nature of the flow, a simple correction could be worse than none at all.

It was stated that the windows for the cavity were roughly checked and found to be "reasonably" flat. The flatness of the glass should be more throughly investigated, though, of course, correcting for nonstraightness of the fringes allows for the use of poorer quality windows.

Where comparisons between interferometrically measured temperatures and directly measured temperatures (by thermocouple) were made in this thesis, they were made only between two walls (as with the cavity) or between a wall and a field (as with the heated plate). Some experiments should be performed where the air temperature at intermediate locations has been measured (as by a group of thermocouples) to further check the measurement accuracy of the MZI.

Finally, considerable care should be exercised in keeping the optical surfaces clean. Lenses and mirrors are for refracting or reflecting light--not for maintaining a fingerprint collection. When the optics become dirty, they should be carefully cleaned and then kept covered when not in use. Dirt and smudges on the optical elements will not usually cause catastrophic destruction of images, but will

contribute to decreased contrast and sharpness. The coated side of the beam splitters is probably the most delicate optical surface in the laboratory; a good technique for cleaning these elements should be devised.

LIST OF REFERENCES

LIST OF REFERENCES

1. Zehnder, L., "Ein neuer Interferenzrefraktor," Z. Instrumentenk, Vol. 12, 1891, pp. 275-285.

2. Mach, L., "Uber einen Interferenzrefraktor," Z. Instrumentenk, Vol. 12, 1892, pp. 89-93.

3. Wilkie, D., Fisher, S.A., "Measurement of Temperature by Mach-Zehnder Interferometry," Proceedings of the Institution of Mechanical Engineers, Vol. 178, Pt. 1, No. 17, 1963-1964, pp. 461-472.

4. Hauf, W., Grigull, U., "Optical Methods in Heat Transfer," Advances in Heat Transfer, Vol. 6, Academic Press, New York, 1970, pp. 133-366.

5. Mehta, J.M., Black, W.Z., "Errors Associated with Interferometric Measurement of Convective Heat Transfer Coefficients," Applied Optics, Vol. 16, No. 6, June 1977, pp. 1720-1726.

6. Kennard, R.B., "An Optical Method for Measuring Temperature Distribution and Convective Heat Transfer," National Bureau of Standards, Journal of Research, Vol. 8, 1932, pp. 787-805.

7. Panarella, "Alignment Technique for the Mach-Zehnder Interferometer," Journal of Physics E: Scientific Instruments, Vol. 6, 1973, p. 523.

8. Yeh, Y., Cummins, H.Z., "Localized Fluid Flow Measurements with a He-Ne Laser Spectrometer," Applied Physics Letters, Vol. 4, No. 10, 1964, pp. 176-178.

9. Eckert, E.R.G., Goldstein, R.J., "Optical Techniques for Temperature Measurement," Measurements in Heat Transfer, 2nd Ed., 1976, Hemisphere Publishing Corp., McGraw-Hill Book Co., pp. 264-282.

10. Linthorst, S.J.M., Schinkel, W.M.M., Hoogendroorn, C.J., "Flow Structure With Natural Convection in Inclined Air-Filled Enclosures," Natural Convection in Enclosures, editors: K.E. Torrance and I. Catton, ASME-HTD-Vol.8, 1980, pp. 39-45.

11. Kline, S.J., McClintock, F.A., "Describing Uncertainties in Single Sample Experiments," Mechanical Engineering, Vol. 25, January 1953, pp. 3-8.

12. Hess, C.F., Miller, C.W., "Natural Convection in a Vertical Cylinder Subject to Constant Heat Flux," International Journal of Heat and Mass Transfer, Vol. 22, 1979, pp. 421-430.

13. Hilsenrath, J., et al., "Tables of Thermal Properties of Gases," National Bureau of Standards Circular 564, United States Department of Commerce, November 1, 1955.

APPENDICES

APPENDIX A

END-EFFECT CALCULATIONS

An end-effect correction for MZI temperature calculations for a heated plate in free air will now be derived.

Here, the assumption is made that the temperature distribution through the plate's end regions follows a parabolic distribution along the z-axis (the light ray path); this situation is illustrated in Figure 8 (p. 41). Thus,

$$T(y,z) = T_M(y) + Az + Bz^2 \qquad [53]$$

At $z = 0$, $T = T_M(y)$. This temperature will be known from uncorrected data (that is, from use of Equation 11 (p. 36) with no correction applied). At $z = \delta'$, $T = T_\infty$, and $dT/dz = 0$. Therefore

$$T = T_M - 2(T_M - T_\infty)\frac{z}{\delta'} + (T_M - T_\infty)(\frac{z}{\delta'})^2 \qquad [54]$$

$$\delta' = \sqrt{\delta^2 - y^2} \qquad [55]$$

$$T = T_M(y) + (T_M - T_\infty)[\frac{z^2}{\delta^2 - y^2} - 2\frac{z}{\sqrt{\delta^2 - y^2}}] \qquad [56]$$

Repeating Equations 9 and 10 (p. 36)

$$n - 1 = (3/2)\bar{r}\rho = (3/2)\bar{r}\frac{P_\infty}{RT}$$

Substituting for T

$$n-1 = \frac{3}{2}\bar{r}\frac{P_\infty}{R}\left[T_M + (T_M - T_\infty)\left[\frac{z^2}{\delta^2 - y^2} - 2\frac{z}{\sqrt{\delta^2 - y^2}}\right]\right] \qquad [57]$$

T_M must be absolute temperature. Equation 16 (p. 40):

$$S\lambda = n_\infty L - \int_0^L n \, dz$$

Substituting and letting $\Delta T = T_M - T_\infty$

$$S\lambda = n_\infty \delta' - \int_0^{\delta'} \left[\frac{\frac{3}{2}\bar{r}\frac{P_\infty}{R}}{\Delta T \frac{z^2}{\delta'^2} - 2\Delta T \frac{z}{\delta} + T_M} + 1\right] dz \qquad [58]$$

$$S\lambda = n_\infty \delta' - \delta' - \frac{3}{2}\bar{r}\frac{P_\infty}{R}\left[\frac{2}{\sqrt{4 T_M \frac{\Delta T}{\delta'^2} - 4\frac{\Delta T^2}{\delta'^2}}}\right.$$

$$\left. - \tan^{-1}\frac{2\frac{\Delta T}{\delta'^2} z - 2\frac{\Delta T}{\delta'}}{\frac{2}{\delta'}\sqrt{T_M \Delta T - \Delta T^2}}\right]_0^{\delta'} \qquad [59]$$

Simplifying and using $n_\infty - 1 = \frac{3}{2}\bar{r}\frac{P_\infty}{R T_\infty}$:

$$S\lambda = \frac{3}{2}\bar{r}\frac{P_\infty \delta'}{R}\left[\frac{1}{T_\infty} - \frac{1}{\sqrt{\Delta T \, T_\infty}}\tan^{-1}\frac{\Delta T}{\sqrt{\Delta T \, T_\infty}}\right] \qquad [60]$$

Doubling the above to account for both ends:

$$\Delta S_2 = 3\bar{r}\frac{P_\infty}{R\lambda}\sqrt{\delta^2 - y^2}\left[\frac{1}{T_\infty} - \frac{1}{\sqrt{\Delta T \, T_\infty}}\tan^{-1}\frac{\Delta T}{\sqrt{\Delta T \, T_\infty}}\right] \qquad [61]$$

Where $\Delta T = T_M - T_\infty$. This correction should be <u>subtracted</u> so as to reduce the resulting temperature (when the plate is <u>above</u> ambient temperature).

Using the values:

$$\bar{r} = 1.504 \times 10^{-4} \quad [m^3/kg]$$

$$R = 287.06 \quad [m^2/sec^2 K^o]$$

$$\lambda = 6328 \times 10^{-7} \quad [mm] \quad \text{(He-Ne laser)}$$

Then:

$$\Delta S_2 = 0.3311\ P_\infty \sqrt{\delta^2 - y^2}\ \left[\frac{1}{T_\infty} - \frac{1}{\sqrt{\Delta T\ T_\infty}} \tan^{-1} \frac{\Delta T}{\sqrt{\Delta T\ T_\infty}}\right] \qquad [62]$$

Where:

P_∞ is in mmHg

δ and y are in mm

T_∞ and T_M are in ^oK

$$\Delta T = T_M - T_\infty$$

If it is chosen to use a mean temperature value instead of the parabolic distribution, then the end-effect correction is as follows.

$$T(y,z) = (T_M(y) + T_\infty)/2 \qquad [63]$$

$$n - 1 = (3\bar{r}P/2R)2/(T_M + T_\infty) \qquad [64]$$

$$S\lambda = n_\infty \delta' - \int_o^{\delta'} \left(1 + \frac{3\bar{r}\ P_\infty}{R(T_M + T_\infty}\right) dz \qquad [65]$$

$$S\lambda = \frac{3\bar{r}\ P_\infty}{R} \sqrt{\delta^2 - y^2}\ \left[\frac{T_M}{T_\infty (T_M + T_\infty)}\right] \qquad [66]$$

Doubling the above to account for both ends of the plate:

$$\Delta S_2 = \frac{6\bar{r}\ P_\infty}{R\lambda} \sqrt{\delta^2 - y^2}\ \left[\frac{T_M}{T_\infty (T_M + T_\infty)}\right] \qquad [67]$$

$$\Delta S_2 = 0.662\ P_\infty \sqrt{\delta^2 - y^2}\ \left[\frac{T_M}{T_\infty (T_M + T_\infty)}\right] \qquad [68]$$

Where:

P_∞ is in mmHg

δ and y are in mm

T_∞ and T_M are in ^oK

APPENDIX B

AN ALTERNATIVE COLLIMATION TECHNIQUE FOR THE MACH-ZEHNDER INTERFEROMETER

The "preferred" collimation technique was described in CHAPTER I. In this appendix another collimation technique is described and is compared to the one in CHAPTER I.

The method here described could be called the "measure-the-diameter method." To use this method, the collimating mirror must be removed and its reflective diameter measured. A bevel on the mirror's edge reduces its effective diameter. Several diameters (or, say, just the horizontal diameter) should be measured. After reattaching the mirror and aligning the light beam, a card with a circle drawn on it the same size as the reflective diameter of the mirror is held in the light beam and the diameter of the light beam is compared to that of the drawn circle. If the diameter of the beam is less than that of the circle, then the light source's aperture is outside the focus of the collimating mirror. If the diameter is greater, then the aperture is inside the focus. The main argument against this collimation technique is that the card with the circle drawn on it can be held no farther from the collimating mirror than just before the first beam splitter (since the edge of the beam is blocked by the

splitter), and at this location it is difficult to check correspondence between the beam and circle since the card can be viewed only obliquely. With the beam projected onto the wall as in the first method, there is no blockage to free viewing of the shadows.

For a rough comparison of the two methods, assume that a mirror exactly 6 inches in diameter reflects a beam with a divergence of 0.5 degrees (angle of the outermost rays). At 56 inches from the mirror, just before the beam splitter, the light beam is 6.50 inches in diameter, an increase of 0.50 inches or 8 per cent. Now consider a collimation tool at the 56 inch location with a wire separation of exactly 5 inches. The wall is about 197 inches along the optical path from the tool. At this location, the separation of the shadows is 6.32 inches, an increase of 1.32 inches or 26 per cent. Thus, the shadow separation method gives greater sensitivity than the measure-the-diameter method.

APPENDIX C

OPERATION OF CAMERA AND FILM DEVELOPMENT

In this appendix, the method of making exposures with the camera and of processing the film will be described.

As stated in CHAPTER I, all photographs for all experimental runs were made with Polaroid Type 55 Positive-Negative film. This film, besides providing the usual positive print, also provides a "recoverable" negative.

The exposures were made as follows. The Type 55 film is manufactured as individual single sheets or film packets. A packet is exposed within a special film holder made by Polaroid. The directions provided with the film and with the film holder illustrate how to insert and remove the film. With the film loaded, the film holder is inserted into the camera; it slips in between the viewing screen and the camera body. The shutter must now be cocked or otherwise set as desired. For most exposures made with the MZI, the "TIME" setting was used. The wing-shaped knob on the camera was turned to its "B" position. Here, the shutter curtain is closed. Now, the "dark slide" or the protective envelope over the film is slipped out of the film holder until it stops (the film itself will now be uncovered but the shutter curtain keeps out the light). The room must now be darkened, since the optical path is

open to any ambient illumination. When it is time to make the exposure, the shutter button is tripped once, which results in the shutter curtain opening, and then tripped again, which results in the curtain closing. For most exposures, the interval between opening and closing of the curtain was made approximately 1 to 2 seconds, which seemed to be right for correct exposure (as found by trial-and-error). With the shutter curtain now closed, the room lights may be turned on, and the dark slide slipped over the film. Now, the film holder may be removed from the camera, and film development started by pulling the film packet (through pinch rollers) from the film holder. The film was allowed to develop for approximately 20 seconds, and then the film packet was torn open to retrieve the print and the negative. The negative was "recovered" by soaking it in a solution of sodiun sulfite for about 2 minutes to deactivate and remove a layer of chemicals adhering to the negative's surface. After the chemical layer was removed, the negative was washed in running water for about 5 minutes for further chemical removal.

When making the actual exposure, considerable care should be exercised so that the camera or its stand are not shaken any more than necessary. A remote shutter release is attached to the camera's shutter trip lever to eliminate having to directly touch the camera to activate the shutter.

APPENDIX D

WALL ANGULAR ALIGNMENT

When a light ray traverses a medium containing a temperature gradient, the ray is deflected in the direction of decreasing temperature. It is desired to be able to calculate the magnitude of the deflection so that the necessary alignment accuracy of the wall to the light beam may be estimated.

Assume that a light ray approaches initally parallel to the surface of a heated plate. Let the z-axis be along the length of the plate (parallel to the approaching ray) and the y-axis be perpendicular to the plate. Further assume that the refractive index gradient, dn/dy, above the plate is a constant.

Hauf and Grigull [4] present the following equation for ray deflections where dn/dy = constant.

$$dy/dz = (dn/dy)(z/n_o) \qquad [69]$$

Here, n_o is the value of refractive index where the ray enters the field. The substitution may be made that dn/dy = (dn/dT)(dT/dy). Thus,

$$dy/dz = (dn/dT)(dT/dy)(z/n_o) \qquad [70]$$

From Appendix K, $n = 1 + 0.0001048(P/T)$; so

$$dn/dT = -0.0001048(P/T^2) \qquad [71]$$

where P is in mmHg and T is in ^{o}K.

For one of the earlier experiments with the heated plate, the data were found to be: P = 740.1 mmHg, T = T_W = 320.7 ^{o}K, $(dT/dy)_W$ = -5 K^{o}/mm, and L = 244.5 mm. Thus, $dn/dT = -7.54 \times 10^{-7}\ K^{o-1}$ and $z/n_o = L/n_o$ = 244.5/1.00024 = 244.4 mm. Multiplying the numbers yields

$$dy/dz(z=L) = 0.00092 \text{ radian}$$

The angular adjustment screw for the cavity's mount has 28 threads per inch. This corresponds to a pitch of 0.907 mm/thread. The scale on the disc attached to the screw had 36 graduations per revolution. It was approximately 120 millimeters from the axis of the screw to the pivot point of the support plate. Thus, a rotation of one graduation would correspond to an angular change, $\emptyset$, of the support plate of

$$\emptyset = (0.907/36)/120 = 0.00021 \text{ radian/graduation}$$

In terms of graduations on the angle scale, the ray was deflected by 0.00092/0.00021 = 4.4. This would indicate that the alignment of the plate to the MZI's test beam should be done to a tolerance of plus or minus 2 graduations on the angular rotation scale.

It might be desired to know the distance that the ray deflects. A light ray follows a parabolic path within a region of constant dn/dy. For a parabola, $y = cz^2$, so

$$dy/dz = 2cz = (dn/dT)(dT/dy)(1/2n_o) \quad [72]$$

$$c = (dn/dT)(dT/dy)(1/2n_o) \quad [73]$$

$$y = (dn/dT)(dT/dy)(1/2n_o)\ z^2 \quad [74]$$

Or, this could have been obtained by integration of dy/dz.

APPENDIX E

OPERATION OF THE CIRCULATING BATHS

Available in the Natural Convection Laboratory are a pair of Haake Model NK-22 "constant temperature circulating baths." These baths contain a reservoir that is filled with some liquid (usually distilled water), and they have a pair of pumps to circulate the liquid through hoses to the experiment. Each circulator has both a suction and a pressure pump with a flow regulating valve on the discharge line so that the device can circulate the fluid to an open container as well as through a closed system. Within the reservoirs are electrical resistance heating elements plus the cooling coil of a conventional refrigeration system. Thus, the baths can circulate liquids that are heated above as well as cooled below ambient temperature. An operating manual was included with the machines. This discussion will partially repeat the information in the manual as well as elaborate upon it.

Temperature control of the circulating liquid (assumed to be water) is set with and regulated by a "thermoregulator" (a thermostat). This device consists of a special mercury-in-glass thermometer contained within a larger diameter glass envelope. The regulator functions as an on-off electrical switch; one contact is the wire in the capillary, while the other is the mercury itself. The

regulator contains two scales: one for reading the temperature indicated by the mercury, and the other for reading the "set" temperature (the temperature determined by the location of the end of the wire at which electrical contact would be made or broken). Neither of these scales is especially accurate or precise. Normally another thermometer or thermocouple is used to indicate temperature while trial-and-error is used to finally adjust the regulator to the desired set temperature. When in place on the baths, the regulators are well immersed in the circulating water, which becomes quite turbulent when the pumps are running.

The thermoregulator controls a solid-state relay that sends electrical power to the heating elements within the reservoir. When electrical contact between the mercury and the wire is made, the power to the heater is shut off so that the temperature of the fluid will cease to increase. Likewise, when contact is broken, the power to the heater is turned on to raise the water's temperature. Another control in the system regulates the percent-of-time that power is actually sent to the heater even when contact within the regulator is broken (when the regulator is "calling for heat"). This control, which is set by a knob on the circulator's control panel, serves to throttle or regulate the rate at which heat is added to the water at the times when heating is needed. (A yellow light on the

control panel turns on when power is applied to the heater.)

As stated in the operating manual, it is desired to set this heater control so that heat will be added to the circulating water at nearly the same rate that it is being removed. Doing this helps to lessen the magnitude of the temperature variations that would occur if the heater ran only either full-on or full-off for extended periods. The operating manual, however, does not state how one can be sure that enough heat is being transferred to the system. One can determine the proper setting for the control knob by adjusting it so that the heater receives power (the yellow light flashes on-and-off) for a time period (about 30 seconds to a minute or more) and then turns off for a shorter time due to the contacts closing in the regulator. This brief off-period in a much longer on-and-off period ensures that the heating rate can be greater than the cooling rate. If this were not done, then the cooling rate might be greater than the heating rate and the water's temperature would continue to decrease, perhaps very slowly so that the decrease would not be easy to detect.

When initally starting a circulator whose water temperature is to be above ambient temperature, the heater control knob should be turned to the position of maximum heat (fully clockwise) so that the operating temperature can be quickly reached.

The circulator's cooling system is controlled by a single on-off switch. Of course, when the circulator's water is desired to be below ambient temperature, the cooling system must be turned on. The operating manual, however, says that it should be run whenever the water's temperature is below about 50 °C. The reason for this is not given; it is presumed that the pump work (converted to heat) might cause the temperature to rise above the set point (if little heat is being drawn from the system).

It has been stated that the thermoregulator controls only the heater. Thus, temperature regulation (when the cooling system is turned on) is dependent upon the heater being able to "overpower" the cooling system, which it can easily do. Actually, the cooling compressor does turn off occasionally; just why it does this is unknown.

APPENDIX F

TEMPERATURE DATA FOR THE HEATED PLATE EXPERIMENT

In this appendix, data from the calibration experiment as well as from the main experiment with the heated plate will be presented.

The calibration procedure, as described in CHAPTER III, consists of placing the plate into the reservoir of a constant temperature circulating bath, adjusting the bath's temperature so that the millivolt output of the thermocouples is approximately the same as that reached during the main experiment, and determining the "true" temperature of the bath and plate by means of a pair of high-accuracy mercury thermometers. As stated, the "true" temperature of the bath was found to be 52.2 ^{o}C.

The data from the calibration experiment are listed in Table 11. Thermocouples numbered 1 through 8 were contained within the plate; thermocouples numbered 22, 23, and 24 were free and had been used to record air temperature during the main experiment. The millivolt readings from the potentiometer are listed. The potentiometer was graduated in increments of 0.005 millivolt; however, the instrument was read to a resolution of 0.0025 millivolt, which corresponds to a temperature resolution of 0.05 C^{o}.

The temperatures listed along the "Temp ^{o}C" row are

Table 11. Temperature data for the heated vertical plate.

	Thermocouple Numbers										
	1	2	3	4	5	6	7	8	22	23	24
	Calibration:										
Pot [mV]	2.1250	2.1250	2.1275	2.1275	2.1275	2.1275	2.1275	2.1275	1.0775	1.0775	1.0775
Temp [°C]	52.10	52.10	52.15	52.15	52.15	52.15	52.15	52.15	27.10	27.10	27.10
Error	0.10	0.10	0.05	0.05	0.05	0.05	0.05	0.05	0.20	0.20	0.20
	Reading No. 2:										
Pot [mV]	2.1650	2.2000	2.2025	2.1925	2.1375	2.1800	2.1850	2.1775	1.0600	1.0775	1.0625
Temp [°C]	53.00	53.85	53.90	53.65	52.40	53.35	53.50	53.30	26.70	27.10	26.75
Corrected	53.10	53.95	53.95	53.70	52.45	53.40	53.55	53.35	26.90	27.30	26.95

those obtained from a plot of millivolt values versus temperature values. One of the plots is reproduced here as Figure 53. This figure is a plot of the millivolt-temperature values listed in the Omega Engineering Inc. catalog for copper-constantan thermocouples. The increments of the grid correspond to the 0.0025 millivolt and 0.05 C^{o} values previously mentioned. As an example, thermocouple number one (TC #1) indicated 2.125 millivolts during the calibration procedure. This corresponds, from the figure, to a temperature of 52.10 ^{o}C. It was stated that the true temperature was 52.20 ^{o}C. The following was used to relate these quantities.

$$Error = T_{corr} - T_{ind} \qquad [75]$$

Here, T_{corr} is the "correct" temperature (52.20 ^{o}C), and T_{ind} is the "indicated" temperature (from the plot; 52.10 ^{o}C for this example). Thus, for this case, Error = 0.10 C^{o}.

The values listed for couples 22, 23, and 24 were obtained from a previous calibration experiment performed primarily for the hot and cold cavity walls. The plot used to reduce these data are presented as Figure 54. During the experiment, a pair of mercury thermometers indicated that the correct temperature was 27.30 ^{o}C. Thus, the error was 0.20 C^{o}.

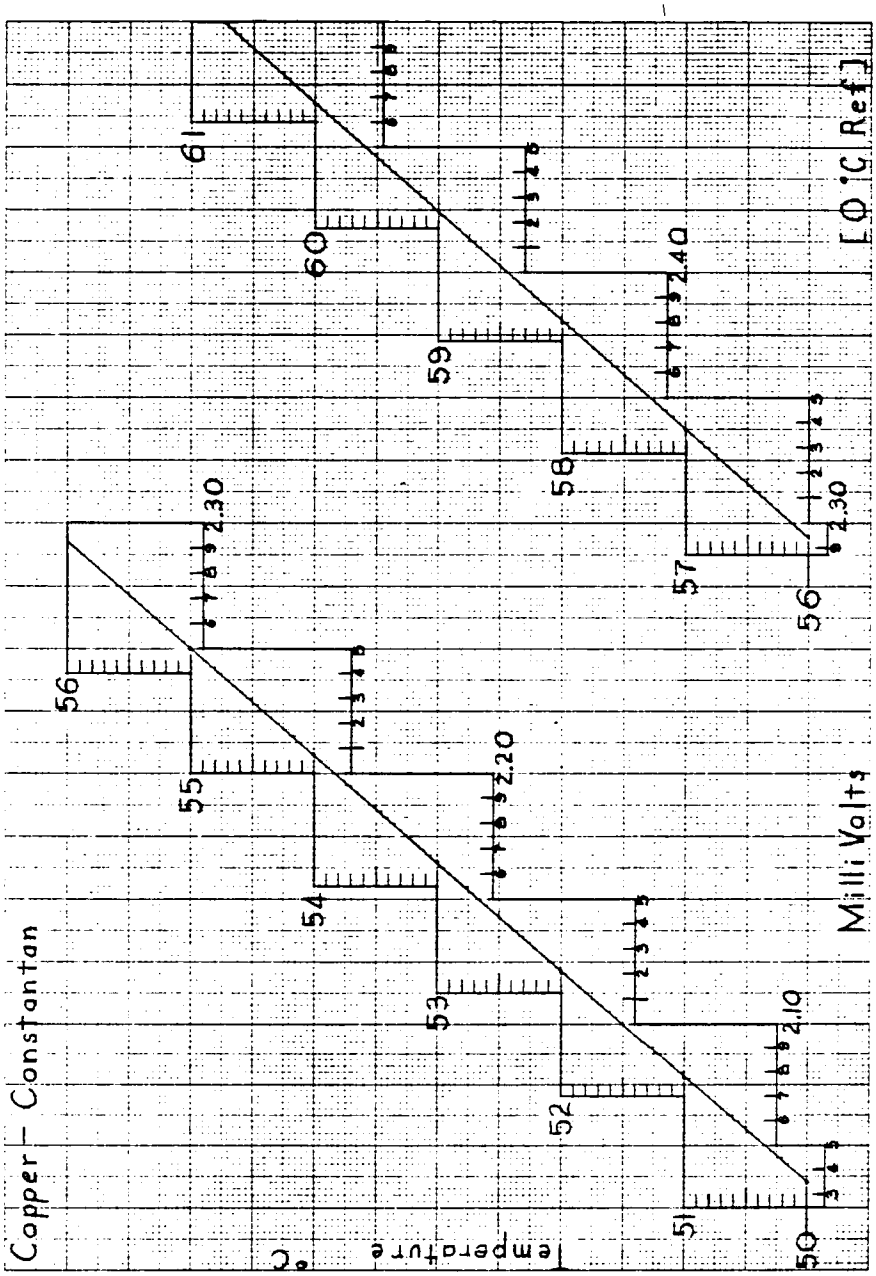


Figure 53. Thermocouple millivolt potential versus temperature as given in the Omega Engineering, Inc. catalog for the 50 - 60 C range.

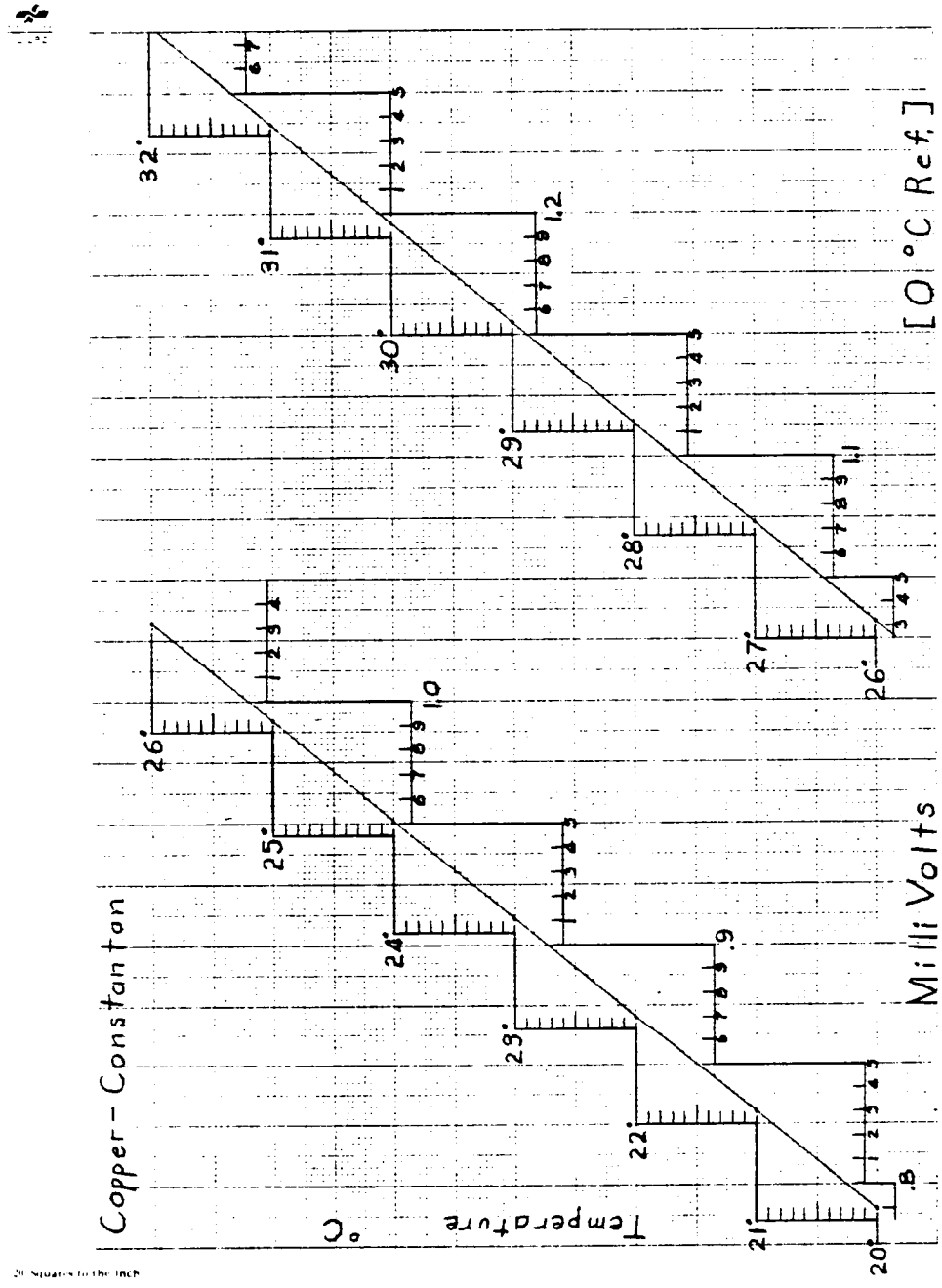


Figure 54. Thermocouple millivolt potential versus temperature for the 20 - 30 C range.

The techniques here described for reading the potentiometer, finding the indicated temperatures, and determining the error are the same ones used to reduce the temperature data for the hot and cold walls as well as for the plate.

When the experiment with the plate was described in CHAPTER III, it was stated that the thermocouples were read between each interferogram exposure as well as before the first and after the last exposures. In CHAPTER IV, an analysis of interferogram 071580-3 only was presented. In Table 11 are listed (under Reading No. 2) the millivolt readings that were recorded just after exposure 071580-3 was made. These data only are listed because they were obtained closer to the time of the exposure than those data recorded before the exposure was made. The millivolt values were reduced to temperature values by using Figures 53 and 54. The corrected temperature values were obtained from

$$T_{corr} = T_{ind} + Error \qquad [76]$$

where T_{corr} now stands for "corrected" temperature.

To determine the temperature profile about the plate, it is necessary to know the ambient air temperature. Also, a value for the plate temperature is desired in order to check the accuracy of the interferometric method. Since thermocouple #23 was at the same approximate location as

the fringe that was examined (on the RHS centerline of the plate), its corrected temperature will be taken as the air temperature. Thus, θ = 27.30 °C (27.30 + 273.15 = 300.45 °K). (One might argue against the selection of this value since both of the other couples indicated nearly the same lower value; however, since thermocouple #23 was so near the location of measurement, its temperature value will be used.) Selecting a suitable temperature value for the plate is not especially easy since the couples indicate a relatively large temperature variation over the plate. The examples of data reduction in CHAPTER IV involve only the RHS of the plate; couples numbered 1 through 4 were on this side. Couple #1 was at one end of the plate at the centerline while couples #2, #3, and #4 were lined up on the vertical centerline with #2 at the top, #3 at the center, and #4 at the bottom of the plate. Couples #1 and #3 were in the plane at which the fringe data was taken; thus, their readings are of greatest interest. The mean of the two temperatures, 53.10 °C and 53.95 °C, is 53.53 °C. This will be taken as the wall temperature.

One can see from looking at the figures that the temperatures on the LHS of the plate (indicated by thermocouples #5 through #8) are lower than than those for the RHS. One can see from the interferograms in Figure 34 and 35, that the fringe system is not exactly symmetrical about the two sides of the plate. If the RHS was hotter,

then a stronger air current would have been present on that side, which would have pulled the air current on the LHS toward the right. That this seems to be happening is most clearly seen in Figure 35.

APPENDIX G

TEMPERATURE DATA FOR THE HOT AND COLD WALLS OF THE CAVITY

A calibration experiment, very similar to the one described in Appendix F, was performed with both the hot and cold walls of the internal cavity within the reservoir of the circulating bath. For this experiment, the calibration was checked at increments of approximately 2.5 C^o from 5 ^oC to 50 ^oC. For temperatures below ambient, only the cold wall data was recorded at each 2.5 C^o increment; the hot wall data was recorded each 5 C^o. For temperatures above ambient, the intervals were reversed.

Three mercury-in-glass thermometers were used to determine the bath's "true" or "correct" temperature. They were generally identified as #1, #2, and #3. Thermometer #1 had a range of 20 to 120 ^oF with a resolution of 0.2 F^o. This thermometer was tested, as described in CHAPTER III, and was found to be accurate. Thermometer #2 had a range of -10 to 25 ^oC with a resolution of 0.1 C^o. It was tested at the ice point and was found to be 0.05 C^o low; so, this value was added to all of its readings. Thermometer #3 had a range of 20 to 130 ^oF with a resolution of 0.2 F^o. It was found to be 0.1 F^o high at the ice point; so, this value was subtracted from its readings.

The experiment with the cavity was performed with the

hot and cold walls at approximately 37.4 °C and 7.4 °C, respectively. The calibration data appropriate to these temperatures are listed in Table 12. The millivolt readings of the thermocouples are listed along with the equivalent temperatures obtained from the plots of Figures 55 and 56 (these plots are explained in Appendix F). In Table 13, the data from the thermometers are listed. As can be seen, the correct temperatures were taken as 37.40 °C or 7.55 °C for the water bath temperatures during the tests. The "Error" values were calculated from Equation 75 in Appendix F.

The hot and cold wall temperature data from the main experiment with the cavity are also listed in Table 12. The thermocouple potentials were reduced to temperatures by again using Figures 55 and 56, and these values were corrected using the listed "Error" values and Equation 76 in Appendix F.

The wall temperature values used in the data reduction process were simply taken as the mean values of the corrected temperatures. For the hot wall, the mean temperature was 37.41 °C (310.56 °K), and for the cold wall, the mean temperature was 7.24 °C (280.39 °K). The hot-to-cold wall difference is 30.17 C°, and the mean of the wall temperatures is 22.32 °C (295.47 °K).

Table 12. Hot and cold wall temperature data for the calibration and main operating tests.

	Thermocouple Numbers								
	1	2	3	4	5	6	7	8	9
	HOT WALL CALIBRATION								
Pot [mV]	1.4975	1.4975	1.4975	1.4975	1.4975	1.4975	1.4975	1.4975	------
Temp [°C]	37.25	37.25	37.25	37.25	37.25	37.25	37.25	37.25	
Error	0.15	0.15	0.15	0.15	0.15	0.15	0.15	0.15	
	Cold Wall Calibration								
Pot [mV]	0.2800	0.2800	0.2800	0.2800	0.2825	0.2825	0.2825	0.2825	0.2825
Temp [°C]	7.20	7.20	7.20	7.20	7.25	7.25	7.25	7.25	7.25
Error	0.35	0.35	0.35	0.35	0.30	0.30	0.30	0.30	0.30
	Hot Wall Test								
Pot [mV]	1.5000	1.4975	1.5000	1.4950	1.5000	1.4975	1.4975	1.4975	------
Temp [°C]	37.30	37.25	37.30	37.20	37.30	37.25	37.25	37.25	
Corrected	37.45	37.40	37.45	37.35	37.45	37.40	37.40	37.40	
	Cold Wall Test								
Pot [mV]	0.2700	0.2650	0.2675	0.2675	0.2750	0.2725	0.2700	0.2675	0.2775
Temp [°C]	6.90	6.80	6.85	6.85	7.05	7.00	6.90	6.85	7.10
Corrected	7.25	7.15	7.20	7.20	7.35	7.30	7.20	7.15	7.40

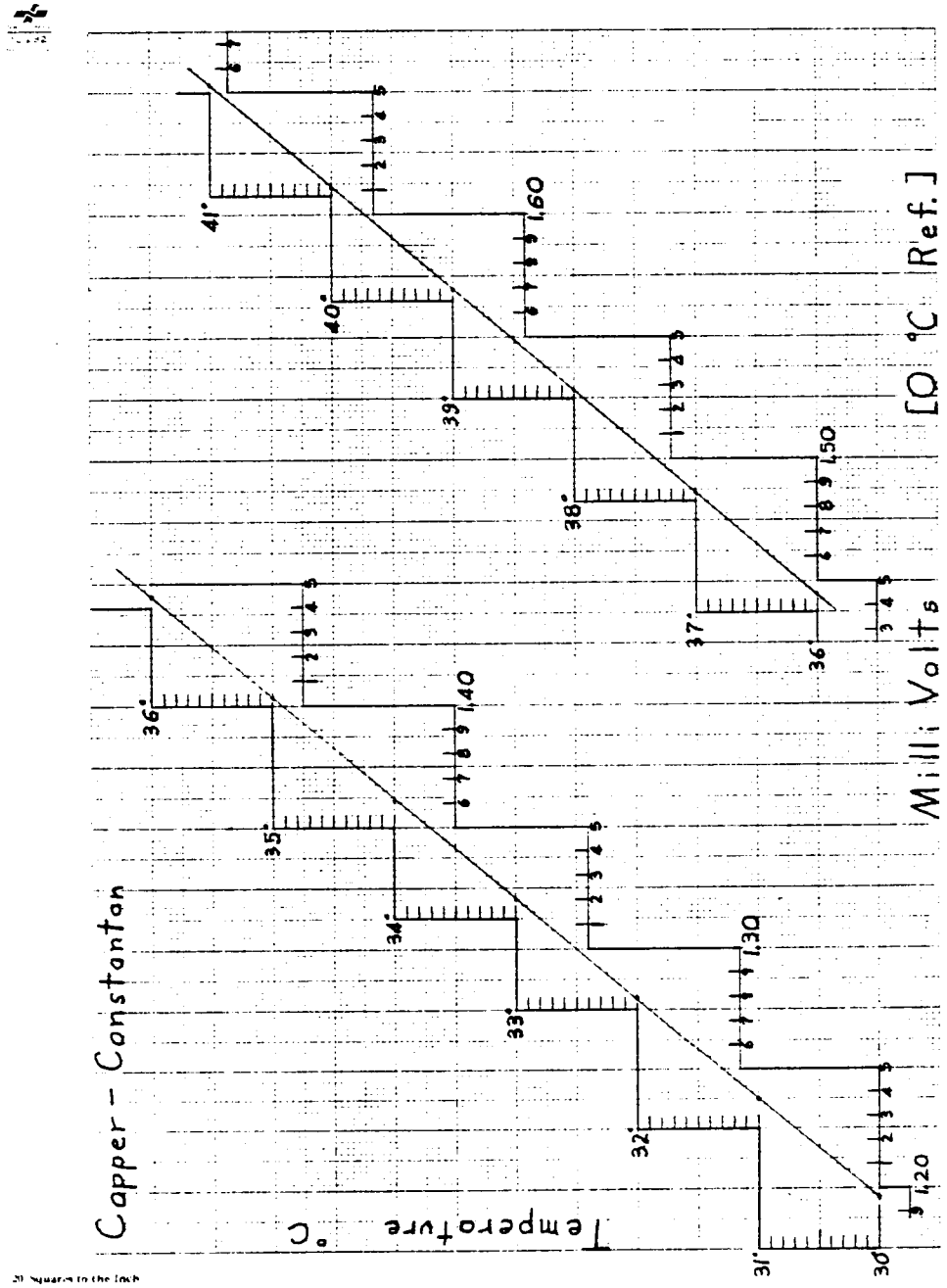


Figure 55. Thermocouple millivolt potential versus temperature for the 30 - 40 C range.

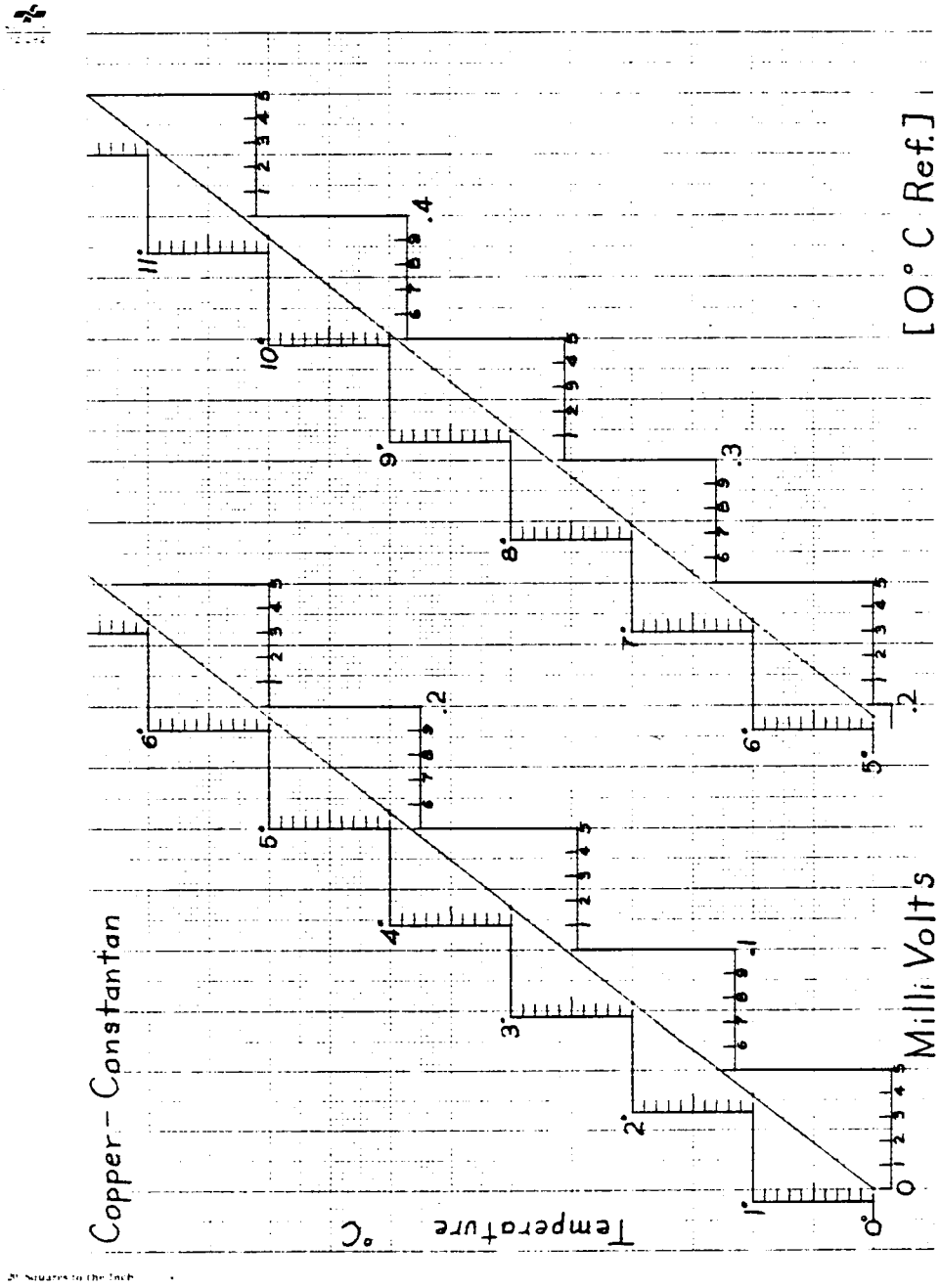


Figure 56. Thermocouple millivolt potential versus temperature for the 0 - 10 C range.

Table 13. Thermometer data for the hot and cold wall calibration tests.

	Thermometers		
	#1	#2	#3
	Hot Wall Calibration		
°F	99.30	-----	99.40
°C	37.39		37.44
Corrected	37.39		37.39
	T_{corr} = 37.40 °C		
	Cold Wall Calibration		
°F	45.60		45.70
°C	7.56	7.50	7.61
Corrected	7.56	7.55	7.55
	T_{corr} = 7.55 °C		

APPENDIX H

PARTICLE GENERATORS FOR SEEDING FLOWS FOR LASER DOPPLER VELOCIMETRY

When the operation of the LDV was described, it was explained that the flow whose velocity is to be measured must be seeded with fine particles of some type in order to scatter the laser light. Thermo-Systems, Inc. makes particle generator devices, one of which was obtained for the Natural Convection Laboratory.

To use the generator, one either dissolves or disperses some solid substance in water. The mixture is then fed into a part of the generator called a "nebulizer" which uses an ultrasonic oscillator and crystal to break the water up into a fog of fine droplets. This fog is then passed through a "diffusion dryer" which uses silica gel to absorb away the water from the fog. With the water evaporated away, the solid material is left as a particulate suspension in the air stream. This stream of particles can then be introduced where seeding is desired. By dissolving greater or lesser amounts of the solid substance in the water, the size of the particles can be controlled.

This generator was used on one occasion to seed the flow within the cavity. Table sugar (sucrose) was selected as the solid material. Sugar was used because it is

nontoxic, noncorrosive, highly soluble in water, and readily available. Its performance as a seeding material was quite acceptable; however, it tended to form a relatively heavy coating on the end-windows.

Because a relatively large amount of effort is needed to set-up and take-apart and clean the particle generator, it was not used for any of the main experiments with the LDV. Instead, a homemade smoke generator was used.

The smoke generator consists of a laboratory thistle-tube inserted through a two-hole stopper which is held in the mouth of a small bottle. Plastic tubing leads from the other hole of the stopper to another diffusion dryer, this one made in the laboratory. It consists of an approximate 1 foot length of plastic tubing about 1.5 inches in diameter with stoppers at both ends. A tube of wire mesh about 0.5 inch in diameter extends between these two stoppers. The space between the two tubes is filled with silica gel. From the end of the dryer opposite the connection to the bottle, another tube leads to the suction side of a rubber squeeze-bulb hand pump. A tube from the discharge of this pump extends to the cavity's fill tube. By squeezing and releasing the bulb, air can be induced to flow in through the bulb of the thistle-tube, through the bottle and dryer, and into the cavity and out the drain tube.

Since numerous other researchers had used tobacco

smoke for LDV measurements or for flow visualization, some pipe tobacco was obtained for use in this generator. It was expected that the tobacco would release tars and other substances, so the bottle was partially filled with water so that the smoky air would bubble through it to try to condense out the substances before they entered the rest of the system. Unfortunately, this filtering did not work very well, and the tubing, some of the silica gel, and the hand pump became fouled with the products from the tobacco.

So, a rolled-up strip of cotton rag was substituted for the tobacco. This smoke, except for its odor, was found to be extremely satisfactory in seeding the flow for LDV measurements. Because the cotton rag did not release substances such as tars, the bottle was not filled with water although the dryer was still used to try to ensure that damp air did not enter the cavity. This author strongly urges the use of a tobacco substitute.

APPENDIX I

CAVITY VELOCITY DATA MEASURED WITH THE LDV

LDV Data Exp. No. 2 Traverse No. 1 Date 12-21-79

$x'_{20} = 30.0$ $x =$ _____ mm. $V_o = 1.98, 4.98$

$y' = 86.0$ $y = 20.0$ mm. $S.F. = 10^{-4}$ Volt sec.

$z' = 62.5$ $z =$ ℄ m.m. $d_f = .003202$ m.m.

#	Axis' X'	Voltage	Axis X	Vel. V	#	Axis' X'	Voltage	Axis X	Vel. V
1	30.0	4.97	20.0	-.32	32	22.0	2.00	28.0	.64
2	32.0	4.97	18.0	-.32	33	20.0	1.97	30.0	-.32
3	34.0	4.96	16.0	-.64	34	19.0	1.92	31.0	-1.92
4	36.0	4.95	14.0	-.96	35	18.0	1.83	32.0	-4.80
5	38.0	4.96	12.0	-.64	36	17.0	1.69	33.0	-9.29
6	40.0	5.02	10.0	1.28	37	16.0	1.46	34.0	-16.65
7	40.0	2.02	10.0	1.28	38	15.0	1.15	35.0	-26.58
8	41.0	2.10	9.0	3.84	39	15.0	4.15	35.0	-26.58
9	42.0	2.24	8.0	8.33	40	14.0	3.78	36.0	-38.42
10	43.0	2.46	7.0	15.37	41	13.0	3.38	37.0	-51.23
11	44.0	2.75	6.0	24.66	42	12.0	3.16	38.0	-58.28
12	45.0	3.12	5.0	36.50	43	11.0	3.41 ±	39.0	-50.27±
13	46.0	3.51	4.0	48.99	44	10.5	3.80 ±	39.5	-37.78±
14	47.0	3.77	3.0	57.32	45	10.0	4.40 ±	40.0	-18.57±
15	47.5	3.80	2.5	58.28	46	12.5	3.23	37.50	-56.04
16	48.0	3.71	2.0	55.39	47	15.0	4.14	35.0	-26.90
17	48.5	3.45	1.5	47.07	48	20.0	4.98	30.0	0
18	49.0	3.05	1.0	34.26	49	25.0	4.99+	25.0	.48
19	49.5	2.45 ±	.5	15.05±	50	30.0	4.98-7	20.0	-.16
20	49.75	2.34 ±	.25	11.53 ±	51				
21	50.0	———			52				
22					53				
23	48.0	3.70	2.0	55.07	54				
24	45.5	3.32	4.5	42.91	55				
25	45.0	3.13	5.0	36.82	56				
26	40.0	2.02	10.0	1.28	57				
27	35.0	1.96	15.0	-.64	58				
28	30.0	1.97	20.0	-.32	59				
29	28.0	1.97-8	22.0	-.16	60				
30	26.0	1.98-9	24.0	.16	61				
31	24.0	1.99	26.0	.32	62				

J.W.J

LDV Data Exp. No. 2 Traverse No. 2 Date 12-24-79

$x' = 30.0$ $x = 20.0$ mm. $V_o = 1.98, 4.98$

$y'_{20} = 86.0$ $y =$ _____ m.m. S.F. $= 10^{-4}$ Volt sec.

$z' = 62.5$ $z =$ ℄ m.m. $d_f = .003202$ m.m.

#	Axis y'	Voltage	Axis y	Vel. U	#	Axis y'	Voltage	Axis y	Vel. U
1	86.0	1.98	20.0	0	32	75.0	1.40	9.0	-18.57
2	88.0	1.97	22.0	-.32	33	74.0	1.26	8.0	-23.05
3	90.0	2.00	24.0	.64	34	73.0	1.11	7.0	-27.86
4	92.0	2.08	26.0	3.20	35	72.0	1.00	6.0	-31.38
5	93.0	2.14	27.0	5.12	36	71.0	.93	5.0	-33.62
6	94.0	2.23	28.0	8.01	37	70.0	.94	4.0	-33.30
7	95.0	2.34	29.0	11.53	38	69.0	1.04	3.0	-30.10
8	96.0	2.46	30.0	15.37	39	68.0	1.22	2.0	-24.34
9	97.0	2.61	31.0	20.17	40	67.0	1.52	1.0	-14.73
10	98.0	2.75	32.0	24.66	41	66.5	1.70	.5	-8.97
11	99.0	2.88	33.0	28.82	42	66.0	1.89 ±	0	-2.88 ±
12	100.0	2.98	34.0	32.02	43				
13	101.0	3.03	35.0	33.62	44	67.5	1.36	1.50	-19.85
14	102.0	3.01	36.0	32.98	45	70.0	.94	4.0	-33.30
15	103.0	2.89	37.0	29.14	46	75.0	1.40	9.0	-18.57
16	104.0	2.69	38.0	22.73	47	80.0	1.91	14.0	-2.24
17	105.0	2.38	39.0	12.81	48	85.0	1.98	19.0	0
18	105.5	2.21	39.5	7.36	49				
19					50				
20	102.5	2.96	36.5	31.38	51				
21	100.0	2.99	34.0	32.02	52				
22	95.0	2.35	29.0	11.85	53				
23	90.0	2.00	24.0	.64	54				
24	86.0	1.98	20.0	0	55				
25	84.0	1.99	18.0	.32	56				
26	82.0	1.97	16.0	-.32	57				
27	80.0	1.91	14.0	-2.24	58				
28	79.0	1.85	13.0	-4.16	59				
29	78.0	1.77	12.0	-6.72	60				
30	77.0	1.66	11.0	-10.25	61				
31	76.0	1.54	10.0	-14.09	62				

J.W.J

Selected LDV data used for the plots in Figure 51.

x [mm]	v [mm/sec]
0.0	0.0
0.5	15.05
1.0	34.26
1.5	47.07
2.0	55.39
2.5	58.28
3.0	57.32
4.0	48.99
5.0	36.50
6.0	24.66
7.0	15.37
8.0	8.33
9.0	3.84
10.0	1.28
12.0	-.64
14.0	-.96
16.0	-.64
18.0	-.32
20.0	-.32
22.0	-.16
24.0	0.16
26.0	0.32
28.0	0.64
30.0	-.32
31.0	-1.92
32.0	-4.80
33.0	-9.29
34.0	-16.65
35.0	-26.58
36.0	-38.42
37.0	-51.23
38.0	-58.28
39.0	-50.27
39.5	-37.78
40.0	0.0

y [mm]	u [mm/sec]
0.0	0.0
0.5	-8.97
1.0	-14.73
2.0	-24.34
3.0	-30.10
4.0	-33.30
5.0	-33.62
6.0	-31.38
7.0	-27.86
8.0	-23.05
9.0	-18.57
10.0	-14.09
11.0	-10.25
12.0	-6.72
13.0	-4.16
14.0	-2.24
16.0	-.32
18.0	0.32
20.0	0.0
22.0	-.32
24.0	0.64
26.0	3.20
27.0	5.12
28.0	8.01
29.0	11.53
30.0	15.37
31.0	20.17
32.0	24.66
33.0	28.82
34.0	32.02
35.0	33.62
36.0	32.98
37.0	29.14
38.0	22.73
39.0	12.81
39.5	7.36
40.0	0.0

APPENDIX J

THE MEASURING MICROSCOPE

Measurements on interferogram negatives were made in the Natural Convection Laboratory by means of an EPOI (Nikon) "Shopscope" measuring microscope. This microscope is shown in Figure 57. An interferogram is in place on the stage. The black cardboard screen attached to the eyepiece tube was added to block the vision of the unused eye (pinching the eye shut becomes painful after a while).

The measuring microscope has an x-y traveling stage with 2 inches by 6 inches of travel. Movement of the stage is controlled from two micrometers, each with 2 inches travel and graduated to 0.0001 inch. For movements greater than 2 inches in the 6 inch travel direction, a V-groove was provided for gage blocks to be added where they would be borne against by the micrometer.

The microscope's optical system consists of an eyepiece with a crosshair reticle and a three objective turret providing magnifications of 10X, 30X, and 50X. This author used the 30X magnification for practically all measurements.

When analyzing an interferogram, the negative was attached by adhesive tape to a 3 inch by 7 inch piece of thin glass (before taping it down, a location for the negative must be found such that the desired points to be

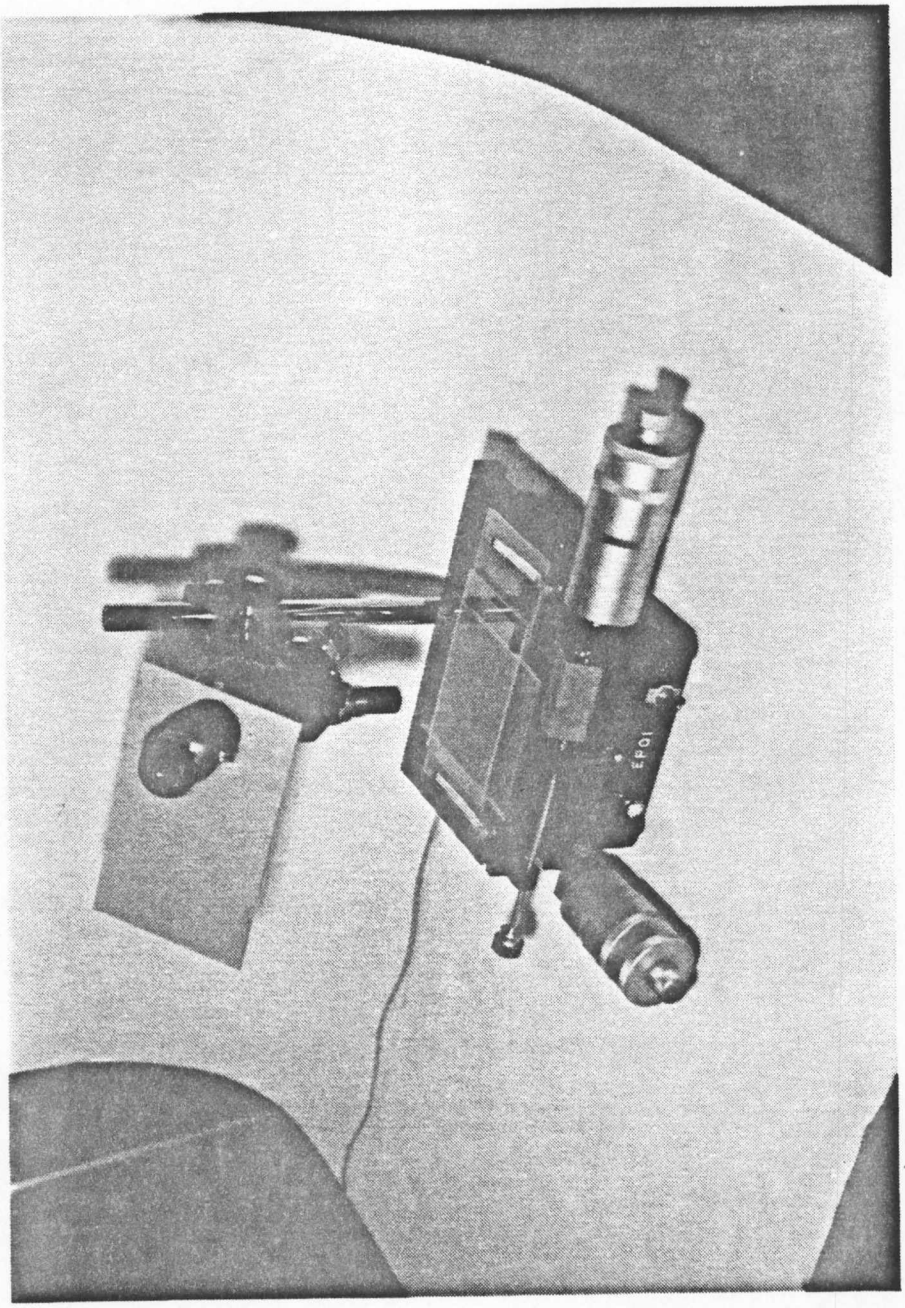


Figure 57. Photograph of the measuring microscope.

viewed are within the range of travel of the stage). A smaller cover glass was placed over the negative to hold it flat for the measurements. Spring clips attached to the stage hold the "negative carrier" glass in place; the ends of the carrier are simply slid back and forth to achieve alignment of the negative with the stage travel.

APPENDIX K

PROPERTY VALUES AND EQUATIONS FOR AIR

Where values for properties of air were needed in this paper, they were obtained from Hilsenrath, et al., [13].

The gas constant, R, for air was taken to be

$$R = 2.15297 \quad (m^3 \text{ mmHg})/(Kg\ ^oK)$$

A convenient form of the ideal gas equation for air is

$$\rho_{air} = 0.46447\ P/T \quad (Kg/m^3) \qquad [77]$$

where P is in mmHg and T is in ^oK.

Hauf and Grigull [4] list values of refractive index, n, and specific refractivity, $\bar{r}$, for air at 20 ^oC and 760 mmHg and for a light wavelength of 6328×10^{-10} meter. The values are

$$n = 1.0002716$$

$$\bar{r} = 1.504 \times 10^{-4} \quad (m^3/Kg)$$

The consistency of these numbers can be checked using Equation 8, which is

$$\bar{r} = (2/3)((n-1)/\rho)$$

Using the listed value for n and the equation for ρ_{air} at 760 mmHg and 20 ^oC, one obtains the above listed value for

$\overline{r}$. Another value for n at the particular wavelength desired was not readily available, so no further checks were made.

Rearranging Equation 8, one obtains

$$n = 1 + (3/2)\overline{r}\rho$$

After substituting in the value for $\overline{r}$ and the equation for ρ_{air},

$$n = 1 + 0.0001048\ (P/T) \qquad [78]$$

where P is in mmHg and T is in ^{o}K.

APPENDIX L

CAVITY END EFFECT ANALYSIS

In this appendix, the magnitude of the error due to end effects within the cavity will be estimated.

After other experiments with the cavity had been completed, another experiment was performed in which three free thermocouples, those identified previously as #22, #23, and #24, were attached to the outside of the glass window at one end of the cavity. The couples were attached with thick tape; it was hoped that the insulating effect of the tape would tend to overcome any measurement error due to heat conduction through the couple's leads.

All of the couples were positioned to be along the horizontal centerline of the cavity. Thermocouple #22 was attached to the glass just at the end of the hot wall. Thermocouple #24 was attached at the center of the cavity (along the vertical centerline as well as the horizontal), and thermocouple #23 was attached midway between the other two on the horizontal centerline. Before operating the cavity, the potential outputs of the couples were checked. They all indicated 22.85 ^{o}C (corrected) while the room air temperature was about 23.1 ^{o}C (it was unclear what caused this difference).

The circulating baths were then started with the thermoregulators set to approximately the same temperatures

used in the main cavity experiments. The cavity was operated for 2 hours, and the outputs of the three couples listed above were checked as well as the outputs of the couples in the center of the hot and cold walls (couples #5, for each wall). The corrected temperatures indicated by the couples were

22:	26.95 ^{o}C
24:	25.20
23:	23.65
5H:	37.35
5C:	7.30

The hot to cold wall temperature difference was 30.05 C^{o}, and the mean temperature was 22.32 ^{o}C. (The room air at this time was 24.7 ^{o}C.) There was a 37.35 - 22.32 = 15.03 C^{o} difference between the hot wall temperature and the cavity mean temperature. There was a 26.95 - 23.65 = 3.30 C^{o} difference between the glass temperature at the hot wall and the glass temperature at the center of the cavity. Thus, the temperature variation over the glass was about 3.30/15.03 = 1/4.5 that of the variation over the cavity. Based on this information (albeit very limited), it might be reasonable to assume, for purposes of estimation, that the glass windows were isothermal at the mean temperature of the cavity. This is the assumption that will be made here.

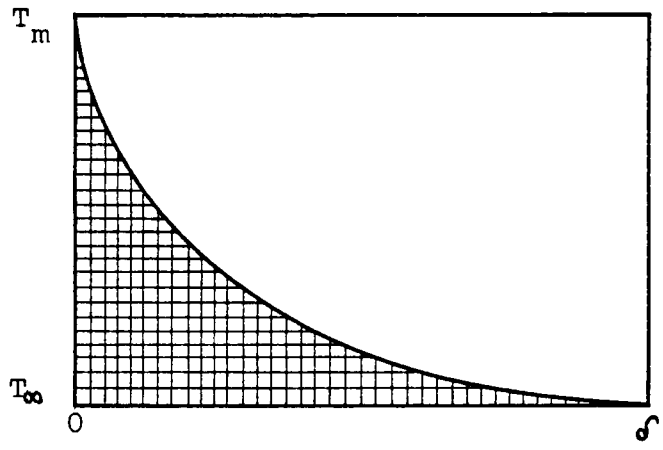
An end effect analysis has already been presented in

Appendix A for the case of a heated plate in free air. That situation is depicted in Figure 58A. The temperature distribution is assumed to be parabolic from the air temperature at some distance along the plate, T_M, to the free air temperature, T_∞. This parabolic distribution extends along a distance, δ. The shaded part of the figure represents that area bounded by the curve that influences the fringe shift; that is, it is this area that contributes to the end effect.

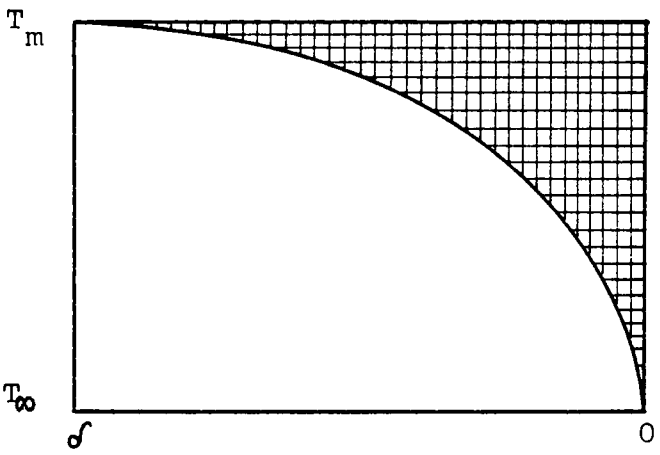
In Figure 58B, the situation for an internal cavity flow is illustrated. Without the end effect, the air temperature at some x,y location would extend up to the end window. With the end effect, the end window influences the air temperature some distance into the cavity. It might be reasonable to assume that the air temperature again follows a parabolic distribution within this end region. This is shown in the figure.

For the free air case, the extent of the boundary layer, δ, in the end region could be estimated from its extent on the sides of the plate (this could be seen on the interferograms). For the cavity case, there is no equivalent method available. Thus, there is no obvious method available for obtaining reasonable values of δ (δ would be a function of both x and y).

Nevertheless, an estimate of the magnitude of the end effect error will be made for one point. This point will



A. Free Air Case



B. Internal Cavity Case

Figure 58. Assumed end effects for a heated plate in free air (A) or for the influence of an end window in an internal cavity (B).

be taken to be along the y = 0.5H traverse and at the S = 2 location; this is at x = 1.64 millimeters (see Table 9). The temperature at this point may be estimated from Equation 44,

$$T = T_M = 310.56/(1 + 0.01011\ S) - 273.15 \qquad [79]$$

The indicated (or measured) temperature at S = 2 is T_M = 31.25 °C (the value S = 2 could be assumed to be the ideal fringe shift (no end effect) for this calculation).

The size of the fringe shift due to the assumed end effect (that of Figure 58B) may be calculated from the equation derived in Appendix A, even though the two cases are not identical. The equation is

$$\Delta S_2 = 0.3311\ P_\infty \delta \left[\frac{1}{T_\infty} - \frac{1}{\sqrt{\Delta T\ T_\infty}} \tan^{-1} \frac{\Delta T}{\sqrt{\Delta T\ T_\infty}}\right] \qquad [80]$$

where δ replaces δ' as used in Appendix A. With the values P_∞ = 744.3 mmHg, T_∞ = 295.47 °K (the mean of the hot and cold wall temperatures), and $\Delta T = T_M - T_\infty$ =304.40 - 295.47 = 8.93 K°, the above equation reduces to

$$\Delta S_2 = 0.00825\,\delta \qquad [81]$$

This includes both ends of the cavity.

The S = 2 fringe was at x = 1.64 millimeter (from the hot wall). Let the boundary layer length, δ, be assumed to be 10 millimeters. Thus,

$$\Delta S_2 = 0.0825$$

For a cavity, the end effects reduce the effective length of the walls. For light rays that pass through air that is above the mean or the outside temperature (that is, for T_M greater than T_∞) there is a fringe shift deficit compared to the ideal fringe shift case. So, for this example, ΔS_2 should be subtracted from S to give a smaller S-value which results in a greater air temperature. (For air temperatures below T_∞, the situation would be reversed.) Thus,

$$S_{ideal} = S - \Delta S_2 = 2 - 0.0825 = 1.9175 \qquad [82]$$

The resulting temperature is 31.50 ^oC. With no correction, the temperature was 31.25 ^oC. The error is thus 0.25 C^o or, relative to the 30.17 C^o difference between the hot and cold walls, 0.83%.

For light rays that just graze the hot and cold walls, the end effect should be relatively small, since the boundary layers on the end windows will not extend to the walls and since half of each endgap was added to the length of the walls where the length was used in calculations. Also, where the air in the cavity is at or near the outside air temperature or the mean temperature (these should be nearly the same), the end effect error will be minimal. Thus, one would expect the end effect error to increase from nearly zero at each wall to some maximum value and then to decrease to zero at some point within the cavity.

As stated, the S = 2 fringe was at x = 1.64 millimeter. The S = 5 fringe, where the temperature had decreased to approximately the mean or room temperature, was at x = 5.67 millimeters. Compared to these distances, the assumption that δ = 10 millimeters seems reasonable.

APPENDIX M

CAVITY TEMPERATURE DATA

FROM THE MZI

The cavity temperature data obtained from interferogram analysis are presented in Tables 14 through 24. Each table contains the data obtained from a single traverse across the interferogram (or the cavity). Table 14 presents the traverse at y = 0.038H, while Table 24 presents the traverse at y = 0.966H. The hot wall is taken to be at x = 0.00 millimeter, while the cold wall is at the highest x value listed in each table (this was its observed location on the interferogram). Fringe number interpolations were performed only at those locations where entries are made in the y' (Upper and Lower) columns. The temperature value on the last line of each table was obtained from a second-order curve fit to the three x,T values closest to the cold wall. In Tables 14, 15, 16, and 24, a fringe number interpolation (and corresponding temperature calculation) was performed just at the observed cold wall location. This x,T data was not used in the second-order curve fit calculation.

Table 14. Temperature data for: y' = 0.2675 inch; y = 1.53 mm; y/H = 0.038.

x' [in]	x [mm]	y' [in] Upper	y' [in] Lower	S	ΔS_1	S_{ideal}	T [°C]
1.6827	0.00			0.000	0.022	0.000	37.41
1.6538	0.80			1.000	0.018	1.004	34.29
1.6213	1.70			2.000	0.013	2.009	31.23
1.5826	2.78			3.000	0.007	3.015	28.22
1.5258	4.35			4.000	0.002	4.020	25.28
1.4103	7.56			5.000	0.001	5.021	22.41
1.2750	11.31	0.2811	0.2596	5.633	0.000	5.655	20.61
1.1740	14.11			6.000	0.000	6.022	19.59
0.9637	19.95	0.2819	0.2617	6.713	0.000	6.735	17.61
0.9610	20.02	0.2821	0.2615	6.709	0.000	6.731	17.62
0.8835	22.17			7.000	0.000	7.022	16.82
0.7500	25.88	0.2783	0.2579	7.529	0.000	7.551	15.38
0.6494	28.67			8.000	0.000	8.022	14.11
0.5450	31.56	0.2770	0.2582	8.505	0.000	8.527	12.76
0.4552	34.06			9.000	0.001	9.021	11.45
0.3177	37.87			10.000	0.002	10.020	8.84
0.2393	40.05	0.2828	0.2654	10.879	0.003	10.898	6.59
0.2393	40.05 (Wall)						7.02

Table 15. Temperature data for: y' = 0.3515 inch; y = 3.86 mm; y/H = 0.097.

x' [in]	x [mm]	y' [in] Upper	y' [in] Lower	S	ΔS_1	S_{ideal}	T [°C]
1.6825	0.00			0.000	0.030	0.000	37.41
1.6586	0.66			1.000	0.027	1.003	34.29
1.6328	1.38			2.000	0.025	2.005	31.24
1.6067	2.10			3.000	0.020	3.010	28.24
1.5747	2.99			4.000	0.011	4.019	25.28
1.5277	4.29			5.000	0.002	5.028	22.39
1.4610	6.15	0.3653	0.3460	5.715	0.000	5.745	20.36
1.4100	7.56			6.000	0.000	6.030	19.56
1.3280	9.84	0.3566	0.3377	6.270	0.000	6.300	18.81
1.2500	12.00	0.3613	0.3420	6.508	0.000	6.538	18.15
1.1250	15.47	0.3662	0.3483	6.821	0.000	6.851	17.29
1.0500	17.55			7.000	0.000	7.030	16.80
0.9635	19.95	0.3552	0.3376	7.210	0.000	7.240	16.23
0.9614	20.01	0.3554	0.3376	7.219	0.000	7.249	16.20
0.8700	22.54	0.3590	0.3422	7.446	0.000	7.476	15.58
0.7750	25.18	0.3622	0.3461	7.665	0.000	7.695	14.99
0.6156	29.60			8.000	0.000	8.030	14.09
0.4950	32.95	0.3564	0.3421	8.343	0.000	8.373	13.17
0.3997	35.59			9.000	0.001	9.029	11.43
0.3450	37.11	0.3583	0.3437	9.466	0.001	9.495	10.21
0.3040	38.25			10.000	0.002	10.028	8.82
0.2402	40.02	0.3649	0.3485	10.817	0.002	10.845	6.72
0.2402	40.02 (Well)						5.58

Table 16. Temperature data for: y' = 0.5025 inch; y = 8.05 mm; y/H = 0.202.

x' [in]	x [mm]	y' [in] Upper	y' [in] Lower	S	ΔS_1	S_{ideal}	T [°C]
				0.000	0.033	0.000	37.41
1.6825	0.00			1.000	0.033	1.000	34.30
1.6599	0.63			2.000	0.033	2.000	31.25
1.6373	1.25			3.000	0.027	3.006	28.25
1.6149	1.88			4.000	0.019	4.014	25.30
1.5822	2.62			5.000	0.008	5.025	22.39
1.5557	3.52			6.000	0.004	6.029	19.57
1.4989	5.09			6.503	0.000	6.536	18.16
1.4250	7.14	0.5108	0.4943	6.618	0.000	6.651	17.84
1.3750	8.53	0.5130	0.4960	6.806	0.000	6.839	17.32
1.2700	11.44	0.5154	0.4994	6.894	0.000	6.927	17.08
1.1500	14.77	0.5169	0.5008	6.939	0.000	6.972	16.96
0.9635	19.95	0.5179	0.5015	6.944	0.000	6.977	16.95
0.9623	19.98	0.5177	0.5016	6.955	0.000	6.988	16.92
0.8640	22.71	0.5172	0.5018	6.906	0.000	6.939	17.05
0.8400	23.37	0.5170	0.5010	6.861	0.000	6.894	17.17
0.8000	24.48	0.5161	0.5003	6.762	0.000	6.795	17.44
0.7250	26.56	0.5140	0.4989	6.622	0.000	6.655	17.83
0.6530	28.56	0.5117	0.4969	6.561	0.000	6.594	18.00
0.5470	31.50	0.5108	0.4960	6.678	0.000	6.711	17.68
0.4950	32.95	0.5126	0.4977	7.000	0.000	7.033	16.79
0.4412	34.44			8.000	0.004	8.029	14.09
0.3645	36.57			9.000	0.007	9.026	11.44
0.3119	38.03			10.000	0.009	10.024	8.83
0.2674	39.26			10.571	0.010	10.594	7.36
0.2420	39.97	0.5118	0.4955				7.14
0.2420	39.97 (Wall)						

Table 17. Temperature data for: y' = 0.6355 inch; y = 11.74 mm; y/H = 0.295.

x' [in]	x [mm]	y' [in] Upper	y' [in] Lower	S	ΔS_1	S_{ideal}	T [°C]
1.6834	0.00			0.000	0.031	0.000	37.41
1.6599	0.65			1.000	0.031	1.000	34.30
1.6367	1.30			2.000	0.030	2.001	31.25
1.6125	1.97			3.000	0.025	3.006	28.25
1.5841	2.75			4.000	0.017	4.014	25.30
1.5491	3.73			5.000	0.007	5.024	22.40
1.4840	5.53			6.000	0.003	6.028	19.57
1.4090	7.61	0.6408	0.6252	6.340	0.000	6.371	18.62
1.3500	9.25	0.6420	0.6262	6.411	0.000	6.442	18.42
1.2850	11.05	0.6420	0.6265	6.419	0.000	6.450	18.40
1.2000	13.41	0.6425	0.6270	6.452	0.000	6.483	18.31
1.1000	16.19	0.6423	0.6273	6.453	0.000	6.484	18.30
0.9694	19.81	0.6411	0.6261	6.373	0.000	6.404	18.52
0.9634	19.98	0.6409	0.6259	6.360	0.000	6.391	18.56
0.9000	21.73	0.6408	0.6253	6.342	0.000	6.373	18.61
0.8100	24.23	0.6390	0.6231	6.220	0.000	6.251	18.95
0.7500	25.90	0.6379	0.6222	6.153	0.000	6.184	19.13
0.6800	27.84			6.000	0.000	6.031	19.56
0.6100	29.78	0.6489	0.6334	5.865	0.000	5.896	19.94
0.5500	31.45	0.6475	0.6319	5.769	0.000	5.800	20.21
0.4950	32.97	0.6481	0.6331	5.840	0.000	5.871	20.01
0.4546	34.09			6.000	0.000	6.031	19.56
0.4050	35.47	0.6426	0.6276	6.473	0.000	6.504	18.25
0.3720	36.38			7.000	0.004	7.027	16.81
0.3269	37.63			8.000	0.010	8.021	14.11
0.2903	38.65			9.000	0.014	9.017	11.46
0.2574	39.56			10.000	0.016	10.015	8.85
0.2434	39.95 (Wall)						7.58

Table 18. Temperature data for: y' = 0.7838 inch; y = 15.85 mm; y/H = 0.399.

x' [in]	x [mm]	y' [in] Upper	y' [in] Lower	S	ΔS_1	S_{ideal}	T [°C]
1.6823	0.00			0.000	0.026	0.000	37.41
1.6566	0.71			1.000	0.025	1.001	34.30
1.6306	1.43			2.000	0.024	2.002	31.25
1.6034	2.19			3.000	0.019	3.007	28.25
1.5712	3.08			4.000	0.011	4.015	25.29
1.5263	4.33			5.000	0.003	5.023	22.40
1.4650	6.03	0.7935	0.7777	5.614	0.000	5.640	20.66
1.3820	8.33	0.7966	0.7810	5.821	0.000	5.847	20.07
1.2950	10.74	0.7955	0.7801	5.760	0.000	5.786	20.25
1.1750	14.08	0.7942	0.7790	5.684	0.000	5.710	20.46
1.0570	17.35	0.7938	0.7786	5.658	0.000	5.684	20.53
0.9694	19.78	0.7938	0.7786	5.658	0.000	5.684	20.53
0.9633	19.95	0.7937	0.7786	5.656	0.000	5.682	20.54
0.8600	22.81	0.7926	0.7775	5.583	0.000	5.609	20.74
0.7250	26.56	0.7909	0.7759	5.473	0.000	5.499	21.05
0.6350	29.06	0.7890	0.7734	5.333	0.000	5.359	21.45
0.5250	32.11	0.7863	0.7713	5.167	0.000	5.193	21.92
0.4500	34.19	0.7897	0.7741	5.378	0.000	5.404	21.32
0.3928	35.78			6.000	0.003	6.023	19.58
0.3447	37.11			7.000	0.010	7.016	16.84
0.3105	38.06			8.000	0.017	8.009	14.14
0.2821	38.85			9.000	0.022	9.004	11.50
0.2551	39.60			10.000	0.026	10.000	8.89
0.2442	39.90 (Wall)						7.77

Table 19. Temperature data for: y' = 0.9318 inch; y = 19.96 mm; y/H = 0.502.

x' [in]	x [mm]	y' [in] Upper	y' [in] Lower	S	ΔS_1	S_{ideal}	T [°C]
1.6848	0.00			0.000	0.021	0.000	37.41
1.6556	0.81			1.000	0.019	1.002	34.30
1.6258	1.64			2.000	0.017	2.004	31.24
1.5925	2.56			3.000	0.013	3.008	28.24
1.5525	6.67			4.000	0.005	4.016	25.29
1.4805	5.67			5.000	0.000	5.021	22.40
1.4030	7.82	0.9353	0.9196	5.223	0.000	5.244	21.77
1.3250	9.98	0.9342	0.9190	5.158	0.000	5.179	21.96
1.2250	12.76			5.000	0.000	5.021	22.40
1.1500	14.84	0.9457	0.9309	4.939	0.000	4.960	22.58
1.0730	16.97	0.9447	0.9296	4.854	0.000	4.875	22.82
0.9694	19.85	0.9440	0.9289	4.808	0.000	4.829	22.95
0.9649	19.97	0.9436	0.9288	4.797	0.000	4.818	22.98
0.8500	23.16	0.9439	0.9282	4.771	0.000	4.792	23.06
0.7000	27.32	0.9431	0.9275	4.724	0.000	4.745	23.19
0.5500	31.48	0.9414	0.9258	4.615	0.000	4.636	23.50
0.4950	33.01	0.9418	0.9262	4.641	0.000	4.662	23.43
0.4261	34.92			5.000	0.003	5.018	22.41
0.3660	36.59			6.000	0.007	6.014	19.61
0.3302	37.58			7.000	0.016	7.005	16.87
0.3018	38.37			8.000	0.024	7.997	14.18
0.2776	39.04			9.000	0.031	8.990	11.53
0.2553	39.66			10.000	0.034	9.987	8.93
0.2450	39.95 (Wall)						7.65

Table 20. Temperature data for: y' = 1.0645 inch; y = 23.64 mm; y/H = 0.595.

x' [in]	x [mm]	y' [in] Upper	y' [in] Lower	S	ΔS_1	S_{ideal}	T [°C]
1.6855	0.00			0.000	0.018	0.000	37.41
1.6513	0.95			1.000	0.015	1.003	34.29
1.6180	1.87			2.000	0.012	2.006	31.24
1.5770	3.01			3.000	0.007	3.011	28.23
1.5235	4.50			4.000	0.000	4.018	25.29
1.4830	5.62	1.0704	1.0550	4.383	0.000	4.401	24.18
1.4250	7.23	1.0749	1.0592	4.662	0.000	4.680	23.38
1.3700	8.75	1.0747	1.0590	4.650	0.000	4.668	23.41
1.2750	11.39	1.0718	1.0561	4.465	0.000	4.483	23.94
1.1950	13.61	1.0691	1.0538	4.301	0.000	4.319	24.42
1.1060	16.08	1.0676	1.0568	4.287	0.000	4.305	24.46
1.0250	18.32	1.0664	1.0508	4.122	0.000	4.140	24.93
0.9694	19.87	1.0651	1.0502	4.040	0.000	4.058	25.17
0.9660	19.96	1.0652	1.0502	4.047	0.000	4.065	25.15
0.8030	24.48	1.0650	1.0496	4.032	0.000	4.050	25.19
0.7060	27.18	1.0648	1.0495	4.020	0.000	4.038	25.23
0.5750	30.81	1.0647	1.0493	4.013	0.000	4.031	25.25
0.4934	33.07	1.0651	1.0499	4.039	0.000	4.057	25.17
0.4350	34.69	1.0708	1.0550	4.399	0.000	4.417	24.13
0.3922	35.88			5.000	0.006	5.012	22.43
0.3498	37.06			6.000	0.013	6.005	19.63
0.3204	37.87			7.000	0.024	6.994	16.90
0.2965	38.54			8.000	0.032	7.986	14.21
0.2749	39.14			9.000	0.040	8.978	11.56
0.2551	39.68			10.000	0.048	9.970	8.97
0.2465	39.92 (Wall)						7.74

Table 21. Temperature data for: y' = 1.2130 inch; y = 27.76 mm; y/H = 0.698.

x' [in]	x [mm]	y' [in] Upper	y' [in] Lower	S	ΔS_1	S_{ideal}	T [°C]
1.6864	0.00			0.000	0.011	0.000	37.41
1.6427	1.21			1.000	0.009	1.002	34.30
1.5999	2.40			2.000	0.007	2.004	31.24
1.5453	3.92			3.000	0.001	3.010	28.24
1.4850	5.59	1.2248	1.2094	3.766	0.000	3.777	25.99
1.3930	8.14	1.2153	1.2000	4.150	0.000	4.161	24.87
1.3100	10.44	1.2142	1.1984	4.076	0.000	4.087	25.09
1.2732	11.46			4.000	0.000	4.011	25.31
1.1900	13.77	1.2261	1.2101	3.819	0.000	3.830	25.83
1.1000	16.27	1.2230	1.2071	3.629	0.000	3.640	26.39
1.0200	18.49	1.2211	1.2052	3.509	0.000	3.520	26.74
0.9694	19.89	1.2202	1.2048	3.468	0.000	3.479	26.86
0.9672	19.95	1.2205	1.2047	3.475	0.000	3.486	26.84
0.8750	22.51	1.2200	1.2042	3.443	0.000	3.454	26.93
0.7950	24.73	1.2203	1.2042	3.453	0.000	3.464	26.90
0.7000	27.37	1.2206	1.2042	3.463	0.000	3.474	26.87
0.5950	30.28	1.2213	1.2053	3.519	0.000	3.530	26.71
0.5000	32.92	1.2236	1.2074	3.654	0.000	3.665	26.31
0.4366	34.67			4.000	0.000	4.011	25.31
0.3730	36.44			5.000	0.007	5.004	22.45
0.3393	37.37			6.000	0.019	5.992	19.67
0.3142	38.07			7.000	0.031	6.980	16.94
0.2926	38.67			8.000	0.040	7.971	14.25
0.2732	39.21			9.000	0.051	8.960	11.61
0.2560	39.68			10.000	0.060	9.951	9.02
0.2480	39.91 (Wall)						7.73

Table 22. Temperature data for: y' = 1.3632 inch; y = 31.93 mm; y/H = 0.803.

x' [in]	x [mm]	y' [in] Upper	y' [in] Lower	S	ΔS_1	S_{ideal}	T [°C]
1.6867	0.00			0.000	0.007	0.000	37.41
1.6283	1.62			1.000	0.005	1.002	34.30
1.5674	3.31			2.000	0.003	2.004	31.24
1.4772	5.81			3.000	0.000	3.007	28.25
1.3950	8.09	1.3690	1.3544	3.397	0.000	3.404	27.08
1.33250	10.04	1.3705	1.3553	3.480	0.000	3.487	26.83
1.2380	12.45	1.3685	1.3534	3.351	0.000	3.358	27.21
1.1550	14.75	1.3661	1.3506	3.187	0.000	3.194	27.69
1.0759	16.95	1.3640	1.3486	3.052	0.000	3.059	28.09
0.9694	19.90	1.3635	1.3473	3.019	0.000	3.026	28.19
0.9681	19.94	1.3634	1.3474	3.013	0.000	3.020	28.21
0.8650	22.80	1.3640	1.3479	3.050	0.000	3.057	28.10
0.7500	25.99	1.3655	1.3489	3.139	0.000	3.146	27.84
0.7000	27.38	1.3659	1.3499	3.169	0.000	3.176	27.75
0.6100	29.87	1.3673	1.3509	3.250	0.000	3.257	27.51
0.5100	32.65	1.3712	1.3542	3.471	0.000	3.478	26.86
0.4500	34.31	1.3759	1.3591	3.756	0.000	3.763	26.03
0.4211	35.11			4.000	0.000	4.007	25.32
0.3670	36.61			5.000	0.009	4.998	22.47
0.3359	37.48			6.000	0.023	5.984	19.69
0.3127	38.12			7.000	0.035	6.972	16.96
0.2917	38.70			8.000	0.044	7.963	14.27
0.2738	39.20			9.000	0.055	8.952	11.63
0.2568	39.67			10.000	0.065	9.942	9.04
0.2495	39.87	(Wall)					7.81

Table 23. Temperature data for: y' = 1.4963 inch; y = 35.62 mm; y/H = 0.896.

x' [in]	x [mm]	y' [in] Upper	y' [in] Lower	S	ΔS_1	S_{ideal}	T [°C]
1.6883	0.00			0.000	0.004	0.000	37.41
1.6361	1.45	1.5049	1.4887	0.531	0.002	0.533	35.75
1.5901	2.72			1.000	0.001	1.003	34.29
1.5310	4.36	1.5037	1.4889	1.500	0.001	1.503	32.76
1.4831	5.69	1.5092	1.4942	1.860	0.000	1.864	31.67
1.3500	9.39	1.5016	1.4870	2.363	0.000	2.367	30.15
1.2200	12.99	1.5058	1.4896	2.586	0.000	2.590	29.48
1.0850	16.74	1.5084	1.4914	2.712	0.000	2.716	29.11
0.9694	19.94	1.5124	1.4947	2.910	0.000	2.914	28.52
0.9184	21.36			3.000	0.000	3.004	28.26
0.7600	25.76	1.5022	1.4841	3.326	0.000	3.330	27.29
0.6300	29.36	1.5083	1.4891	3.625	0.000	3.629	26.42
0.5045	32.84			4.000	0.000	4.004	25.33
0.3912	35.99			5.000	0.003	5.001	22.46
0.3482	37.18			6.000	0.013	5.991	19.67
0.3197	37.97			7.000	0.026	6.978	16.94
0.2973	38.59			8.000	0.037	7.967	14.26
0.2771	39.15			9.000	0.045	8.959	11.61
0.2588	39.66			10.000	0.050	9.954	9.01
0.2502	39.90 (Wall)						7.70

Table 24. Temperature data for: y' = 1.5965 inch; y = 38.40 mm; y/H = 0.966.

x' [in]	x [mm]	y' [in]		S	ΔS_1	S_{ideal}	T [°C]
		Upper	Lower				
1.6895	0.00			0.000	0.001	0.000	37.41
1.5754	3.17			1.000	0.001	1.000	34.30
1.4650	6.23	1.6096	1.5914	1.720	0.000	1.721	32.10
1.4030	7.95			2.000	0.000	2.001	31.25
1.2850	11.22	1.6063	1.5870	2.508	0.000	2.509	29.73
1.1470	15.05			3.000	0.000	3.001	28.26
0.9705	19.95	1.6074	1.5870	3.534	0.000	3.535	26.69
0.9696	19.97	1.6076	1.5871	3.541	0.000	3.542	26.67
0.8090	24.43			4.000	0.000	4.001	25.33
0.6600	28.56	1.6066	1.5857	4.483	0.000	4.484	23.94
0.6000	30.23	1.6116	1.5896	4.686	0.000	4.687	23.36
0.5370	31.97			5.000	0.000	5.001	22.46
0.4580	34.17	1.6090	1.5844	5.508	0.000	5.509	21.02
0.4096	35.51			6.000	0.002	5.999	19.65
0.3521	37.10			7.000	0.008	6.993	16.90
0.3154	38.12			8.000	0.016	7.985	14.21
0.2868	38.92			9.000	0.025	8.976	11.57
0.2632	39.57			10.000	0.031	9.970	8.97
0.2497	39.95	1.6072	1.5897	10.611	0.034	10.578	7.40
0.2497	39.95 (Wall)						7.29

VITA

Jon William Jessee, the first born and only son of Harold and Edith Jessee, of Dryden, Virginia was born January 7, 1953.

He attended Dryden High School, and graduated as salutatorian in 1971. He then entered Emory and Henry College where he was named an Emory and Henry Scholar.

After completing two years at Emory and Henry, Jon transferred to the University of Tennessee in Knoxville. He was admitted to the Cooperative Education Program and worked for the Champion Paper Company in Canton, North Carolina. Jon graduated from the University of Tennessee in June of 1977, earning a Bachelor of Science Degree in Mechanical Engineering with high honors.

In September of 1977, Jon entered the graduate program in Mechanical Engineering at the University of Tennessee, and was awarded an assistantship through the National Science Foundation.

Jon was awarded the Master of Science Degree in Mechanical Engineering posthumously in August of 1985.